Chapter 15

Sorption Processes: Chromatography, Adsorption, and Ion Exchange

Adsorption, ion exchange, and chromatography are *sorption* operations, in which certain components of a fluid phase, called solutes, are selectively transferred to insoluble, rigid particles suspended in a vessel or packed in a column. Sorption, which is a general term introduced by J.W. McBain [*Phil. Mag.*, **18,** 916–935 (1909)], includes selective transfer to the surface and/or into the bulk of a solid or liquid. Thus, absorption of gas species into a liquid and penetration of fluid species into a nonporous membrane are also sorption operations. In a general sorption process, the sorbed solutes are referred to as *sorbate,* and the sorbing agent is the *sorbent.*

In an *adsorption* process, molecules, as shown in Figure 15.1a, or atoms or ions, in a gas or liquid diffuse to the surface of a solid, where they bond with the solid surface or are held there by weak intermolecular forces. The adsorbed solutes are referred to as *adsorbate,* whereas the solid material is the *adsorbent.* To achieve a very large surface area for adsorption per unit volume, highly porous solid particles with small-diameter interconnected pores are used, with the bulk of the adsorption occurring within the pores.

In an *ion-exchange* process, as shown in Figure 15.1b, ions of positive charge (*cations*) or negative charge (*anions*) in a liquid solution, usually aqueous, replace dissimilar and displaceable ions of the same charge contained in a solid *ion exchanger,* which also contains immobile, insoluble, and permanently bound co-ions of the opposite charge. Thus, ion exchange can be cation or anion exchange. Water softening by ion exchange involves a cation exchanger, in which the following reaction occurs to replace calcium ions with sodium ions.

$$Ca^{2+}_{(aq)} + 2NaR_{(s)} \leftrightarrow CaR_{2_{(s)}} + 2Na^{+}_{(aq)}$$

where R is the residual material of the ion exchanger. The exchange of ions is reversible and does not cause any permanent change to the structure of the solid ion exchanger. Thus, it can be used and reused unless fouled by organic compounds in the liquid feeds that attach to exchange sites on and within the ion exchanger. The ion-exchange concept can be extended to the removal of essentially all inorganic salts from water by a two-step process called *demineralization* or *deionization.* In the first step, a cation resin exchanges hydrogen ions for cations such as calcium, magnesium, and sodium. In the second step, an anion resin exchanges hydroxyl ions for strongly and weakly ionized anions such as sulfate, nitrate, chloride, and bicarbonate. The hydrogen and hydroxyl ions that enter the water combine to form water. Regeneration of the cation and anion resins is usually accomplished with sulfuric acid and sodium hydroxide, respectively.

In *chromatography,* the sorbent may be a solid adsorbent, an insoluble, nonvolatile, liquid absorbent contained in the pores of a granular solid support, or an ion exchanger. In either case, the solutes to be separated move through the chromatographic separator, with an inert, eluting fluid, at different rates because of repeated sorption, desorption cycles.

During adsorption and ion exchange, the solid separating agent becomes saturated or nearly saturated with the molecules, atoms, or ions transferred from the fluid phase. To recover the sorbed substances and allow the adsorbent to be reused, it is regenerated by desorbing the sorbed substances. Accordingly, these two separation operations are carried out in a cyclic manner. In chromatography, regeneration occurs continuously, but at changing locations in the separator.

Adsorption processes may be classified as *purification* or *bulk separation,* depending on the concentration in the feed fluid of the components to be adsorbed. Although there is no sharp dividing concentration, Keller [1] has suggested 10 wt%. Early applications of adsorption involved only purification. For example, adsorption with charred wood to improve the taste of water has been known for centuries. The decolorization of liquid solutions by adsorption with bone char and other materials has been practiced for at least five centuries. Adsorption of gases by a solid (charcoal) was first described by C.W. Scheele in 1773. Commercial applications of bulk separation by gas adsorption began in the early 1920s, but did not escalate until the 1960s, following the inventions by Milton [2] of synthetic molecular-sieve zeolites, which provide high adsorptive selectivity, and by Skarstrom [3] of the *pressure-swing cycle,* which made possible the efficient operation of a fixed-bed, cyclic, gas-adsorption process. The commercial-scale bulk separation

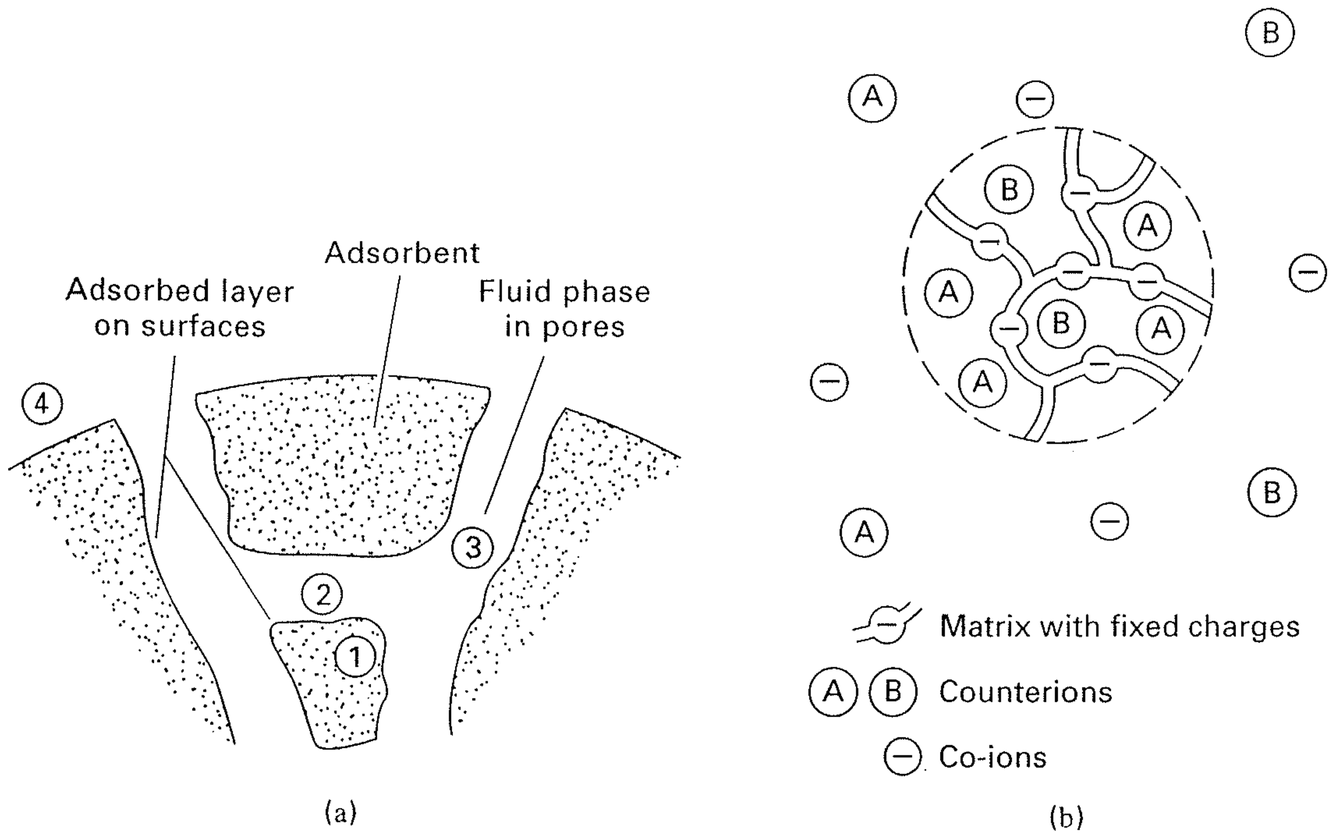

Figure 15.1 Sorption operations with solid-particle sorbents. (a) Adsorption. (b) Ion exchange.

of liquid mixtures also began in the 1960s, following the invention by Broughton and Gerhold [4] of the simulated moving bed for adsorptive separation.

The use of ion exchange dates back to at least the time of Moses, who, while leading his followers out of Egypt into the wilderness, sweetened the bitter waters of Marah with a tree [Exodus 15:23–26]. In ancient Greece, Aristotle observed that the salt content of water is reduced when it percolates through certain sands. Systematic studies of ion exchange were published in 1850 by both Thompson and Way, who experimented with cation exchange in soils before the discovery of the existence of ions.

The first major application of ion exchange, which occurred about 100 years ago, was for water treatment to remove the ions responsible for water hardness, such as calcium. Initially, the ion exchanger was a porous, natural, mineral zeolite containing silica. In 1935, synthetic, insoluble, polymeric-resin ion exchangers were introduced. Today they are dominant for water-softening and deionizing applications, but natural and synthetic zeolites still find some use.

Since the invention of chromatography by M.S. Tswett [5], a Russian botanist, in 1903, it has found widespread use as an analytical and preparative laboratory technique. Tswett separated a mixture of structurally similar yellow and green chloroplast pigments in leaf extracts by dissolving the extracts in carbon disulfide and passing the solution through a column packed with chalk particles. The pigments were separated by color. Hence, the name chromatography was coined by Tswett in 1906 from the Greek words *chroma,* meaning color, and *graphe,* meaning writing. Chromatography has revolutionized the laboratory chemical analysis of liquid and, particularly, gas mixtures. The large-scale, commercial applications described by Bonmati et al. [6] and Bernard et al. [7], however, did not begin until the 1980s.

15.0 INSTRUCTIONAL OBJECTIVES

After completing this chapter, you should be able to:

- List the major types of porous adsorbents and their most significant properties.
- Explain why a few grams of porous adsorbent can have an adsorption area as large as a football field.
- Differentiate between chemisorption and physical adsorption.
- Explain how ion-exchange resins work.
- List types of sorbents used in chromatography.
- Compare three major expressions (so-called isotherms) used for correlating single-component adsorption equilibria.
- List steps involved in adsorption of a solute, and which steps may control rate of adsorption.
- Estimate external and internal rates of adsorption.
- Describe major modes for contacting the adsorbent with a fluid containing solute(s) to be adsorbed.
- Describe major methods for regenerating adsorbent.
- Calculate vessel size or residence time for any of the major modes of slurry adsorption.
- List and explain assumptions for ideal fixed-bed adsorption and explain the concept of width of mass-transfer zone.

- Explain the concept of breakthrough in fixed-bed adsorption.
- Calculate bed height, bed diameter, and cycle time for fixed-bed adsorption.
- Compute separations for a simulated moving bed operation.
- Make design calculations for ion-exchange cycles.
- Calculate rectangular and Gaussian-distribution pulses in chromatography.

Industrial Example

The pressure-swing gas adsorption process is primarily used for the dehydration of air and for the separation of air into nitrogen and oxygen. A small unit for the dehydration of compressed air is described by White and Barkley [8] and shown in Figure 15.2. The unit consists of two fixed-bed adsorbers, each 12.06 cm in diameter and packed with 11.15 kg of 3.3-mm-diameter Alcoa F-200 activated-alumina beads to a height of 1.27 m. The external porosity (void fraction) of the bed is 0.442 and the alumina-bead bulk density is 769 kg/m^3.

The unit operates on a 10-min cycle, with 5 min for adsorption of water vapor from the air and 5 min for regeneration, which consists of depressurization, purging of the water vapor, and a 30-s repressurization. While one bed is adsorbing, the other bed is being regenerated. The adsorption (drying) step takes place with air entering at 21°C and 653.3 kPa (6.45 atm) with a flow rate of 1.327 kg/min, passing up through the bed with a pressure drop of 2.386 kPa. The dew-point temperature of the air at system pressure is reduced from 11.2 to –61°C by the adsorption process. During the 270-second period of purging, about a third of the dry air leaving one bed is directed to the other bed as a downward-flowing purge to regenerate the adsorbent. The purge is exhausted at a pressure of 141.3 kPa. By conducting the purge flow countercurrent to the entering air flow, the highest degree of water-vapor desorption is achieved.

Other equipment, shown in Figure 15.2, includes an air compressor; an aftercooler; piping and valving to switch the beds from one step in the cycle to the other; a coalescing filter

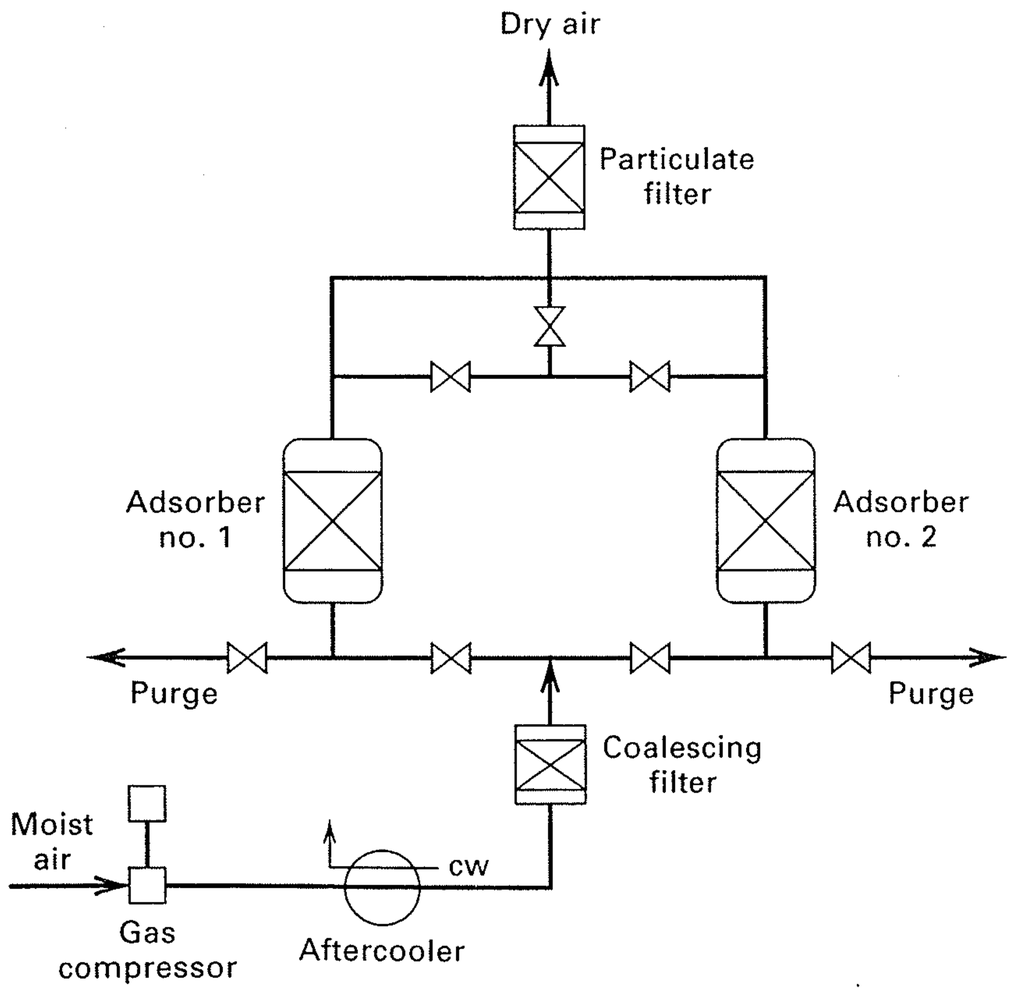

Figure 15.2 Pressure-swing adsorption for the dehydration of air.

Table 15.1 Industrial Applications of Sorption Operations

1. Adsorption
   - Gas purifications:
     - Removal of organics from vent streams
     - Removal of SO_2 from vent streams
     - Removal of sulfur compounds from gas streams
     - Removal of water vapor from air and other gas streams
     - Removal of solvents and odors from air
     - Removal of NO_x from N_2
     - Removal of CO_2 from natural gas
   - Gas bulk separations:
     - N_2/O_2
     - H_2O/ethanol
     - Acetone/vent streams
     - C_2H_4/vent streams
     - Normal paraffins/isoparaffins, aromatics
     - CO, CH_4, CO_2, N_2, A, NH_3/H_2
   - Liquid purifications:
     - Removal of H_2O from organic solutions
     - Removal of organics from H_2O
     - Removal of sulfur compounds from organic solutions
     - Decolorization of solutions
   - Liquid bulk separations:
     - Normal paraffins/isoparaffins
     - Normal paraffins/olefins
     - *p*-xylene/other C_8 aromatics
     - *p*- or *m*-cymene/other cymene isomers
     - *p*- or *m*-cresol/other cresol isomers
     - Fructose/dextrose, polysaccharides
2. Ion Exchange
   - Water softening
   - Water demineralization
   - Water dealkalization
   - Decolorization of sugar solutions
   - Recovery of uranium from acid leach solutions
   - Recovery of antibiotics from fermentation broths
   - Recovery of vitamins from fermentation broths
3. Chromatography
   - Separation of sugars
   - Separation of perfume ingredients
   - Separation of C_4–C_{10} normal and isoparaffins

to remove aerosols from the entering air; and a particulate filter for the exiting dry air to remove adsorbent fines. If the dry air is needed only at low-to-moderate pressures, an air turbine can be installed to recover energy while reducing the air pressure.

During the 5-min adsorption period of the cycle, the capacity of the adsorbent for water must not be exceeded. In this example, the water content of the air is reduced from 1.27×10^{-3} kg H_2O/kg air to the very low value of 9.95×10^{-7} kg H_2O/kg air. To achieve this exiting water vapor content, only a small fraction of the adsorbent capacity is utilized during the adsorption step, with most of the adsorption occurring in the first 0.2 m of the 1.27-m bed height.

The bulk separation of gas and liquid mixtures by adsorption is an emerging separation operation. Important progress is being made in the development of new and more-selective adsorbents and in more-efficient operation cycles. In addition, attention is being directed to hybrid systems that include membrane and other types of separation steps. Already, the three sorption operations addressed in this chapter have found numerous applications, some of which are listed in Table 15.1, compiled from listings in Rousseau [9]. The applications cover a very wide range of species molecular weight.

This chapter discusses sorbents, including their equilibrium, sieving, transport, and kinetic properties with respect to solutes being removed from solutions; techniques for conducting cyclic operations; and equipment configuration and design. Both equilibrium-stage and rate-based models are developed. Although emphasis is on adsorption, the basic principles of ion exchange and chromatography are also presented. Further descriptions of the three sorption operations are given by Rousseau [9] and Ruthven [10].

15.1 SORBENTS

To be suitable for commercial applications, a sorbent should have (1) high selectivity to enable sharp separations, (2) high capacity to minimize the amount of sorbent needed, (3) favorable kinetic and transport properties for rapid sorption, (4) chemical and thermal stability, including extremely low solubility in the contacting fluid, to preserve the amount of sorbent and its properties, (5) hardness and mechanical strength to prevent crushing and erosion, (6) a free-flowing tendency for ease of filling or emptying vessels, (7) high resistance to fouling for long life, (8) no tendency to promote undesirable chemical reactions, (9) the capability of being regenerated when used with commercial feedstocks that contain trace quantities of high-molecular-weight species that are strongly sorbed and difficult to desorb, and (10) relatively low cost.

Adsorbents

Most solids are able to adsorb species from gases and liquids. However, only a few have a sufficient selectivity and capacity to make them serious candidates for commercial adsorbents. Of considerable importance is a large specific surface area (area per unit volume), which is achieved by adsorbent manufacturing techniques that result in solids with a microporous structure. By the definition of the International Union of Pure and Applied Chemistry (IUPAC), a micropore is <20 Å, a mesopore is 20–500 Å, and a macropore is >500 Å (50 nm). Typical commercial adsorbents, which may be granules, spheres, cylindrical pellets, flakes, and/or powders of size ranging from 50 μm to 1.2 cm, have specific surface areas from 300 to 1,200 m^2/g. Thus, just a few grams of adsorbent can have a surface area equal to that of a football field (120 × 53.3 yards or 5,350 m^2)! Such a large area is made possible by a particle porosity from 30 to 85 vol% with average pore diameters from 10 to 200 Å. To quantify this, consider a cylindrical pore of diameter d_p and length L. The surface area-to-volume ratio is

$$S/V = \pi d_p L/(\pi d_p^2 L/4) = 4/d_p \qquad (15\text{-}1)$$

If the fractional particle porosity is ϵ_p and the particle density is ρ_p, the specific surface area, S_g, in area per unit mass of adsorbent is

$$S_g = 4\epsilon_p/\rho_p d_p \qquad (15\text{-}2)$$

Thus, if ϵ_p is 0.5, ρ_p is 1 g/cm^3 = 1×10^6 g/m^3, and d_p is 20 Å (20×10^{-10} m), substitution into (15-2) gives S_g = 1,000 m^2/g, a desirable value.

Depending upon the type of forces between the fluid molecules and the molecules of the solid, adsorption may be classified as *physical adsorption* (van der Waals adsorption) or *chemisorption* (activated adsorption). Physical adsorption from a gas occurs when the intermolecular attractive forces between molecules of a solid and the gas are greater than those between molecules of the gas itself. In effect, the resulting adsorption is like condensation, which is exothermic and thus is accompanied by a release of heat. The magnitude of the heat of adsorption can be less than or greater than the heat of vaporization, and changes with the extent of adsorption. Physical adsorption, which may be a monomolecular (unimolecular) layer, or may be two, three or more layers thick (multimolecular), occurs rapidly. If unimolecular, it is reversible; if multimolecular, such that capillary pores are filled, hysteresis may occur. The density of the adsorbate is of the order of magnitude of the liquid rather than the vapor state. As physical adsorption takes place, it begins as a monolayer, becomes multilayered, and then, if the pores are close to the size of the molecules, capillary condensation occurs, and the pores fill with adsorbate. Accordingly, the maximum capacity of a porous adsorbent can be more related to the pore volume than to the surface area. However, for gases at temperatures above their critical temperature, adsorption is confined to a monolayer.

In contrast, chemisorption involves the formation of chemical bonds between the adsorbent and adsorbate in a monolayer, often with a release of heat much larger than the heat of vaporization. Chemisorption from a gas generally takes place only at temperatures greater than 200°C and may be slow and irreversible. Commercial adsorbents rely on physical adsorption; catalysis relies on chemisorption.

Adsorption from a liquid is a more difficult phenomenon to measure experimentally or describe. When the fluid is a gas, experiments are conducted with pure gases or with mixtures. The amount of gas adsorbed in a confined space is determined from the measured decrease in total pressure. When the fluid is a liquid, no simple procedure for determining the extent of adsorption from a pure liquid exists; consequently, experiments are only conducted using liquid mixtures, including dilute solutions. When porous particles of adsorbent are immersed in a liquid mixture, the pores, if sufficiently larger in diameter than the molecules in the liquid, fill with liquid. At equilibrium, because of differences in the extent of physical adsorption among the different molecules of the liquid mixture, the composition of the liquid in the pores differs from that of the bulk liquid surrounding the adsorbent particles. The observed exothermic heat effect is referred to as the *heat of wetting,* which is much smaller than the heat of adsorption from the gas phase. As with gases, the extent of equilibrium adsorption of a given solute increases with concentration and decreases with temperature. Chemisorption can also occur with liquids.

Listed in Table 15.2 are six major types of solid adsorbents in use. Included are the nature of the adsorbent and representative values of the mean pore diameter, d_p; particle porosity (internal void fraction), ϵ_p; particle density, ρ_p; and specific surface area, S_g. In addition, for some adsorbents, the capacity for adsorbing water vapor at a partial pressure of 4.6 mmHg in air at 25°C is listed, as taken from Rousseau [9]. Not included is the specific pore volume, V_p, which can be computed from the other properties by

$$V_p = \epsilon_p / \rho_p \tag{15-3}$$

Also not included in Table 15.2, but of interest when the adsorbent is used in fixed beds, are the bulk density, ρ_b, and the bed porosity (external porosity), ϵ_b, which are related:

$$\epsilon_b = 1 - \frac{\rho_b}{\rho_p} \tag{15-4}$$

In addition, the true solid density (also called the crystalline density), ρ_s, can be computed from a similar expression:

$$\epsilon_p = 1 - \frac{\rho_p}{\rho_s} \tag{15-5}$$

The specific surface area of an adsorbent, S_g, is measured by adsorbing gaseous nitrogen, using the well-accepted BET method (Brunauer, Emmett, and Teller [11]). Typically, the BET apparatus operates at the normal boiling point of N_2 (–195.8°C) by measuring the equilibrium volume of pure N_2 physically adsorbed on several grams of the adsorbent at a number of different values of the total pressure in the vacuum range of 5 to at least 250 mmHg. Brunauer, Emmett, and Teller derived a theoretical equation to model the adsorption by allowing for the formation of multimolecular layers. Furthermore, they assumed that the heat of adsorption during monolayer formation (ΔH_{ads}) is constant and that the heat effect associated with subsequent layers is equal to the heat of condensation (ΔH_{cond}). The BET equation is

$$\frac{P}{v(P_0 - P)} = \frac{1}{v_m c} + \frac{(c-1)}{v_m c}\left(\frac{P}{P_0}\right) \tag{15-6}$$

where

P = total pressure

P_0 = vapor pressure of adsorbate at test temperature

v = volume of gas adsorbed at STP (0°C, 760 mmHg)

Table 15.2 Representative Properties of Commercial Porous Adsorbents

Adsorbent	Nature	Pore Diameter d_p, Å	Particle Porosity, ϵ_p	Particle Density ρ_p, g/cm^3	Surface Area S_g, m^2/g	Capacity for H_2O Vapor at 25°C and 4.6 mmHg, wt% (Dry Basis)
Activated alumina	Hydrophilic, amorphous	10–75	0.50	1.25	320	7
Silica gel:	Hydrophilic/					
Small pore	hydrophobic,	22–26	0.47	1.09	750–850	11
Large pore	amorphous	100–150	0.71	0.62	300–350	—
Activated carbon:	Hydrophobic,					
Small pore	amorphous	10–25	0.4–0.6	0.5–0.9	400–1200	1
Large pore		>30	—	0.6–0.8	200–600	—
Molecular-sieve carbon	Hydrophobic	2–10	—	0.98	400	—
Molecular-sieve zeolites	Polar-hydrophilic, crystalline	3–10	0.2–0.5	1.4	600–700	20–25
Polymeric adsorbents	—	40–25	0.4–0.55	—	80–700	—

v_m = volume of monomolecular layer of gas adsorbed at STP

c = constant related to the heat of adsorption $\approx \exp[(\Delta H_{\text{cond}} - \Delta H_{\text{ads}})/RT]$

Experimental data for v as a function of P are plotted, according to (15-6), as $P/[v(P_0 - P)]$ versus P/P_0, from which v_m and c are determined from the slope and intercept of the best straight-line fit of the data. The value of S_g is then computed from

$$S_g = \frac{\alpha v_m N_{\text{A}}}{V} \tag{15-7}$$

where

N_{A} = Avogadro's number = 6.023×10^{23} molecules/mol

V = Volume of gas per mole at STP conditions (0°C, 1 atm) = 22,400 cm^3/mol

The quantity α is the surface area covered per adsorbed molecule. If we assume spherical molecules arranged in close two-dimensional packing, the projected surface area is:

$$\alpha = 1.091 \left(\frac{M}{N_A \rho_L} \right)^{2/3} \tag{15-8}$$

where

M = molecular weight of the adsorbate

ρ_L = density of the adsorbate in g/cm^3, taken as the liquid at the test temperature

Although the BET surface area may not always represent the surface area available for adsorption of a particular molecule, the BET test is reproducible and widely used in the characterization of adsorbents.

The specific pore volume, typically cm^3 of pore volume/g of adsorbent, is determined for a small mass of adsorbent, m_p, by measuring the volumes of helium, V_{He}, and mercury, V_{Hg}, displaced by the adsorbent. The helium is not adsorbed, but fills the pores. At ambient pressure, the mercury cannot enter the pores because of unfavorable interfacial tension and contact angle. The specific pore volume, V_p, is then determined from

$$V_p = (V_{\text{Hg}} - V_{\text{He}})/m_p \tag{15-9}$$

The particle density is obtained from

$$\rho_p = \frac{m_p}{V_{\text{Hg}}} \tag{15-10}$$

The true solid density is obtained from

$$\rho_s = \frac{m_p}{V_{\text{He}}} \tag{15-11}$$

The particle porosity is then obtained from (15-3) or (15-5).

The distribution of pore volume over the range of pore size, which is of great importance in adsorption, is measured by mercury porosimetry for large-diameter pores (>100 Å); by gaseous-nitrogen desorption for pores of 15–250 Å in diameter; and by molecular sieving, using molecules of different diameter, for pores <15 Å in diameter. In mercury porosimetry, the extent of mercury penetration into the pores is measured as a function of applied hydrostatic pressure. A force balance along the axis of a straight pore of circular cross-section for the pressure and the interfacial tension between the mercury and the adsorbent surface gives

$$d_p = -\frac{4\sigma_{\text{I}} \cos \theta}{P} \tag{15-12}$$

where for mercury: σ_{I} = interfacial tension = 0.48 N/m and θ = contact angle = 140°. With these values, (15-12) becomes

$$d_p(\text{Å}) = \frac{21.6 \times 10^5}{P \text{ (psia)}} \tag{15-13}$$

Thus, forcing mercury into a 100-Å-diameter pore requires a very high pressure of 21,600 psia.

The nitrogen desorption method for determining pore-size distribution in the more important 15–250-Å-diameter range is an extension of the BET method described earlier for measuring specific surface area. By increasing the nitrogen pressure above 600 mmHg, the multilayer adsorbed films reach the point where they bridge the pore, resulting in capillary condensation. At $P/P_0 = 1$, the entire pore volume is filled with nitrogen. Then, by reducing the pressure in steps, nitrogen is desorbed selectively, starting with the larger pores. This selectivity occurs because of the effect of pore diameter on the vapor pressure of the condensed phase in the pore, as given by the Kelvin equation:

$$P_p^s = P^s \exp\left(-\frac{4\sigma v_L \cos \theta}{RT d_p} \right) \tag{15-14}$$

where

P_p^s = vapor pressure of liquid in pore

P^s = the normal vapor pressure of liquid on a flat surface

σ = surface tension of liquid in pore

v_L = molar volume of liquid in pore

Thus, the vapor pressure of the condensed phase in the pore is less than its normal vapor pressure for a flat surface. The effect of d_p on P_p^s can be significant. For example, for liquid nitrogen at −195.8°C, P^s = 760 torr, σ = 0.00827 N/m, $\theta = 0$, and v_L = 34.7 cm^3/mol. Equation (15-14) then becomes

$$d_p(\text{Å}) = 17.9/\ln\left(P^s/P_p^s\right) \tag{15-15}$$

From (15-15), for d_p = 30 Å, P_p^s = 418 torr, a reduction in vapor pressure of almost 50%. At 200 Å, the reduction is only about 10%. At 418 torr pressure, only pores less than 30 Å in diameter remain filled with liquid nitrogen. For greater accuracy in applying the Kelvin equation, a correction is needed for the thickness of the adsorbed layer. The use of this correction is discussed in detail by Satterfield [12]. For a monolayer, this thickness for nitrogen is about 0.354 nm, corresponding to a P/P_0 in (15-6) of between 0.05 and 0.10. At $P/P_0 = 0.60$ and 0.90, the adsorbed thicknesses are 0.75 and 1.22 nm, respectively. The correction is applied by subtracting twice the adsorbed thickness from d_p in (15-14) and (15-15).

EXAMPLE 15.1

Using data from Table 15.2, determine the volume fraction of pores in silica gel (small-pore type) filled with adsorbed water vapor when its partial pressure is 4.6 mmHg and the temperature is 25°C. At these conditions, the partial pressure is considerably below the vapor pressure of 23.75 mmHg. In addition, determine whether the amount of water adsorbed is equivalent to more than a monolayer, if the area of an adsorbed water molecule is given by (15-8) and the specific surface area of the silica gel is 830 m^2/g.

SOLUTION

Take 1 g of silica gel particles as a basis. From (15-3) and data in Table 15.2, $V_p = 0.47/1.09 = 0.431$ cm^3/g. Thus, for 1 g, pore volume is 0.431 cm^3. From the capacity value in Table 15.2, amount of adsorbed water $= 0.11/(1 + 0.11) = 0.0991$ g. Assume density of adsorbed water is 1 g/cm^3, volume of adsorbed water $= 0.0991$ cm^3, fraction of pores filled with water $= 0.0991/0.431 = 0.230$, and surface area of 1 g $= 830$ m^2. From (15-8):

$$\alpha = 1.091\left[\frac{18.02}{(6.023 \times 10^{23})(1.0)}\right]^{2/3} = 10.51 \times 10^{-16}\ cm^2/\text{molecule}$$

Number of water molecules adsorbed $= \frac{(0.0991)(6.023\times10^{23})}{18.02} = 3.31 \times 10^{21}$ molecules

Number of water molecules in a monolayer for 830 $m^2 = \frac{830(100)^2}{10.51\times10^{-16}} = 7.90 \times 10^{21}$

Therefore, only 3.31/7.90 or 42% of one monolayer is adsorbed.

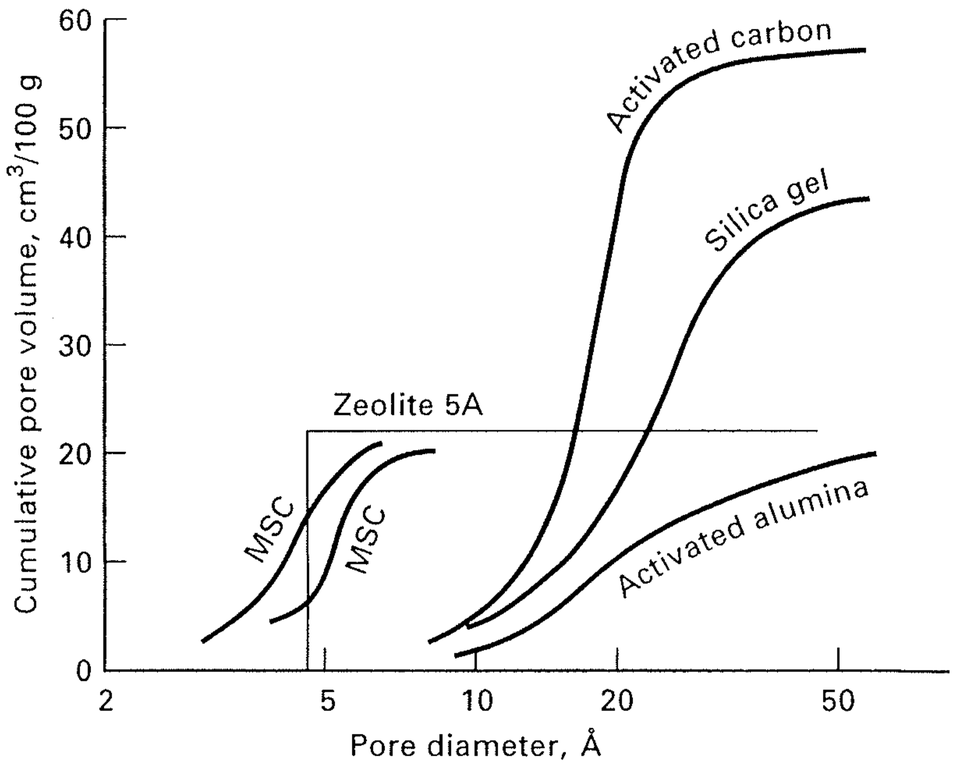

Figure 15.3 Representative cumulative pore-size distributions of adsorbents.

The four most widely used adsorbents in decreasing order of commercial usage are carbon (activated and molecular-sieve), molecular-sieve zeolites, silica gel, and activated alumina. In Table 15.2, activated alumina, Al_2O_3, which includes activated bauxite, is made by removing water from hydrated colloidal alumina. Activated alumina has a moderately high specific surface area, with a capacity for adsorption of water sufficient to dry gases to less than 1 ppm moisture content. Because of its great affinity for water, activated alumina is widely used for the removal of water from gases and liquids.

Silica gel, SiO_2, which is made from colloidal silica, has a high surface area and high affinity for water and other polar compounds. Related silicate adsorbents include magnesium silicate, calcium silicate, various clays, Fuller's earth, and diatomaceous earth. Silica gel is also highly desirable for water removal. Both small-pore and large-pore types are available.

Activated carbon is made by processes that involve the partial oxidation of a number of materials, including coconut shells, fruit nuts, wood, coal, lignite, peat, petroleum residues, and bones. Because activated carbon is hydrophobic and has a high specific surface area, it is particularly useful for processes involving nonpolar and weakly polar organic molecules. Macropores within the carbon particles help transfer molecules to the micropores. Two commercial grades are produced, one with large pores for liquid applications and one with small pores for gas adsorption. As shown in Table 15.2, activated carbon is relatively hydrophobic and has a large surface area. Accordingly, it has found wide application for the purification and separation of gas and liquid mixtures containing nonpolar and weakly polar organic compounds, which adsorb much more strongly than water. In addition, the bonding strength of adsorption on activated carbon is low, resulting in a low heat of adsorption and ease of regeneration of the adsorbent.

Unlike activated carbon, which typically has pore diameters starting from 10 Å, molecular-sieve carbon (MSC) has much smaller pores ranging from 2 to 10 Å, making it possible to separate N_2 from air. The small pores, in one process, are made by depositing coke in the pore mouths of activated carbon.

Most commercial adsorbents have a range of pore sizes, as shown in Figure 15.3, where the cumulative pore volume is plotted against pore diameter. Exceptions are the molecular-sieve zeolites, which are crystalline, inorganic polymers of aluminosilicates and alkali or alkali-earth cation elements, such as Na, K, Mg, and Ca, with the general stoichiometric, unit-cell formula

$$M_{x/m}[(AlO_2)_x(SiO_2)_y]z\,H_2O$$

where M is the cation with valence m, z is the number of water molecules in each unit cell, and x and y are integers such that $y/x \geq 1$. The cations balance the charge of the AlO_2 groups, each having a net charge of -1. To activate the zeolite, the water molecules are removed by raising the temperature or pulling a vacuum. This leaves the remaining atoms spatially intact in interconnected, cagelike structures with six identical window apertures each, the size of which ranges from 3.8 to about 10 Å, depending on the cation and the crystal structure. These apertures act as sieves, which permit small molecules to enter the crystal cage, but exclude large molecules. Thus, compared to the other types of adsorbents, molecular-sieve zeolites are highly selective because all apertures have the same size. The properties and applications of five of the most commonly used molecular-sieve

Table 15.3 Properties and Applications of Some Molecular-Sieve Zeolites

Designation	Cation	Unit Cell Formula	Aperture Size, Å	Typical Applications
3A	K^+	$K_{12}[(AlO_2)_{12}(SiO_2)_{12}]$	2.9	Drying of reactive gases
4A	Na^+	$Na_{12}[(AlO_2)_{12}(SiO_2)_{12}]$	3.8	H_2O, CO_2 removal; air separation
5A	Ca^{2+}	$Ca_5Na_2[(AlO_2)_{12}(SiO_2)_{12}]$	4.4	Separation of air; separation of linear paraffins
10X	Ca^{2+}	$Ca_{43}[(AlO_2)_{86}(SiO_2)_{106}]$	8.0	Separation of air; removal of mercaptans
13X	Na^+	$Na_{86}[(AlO_2)_{86}(SiO_2)_{86}]$	8.4	

zeolites are given in Table 15.3, taken from Ruthven [13]. The zeolites separate not only by molecular size and shape, but also by polarity. Thus, they can also separate molecules of similar size. Some zeolites have circular apertures, whereas others have elliptical apertures. Adsorption in zeolites is actually a selective and reversible filling of crystal cages, so surface area is not a pertinent factor. Although naturally occurring zeolite minerals have been known for more than 200 years, molecular-sieve zeolites were first synthesized by Milton [2], who used very reactive materials at temperatures of 25–100°C.

The structure of the unit cell of a type A zeolite is shown in Figure 15.4a as a three-dimensional structure of silica and alumina tetrahedra, each formed by four oxygen atoms surrounding a silicon or aluminum atom. Oxygen and silicon atoms have two negative and four positive charges, respectively, causing the tetrahedra to build uniformly in four directions. Aluminum, with a valence of 3, causes the alumina tetrahedron to be negatively charged. The added cation provides the balance. In Figure 15.4a, an octahedron of tetrahedra is evident with six faces, with one near-circular window aperture at each face. A type X zeolite is shown in Figure 15.4b. This unit-cell structure results in a larger window aperture. Monographs by Barrer [14] and Breck [15] cover many important aspects of zeolites.

Of lesser commercial importance are polymeric adsorbents. Typically, they are spherical beads, 0.5 mm in diameter, made from microspheres about 10^{-4} mm in diameter. They are produced by polymerizing styrene and divinylbenzene for adsorbing nonpolar organics from aqueous solutions, and by polymerizing acrylic esters for adsorbing polar solutes. They are regenerated by leaching with organic solvents.

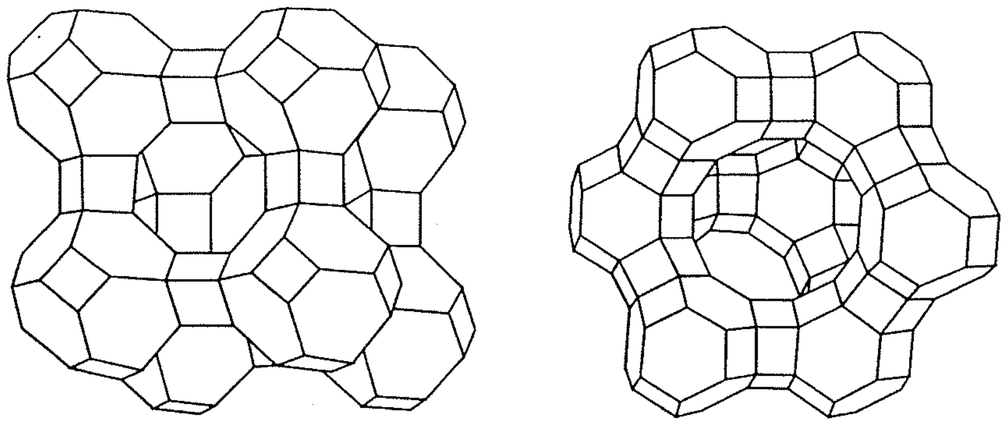

Figure 15.4 Line structures of molecular-sieve zeolites: (a) Type A unit cell. (b) Type X unit cell.

Ion Exchangers

The first ion exchangers were naturally occurring inorganic aluminosilicates (zeolites), used in experiments in the 1850s to exchange between ammonium ions in fertilizers and calcium ions in soils. Industrial water softeners using zeolites were introduced about 1910. However, the zeolites were unstable in the presence of mineral acids. The instability problem was solved by Adams and Holmes [16] in 1935, when they synthesized the first organic-polymer, ion-exchange resins by the polycondensation of phenol and aldehydes. Depending upon the nature of the phenolic group, the resin contains either sulfonic ($-SO_3^-$) or amine ($-NH_3^+$) groups, used for the reversible exchange of cations or anions. Today, the most widely used ion exchangers are synthetic, organic-polymer resins based on styrene- or acrylic-acid-type monomers, as described by D'Alelio in U.S. Patent 2,366,007 (Dec. 26, 1944).

Ion-exchange resins are generally solid gels in spherical or granular form, which consist of (1) a three-dimensional polymeric network, (2) ionic functional groups attached to the network, (3) counterions, and (4) a solvent. Strong-acid, cation-exchange resins and strong-base, anion-exchange resins that are fully ionized over the entire pH range are based on the copolymerization of styrene and a cross-linking agent, divinylbenzene, to produce the three-dimensional, cross-linked structure shown in Figure 15.5a. The degree of cross-linking is governed by the ratio of divinylbenzene to styrene. Weakly acid, cation exchangers are sometimes based on the copolymerization of acrylic acid and methacrylic acid, as shown in Figure 15.5b. These two cross-linked copolymers swell in the presence of organic solvents and have no ion-exchange properties.

To convert the copolymers to water-swellable gels with ion-exchange properties, ionic functional groups are added to the polymeric network by reacting the copolymers with various chemicals. For example, if the styrene–divinylbenzene copolymer is sulfonated, as shown in Figure 15.6a, a cation-exchange resin, as shown in Figure 15.6b, is obtained with ($-SO_3^-$) groups permanently attached or fixed to the polymeric network to give a negatively charged matrix and exchangeable, mobile, positive hydrogen ions (cations). The hydrogen ion can be exchanged on an equivalent basis with other cations, such as Na^+, Ca^{2+}, K^+, or Mg^{2+}, to maintain neutrality of the polymer. For example, two H^+ ions are

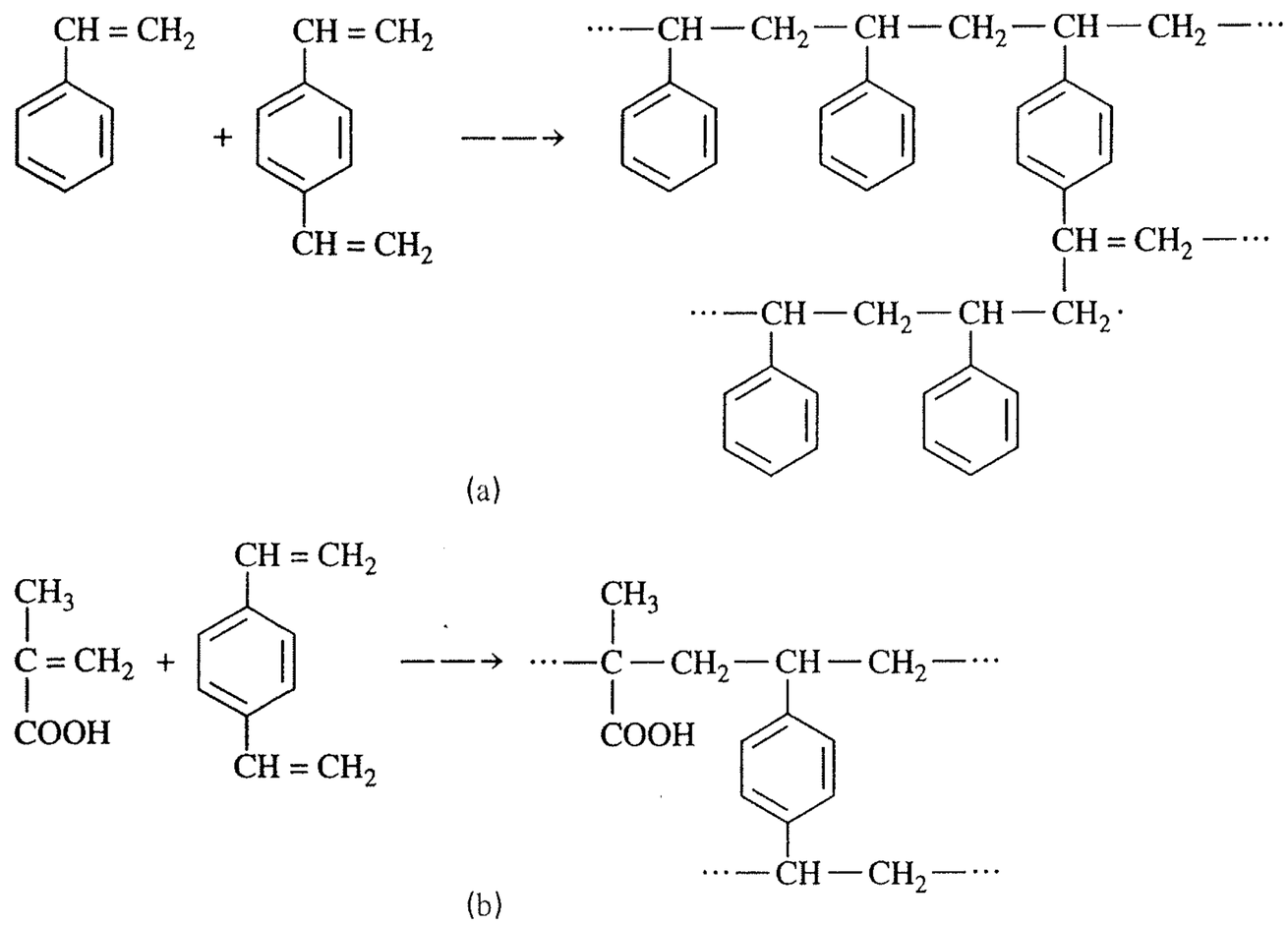

Figure 15.5 Ion-exchange resins: (a) Resin from styrene and divinylbenzene; (b) Resin from acrylic and methacrylic acid.

exchanged for one Ca^{2+} ion. The exchangeable ions are called *counterions.* The liquid whose ions are being exchanged also contains other ions of unlike charge, such as Cl^- for a solution of NaCl, where Na^+ is exchanged. These other ions are called *co-ions.* Often the liquid treated is water, which dissolves to some extent in the resin and causes it to swell. Other solvents, such as methanol, are also soluble in the resin. If the styrene–divinylbenzene copolymer is chloromethylated and then aminated, a strong-base, anion-exchange resin is formed, as shown in Figure 15.6c, which can exchange Cl^- ions for other anions, such as OH^-, HCO_3^-, SO_4^{2-}, and NO_3^-.

Commercial ion exchangers in the hydrogen, sodium, and chloride form are available under the trade names of Amberlite, Duolite, Dowex, Ionac, and Purolite. Typically, they are in the form of spherical beads from about 40 μm

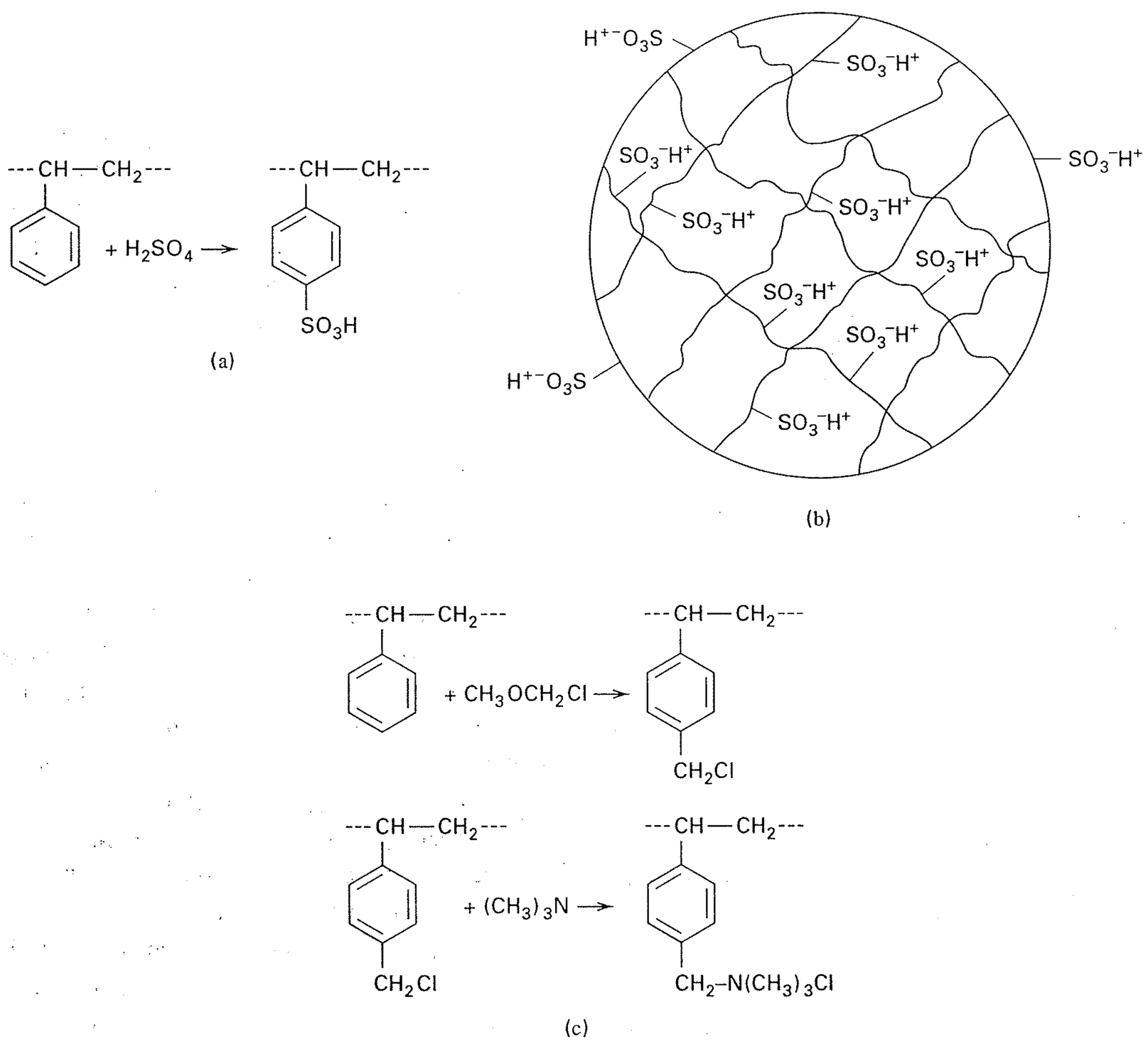

Figure 15.6 Introducing ionic functional groups into resins. (a) Sulfonation to a cation exchanger. (b) Fixed and mobile ions in a cation exchanger. (c) Chloromethylation and amination to an anion exchanger.

to 1.2 mm in diameter. When saturated with water, the beads have typical moisture contents from 40 to 65 wt%. When water-swollen, they have a particle density of 1.1–1.5 g/cm^3. When packed into a bed, they have bulk densities from 0.56 to 0.96 g/cm^3 with fractional bed porosities of 0.35–0.40.

When water is demineralized by ion exchange, potential organic foulants must be removed from the water feed. As discussed by McWilliams [17], this can be accomplished by coagulation, clarification, prechlorination, and the use of ion-exchanger traps.

The maximum ion-exchange capacity of a strong-acid cation or strong-base anion exchanger is stoichiometric, based on the number of equivalents of mobile charge in the resin. Thus, 1 mol H^+ is one equivalent, whereas 1 mol Ca^{2+} is two equivalents. The exchanger capacity is usually quoted as eq/kg of dry resin or eq/L of wet resin. The wet capacity depends on the water content and degree of swelling of a given resin, whereas the dry capacity is fixed. For the copolymer of styrene and divinylbenzene, the maximum capacity is determined on the assumption that each benzene ring in the resin contains one sulfonic-acid group.

EXAMPLE 15.2

A commercial, ion-exchange resin is made from 88 wt% styrene and 12 wt% divinylbenzene. Estimate the maximum ion-exchange capacity in eq/kg resin (same as meq/g resin).

SOLUTION

Basis: 100 g of resin before sulfonation.

	M	g	gmol
Styrene	104.14	88	0.845
Divinylbenzene	130.18	12	0.092
		100	0.937

Therefore, sulfonation at one location on each benzene ring requires 0.937 mol of H_2SO_4 to attach the sulfonic acid group ($M = 81.07$) and split out one water molecule. This is 0.937 equivalents with the addition in weight of 0.937(81.07) = 76 g. Total dry weight of sulfonated resin = 100 + 76 = 176 g maximum ion-exchange capacity, or

$$\frac{0.937}{(176/1{,}000)} = 5.3 \text{ eq/kg(dry)}$$

Depending on the extent of cross-linking, resins from copolymers of styrene and divinylbenzene are listed as having actual capacities of from 3.9 (high degree of cross-linking) to 5.5 (low degree of cross-linking). Although a low degree of cross-linking favors dry capacity, almost every other ion-exchanger property, including wet capacity and selectivity, is improved by cross-linking, as discussed by Dorfner [18].

Sorbents for Chromatography

Sorbents (called *stationary phases*) for chromatographic separations come in a wide variety of forms and chemical compositions because of the many ways in which chromatography is applied. Figure 15.7 shows a classification of analytical chromatographic systems, taken from Sewell and Clarke [19]. The mixture to be separated, after injection into the carrier fluid to form the *mobile phase,* may be a liquid (*liquid chromatography*) or a gas (*gas chromatography*). Often, the mixture is initially a liquid, but is vaporized without decomposition by the carrier gas, giving a gas mixture for the mobile phase. Gas carriers are inert and do not interact with the sorbent or components of the feed. Liquid carriers (solvents) can interact and must be selected carefully.

The stationary sorbent phase is a solid, a liquid supported on or bonded to a solid, or a gel. With a porous-solid adsorbent, the mechanism or mode of separation is adsorption. If an ion-exchange mechanism is desired, a synthetic, polymer-resin ion exchanger is used. With a polymer gel or a microporous solid, a separation based on sieving, called *exclusion,* can be applied. Unique to chromatography are the liquid-supported or liquid-bonded solids, where the mechanism is absorption into the liquid, also referred to as a *partition mode* of separation or *partition chromatography.* With mobile liquid phases, there is a tendency for the stationary liquid phase to be stripped or dissolved. Therefore, methods of chemically bonding the stationary liquid phase to the solid bonding support have been developed.

All sorbents can be used in columns. In packed columns >1 mm inside diameter, the sorbents are in the form of particles. In capillary columns <0.5 mm inside diameter, the sorbent is the inside wall or is a coating on the wall. If the inside wall of the capillary is liquid coated, the capillary column is referred to as a wall-coated, open-tubular (WCOT) column. If the coating is a layer of fine particulate support material to which a liquid adsorbent is added, the column is called a support-coated, open-tubular (SCOT) column. If the wall is coated with a porous adsorbent only, the column is referred to as a porous-layer, open-tubular (PLOT) column.

Each type of sorbent can be applied to sheets of glass, plastic, or aluminum for use in *thin-layer* (or planar) *chromatography* or to a sheet of cellulose material for use in *paper chromatography.* If a pump, rather than gravity, is used to pass a liquid mobile phase through a packed column, the name *high-performance liquid chromatography* (HPLC) is used.

The two most common adsorbents used in chromatography are porous alumina and porous silica gel. Of lesser importance are carbon, magnesium oxide, and various carbonates. Alumina is a polar adsorbent and is preferred for the separation of components that are weakly or moderately polar, with the more polar compounds retained more selectively by the adsorbent and, therefore, eluted from the column last. In addition, alumina is a basic adsorbent, preferentially retaining acidic compounds. Silica gel is less polar than alumina and is an acidic adsorbent, preferentially retaining basic compounds, such as amines. Carbon is a nonpolar (apolar) stationary phase with the highest attraction for larger nonpolar molecules.

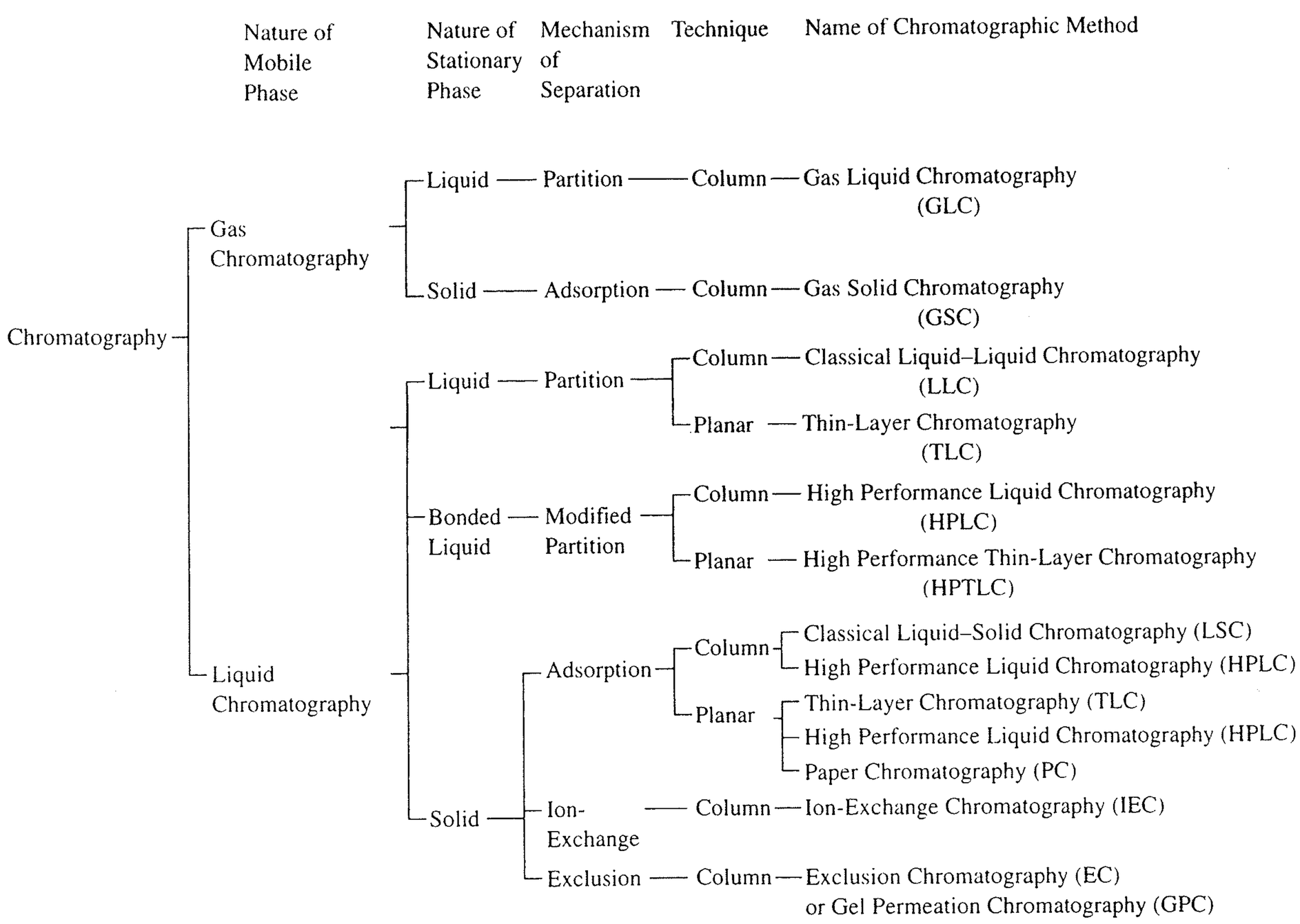

Figure 15.7 Classification of analytical chromatographic systems.
[From P.A. Sewell and B. Clarke, *Chromatographic Separations,* John Wiley and Sons, New York (1987) with permission.]

Adsorbent-type sorbents are better suited for the separation of a mixture on the basis of chemical type (e.g., olefins, esters, acids, aldehydes, alcohols) than for separation of individual members of a homologous series. For the latter, partition chromatography is preferred, wherein an inert-solid support, often silica gel, is coated with a liquid phase. For application to gas chromatography, the liquid must be nonvolatile. For liquid chromatography, the stationary liquid phase must be insoluble in the mobile phase. Since this is difficult to achieve, the stationary liquid phase is usually bonded to the solid support. An example of a bonded phase is the result of reacting silica with a chlorosilane. Both monofunctional and bifunctional silanes are used, as shown in Figure 15.8, where R is a methyl (CH_3) group and R′ is a hydrocarbon chain (C_6, C_8, or C_{18}) where the terminal CH_3 group is replaced with a polar group, such as $-CN$ or $-NH_2$.

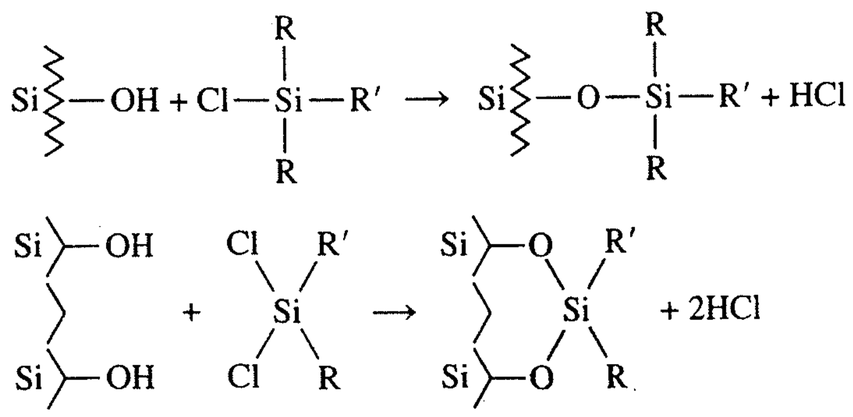

Figure 15.8 Bonded phases from the reaction of surface silanol groups with (a) Monofunctional and (b) Bifunctional chlorosilanes.

If the resulting stationary phase is more polar than the mobile phase, the technique is referred to as *normal-phase chromatography.* Otherwise, the name *reverse-phase chromatography* is used.

In liquid chromatography, the order of elution from the column of the solutes in the mobile phase can also be influenced by the solvent carrier of the mobile phase by matching the solvent polarity with the solutes and using more-polar adsorbents for less-polar solutes and less-polar adsorbents for more-polar solutes.

EXAMPLE 15.3

For the separation of each of the following mixtures, select an appropriate mode of chromatography from Figure 15.7: (a) gas mixture of O_2, CO, CO_2, and SO_2, (b) vaporized mixture of anthracene, phenanthrene, pyrene, and chrysene, and (c) aqueous solution containing Ca^{2+} and Ba^{2+}.

SOLUTION

(a) Use gas–solid chromatography, that is, with a gas mobile phase and a solid-adsorbent stationary phase.

(b) Use partition or gas–liquid chromatography, that is, with a gas mobile phase and a bonded liquid coating on a solid for the stationary phase.

(c) Use ion-exchange chromatography, that is, with a liquid as the mobile phase and polymer resin beads as the stationary phase.

15.2 EQUILIBRIUM CONSIDERATIONS

In adsorption, a dynamic phase equilibrium is established for the distribution of the solute between the fluid and the solid surface. This equilibrium is usually expressed in terms of (1) concentration (if the fluid is a liquid) or partial pressure (if the fluid is a gas) of the adsorbate in the fluid and (2) solute *loading* on the adsorbent, expressed as mass, moles, or volume of adsorbate per unit mass or per unit BET surface area of the adsorbent. Unlike vapor–liquid and liquid–liquid equilibria, where theory is often applied to estimate phase distributions, particularly in the form of K-values for the former type of equilibrium, no acceptable theory has been developed to estimate fluid–solid adsorption equilibria. Thus, it is necessary to obtain experimental equilibrium data for a particular solute, or mixture of solutes and/or solvent, and a sample of the actual solid-adsorbent material of interest. If the data are taken over a range of fluid concentrations at a constant temperature, a plot of solute loading on the adsorbent versus concentration or partial pressure in the fluid, called an *adsorption isotherm,* is made. This equilibrium isotherm places a limit on the extent to which a solute is adsorbed from a given fluid mixture on an adsorbent of given chemical composition and geometry for a given set of conditions. The rate at which the solute is adsorbed is also an important consideration and is discussed in Section 15.3.

Pure Gas Adsorption

For pure gases, experimental physical-adsorption isotherms have shapes, that are classified into five types by Brunauer et al. [20], as shown in Figure 15.9 and discussed in considerable detail by Brunauer [21]. The simplest isotherm is Type I, which corresponds to unimolecular adsorption, as characterized by a maximum limit in the amount adsorbed. This type applies often to gases at temperatures above their critical temperature. The more complex Type II isotherm is associated with multimolecular adsorption of the BET type and is observed for gases at temperatures below their critical temperature and for pressures below, but approaching, the saturation pressure (vapor pressure). The heat of adsorption for the first adsorbed layer is greater than that for the succeeding layers, each of which is assumed to have a heat of adsorption equal to the heat of condensation (vaporization). Both Types I and II are desirable isotherms, exhibiting strong adsorption.

The Type III isotherm in Figure 15.9, with its convex nature, is undesirable because the extent of adsorption is low except at high pressures. According to the BET theory, it corresponds to multimolecular adsorption where the heat of adsorption of the first layer is less than that of succeeding layers. Fortunately, this type of isotherm is rarely observed, an example being the adsorption of iodine vapor on silica gel. In the limit, as the heat of adsorption of the first layer approaches zero, adsorption is delayed until the saturation pressure is approached.

The derivation of the BET equation (15-6) assumes that an infinite number of molecular layers can be adsorbed.

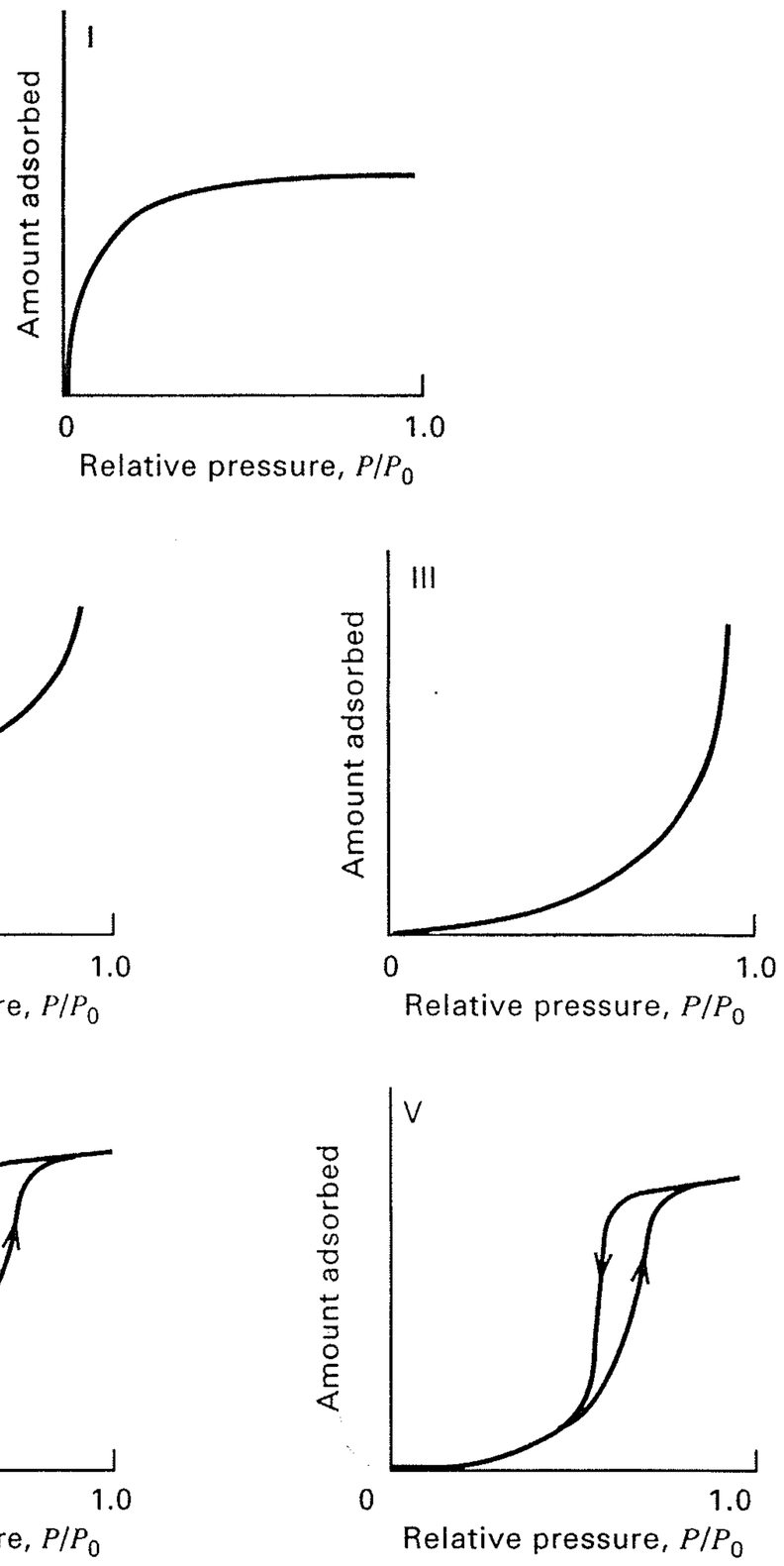

Figure 15.9 Brunauer's five types of adsorption isotherms. (P/P_0 = total pressure/vapor pressure.)

Thus, the equation precludes the possibility of capillary condensation. In a development by Brunauer et al. [20], subsequent to the BET equation, the number of layers is restricted by pore size, and capillary condensation is assumed to occur at a reduced vapor pressure in accordance with the Kelvin equation (15-14). The resulting equation is quite complex, but predicts adsorption isotherms of Types IV and V in Figure 15.9, where we see that the maximum extent of adsorption occurs before the saturation pressure is reached. Type IV is the capillary-condensation version of Type II; Type V is the capillary-condensation version of Type III.

As shown in Figure 15.9, a hysteresis phenomenon can occur in multimolecular adsorption regions for isotherms of types IV and V. The upward adsorption branch of the hysteresis loop is due to simultaneous, multimolecular adsorption and capillary condensation. Only capillary condensation occurs during the downward desorption branch of the loop. Hysteresis can also occur throughout any isotherm when strongly adsorbed impurities are present. Thus, measurements of pure-gas adsorption require adsorbents with clean pore surfaces, normally achieved by preevacuation.

Physical adsorption data of Titoff [22] for ammonia gas on charcoal, as discussed by Brunauer [21], are shown in Figure 15.10. The five adsorption isotherms of Figure 15.10a

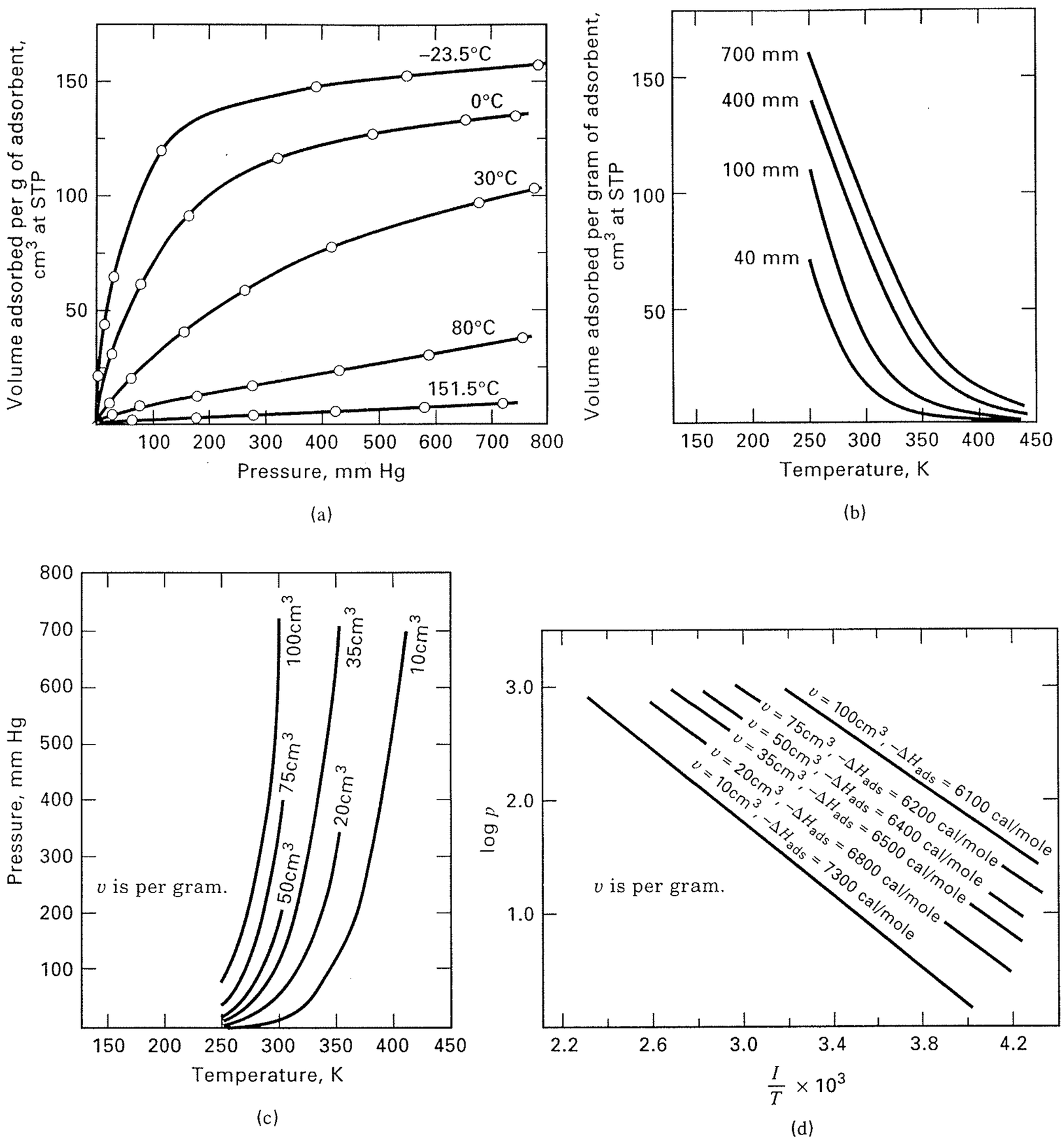

Figure 15.10 Different displays of adsorption equilibrium data for NH_3 on charcoal. (a) Adsorption isotherms. (b) Adsorption isobars. (c) Adsorption isosteres. (d) Isosteric heats of adsorption. [From S. Brunauer, *The Adsorption of Gases and Vapors,* Vol. I, Princeton University Press (1943) with permission.]

cover pressures from vacuum to almost 800 mmHg and temperatures from –23.5 to 151.5°C. For ammonia, the normal boiling point is –33.3°C and the critical temperature is 132.4°C. For the lowest-temperature isotherm, up to 160 cm^3 (STP) of ammonia per gram of charcoal is adsorbed, which is equivalent to 0.12 g NH_3/g charcoal. All five isotherms are of Type I. When the amount adsorbed is low (<25 cm^3/g), the isotherms are almost linear and the following form of Henry's law, called the *linear isotherm,* is obeyed:

$$q = kp \tag{15-16}$$

where q is equilibrium *loading* or amount adsorbed/unit mass of adsorbent (specific amount adsorbed), k is an empirical, temperature-dependent constant, and p is the partial pressure of the component in the gas. As the temperature increases, the amount adsorbed decreases because of Le Chatelier's principle for an exothermic process. This is shown more clearly for the same data in the crossplot of *adsorption isobars* in Figure 15.10b, where absolute temperature is employed. A third method of displaying the experimental data is in the form of *adsorption isosteres,* also obtained by crossplotting, as shown in Figure 15.10c. These curves, representing constant amounts adsorbed, resemble vapor-pressure plots, for which the adsorption form of the Clausius–Clapeyron equation,

$$\frac{d \ln p}{dT} = \frac{-\Delta H_{ads}}{RT^2} \tag{15-17}$$

or

$$\frac{d \log p}{d(1/T)} = \frac{-\Delta H_{ads}}{2.303RT} \tag{15-18}$$

is applied to determine the heat of adsorption; which is negative because the effect is exothermic. The result is shown in Figure 15.10d, where it is seen that $-\Delta H_{ads}$ is initially 7,300 cal/mol, but decreases as the amount adsorbed increases, reaching 6,100 cal/mol at 100 cm^3/g. These values can be compared to the heat of vaporization of NH_3, which at 30°C is 4,600 cal/mol.

Experimental, adsorption-isotherm data for 18 different pure gases and a variety of solid adsorbents are summarized and analyzed by Valenzuela and Myers [23]. The data show

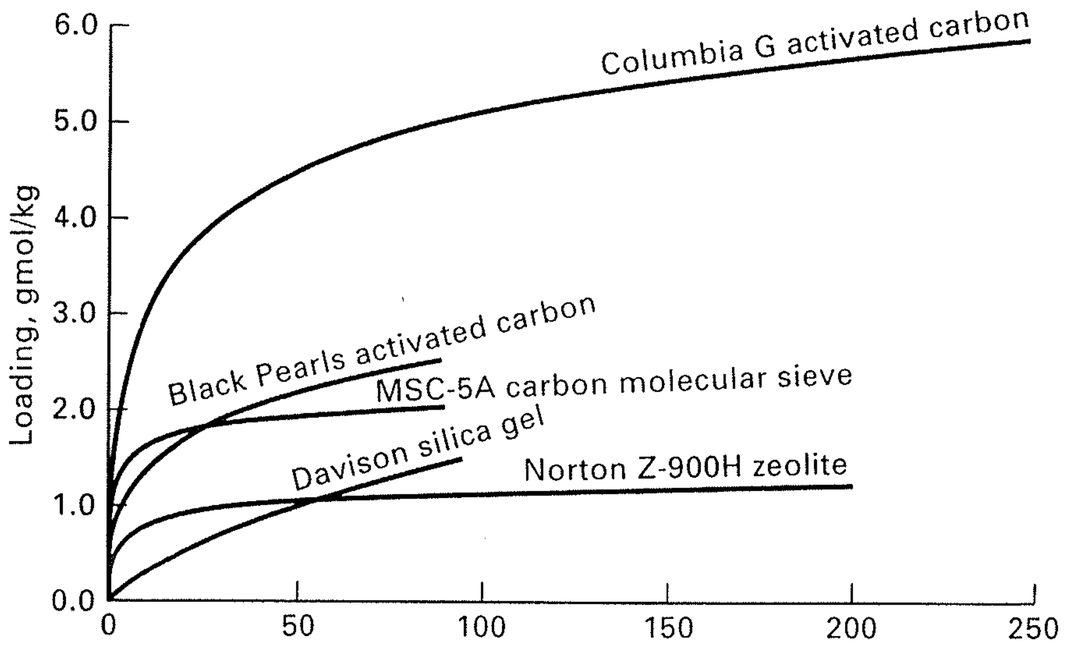

Figure 15.11 Adsorption isotherms for pure propane vapor at 298–303 K.

that adsorption isotherms for a given pure gas at a fixed temperature vary considerably with the adsorbent. This is shown for pure propane vapor in the narrow temperature range of 25–30°C in Figure 15.11 for pressures up to about 101.3 kPa. The highest specific adsorption is with Columbia G-grade activated carbon, while the lowest is with Norton Z-900H, a zeolite molecular sieve. Columbia G-grade activated carbon has about twice the adsorbate capacity of Cabot Black Pearls activated carbon.

The literature data compiled by Valenzuela and Myers [23] also show that for a given adsorbent, the loading depends strongly on the gas. This is illustrated in Table 15.4 for a temperature of 38°C and a narrow pressure range of 97.9 to 100 kPa from the data of Ray and Box [24] for Columbia L activated carbon. Included in the table are normal boiling points and critical temperatures. As might be expected, the species are adsorbed in approximately the inverse order of volatility.

The correlation of experimental adsorption isotherms for pure gases is the subject of a number of published articles and books. As summarized by Yang [25], approaches have ranged from empirical to theoretical. For practical applications, the classical equations of Freundlich and Langmuir are still dominant because of their simplicity and ability to correlate isotherms of Type I in Figure 15.9.

Table 15.4 Comparison of Equilibrium Adsorption of Pure Gases on 20–40 mesh Columbia L Activated Carbon Particles ($S_g = 1{,}152$ m^2/g) at 38°C and ~1 atm

Pure gas	q, mol/kg	T_b, °F	T_c, °F
H_2	0.0241	−423.0	−399.8
N_2	0.292	−320.4	−232.4
CO	0.374	−313.6	−220.0
CH_4	0.870	−258.7	−116.6
CO_2	1.64	−109.3	87.9
C_2H_2	2.67	−119	95.3
C_2H_4	2.88	−154.6	48.6
C_2H_6	3.41	−127.5	90.1
C_3H_6	4.54	−53.9	196.9
C_3H_8	4.34	−43.7	216.0

Freundlich Isotherm

The equation attributed to Freundlich [26], but which was actually devised earlier by Boedecker and van Bemmelen, according to Mantell [27], is empirical and nonlinear in pressure:

$$q = kp^{1/n} \tag{15-19}$$

where k and n are temperature-dependent constants. Generally, n lies in the range of 1 to 5. With $n = 1$, (15-19) reduces to the Henry's law equation (15-16). Experimental q–p isothermal data can be fitted to (15-19) by a nonlinear, curve-fitting computer program or by converting (15-19) to a linear form as follows, and using a graphical method or a linear-regression program:

$$\log q = \log k + (1/n) \log p \tag{15-20}$$

If the graphical method is employed, the data are plotted as $\log q$ versus $\log p$. The best straight line through the data has a slope of $(1/n)$ and an intercept of $\log k$. In general, k decreases with increasing temperature, while n increases with increasing temperature and approaches a value of 1 at high temperatures. Equation (15-19) is derived by assuming a heterogeneous surface with a nonuniform distribution of the heat of adsorption over the surface, as discussed by Brunauer [21].

Langmuir Isotherm

The Langmuir equation [28], which is restricted to Type I isotherms, is derived from simple mass-action kinetics, assuming chemisorption. Assume that the surface of the pores of the adsorbent is homogeneous ($\Delta H_{ads} =$ constant) and that the forces of interaction between adsorbed molecules are negligible. Let θ be the fraction of the surface covered by adsorbed molecules. Therefore, $(1 - \theta)$ is the fraction of the bare surface. Then, the net rate of adsorption is the difference between the rates of adsorption on the bare surface and desorption on the covered surface:

$$dq/dt = k_a p(1 - \theta) - k_d \theta \tag{15-21}$$

At equilibrium, $dq/dt = 0$ and (15-21) reduces to

$$\theta = \frac{Kp}{1 + Kp} \tag{15-22}$$

where K is the adsorption-equilibrium constant ($= k_a/k_d$). Here,

$$\theta = q/q_m \tag{15-23}$$

where q_m is the maximum loading corresponding to complete coverage of the surface by the gas. Thus, the Langmuir adsorption isotherm is restricted to a monomolecular layer. Combining (15-23) with (15-22), we obtain the *Langmuir isotherm:*

$$q = \frac{Kq_m p}{1 + Kp} \tag{15-24}$$

At low pressures, if $Kp \ll 1$, (15-24) reduces to the linear Henry's law form (15-16), while at high pressures where $Kp \gg 1$, $q = q_m$. At intermediate pressures, (15-24) is nonlinear in pressure. Although originally devised by Langmuir for chemisorption, (15-24) has been widely applied to physical adsorption data.

The quantities K and q_m in (15-24) are treated as empirical constants, obtained by fitting the nonlinear equation directly to experimental data or by employing the following linearized form, numerically or graphically:

$$\frac{p}{q} = \frac{1}{q_m K} + \frac{p}{q_m} \tag{15-25}$$

Using (15-25), the best straight line is drawn through a plot of points p/q versus p, giving a slope of $(1/q_m)$ and an intercept of $1/(q_m K)$. If the theory is reasonable, K should change rapidly with temperature, but q_m should not because it is related through v_m by (15-7) to the specific surface area of the adsorbent, S_g. It should be noted that the Langmuir isotherm predicts an asymptotic limit for q at high pressure, whereas the Freundlich isotherm does not.

Other Adsorption Isotherms

Valenzuela and Myers [23] fit pure gas adsorption-isotherm data to the more complex three-parameter isotherms of (1) Toth:

$$q = \frac{mp}{(b + p^t)^{1/t}} \tag{15-26}$$

where m, b, and t are constants for a given adsorbate–adsorbent system and temperature, and (2) Honig and Reyerson (called the UNILAN equation):

$$q = \frac{n}{2s} \ln\left[\frac{c + pe^s}{c + pe^{-s}}\right] \tag{15-27}$$

where n, s, and c are constants for a given adsorbate–adsorbent system and temperature. The Toth and UNILAN isotherms reduce to the Langmuir isotherm for $t = 1$ and $s = 0$, respectively.

EXAMPLE 15.4

The following experimental data for the equilibrium adsorption of pure methane gas on activated carbon (PCB from Calgon Corp.) at 296 K were obtained by Ritter and Yang [*Ind. Eng. Chem. Res.*, **26,** 1679–1686 (1987)]:

q, cm^3 (STP) of CH_4/g carbon	45.5	91.5	113	121	125	126	126
$P = p$, psia	40	165	350	545	760	910	970

Fit the data to: (a) the Freundlich isotherm, and (b) the Langmuir isotherm. Which isotherm provides a better fit to the data?

SOLUTION

By using the linearized forms of the isotherm equations, a spreadsheet or other computer program can be used to do a linear regression to obtain the constants.

(a) Using (15-20), we obtain $\log k = 1.213$, $k = 16.34$, $1/n = 0.3101$, and $n = 3.225$.

Thus, the Freundlich equation is $q = 16.34\, p^{0.3101}$.

(b) Using (15-25), we obtain $1/q_m = 0.007301$, $q_m = 137.0$, $1/(q_m K) = 0.5682$, and $K = 0.01285$.

Thus, the Langmuir equation is $q = \dfrac{1.760p}{1 + 0.01285p}$

The predicted values of q from the two isotherms are as follows:

	q, cm^3 (STP) of CH_4/g carbon		
p, psia	Experimental	Freundlich	Langmuir
40	45.5	51.3	46.5
165	91.5	79.6	93.1
350	113	101	112
545	121	115	120
760	125	128	124
910	126	135	126
970	126	138	127

For this example, the Langmuir isotherm fits the data significantly better than the Freundlich isotherm. Average percent deviations, in q, are computed to be 1.01% and 8.64%, respectively. One reason for the better fit of the Langmuir isotherm is the trend of the data to an asymptotic value for q at the highest pressures.

Gas Mixtures and Extended Isotherms

Commercial applications of physical adsorption involve mixtures rather than pure gases. If the adsorption of all components in the gas except one (A) is negligible, then the adsorption of A is estimated from its pure gas-adsorption isotherm using the partial pressure of A. If the adsorption of two or more components in the mixture is significant, the situation is quite complicated. Experimental data show that one component can increase, decrease, or have no influence on the adsorption of the other, depending on interactions of adsorbed molecules. A simple theoretical treatment is the extension of the Langmuir equation by Markham and Benton [29], who neglect interactions and assume that the only effect is the reduction of the vacant surface area for the adsorption of A because of the adsorption of other components. Consider a binary gas mixture of A and B. Let θ_A = fraction of the surface covered by A and θ_B = fraction of the surface covered by B. Then, $(1 - \theta_A - \theta_B)$ = fraction of vacant surface. At equilibrium:

$$(k_A)_a p_A (1 - \theta_A - \theta_B) = (k_A)_d \theta_A \tag{15-28}$$

$$(k_B)_a p_B (1 - \theta_A - \theta_B) = (k_B)_d \theta_B \tag{15-29}$$

Solving these equations simultaneously, and combining the results with (15-23) for each component, gives

$$q_A = \frac{(q_A)_m K_A p_A}{1 + K_A p_A + K_B p_B} \tag{15-30}$$

$$q_B = \frac{(q_B)_m K_B p_B}{1 + K_A p_A + K_B p_B} \tag{15-31}$$

where $(q_i)_m$ is the maximum amount of adsorption of species i for coverage of the entire surface. Equations (15-30) and (15-31) are readily extended to a multicomponent mixture of j components:

$$q_i = \frac{(q_i)_m K_i p_i}{1 + \sum_j K_j p_j} \tag{15-32}$$

In a similar fashion, as shown by Yon and Turnock [30], the Freundlich equation can be combined with the Langmuir equation to give the following extended relation for gas mixtures:

$$q_i = \frac{(q_i)_0 k_i p_i^{1/n_i}}{1 + \sum_j k_j p_j^{1/n_j}} \tag{15-33}$$

where $(q_i)_0$ is the maximum loading, which may differ from $(q_i)_m$ for a monolayer. Equation (15-33) represents data for nonpolar, multicomponent mixtures in molecular sieves reasonably well. Unfortunately, Broughton [31] has shown that the extended-Langmuir equation lacks thermodynamic consistency; such is also the case for the extended-Langmuir–Freundlich equation. Accordingly, both (15-32) and (15-33) are frequently referred to as nonstoichiometric isotherms. Nevertheless, for practical application, their simplicity often makes them the isotherms of choice. In particular, both the extended Langmuir and Freundlich adsorption isotherms of (15-32) and (15-33) are frequently referred to as *constant-selectivity-equilibrium* equations because they predict a separation factor (selectivity), $\alpha_{i,j}$, for each pair of components, i, j, in a multicomponent mixture that is constant for a given temperature and independent of mixture composition. For example, (15-32) gives

$$\alpha_{i,j} = \frac{q_i/q_j}{p_i/p_j} = \frac{(q_i)_m K_i}{(q_j)_m K_j}$$

As with multicomponent (three or more components) vapor–liquid and liquid–liquid phase equilibria, experimental data for binary and multicomponent gas–solid adsorbent equilibria are scarce and less accurate than corresponding pure gas data. Valenzuela and Myers [23] include experimental data on adsorption of gas mixtures from nine published studies on 29 binary systems, for which pure gas-adsorption isotherms were also obtained. They also describe procedures for applying the Toth and UNILAN equations to multicomponent mixtures based on the ideal-adsorbed-solution (IAS) theory of Myers and Prausnitz [32]. Unlike the extended-Langmuir equation (15-32), which is explicit in the amount adsorbed, the IAS theory, though more accurate, is not explicit and requires an iterative solution procedure. Additional experimental data for higher-order (ternary and/or higher) gas mixtures are given by Miller, Knaebel, and Ikels [33] for 5A molecular sieves and by Ritter and Yang [34] for activated carbon. Yang [25] presents a discussion of existing theories on adsorption of gas mixtures, together with comparisons of these theories with mixture data for activated carbon and zeolites. The data on zeolites are the most difficult to correlate, with the simplified statistical thermodynamic model (SSTM) of Ruthven and Wong [35] giving best results.

EXAMPLE 15.5

The experimental work of Ritter and Yang, cited in Example 15.4, also includes adsorption isotherms for pure CO and CH_4, and a binary mixture of CH_4(A) and CO(B). For the pure gases, Ritter and Yang give relations over a temperature range of 296–480 K, for the two Langmuir constants. At 294 K, these constants are as follows:

	q_m, cm^3(STP)/g	K, psi^{-1}
CH_4	133.4	0.01370
CO	126.1	0.00624

With these constants, use the extended-Langmuir equation to predict the specific adsorption volumes (STP) of CH_4 and CO for a vapor mixture of 69.6 mol% CH_4 and 30.4 mol% CO at 294 K and a total pressure of 364.3 psia. Compare the results with the following experimental data of Ritter and Yang:

Total volume adsorbed, cm^3/(STP)/g	114.1
Mole fractions in adsorbate:	
CH_4	0.867
CO	0.133

SOLUTION

$$p_A = y_A P = 0.696(364.3) = 253.5 \text{ psia}$$
$$p_B = y_B P = 0.304(364.3) = 110.8 \text{ psia}$$

From (15-30):

$$q_A = \frac{133.4(0.0137)(253.5)}{1 + (0.0137)(253.5) + (0.00624)(110.8)} = 89.7 \text{ cm}^3\text{(STP)/g}$$

$$q_B = \frac{126.1(0.00624)(110.8)}{1 + (0.0137)(253.5) + (0.00624)(110.8)} = 16.9 \text{ cm}^3\text{(STP)/g}$$

The total amount adsorbed $= q = q_A + q_B = 89.7 + 16.9 = 106.6$ cm^3(STP)/g, which is 6.6% lower than the experimental value. Estimated mole fractions in the adsorbate are $x_A = q_A/q = 89.7/106.6 = 0.841$ and $x_B = 1 - 0.841 = 0.159$. These adsorbate mole fractions deviate from the experimental values by a mole fraction of 0.026. For this example, the extended-Langmuir isotherm gives reasonable results.

Liquid Adsorption

When porous adsorbent particles are immersed in a pure gas, the pores fill with the gas, and the amount of adsorbed gas is determined by the decrease in total pressure. With a liquid, the pressure does not change, and no simple experimental procedure has been devised for determining the extent of adsorption of a pure liquid. If the liquid is a homogeneous binary mixture, it is customary to designate one component the solute (1) and the other the solvent (2). The assumption is then made that the change in composition of the bulk liquid in contact with the porous solid is due entirely to adsorption

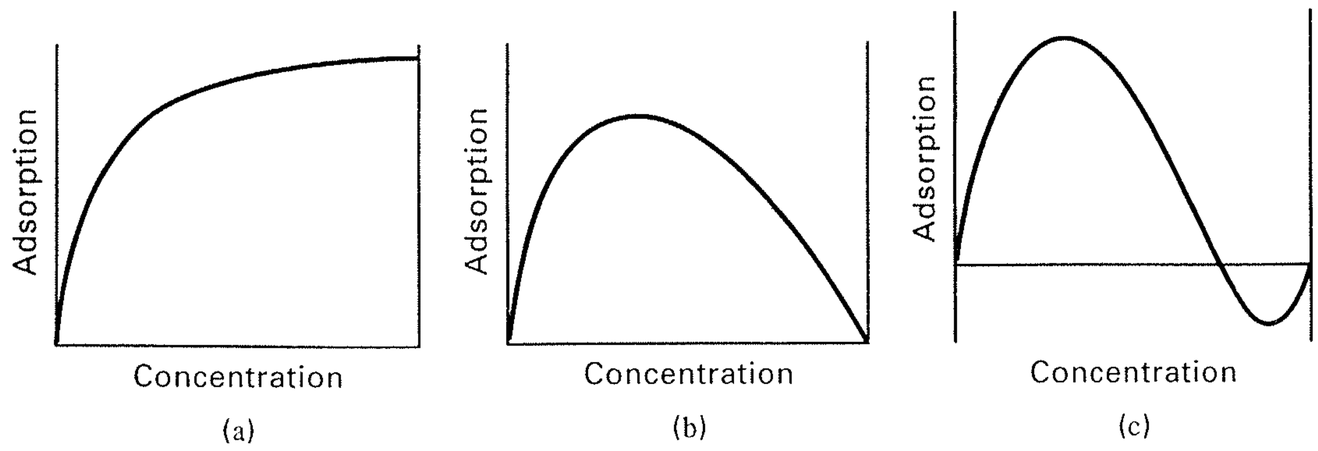

Figure 15.12 Representative isotherms of concentration change for liquid adsorption.

of the solute. That is, adsorption of the solvent is tacitly assumed not to occur. If the liquid mixture is dilute in the solute, the consequences are not serious. If, however, experimental data are obtained over the entire concentration range, the distinction between solute and solvent is arbitrary and the resulting adsorption isotherms, as discussed by Kipling [36], can exhibit curious shapes that are unlike those obtained for pure gases or gas mixtures. To demonstrate this, let

n^0 = total moles of binary liquid brought into contact with adsorbent

m = mass of adsorbent

x_1^0 = mole fraction of solute in the mixture before contact with adsorbent

x_1 = mole fraction of solute in the bulk solution after adsorption equilibrium is achieved

q_1^e = apparent moles of solute adsorbed per unit mass of adsorbent

A solute material balance, assuming no adsorption of solvent and a negligible change in the total moles of liquid mixture, gives

$$q_1^e = \frac{n^0(x_1^0 - x_1)}{m} \tag{15-34}$$

If data are obtained at constant temperature over the entire concentration range and then processed with (15-34) and plotted as adsorption isotherms, the resulting curves are not of the expected type shown in Figure 15.12a. Instead, curves of the type shown in Figures 15.12b and c are obtained, where negative adsorption appears to occur in Figure 15.12c. Such isotherms are probably best referred to as *composite isotherms* or *isotherms of concentration change,* as suggested by Kipling [36]. Likewise, the adsorption loading, q_1^e, of (15-34) is more correctly referred to as the *surface excess.*

Under what conditions are composite isotherms of the form shown in Figures 15.12b and c obtained? This is shown by several examples in Figure 15.13, where various combinations of hypothetical adsorption isotherms for solute (A) and solvent (B) are shown together with the resulting composite isotherms. Thus, when the solvent is not adsorbed, as seen in Figure 15.13a, a composite curve without negative adsorption is obtained. In all other cases of Figure 15.13, negative values of the surface excess are obtained.

Valenzuela and Myers [23] tabulate literature values for the equilibrium adsorption of 25 different binary-liquid mixtures. With one exception, all 25 mixtures give composite isotherms of the forms shown in Figures 15.12b and c. The one exception is a mixture of cyclohexane and *n*-heptane with silica gel, for which the surface excess is almost negligible (0 ± 0.05 mmol/g) over the composition range of $x_1 = 0.041$ to 0.911. They also include literature references to 354 sets of binary-mixture data, 25 sets of ternary-mixture data, and 3 sets of data for higher-order mixtures.

When data for the binary mixture are only available in the dilute region, the amount of adsorption, if any, of the solvent may be constant and all changes in the total amount adsorbed are due to just the solute. In that case, the adsorption isotherms are of the form of Figure 15.12a, which resembles the form obtained with pure gases. It is then common to fit the data with concentration forms of the Freundlich equation

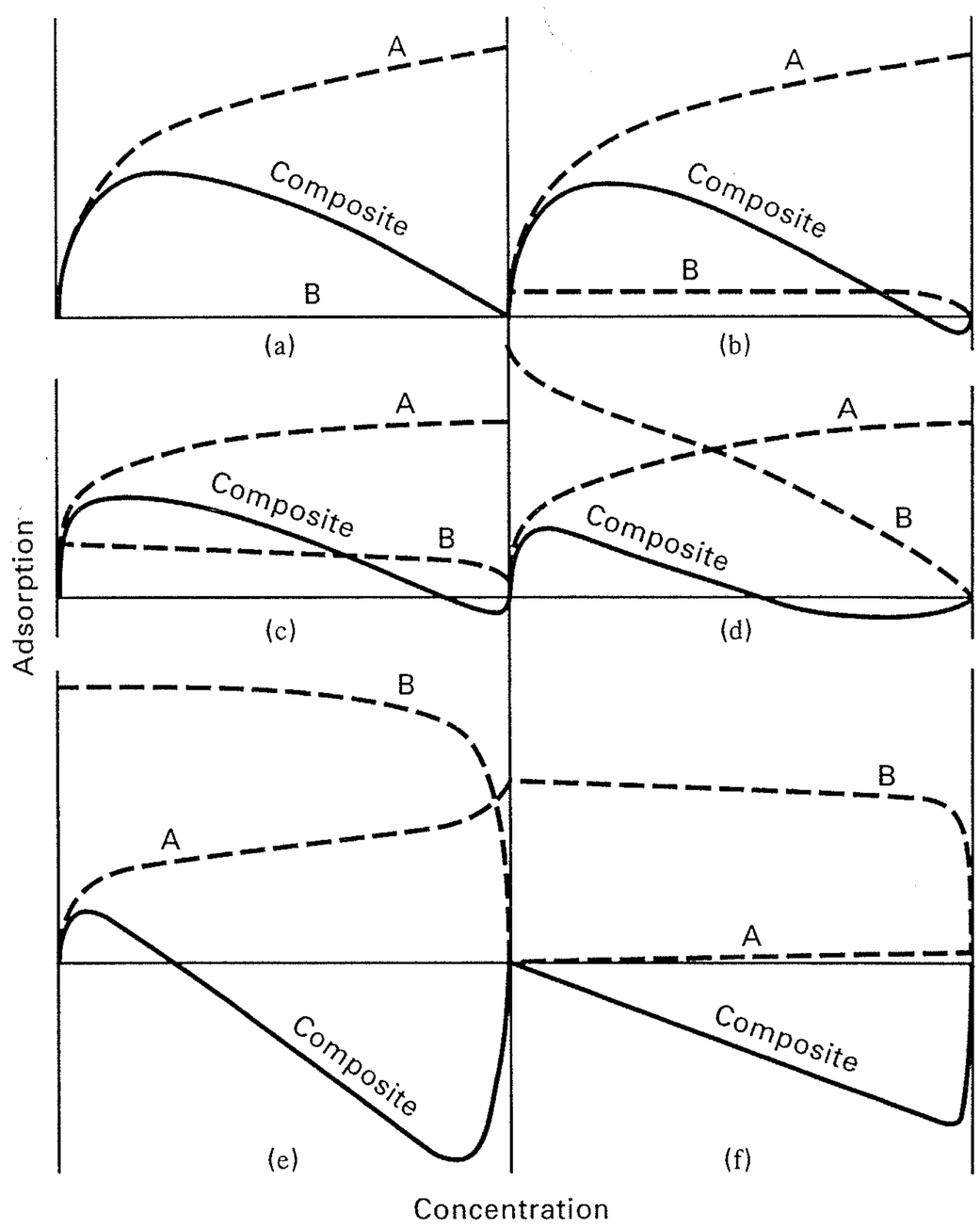

Figure 15.13 Origin of various types of composite isotherms for binary liquid adsorption.

[From J.J. Kipling, *Adsorption from Solutions of Non-electrolytes,* Academic Press, London (1965) with permission.]

(15-19) or the Langmuir equation (15-24):

$$q = kc^{1/n} \tag{15-35}$$

$$q = \frac{Kq_m c}{1 + Kc} \tag{15-36}$$

Candidate systems for this case are small amounts of organic compounds dissolved in water and small amounts of water dissolved in hydrocarbons. For liquid mixtures that are dilute in two or more solutes, the multicomponent adsorption may be estimated from a concentration form of the extended Langmuir equation (15-32) based on the constants, q_m and K, obtained from experiments on the single solutes. However, when solute–solute interactions are suspected, it may be necessary to determine the constants from multicomponent data. As with gas mixtures, the concentration form of (15-32) also predicts a constant selectivity for each pair of components in a multicomponent mixture.

EXAMPLE 15.6

Small amounts of VOCs in water can be removed by adsorption. Generally, two or more VOCs are present. An aqueous stream containing small amounts of acetone (1) and propionitrile (2) is to be treated with activated carbon. Single-solute equilibrium data available from Radke and Prausnitz [37] have been fitted to the Freundlich and Langmuir isotherms, (15-35) and (15-36), with the average deviations indicated, for solute concentrations up to 50 mmol/L:

		Absolute Average Deviation of q, %
Acetone in Water (25°C):		
$q_1 = 0.141c_1^{0.597}$	**(1)**	14.2
$q_1 = \dfrac{0.190c_1}{1 + 0.146c_1}$	**(2)**	27.3
Propionitrile in water (25°C):		
$q_2 = 0.138c_2^{0.658}$	**(3)**	10.2
$q_2 = \dfrac{0.173c_2}{1 + 0.0961c_2}$	**(4)**	26.2

where

q_i = amount of solute adsorbed, mmol/g

c_i = solute concentration in aqueous solution, mmol/L

Use these single-solute results with an extended Langmuir-type isotherm to predict the equilibrium adsorption in a binary-solute aqueous system containing 40 and 34.4 mmol/L, respectively, of acetone and propionitrile at 25°C with the same adsorbent. Compare the results with the following experimental values from Radke and Prausnitz [37]:

$q_1 = 0.715$ mmol/g, $q_2 = 0.822$ mmol/g, and $q_{\text{total}} = 1.537$ mmol/g

SOLUTION

From (15-32), the extended Langmuir isotherm for the liquid phase is

$$q_i = \frac{(q_i)_m K_i c_i}{1 + \sum_j K_j c_j} \tag{5}$$

From (2), $(q_1)_m = 0.190/0.146 = 1.301$ mmol/g.
From (4), $(q_2)_m = 0.173/0.0961 = 1.800$ mmol/g.
From (5):

$$q_1 = \frac{1.301(0.146)(40)}{1 + (0.146)(40) + (0.0961)(34.4)} = 0.749 \text{ mmol/g}$$

$$q_2 = \frac{1.800(0.0961)(34.4)}{1 + (0.146)(40) + (0.0961)(34.4)} = 0.587 \text{ mmol/g}$$

$$q_{\text{total}} = 1.336 \text{ mmol/g}$$

Compared to experimental data, the percent deviations for q_1, q_2, and q_{total}, respectively, are 4.8%, −28.6%, and −13.1%. Better agreement is obtained by Radke and Prausnitz using an IAS theory. It is expected that a concentration form of (15-33) would also give better agreement, but that requires that the single-solute data be refitted for each solute to a Langmuir–Freundlich isotherm of the form

$$q = \frac{q_0 kc^{1/n}}{1 + kc^{1/n}} \tag{6}$$

Ion Exchange Equilibria

Ion exchange differs from adsorption in that one sorbate (a counterion) is exchanged for a solute ion, and the exchange is governed by a reversible, stoichiometric, chemical-reaction equation. Thus, the selectivity of the ion exchanger for one counterion over another may be just as important as the capacity of the ion exchanger. Accordingly, for ion exchange, we apply the law of mass action to obtain an equilibrium ratio rather than fit data to a sorption isotherm such as the Langmuir or Freundlich equation.

As discussed by Anderson [38], two cases are important. In the first case, the counterion initially in the ion exchanger is exchanged with a counterion from an acid or base. For example:

$$\text{Na}^+_{(\text{aq})} + \text{OH}^-_{(\text{aq})} + \text{HR}_{(\text{s})} \leftrightarrow \text{NaR}_{(\text{s})} + \text{H}_2\text{O}_{(l)}$$

Note that the hydrogen ion leaving the ion exchanger immediately reacts with the hydroxyl ion in the aqueous solution to form water, leaving no counterion on the right-hand side of the reaction. Accordingly, the ion exchange will continue until the aqueous solution is depleted of sodium ions or the ion exchanger is depleted of hydrogen ions.

In the second case, which is more common than the first, the counterion being transferred from the ion exchanger to the fluid phase remains as an ion. For example, the exchange of counterions A and B is expressed by the reaction

$$\text{A}^{n\pm}_{(l)} + n\text{BR}_{(\text{s})} \leftrightarrow \text{AR}_{n_{(\text{s})}} + n\text{B}^{\pm}_{(l)} \tag{15-37}$$

where A and B must both be either cations (positive charge) or anions (negative charge). For this case, at equilibrium, we can define a conventional chemical-equilibrium constant according to the law of mass action:

$$K_{\text{A,B}} = \frac{q_{\text{AR}_n} c^n_{\text{B}^\pm}}{q^n_{\text{BR}} c_{\text{A}^{n\pm}}} \tag{15-38}$$

where molar concentrations c_i and q_i refer to the liquid and ion-exchanger phases, respectively. The constant, $K_{\text{A,B}}$ is

not a rigorous thermodynamic equilibrium constant because (15-38) is written in terms of concentrations instead of activities. Although (15-38) could be corrected by including activity coefficients, it is usually applied in the form shown, with $K_{A,B}$ referred to as a *molar selectivity coefficient* for A entering the ion exchange resin and displacing B. For the resin phase, concentrations are in equivalents per unit mass or unit bed volume of ion exchanger. For the liquid solution, concentrations are in equivalents per unit volume of solution. For dilute liquid solutions, $K_{A,B}$ is reasonably constant for a given pair of counterions and a particular resin of a given degree of cross-linking.

When exchange is between two counterions of equal charge, (15-38) can be reduced to a simple equation in terms of just the equilibrium concentrations of A in the liquid solution and in the ion exchange resin. Because of (15-37), the total concentrations C and Q in equivalents of counterions in the liquid solution and the resin, respectively, remain constant during the exchange process. Accordingly:

$$c_i = Cx_i/z_i \tag{15-39}$$

$$q_i = Qy_i/z_i \tag{15-40}$$

where x_i and y_i are equivalent fractions, rather than mole fractions, of A and B, such that

$$x_A + x_B = 1 \tag{15-41}$$

$$y_A + y_B = 1 \tag{15-42}$$

and z_i = valence of counterion i. Combining (15-38) to (15-42) results in

$$K_{A,B} = \frac{y_A(1 - x_A)}{x_A(1 - y_A)} \tag{15-43}$$

Thus, at equilibrium, x_A and y_A are independent of the total equivalent concentrations C and Q. Such is not the case when the two counterions are of unequal charge, as in the exchange of Ca^{2+} and Na^+. A derivation for this general case gives

$$K_{A,B} = \left(\frac{C}{Q}\right)^{n-1} \frac{y_A(1 - x_A)^n}{x_A(1 - y_A)^n} \tag{15-44}$$

For unequal counterion charges, we see that $K_{A,B}$ depends on the ratio C/Q and on the ratio of charges, n.

When experimental data for $K_{A,B}$ for a particular binary system of counterions with a particular ion exchanger are not available, the method of Bonner and Smith [39], as modified by Anderson [38], is used for screening purposes or preliminary calculations. In this method, the molar selectivity coefficient is

$$K_{ij} = K_i/K_j \tag{15-45}$$

where values for relative molar selectivities K_i and K_j are given in Table 15.5 for cations with an 8% cross-linked strong-acid resin and in Table 15.6 for anions with strong-base resins. For values of K in these tables, the units of C and Q are, respectively, eq/L of solution and eq/L of bulk bed volume of water-swelled resin.

A typical cation-exchange resin of the sulfonated styrene–divinylbenzene type, such as Dowex 50, as described by Bauman and Eichhorn [40] and Bauman, Skidmore, and Osmun [41], has an exchangeable ion capacity of 5 ± 0.1 meq/g of dry resin. As shipped, the water-wet resin might contain 41.4 wt% water. Thus, the wet capacity is $5(58.6/100) = 2.9$ meq/g of wet resin. If the bulk density of a drained bed of wet resin is 0.83 g/cm^3, the bed capacity is 2.4 eq/L of resin bed.

As with other separation processes, a separation factor, $S_{A,B}$, which ignores the valence of the exchanging ions, can be defined for an equilibrium stage. For the binary case, in terms of equivalent ionic fractions:

$$S_{A,B} = \frac{y_A(1 - x_A)}{x_A(1 - y_A)} \tag{15-46}$$

which is identical to (15-43). Experimental data for an exchange between Cu^{2+} (A) and Na^+ (B) (counterions of unequal charge) with Dowex 50 cation resin over a wide range of total-solution normality at ambient temperature are shown in terms of y_A and x_A in Figure 15.14, from Subba Rao and David [42]. At low, total-solution concentration, the resin is highly selective for copper ion, whereas at high, total-solution concentration, the selectivity is reversed to favor sodium ion slightly. A similar trend was observed by Selke and Bliss [43, 44] for exchange between Ca^{2+} and H^+ using a similar resin, Amberlite IR-120. This sensitivity of the selectivity is shown dramatically in Figure 15.15, from Myers and Byington [45], where the natural logarithm of the separation factor, S_{Cu^{2+},Na^+}, as computed from the data of Figure 15.14 with (15-46), is plotted as a function of

Table 15.5 Relative Molar Selectivities for Cations with 8% Cross-linked Strong-Acid Resin

Li^+	1.0	Zn^{2+}	3.5
H^+	1.3	Co^{2+}	3.7
Na^+	2.0	Cu^{2+}	3.8
NH_4^+	2.6	Cd^{2+}	3.9
K^+	2.9	Be^{2+}	4.0
Rb^+	3.2	Mn^{2+}	4.1
Cs^+	3.3	Ni^+	3.9
Ag^+	8.5	Ca^{2+}	5.2
UO_2^{2+}	2.5	Sr^{2+}	6.5
Mg^{2+}	3.3	Pb^{2+}	9.9
		Ba^{2+}	11.5

Table 15.6 Approximate Relative Molar Selectivities for Anions with Strong-Base Resins

I^-	8	OH^- (Type II)	0.65
NO_3^-	4	HCO_3^-	0.4
Br^-	3	CH_3COO^-	0.2
HSO_4^-	1.6	F^-	0.1
NO_2^-	1.3	OH^- (Type I)	0.05–0.07
CN^-	1.3	SO_4^{2-}	0.15
Cl^-	1.0	CO_3^{2-}	0.03
BrO_3^-	1.0	HPO_4^{2-}	0.01

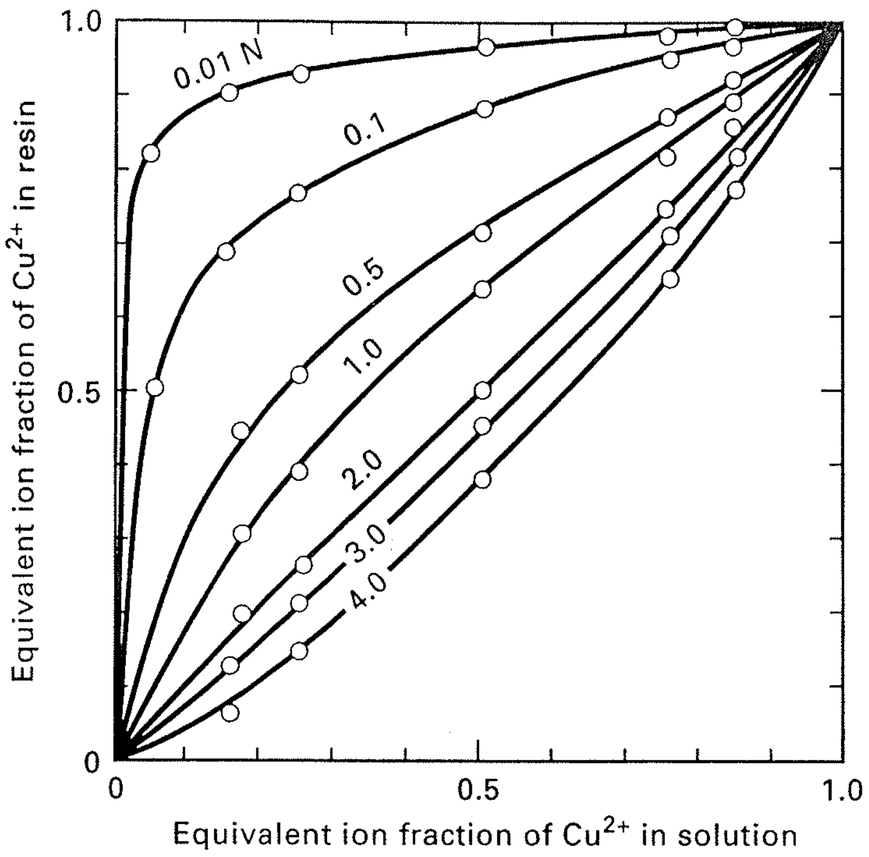

Figure 15.14 Isotherms for ion exchange of Cu^{2+} and Na^{+} on Dowex 50-X8 as a function of total normality in the bulk solution.
[From A.L. Myers and S. Byington, *Ion Exchange Science and Technology,* M. Nijhoff, Boston (1986) with permission.]

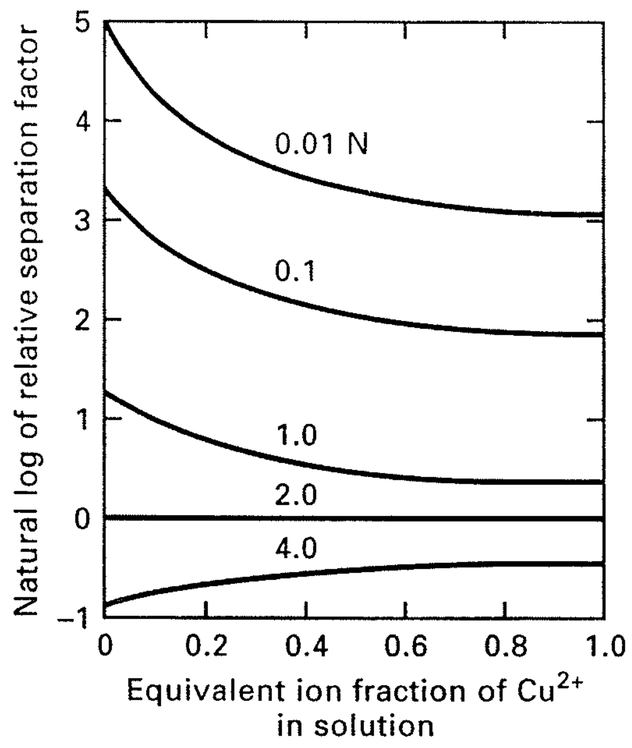

Figure 15.15 Relative separation factor of Cu^{2+} and Na^{+} for ion exchange on Dowex 50-X8 as a function of total normality in the bulk solution.
[From A.L. Myers and S. Byington, *Ion Exchange Science and Technology,* M. Nijhoff, Boston (1986) with permission.]

equivalent ionic fraction, $x_{Cu^{2+}}$. For dilute solutions of Cu^{2+}, $S_{Cu^{2+},Na^{+}}$ ranges from about 0.5 at a total concentration of 4 N to 60 at 0.01 N. In terms of $K_{Cu^{2+},Na^{+}}$ of (15-44), with $n = 2$, the corresponding variation is computed to be only from about 0.6 to 2.2.

EXAMPLE 15.7

An Amberlite IR-120 ion-exchange resin similar to that of Example 15.2, but with a maximum ion-exchange capacity of 4.90 meq/g of dry resin, is used to remove cupric ion from a waste stream containing 0.00975-M $CuSO_4$ (19.5 meq Cu^{2+}/L solution). The spherical resin particles range in diameter from 0.2 to just over 1.2 mm. The equilibrium ion-exchange reaction is of the divalent–monovalent type:

$$Cu^{2+}_{(aq)} + 2HR_{(s)} \leftrightarrow CuR_{2(s)} + 2H^{+}_{(aq)}$$

As ion exchange takes place, the milliequivalents of cations in the aqueous solution and in the resin remain constant.

Experimental measurements by Selke and Bliss [43, 44] show an equilibrium curve of the type of Figure 15.14 at ambient temperature that is markedly dependent on the total equivalent concentration of the aqueous solution, with the following equilibrium data for the cupric ion with a 19.5 meq/liter solution:

c, meq Cu^{2+}/L Solution	0.022	0.786	4.49	10.3
q, meq Cu^{2+}/g Resin	0.66	3.26	4.55	4.65

These data follow a highly nonlinear isotherm.

(a) From the data, compute the molar selectivity coefficient, K, at each value of c for Cu^{2+} and compare it to the value estimated from (15-45) using Table 15.5.

(b) Predict the milliequivalents of Cu^{2+} exchanged at equilibrium from 10 L of 20 meq Cu^{2+}/L using 50 g of dry resin with 4.9 meq of H^{+}/g.

SOLUTION

(a) Selke and Bliss do not give a value for the resin capacity, Q, in eq/L of bed volume. Assume a value of 2.3. From (15-44):

$$K_{Cu^{2+},H^{+}} = \left(\frac{C}{Q}\right)\frac{y_{Cu^{2+}}(1 - x_{Cu^{2+}})^2}{x_{Cu^{2+}}(1 - y_{Cu^{2+}})^2}$$

where $(C/Q) = 0.0195/2.3 = 0.0085$

$$x_{Cu^{2+}} = c_{Cu^{2+}}/19.5 \quad \text{and} \quad y_{Cu^{2+}} = q_{Cu^{2+}}/4.9$$

Using the above values of c and q from Selke and Bliss:

q, meq Cu^{2+}/g	$x_{Cu^{2+}}$	$y_{Cu^{2+}}$	$K_{Cu^{2+},H^{+}}$
0.66	0.00113	0.135	1.35
3.26	0.0403	0.665	1.15
4.55	0.230	0.929	4.04
4.65	0.528	0.949	1.30

The average value of K is 2.0. The values in Table 15.5 when substituted into (15-45) predict

$$K_{Cu^{2+},H^{+}} = 3.8/1.3 = 2.9$$

which is somewhat higher.

(b) Assume a value of 2.0 for $K_{Cu^{2+},H^{+}}$ with $Q = 2.3$ eq/L. The total solution concentration, C, is 0.02 eq/L. Equation (15-44) becomes

$$2.0 = \left(\frac{0.02}{2.3}\right)\frac{y_{Cu^{2+}}(1 - x_{Cu^{2+}})^2}{x_{Cu^{2+}}(1 - y_{Cu^{2+}})^2} \tag{1}$$

Initially, the solution contains $(0.02)(10) = 0.2$ equivalents of cupric ion with $x_{Cu^{2+}} = 1.0$. Let a = equivalents of Cu exchanged. Then, at equilibrium, by material balance:

$$x_{Cu^{2+}} = \frac{0.02 - (a/10)}{0.02} \tag{2}$$

$$y_{Cu^{2+}} = \frac{(a/50)}{0.0049} \tag{3}$$

Substitution of (2) and (3) into (1) gives

$$2.0 = 0.0087 \frac{\left[\dfrac{(a/50)}{0.0049}\right]\left[1 - \dfrac{0.02 - (a/10)}{0.02}\right]^2}{\left[\dfrac{0.02 - (a/10)}{0.02}\right]\left[1 - \dfrac{(a/50)}{0.0049}\right]^2} \tag{4}$$

Solving (4), a nonlinear equation, for a gives 0.1887 equivalents of Cu exchanged. Thus, 0.1887/[(0.020)(10)] = 0.944 or 94.4% of the cupric ion is exchanged.

Equilibria in Chromatography

As discussed in Section 15.1, separation by chromatography involves sorption mechanisms of many types, including adsorption on porous solids, absorption or extraction (partitioning) in liquid-supported or bonded solids, and ion exchange in synthetic resins. Thus, at equilibrium, depending upon the sorption mechanism, equations such as (15-19), (15-24), (15-32), and (15-33) for gas adsorption; (15-35) and (15-36) for liquid adsorption; (6-17) to (6-20) for gas absorption; (8-1) for liquid extraction; and (15-38), (15-43), and (15-44) for ion exchange apply.

When the equilibrium (distribution or partition) constant is defined as

$$K_i = q_i / c_i \tag{15-47}$$

where q is concentration in the stationary phase and c is concentration in the mobile phase, solutes with the highest equilibrium constants will elute from the chromatographic column at a slower rate than solutes with the smallest equilibrium constants.

15.3 KINETIC AND TRANSPORT CONSIDERATIONS

For the adsorption of a solute onto the porous surface of an adsorbent, the following steps are required:

1. External (interphase) mass transfer of the solute from the bulk fluid by convection, through a thin film or boundary layer, to the outer, solid surface of the adsorbent
2. Internal (intraphase) mass transfer of the solute by pore diffusion from the outer surface of the adsorbent to the inner surface of the internal porous structure
3. Surface diffusion along the porous surface
4. Adsorption of the solute onto the porous surface

For chemisorption, which involves bond formation, the rate of the fourth kinetic step may be slow and even controlling; for physical adsorption, however, step 4 is almost instantaneous because it depends only on the collision frequency and orientation of the molecules with the porous surface. Thus, only the first three steps need be considered here.

During regeneration of the adsorbent, the reverse of the four steps occurs, where the rate of physical desorption is instantaneous. Adsorption and desorption are accompanied

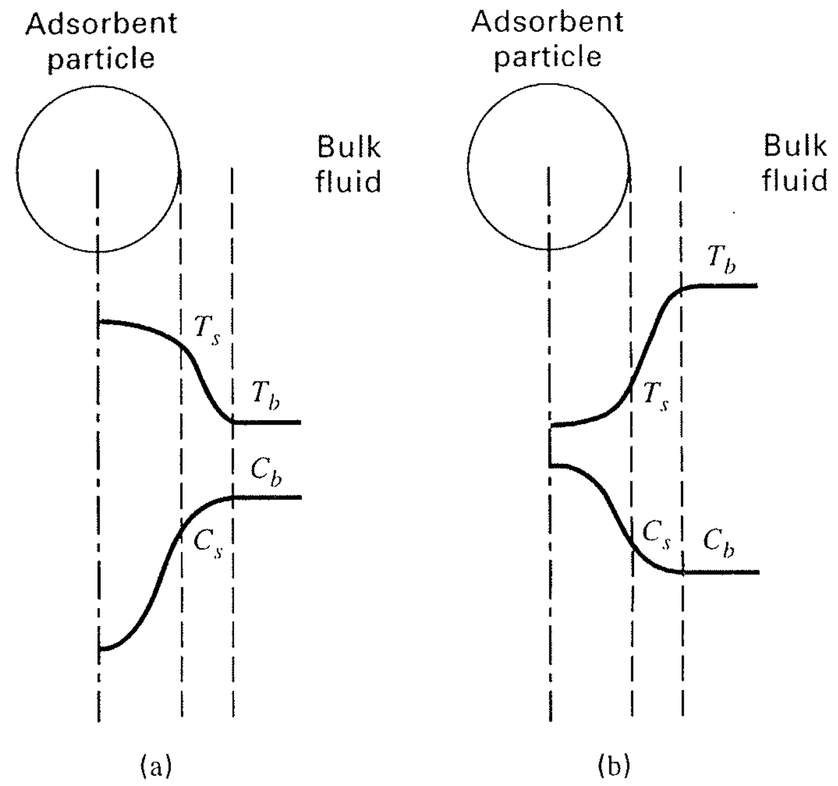

Figure 15.16 Solute concentration and temperature profiles for a porous adsorbent particle surrounded by a fluid: (a) Adsorption. (b) Desorption.

by heat transfer because of the exothermic heat of adsorption and the endothermic heat of desorption. However, although external mass transfer is limited to a convective mechanism, external heat transfer from the particle outer surface occurs not only by convection through the film or boundary layer surrounding each solid particle in the bed, but also by thermal radiation between particles when the fluid is a gas, and by conduction at points of contact by adjacent particles. Conduction and radiation mechanisms for heat transfer can also exist within the particle, in addition to convective heat transfer by the fluid within the pores.

In a fixed bed of adsorbent particles, solute concentration and temperature change continuously with time and location. For a given particle at a particular time, profiles of temperature and solute concentration in the fluid are as shown in Figures 15.16a and b for adsorption and desorption, respectively, where subscripts b and s refer to bulk fluid and particle outer surface, respectively. The fluid concentration gradient is usually steepest within the particle, whereas the temperature gradient is usually steepest in the fluid film or boundary layer surrounding the particle. Thus, although the major resistance to heat transfer is usually external to the adsorbent particle, the major resistance to mass transfer usually resides in the adsorbent particle. All four gradients in Figure 15.16 approach asymptotic values at the end points.

External Transport

Rates of convective mass and heat transfer between the outer surface of a particle and the surrounding bulk fluid during an adsorption process are given, respectively, by

$$n_i = \frac{d\mathcal{N}_i}{dt} = k_c A(c_{b_i} - c_{s_i}) \tag{15-48}$$

$$q = \frac{dQ}{dt} = hA(T_s - T_b) \tag{15-49}$$

For a spherical particle surrounded by an infinite, quiescent fluid, the mass- and heat-transfer coefficients are at their minimum values. Assume an insoluble, solid, spherical particle of radius R_p and diameter $D_p = 2R_p$, suspended in an infinite-fluid medium. The particle is heated so that, at steady state, its surface temperature is constant at T_s. The fluid medium is absolutely quiescent (no free convection) and radiation is ignored so that heat transfer through the fluid is by conduction only. The thermal conductivity k of the fluid is constant, and the temperature far from the particle is T_b. Fourier's second law of heat conduction in the fluid, for spherical coordinates, is

$$\frac{d}{dr}\left(kr^2\frac{dT}{dr}\right) = 0 \tag{15-50}$$

for $r \geq R_p$, where r is the radial distance from the center of the particle. The boundary conditions are

$$T\{r = R_p\} = T_s \tag{15-51}$$

$$T\{r = \infty\} = T_b \tag{15-52}$$

If (15-50) is integrated twice with respect to r, we obtain:

$$T = -\frac{C_1}{r} + C_2 \tag{15-53}$$

Substitution of the boundary conditions, (15-51) and (15-52), results in an expression for the temperature profile in the fluid:

$$\frac{T - T_b}{T_s - T_b} = \frac{R_p}{r}, \quad r \geq R_p \tag{15-54}$$

The heat flux at the outer surface of the particle is given by Fourier's first law of heat conduction applied to the fluid adjacent to the particle:

$$\left.\frac{q}{A}\right|_{r=R_p} = -k\left.\frac{dT}{dr}\right|_{r=R_p} \tag{15-55}$$

From (15-54):

$$\left.\frac{dT}{dr}\right|_{r=R_p} = -\frac{(T_s - T_b)}{R_p} \tag{15-56}$$

We can also apply Newton's law of cooling for the heat flux at the outer surface of the particle:

$$\left.\frac{q}{A}\right|_{r=R_p} = h(T_s - T_b) \tag{15-57}$$

Combining (15-55) to (15-57):

$$h = k/R_p \tag{15-58}$$

which rearranges into a Nusselt number form:

$$N_{\mathrm{Nu}} = hD_p/k = 2 \tag{15-59}$$

A similar development for convective mass transfer using Fick's laws of diffusion gives

$$N_{\mathrm{Sh}_i} = k_{c_i}D_p/D_i = 2 \tag{15-60}$$

where D_i is the diffusivity of component i in the mixture.

When the fluid flows past a single particle, convection increases the convective mass- and heat-transfer coefficients above the values computed from (15-59) and (15-60). Furthermore, the transport coefficients now vary around the periphery of the particle, with the largest value occurring where the fluid flow first impinges on the particle. Correlations of experimental transport data are usually developed for coefficients averaged over the surface of the particle. Typical correlations are those of Ranz and Marshall [46, 47] for Nusselt numbers as high as 30 and Sherwood numbers to 160:

$$N_{\mathrm{Nu}} = 2 + 0.60\,N_{\mathrm{Re}}^{1/2}N_{\mathrm{Pr}}^{1/3} \tag{15-61}$$

$$N_{\mathrm{Sh}_i} = 2 + 0.60\,N_{\mathrm{Re}}^{1/2}N_{\mathrm{Sc}_i}^{1/3} \tag{15-62}$$

where

N_{Pr} = Prandtl number = $C_P\mu/k$

N_{Sc_i} = Schmidt number = $\mu/\rho D_i$

N_{Re} = Reynolds number = D_pG/μ

All fluid properties are evaluated at the average temperature of the film or boundary layer. Equations (15-61) and (15-62) reduce to (15-59) and (15-60), respectively, when the fluid mass velocity, G, is zero.

When particles are packed in a bed, the fluid-flow patterns are restricted, and the single-particle correlations of (15-61) and (15-62) cannot be used to estimate the average external-transport coefficients for the particles in the bed. However, Ranz [48] showed that equations of the same form as (15-61) and (15-62) correlate external-transport data for beds packed with spherical particles. Nevertheless, most early investigators, starting with Gamson, Thodos, and Hougen [49], developed correlations in the form of the Chilton and Colburn [50] j-factors:

$$j_D = (N_{\mathrm{St_M}})(N_{\mathrm{Sc}})^{2/3} = f\{N_{\mathrm{Re}}\} \tag{15-63}$$

$$j_H = (N_{\mathrm{St}})(N_{\mathrm{Pr}})^{2/3} = f\{N_{\mathrm{Re}}\} \tag{15-64}$$

with

$$N_{\mathrm{St_M}} = k_c\rho/G \quad \text{and } N_{\mathrm{St}} = h/C_PG$$

where different Reynolds-number functions apply to different regions. Various forms of the Reynolds number have been used, including D_pG/μ and $D_pG/\epsilon_b\mu$, in attempts to account for bed void fraction, ϵ_b, where G is the superficial mass velocity based on the empty-bed cross-sectional area, and G/ϵ_b (a larger value) is the effective mass velocity through the void region of the bed. Notable among correlations of this type are those of Sen Gupta and Thodos [51], Petrovic and Thodos [52], and Dwivedi and Upadhay [53].

A more-recent study by Wakao and Funazkri [54] reanalyzed 37 sets of previously published mass-transfer data, with Sherwood number corrections for axial dispersion. The resulting correlation, which represents a return to the form of (15-62), is

$$N_{\mathrm{Sh}_i} = \frac{k_{c_i}D_p}{D_i} = 2 + 1.1\left(\frac{D_pG}{\mu}\right)^{0.6}\left(\frac{\mu}{\rho D_i}\right)^{1/3} \tag{15-65}$$

The correlation is compared to 12 sets of gas-phase and 11 sets of liquid-phase data in Figure 15.17. The data cover

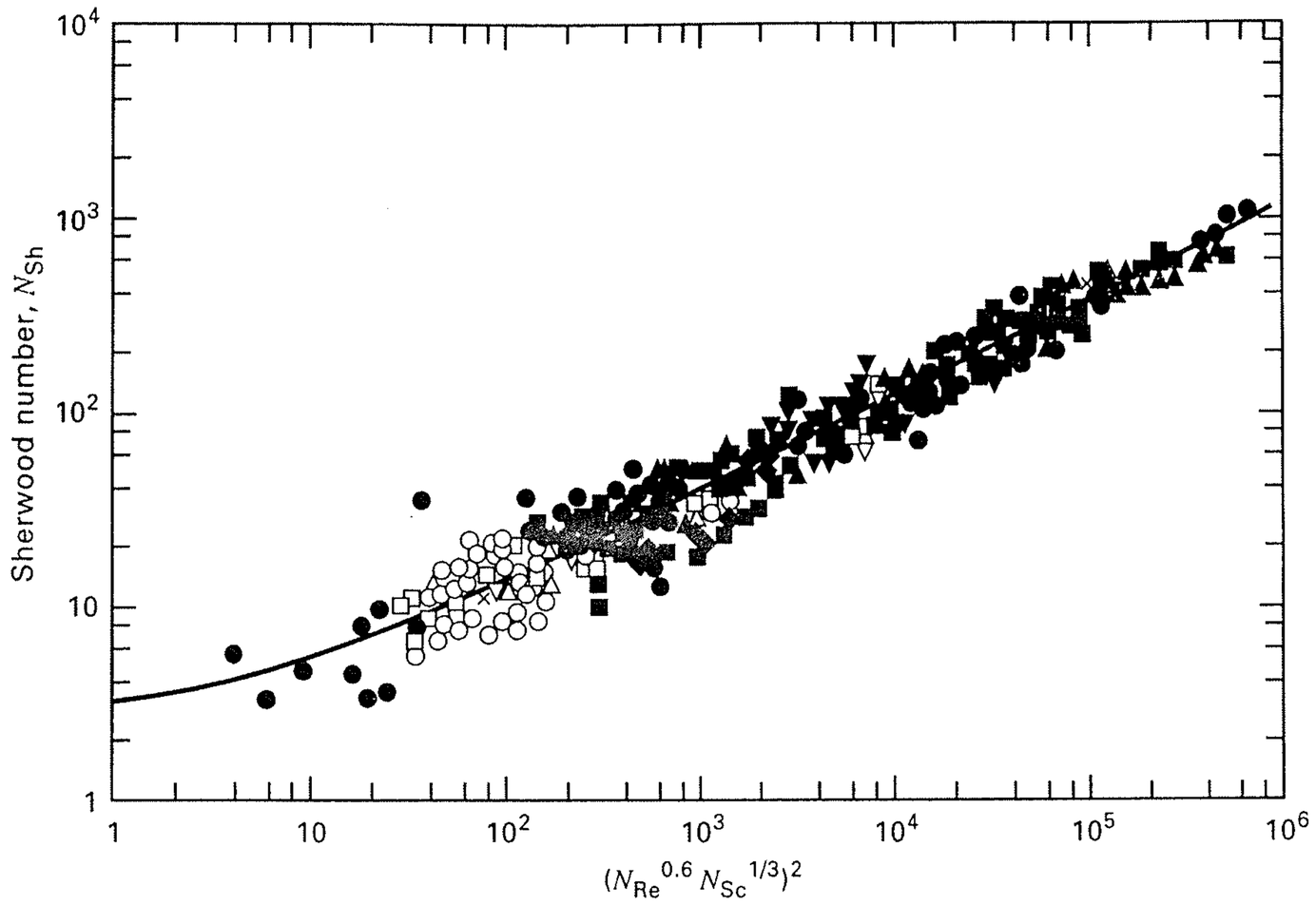

Figure 15.17 Correlation of experimental data for Sherwood number of external mass transfer in a packed bed.
[From N. Wakao and T. Funazkri, *Chem. Eng. Sci.*, **33,** 1375 (1978) with permission.]

a Schmidt number range of 0.6 to 70,600, a Reynolds number range of 3 to 10,000, and a particle diameter from 0.6 to 17.1 mm. Particle shapes include spheres, short cylinders, flakes, and granules. By analogy, the corresponding equation for fluid-particle convective heat transfer in packed beds is

$$N_{\text{Nu}} = \frac{hD_p}{k} = 2 + 1.1\left(\frac{D_p G}{\mu}\right)^{0.6}\left(\frac{C_P \mu}{k}\right)^{1/3} \qquad (15\text{-}66)$$

When (15-65) and (15-66) are used with beds packed with nonspherical particles, D_p is the equivalent diameter of a spherical particle. The following suggestions have been proposed for computing the equivalent diameter from geometric properties of the particle. These suggestions may be compared by considering a short cylinder with diameter, D, equal to the length, L.

1. D_p = diameter of a sphere with the same external surface area:

$$\pi D_p^2 = \pi DL + \pi D^2/2$$

and $$D_p = (DL + D^2/2)^{0.5} = 1.225D$$

2. D_p = diameter of a sphere with the same volume:

$$\pi D_p^3/6 = \pi D^2 L/4 \text{ and } D_p = (3D^2L/2)^{1/3} = 1.145D$$

3. $D_p = 4$ times the hydraulic radius, r_H, where for a packed bed,

$$4r_H = 6/a_v$$

a_v = external particle surface area/volume of particle

Thus,

$$a_v = \frac{\pi DL + \pi D^2/2}{\pi D^2 L/4} = \frac{6}{D} \text{ and } D_p = 4r_H = \frac{6D}{6} = 1.0D$$

The use of the hydraulic radius concept is equivalent to replacing D_p in the Reynolds number by $\Psi D_p'$ where Ψ is the sphericity and D_p' is given by Suggestion 2: The sphericity is defined by:

$$\Psi = \frac{\text{Surface area of a sphere of same volume as particle}}{\text{Surface area of particle}}$$

For a cylinder of $D = L$,

$$\Psi = \frac{\pi D_p^2}{\pi DL + 2\left(\frac{\pi D^2}{4}\right)} = \frac{\pi(1.145D)^2}{\frac{3}{2}\pi D^2} = 0.874$$

and $\Psi D_p' = (0.874)(1.145D) = D$, the diameter of the cylinder.

Suggestions 2 and 3 are widely used. Suggestion 3 is conveniently applied to crushed particles of irregular surface, but with no obvious longer or shorter dimension, that is, isotropic in shape. In that case, D_p' is taken as the size of the particle and the sphericity is approximately 0.65, as discussed by Kunii and Levenspiel [55].

EXAMPLE 15.8

Acetone vapor in a nitrogen stream is removed by adsorption in a fixed bed of activated carbon. At a location in the bed where the pressure is 136 kPa, the bulk gas temperature is 297 K, and the bulk mole fraction of acetone is 0.05, estimate the external gas-to-particle mass-transfer coefficient for acetone and the external particle-to-gas heat-transfer coefficient. Additional data are as follows:

Average particle diameter = 0.0040 m and Gas superficial molar velocity = 0.00352 kmol/m^2-s

SOLUTION

Because the temperature and composition are known only for the bulk gas and not at the particle external surface, use gas properties at bulk gas conditions. From the ChemCAD process simulation program, relevant properties for use in (15-65) and (15-66) are as follows:

Viscosity $\mu = 0.0000165$ Pa-s (kg/m-s); Density $\rho = 1.627$ kg/m^3
Thermal conductivity $k = 0.0240$ W/m-K $= 0.024 \times 10^{-3}$ kJ/m-K-s
Heat capacity at constant pressure = 31.45 kJ/kmol-K
Molecular weight = M = 29.52
Thus, specific heat $C_P = 31.45/29.52 = 1.065$ kJ/kg-K

Other parameters are

Gas mass velocity $G = 0.00352(29.52) = 0.1039$ kg/m^2-s
Assume a sphericity, ψ, of 0.65; therefore, $D_p = 0.65(0.004)$
$= 0.0026$ m

The diffusivity, D_i, of acetone in nitrogen at 297 K and 136 kPa is independent of the composition and is approximately 0.085×10^{-4} m^2/s.

$$N_{Re} = D_p G/\mu = 0.0026(0.1039)/(0.0000165) = 16.4$$
$$N_{Sc} = \mu/\rho D_i = 0.0000165/(1.627)(0.0000085) = 1.19$$
$$N_{Pr} = C_P \mu/k = (1.065)(0.0000165)/(0.000024) = 0.73$$

From (15-65):

$$N_{Sh} = 2 + 1.1(16.4)^{0.6}(1.19)^{1/3} = 8.24$$

which from Figure 15.17 is well within the data range of the correlation. Thus, the mass-transfer coefficient for acetone is

$$k_{ci} = N_{Sh}(D_i/D_p) = 8.24(0.0000085/0.0026)$$
$$= 0.027 \text{ m/s} = 0.088 \text{ ft/s}$$

From (15-66):

$$N_{Nu} = 2 + 1.1(16.4)^{0.6}(0.73)^{1/3} = 7.31$$
$$h = N_{Nu}(k/D_p) = 7.31(0.0240/0.0026)$$
$$= 67.5 \text{ W/m}^2\text{-K} \quad \text{or } 11.9 \text{ Btu/h-ft}^2\text{-}^\circ\text{F}$$

Internal Transport

Porous-adsorbent particles have a sufficiently high, effective thermal conductivity that temperature gradients within the particle are usually negligible. However, internal (intraphase) mass transfer in the particle must be considered. Mechanisms for mass transfer in the pores are those described for porous membranes in Section 14.3. However, in membranes, the transport is through the membrane. In sorption applications, transport is only into the interior of the particle during sorption and from the interior of the particle in desorption.

The mathematical model of internal transport in porous particles during adsorption or desorption is very similar to that for catalytic chemical reactions in porous catalyst pellets. The first pore model was that of Thiele [56], who considered a first-order irreversible reaction taking place isothermally on the surface of a single, straight, cylindrical pore, closed at one end. Thiele's treatment was extended to a porous spherical pellet by Wheeler [57], who utilized an effective diffusivity applied to the case of sorption.

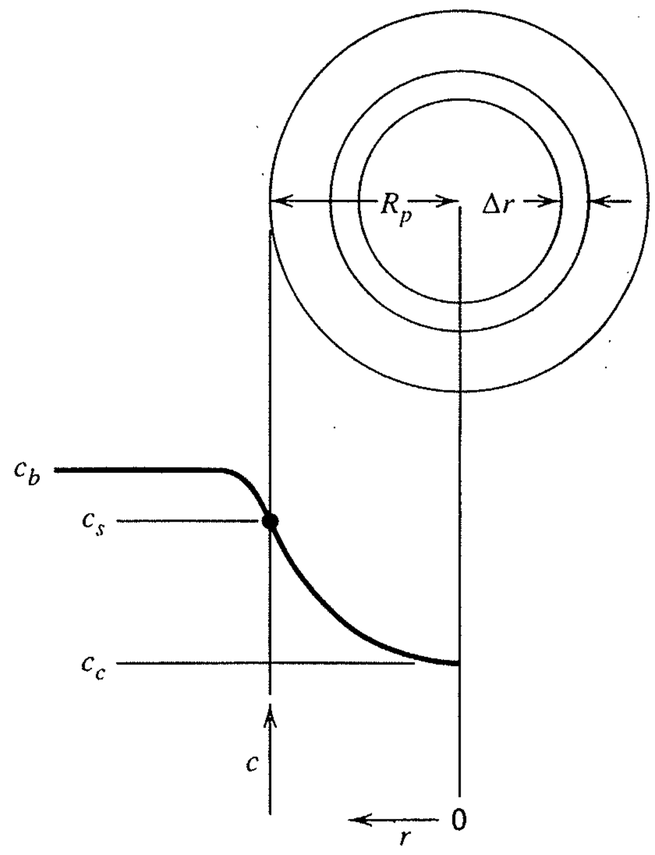

Figure 15.18 Typical solute concentration profile in adsorbent particle.

Consider the porous spherical pellet in Figure 15.18, where the fluid concentration, c, refers to the solute. A material balance in moles or mass per unit time over the spherical-shell volume of thickness Δr involves diffusion of the solute into the shell at radius $r + \Delta r$, adsorption within the shell, and diffusion out of the shell at radius r. Using Fick's first law:

$$4\pi(r + \Delta r)^2 D_e \left.\frac{\partial c}{\partial r}\right|_{r+\Delta r} = 4\pi r^2 \Delta r \frac{\partial q}{\partial t} + 4\pi r^2 D_e \left.\frac{\partial c}{\partial r}\right|_r \tag{15-67}$$

Dividing by $4\pi\Delta r$, taking the limit as $\Delta r \to 0$, and collecting terms gives

$$D_e\left(\frac{\partial^2 c}{\partial r^2} + \frac{2}{r}\frac{\partial c}{\partial r}\right) = \frac{\partial q}{\partial t} \tag{15-68}$$

The variable q is the amount adsorbed per unit volume of porous pellet. The effective diffusivity, D_e, applies to the entire surface area of the spherical shell, even though only about 50% of it is available as pores for diffusion. For liquid-phase diffusion in the pores, the effective diffusivity is given by (14-14), which involves the volume fraction of pores in the pellet, the solute molecular diffusivity in the fluid within the pore, the pore tortuosity, and a possible restrictive factor for relatively large solute molecules. For gas-phase diffusion in the pores, the effective diffusivity is given by (14-18), which accounts for the possibility of Knudsen diffusion, with diffusivity D_K for very small pore diameters and/or low total pressures. Although (14-14) and (14-18) strictly apply only to equimolar counterdiffusion, they can be used as an approximation for unimolecular diffusion for fluids dilute in the solute molecules. A diffusion mechanism not accounted for directly in (14-18) is that of surface diffusion along the pore wall due to the concentration gradient of the adsorbate (adsorbed solute) along the wall.

Fick's first law for molecular diffusion through a fluid in a pore can be written

$$n_i = -D_i A(dc_i/dx) \tag{15-69}$$

where n is the molar rate of ordinary diffusion of i through the fluid in the x-direction, perpendicular to the cross-sectional area, A, for diffusivity, D_i, and concentration, c_i, in moles/unit volume of fluid. A modified Fick's first law applies to surface diffusion, as suggested by Schneider and Smith [58]. Thus,

$$(n_i)_s = -(D_i)_s b d(c_i)_s/dx \tag{15-70}$$

where b is the perimeter of the surface, $(c_i)_s$ is the surface concentration of adsorbate in moles/unit surface area, and $(D_i)_s$ is the surface diffusivity as defined by (15-70).

For convenience, (15-70) is converted, as follows, to the flux form of (15-69) so that the two mechanisms of diffusion

can be combined in a single transport rate equation. The flux form of (15-69) is

$$N_i = n_i/A = -D_i(dc_i/dx) \qquad (15\text{-}71)$$

The corresponding flux form of (15-70) is obtained by dividing both sides by the cross-sectional area of the pore and converting the surface concentration, $(c_i)_s$, in moles/unit surface area to the concentration, q, in mol/g of adsorbent, by using the product of the pore surface/pore volume times the reciprocal of the adsorbent particle density times the particle porosity. The result is

$$(N_i)_s = -(D_i)_s \frac{\rho_p}{\epsilon_p}\left(\frac{dq_i}{dx}\right) \qquad (15\text{-}72)$$

Assuming linear adsorption according to Henry's law:

$$q_i = K_i c_i \qquad (15\text{-}73)$$

Substituting (15-73) into (15-72) and adding the result to (15-71), the total flux is

$$N_i = -\left[D_i + (D_i)_s \frac{\rho_p K_i}{\epsilon_p}\right]\frac{dc_i}{dx} \qquad (15\text{-}74)$$

In terms of the effective diffusity employed in (15-68):

$$D_e = \frac{\epsilon_p}{\tau}\left\{\left[\frac{1}{(1/D_i)+(1/D_K)}\right] + (D_i)_s \frac{\rho_p K_i}{\epsilon_p}\right\} \qquad (15\text{-}75)$$

Equation (15-75) needs to be used with caution, because, as discussed by Riekert [59], the tortuosity, τ, for pore-volume diffusion is not necessarily the same as that for surface diffusion.

Based on the study by Sladek, Gilliland, and Baddour [60], values of the surface diffusivity of light gases for physical adsorption are typically in the range of 5×10^{-3} to 10^{-6} cm^2/s, with the larger values applying to cases of a low differential heat of adsorption. For nonpolar adsorbates, the surface diffusivity in cm^2/s may be estimated from the correlation [60],

$$D_s = 1.6 \times 10^{-2} \exp[-0.45(-\Delta H_{ads})/mRT] \qquad (15\text{-}76)$$

where $m = 2$ for conducting adsorbents such as carbon and $m = 1$ for insulating adsorbents.

EXAMPLE 15.9

Porous silica gel of 1.0 mm particle diameter, with a particle density of 1.13 g/cm^3, a porosity of 0.486, an average pore radius of 11 Å, and a tortuosity of 3.35 is to be used to adsorb propane from helium. At 100°C, diffusion in the pores is controlled by Knudsen and surface diffusion. Estimate the effective diffusivity. The differential heat of adsorption is −5,900 cal/mol. At 100°C, the adsorption constant (for a linear isotherm) is 19 cm^3/g.

SOLUTION

From (14-21), the Knudsen diffusivity for propane is $D_K = 4{,}850(22 \times 10^{-8})(373/44.06)^{1/2} = 3.7 \times 10^{-3}$ cm^2/s. From (15-76), using $m = 1$, $D_s = 1.6 \times 10^{-2} \exp\{(-0.45)(5{,}900)/[(1)(1.987)(373)]\} = 4.45 \times 10^{-4}$ cm^2/s.

Equation (15-75) reduces to $D_e = \frac{\epsilon_p}{\tau}D_K + \frac{\rho_p K}{\tau}D_s = \frac{0.486}{3.35}(3.17 \times 10^{-3}) + \frac{(1.13)(19)}{3.35}(4.45 \times 10^{-4}) = 0.46 \times 10^{-3} + 2.85 \times 10^{-3} = 3.31 \times 10^{-3}$ cm^2/s

Experiments by Schneider and Smith [58] give a value of 1.22×10^{-3} cm^2/s for D_e with a value of 0.88×10^{-3} for the contribution of surface diffusion. Thus, the estimated contribution from surface diffusion is high by a factor of about 3. In either case, the fractional contribution due to surface diffusion is large. A detailed review of surface diffusion is given by Kapoor, Yang, and Wong [61].

Mass Transfer in Ion Exchange and Chromatography

As discussed by Helfferich [62], two major mass-transfer resistances occur in ion exchange. The first is the external mass-transfer resistance due to the film or boundary layer surrounding the ion-exchange bead. The second is the internal diffusional resistance due to the resin bead. Either or both resistances can be rate-controlling; in either case, the diameter of the resin bead is an important factor. In general, external mass-transfer film diffusion is rate-controlling at very low exchange-ion concentrations, say below 0.01 N, whereas internal mass transfer (particle diffusion) controls at high concentrations (say above 1.0 N). It has also been observed that a large separation factor, as defined by (15-46), favors external mass-transfer control, and that divalent ions diffuse appreciably more slowly than monovalent ions through the resin bead. Usually, the rate-determining step is not the chemical reaction between the exchanging ions and the resin.

The external mass-transfer coefficient for flow of fluid through a fixed bed of ion-exchange resin beads is estimated from the same relation, (15-65), that is used for applications to adsorption in fixed beds. For internal mass transfer, it is customary to assume that the ion-exchange resin bead is a single quasi-homogeneous phase and that the diffusivity of the diffusing ion is constant at a given temperature. Under these conditions, (15-68) can be applied, where D_e is a diffusivity determined by experiment. In general, such diffusivities depend upon (1) the size and charge of the ion, with the smaller, monovalent ions diffusing the fastest; (2) the degree of cross-linking and resin swelling, with larger diffusivities favored by swelling and a small degree of cross-linking; and (3) temperature.

The most fundamental measurements of diffusivity in ion-exchange resins have been made with isotopes of the ions to obtain self-diffusion coefficients that are independent of ion concentration. Typical data are those of Soldano [63], shown in Figure 15.19 for Na^+, Zn^{2+}, and Y^{3+} in a sulfonated styrene–divinylbenzene cation exchanger at temperatures of 0.2 and 25°C. Recall that typical order-of-magnitude diffusivities for small molecules are as follows:

0.1 cm^2/s in the gas phase
1×10^{-5} cm^2/s in the liquid phase
1×10^{-7} cm^2/s in polymers

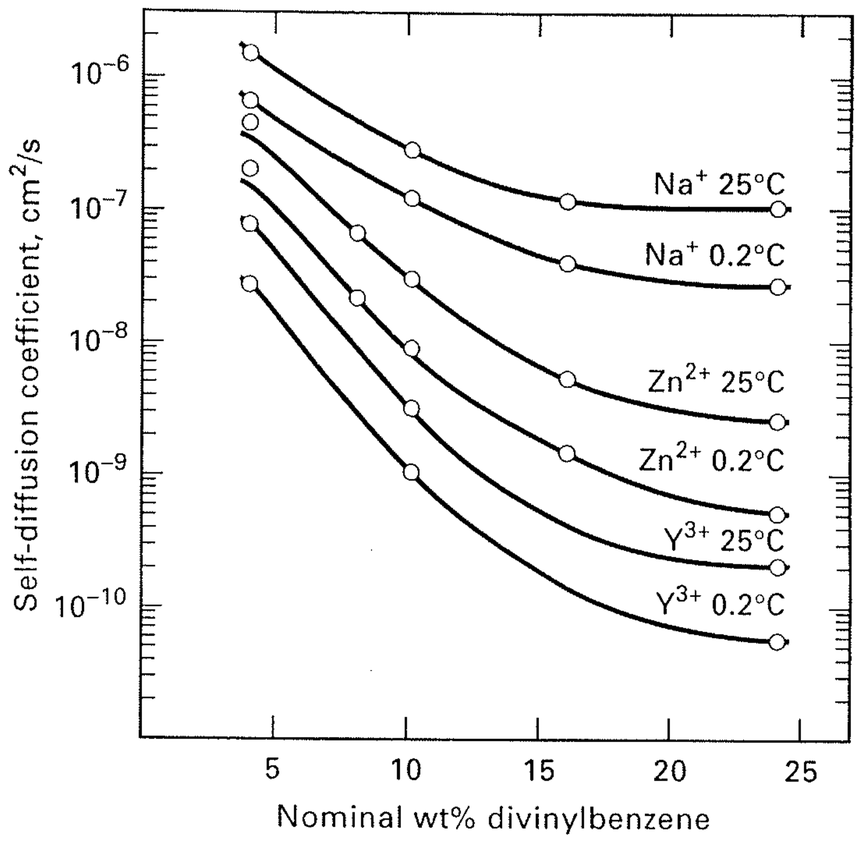

Figure 15.19 Self-diffusion coefficients for cations in a resin as a function of cross-linking with divinylbenzene.
[From B.A. Soldano, *Ann. NY Acad. Sci.*, **57,** 116 (1953) with permission.]

From Figure 15.19, it is seen that diffusivities depend strongly on the degree of cross-linking and the charge on the ion, with values much less than those found in liquids, especially for the divalent and trivalent ions, which have diffusivities even smaller than those observed for small molecules in polymers.

No new fundamental principles are required for formulating mass-transfer relations for chromatography. When packed beds are used, (15-65) and (15-66) are applied to determine external transport coefficients. If a coated flat plate or a tube with a coated inner wall is used, correlations of the type discussed in Chapter 3 are applicable. In some cases, an entry region of finite length exists, particularly for laminar flow, such that the transport coefficients vary with axial location, decrease in value with length, and eventually approach an asymptotic value. For internal diffusion in the sorbent, Fick's second law is applied where the effective diffusivity depends on factors discussed earlier in this section.

15.4 SORPTION SYSTEMS

A variety of equipment configurations and operating procedures are employed for commercial, sorption-separation operations. This variety is due mainly to the wide range of sorbent particle sizes used and the need, in most applications, to regenerate the solid sorbent.

Adsorption

For adsorption, the most widely used equipment configurations and operating procedures are listed in Table 15.7. For analysis purposes, the listed devices may be classified into the three modes of operations, shown schematically in Figure 15.20. An agitated vessel, shown in Figure 15.20a, is used with a batch of liquid to which is added a powdered adsorbent such as activated carbon, of particle diameter typically less than 1 mm, to form a slurry. With good agitation and small particles, the external resistance to mass transfer from the bulk liquid to the external surface of the adsorbent particles is small. For small adsorbent particles, the internal resistance to mass transfer within the pores of the particles is also small. Accordingly, the rate of adsorption is rapid. The required residence time of the slurry in a well-mixed agitated vessel is determined by how fast equilibrium is approached. The main application of this mode of operation is the removal of very small amounts of dissolved, and relatively large molecules, such as coloring agents, from water. Generally, the spent adsorbent, which is removed from the slurry by sedimentation or filtration, is discarded because of the difficulty of desorbing large molecules. The slurry adsorption system, also called *contact filtration,* is also operated continuously.

The cyclic-batch operating mode using a fixed bed, shown schematically in Figure 15.20b, is widely used with both liquid and gas feeds. Adsorbent particle size ranges from 0.05 to 1.2 cm. Bed pressure drop decreases with increasing particle size, but the solute transport rate increases with decreasing particle size. The optimal particle size is determined mainly from these two factors. To avoid jiggling

Table 15.7 Common Commercial Methods for Adsorption Separations

Phase Condition of Feed	Contacting Device	Adsorbent Regeneration Method	Main Application
Liquid	Slurry in an agitated vessel	Adsorbent discarded	Purification
Liquid	Fixed bed	Thermal reactivation	Purification
Liquid	Simulated moving bed	Displacement purge	Bulk separation
Gas	Fixed bed	Thermal swing (TSA)	Purification
Gas	Combined fluidized bed-moving bed	Thermal swing (TSA)	Purification
Gas	Fixed bed	Inert-purge swing	Purification
Gas	Fixed bed	Pressure swing (PSA)	Bulk separation
Gas	Fixed bed	Vacuum swing (VSA)	Bulk separation
Gas	Fixed bed	Displacement purge	Bulk separation

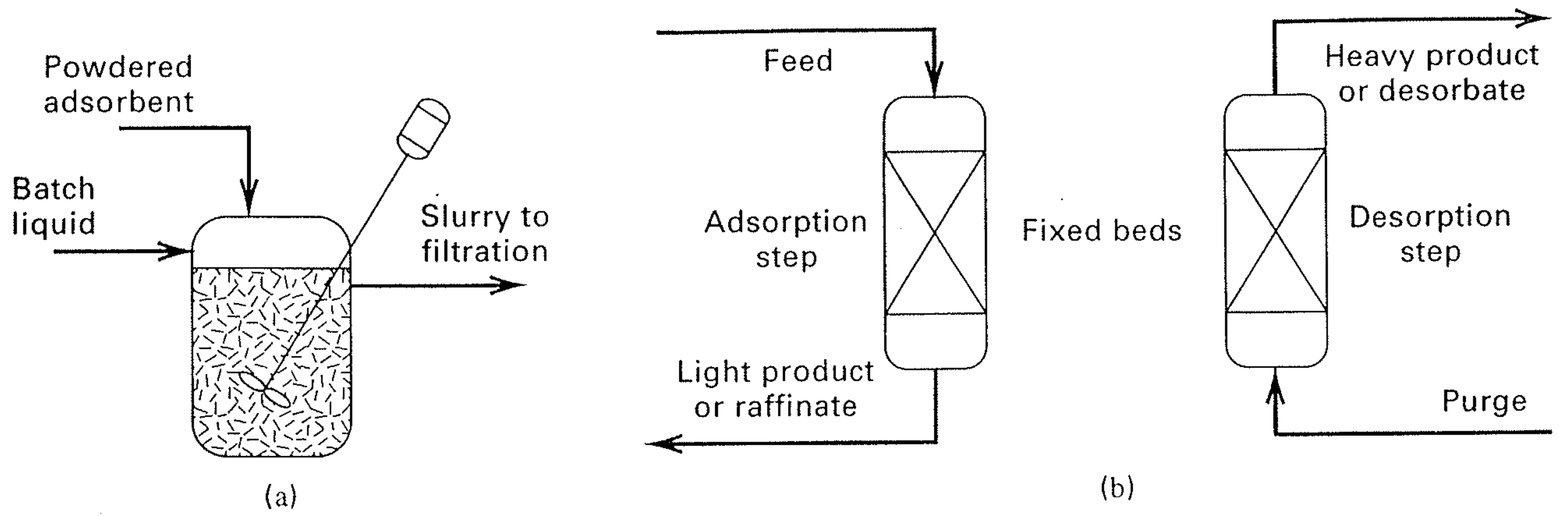

Figure 15.20 Contacting modes for adsorption. (a) Stirred-tank, slurry operation. (b) Cyclic fixed-bed, batch operation. (c) Continuous countercurrent operation.

or fluidizing the bed during adsorption, the flow of the liquid or gas feed is often downward. For removal of small amounts of dissolved hydrocarbons from water, the spent adsorbent is removed from the vessel and reactivated thermally at high temperature or it is discarded. Applications of fixed-bed adsorption, also called *percolation,* include the removal of dissolved organic compounds from water. For purification or bulk separation of gases, the adsorbent is almost always regenerated in place by one of the five methods listed in Table 15.7.

In the *thermal (temperature)-swing-adsorption* (TSA) method, the adsorbent is regenerated by desorption at a temperature higher than that used during the adsorption step of the cycle, as shown in Figure 15.21. The temperature of the bed is increased by (1) heat transfer from heating coils located in the bed followed by pulling a moderate vacuum or (2) more commonly, by heat transfer from an inert, nonadsorbing, hot purge gas, such as steam. Following desorption, the bed is cooled before the adsorption step of the cycle is resumed. Because heating and cooling of the bed requires hours, a typical cycle time for TSA is hours to days. Therefore, if the quantity of adsorbent in the bed is to be reasonable, TSA is practical only for purification involving small rates of adsorption. Instead of using a fixed bed, a fluidized bed can be used for adsorption and a moving bed for desorption, as shown in Figure 15.22, provided that the adsorbent particles are attrition-resistant. In the adsorption section, sieve trays are used with the raw gas passing up through the perforations and fluidizing the adsorbent particles. The fluidized solids flow like a liquid across the tray, into the downcomer, and onto the tray below. From the adsorption section, the solids pass to the desorption section, where, as moving beds, they first flow down through preheating tubes and then through desorption tubes. Steam is used for indirect heating in both sets of tubes and for stripping in the desorption tubes. Moving beds, rather than fluidized beds on trays, are used in the desorption section because the stripping-steam flow rate is insufficient for fluidizing the solids. At the bottom of the unit, the regenerated solids are picked up by a carrier gas, which flows up through a gas-lift line to the top, where the solids settle out onto the top tray to repeat the adsorption part of the cycle. According to Keller [64], this configuration, which was announced in 1977, is used in more than 50 units worldwide to remove small amounts of solvents from air. Other applications of TSA include the removal of moisture, CO_2, and pollutants from gas streams.

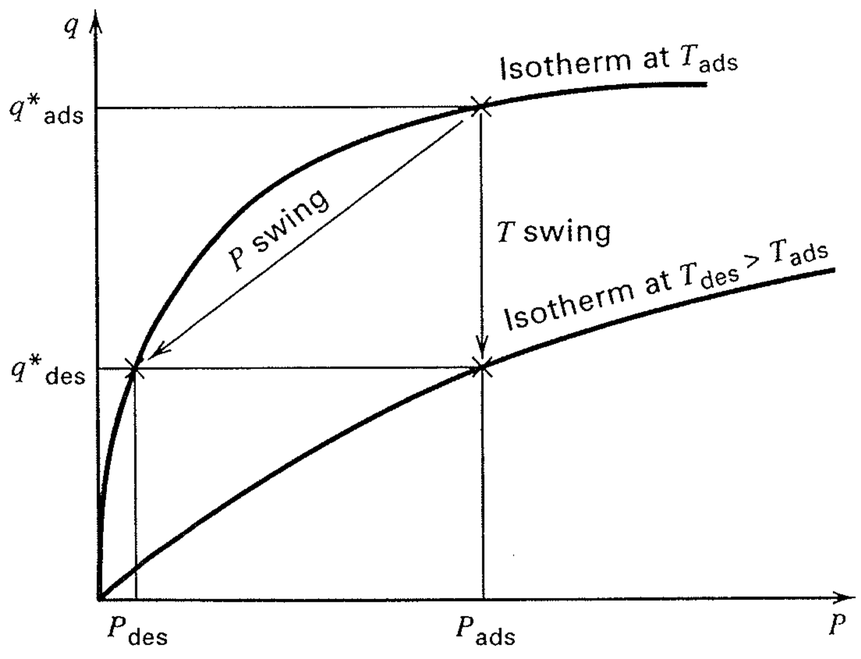

Figure 15.21 Schematic representation of pressure-swing and thermal-swing adsorption.

In the *inert-purge-swing* method of regeneration, desorption is at the same temperature and pressure as the adsorption step, because the gas used for purging is nonadsorbing (inert) or only weakly adsorbing. This method is used only when the solute is weakly adsorbed, easily desorbed, and of little or no value. The purge gas must be inexpensive so that it does not have to be purified before recycle.

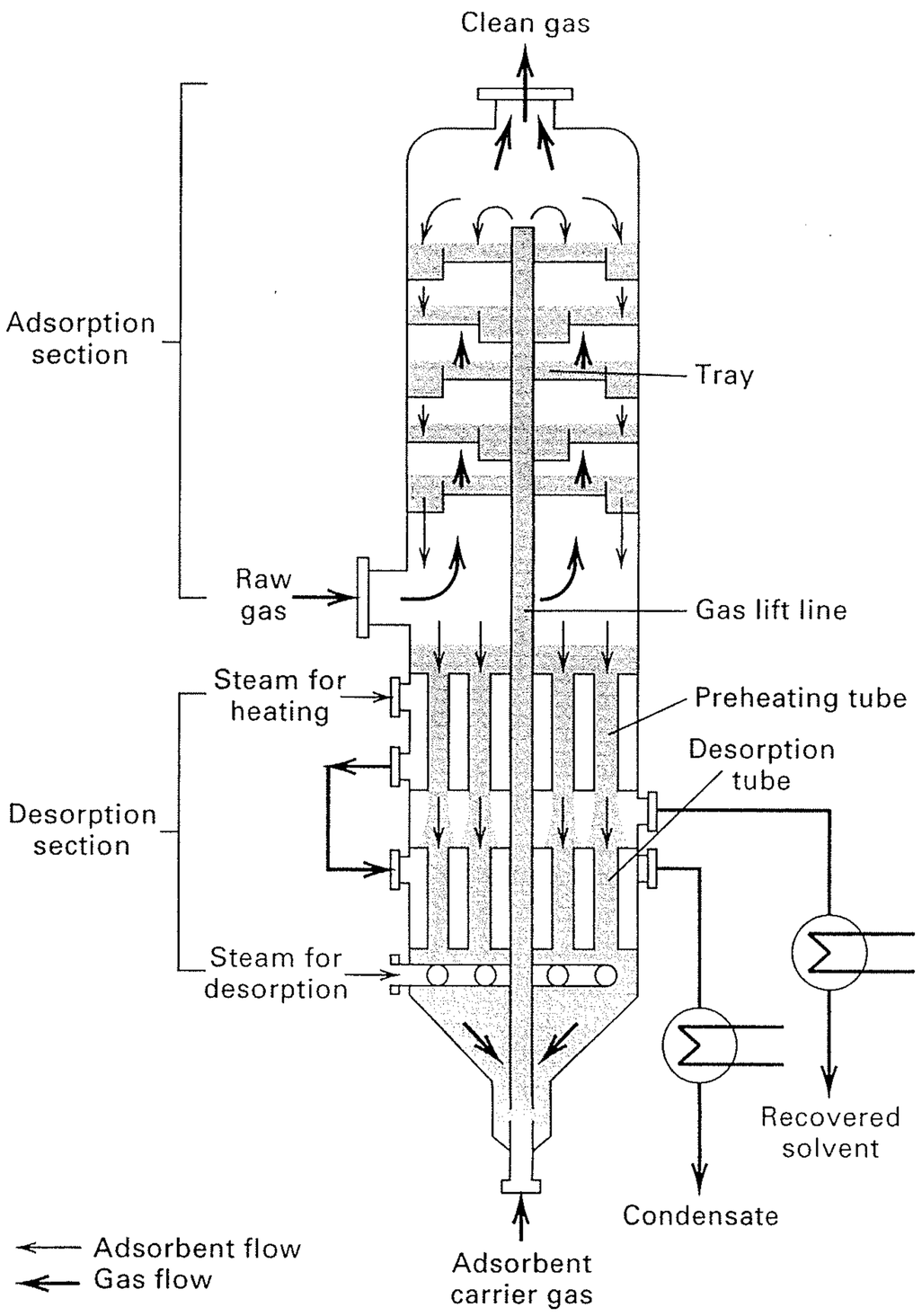

Figure 15.22 Purasiv process with a fluidized bed for adsorption and moving bed for desorption.
[From G.E. Keller, "Separations: New Directions for an Old Field," *AIChE Monograph Series,* **83** (17) (1987) with permission.]

In the *pressure-swing-adsorption* (PSA) cycle, adsorption takes place at an elevated pressure, whereas desorption occurs at near-ambient pressure, as is shown in Figure 15.21. PSA is used for bulk separations because the bed can be depressurized and repressurized rapidly, making it possible to operate at cycle times of seconds to minutes. Because of these short times, the beds need not be large even when a substantial fraction of the feed gas is adsorbed. If adsorption takes place at near-ambient pressure and desorption under vacuum, the cycle is referred to as *vacuum-swing-adsorption* (VSA). PSA and VSA are widely used for the bulk separation of air. If a zeolite adsorbent is used, equilibrium is rapidly established and nitrogen is preferentially adsorbed. The nonadsorbed, high-pressure product gas is a mixture of oxygen and argon with a small amount of nitrogen. If a carbon molecular-sieve adsorbent is used, the particle diffusivity of oxygen is observed to be about 25 times that of nitrogen. As a result, the selectivity of adsorption is controlled by mass transfer, and oxygen is preferentially adsorbed. The resulting high-pressure product gas is nearly pure nitrogen. In both cases, the adsorbed gas, which is desorbed at low pressure, is quite impure. For the separation of air, large plants use VSA because it is more energy-efficient than PSA. Small plants often use PSA because that cycle is simpler.

In the *displacement-purge* (*displacement desorption*) *cycle,* a strongly adsorbed purge gas is used in the desorption step to displace the adsorbed species. Another step is required to recover the purge gas. The displacement-purge cycle is considered only where TSA, PSA, and VSA cannot be used because of pressure or temperature limitations. One application is the separation of medium-molecular-weight linear paraffins (C_{10}-C_{18}) from mixtures of branched-chain and cyclic hydrocarbons by adsorption on 5A zeolite. Ammonia, which is easily separated from the paraffins by flash vaporization, is used as the purge.

Most commercial applications of adsorption involve fixed beds that cycle between adsorption and desorption. Thus, compositions, temperature, and/or pressure at a given location in the bed vary with time. Alternatively, a continuous, countercurrent operation, where such variations do not occur, can be envisaged, as shown in Figure 15.20c and discussed in detail by Ruthven and Ching [65]. The main difficulty with such a scheme is the need to circulate the solid adsorbent, as a moving bed, to achieve a steady-state operation. The first commercial application of countercurrent adsorption and desorption was the moving-bed Hypersorption process for the recovery, by adsorption on activated carbon, of light hydrocarbons from various gas streams in petroleum refineries, as discussed by Berg [66]. Only a few units were installed because of problems with attrition of the adsorbent, difficulties in regenerating the adsorbent when heavier hydrocarbons were present in the feed gas, and unfavorable economics compared to those of distillation. Newer adsorbents with a much higher resistance to attrition and possible applications to more difficult separations are reviving interest in moving-bed units.

A successful alternative countercurrent system for commercial application to the separation of liquid mixtures is the simulated moving-bed system, shown in a hybrid system with two distillation columns in Figure 15.23 and known generally as the UOP Sorbex process. As described by Broughton [67], the bed is held stationary in one column, which is equipped with a number (perhaps 12) of liquid feed entry and discharge locations. By shifting, with a rotary valve (RV), the locations of feed entry, desorbent entry, extract (adsorbed) removal, and raffinate (non-adsorbed) removal, a countercurrent movement of solids is simulated by a downward movement of liquid. For the valve positions shown in Figure 15.23, locations 2 (entering desorbent), 5 (exiting extract), 9 (entering feed), and 12 (exiting raffinate) are operational, with all other numbered lines closed. However, liquid is also circulated down through and back up (external to the column) to the top of the column by a pump. Ideally, an infinite number of entry and exit locations on the column would exist and the valve would continuously change the four operational locations. Since this is impractical, a finite number of locations are used and valve changes are made periodically. In Figure 15.23, when the valve is

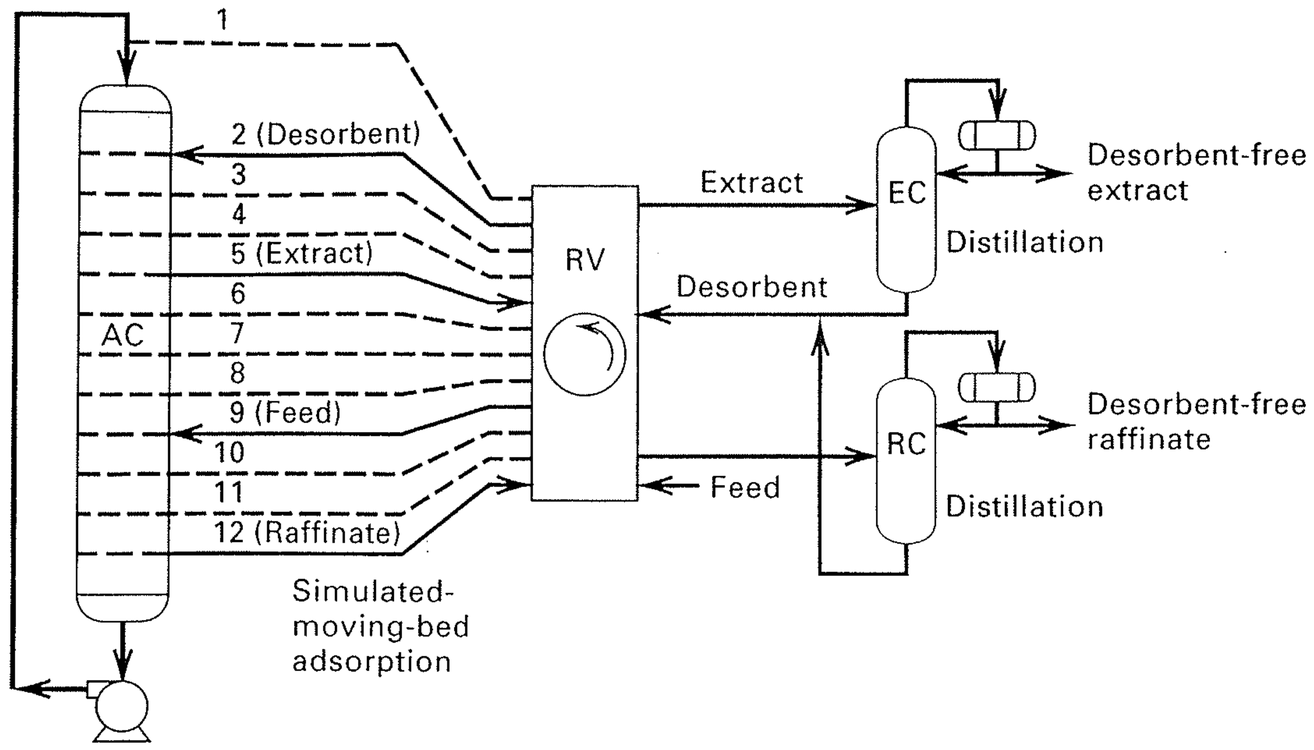

Figure 15.23 Sorbex hybrid simulated moving-bed process for bulk separation. AC, adsorbent chamber; RV, rotary valve; EC, extract column; RC, raffinate column.

[From D.B. Broughton, *Chem. Eng., Progress,* **64** (8), 60–65 (1968) with permission.]

moved to the next position, Lines 3, 6, 10, and 1 become operational. Thus, raffinate removal is relocated from the bottom of the bed to the top of the bed. The result is that the bed has no top or bottom. As discussed by Gembicki et al. [68], 78 Sorbex-type commercial units were installed during 1962–1989 for the bulk separation of *p*-xylene from C_8 aromatics; *n*-paraffins from branched and cyclic hydrocarbons; olefins from paraffins; *p*- or *m*-cymene (or cresol) from cymene (or cresol) isomers; and fructose from dextrose and polysaccharides. Humphrey and Keller [101] cite 100 commercial installations of Sorbex-type units and more than 50 different demonstrated separations.

Ion Exchange

Ion exchange employs the same modes of operation as shown for adsorption in Figure 15.20. Although the use of fixed beds in a cyclic operation is most common, stirred tanks are used for batch contacting, with an attached strainer or filter to separate the resin beads from the solution after equilibrium conditions are approached. Agitation is mild to avoid resin attrition, but sufficient to achieve complete suspension of the resin. To increase resin utilization and achieve high ion-exchange reaction efficiency, much effort has been expended in the development of continuous, countercurrent contactors, two of which are shown in Figure 15.24. The Higgins contactor [69] operates as a moving, packed bed by using intermittent hydraulic pulses to move incremental portions of the bed from the contacting section, where ion exchange takes place, up, around, and down to the backwash region, down to the regenerating section, and back up through the rinse section to the contacting section to repeat the cycle. Liquid moves countercurrently to the resin. The Himsley contactor [70] has a series of trays, on each of which the resin beads are fluidized by the upward flow of liquid. Periodically, the flow is reversed to move incremental amounts of resin from one stage to the stage below. The batch of resin at the bottom is lifted to the wash column, then to the regeneration column, and then back to the top of the ion-exchange column for reuse.

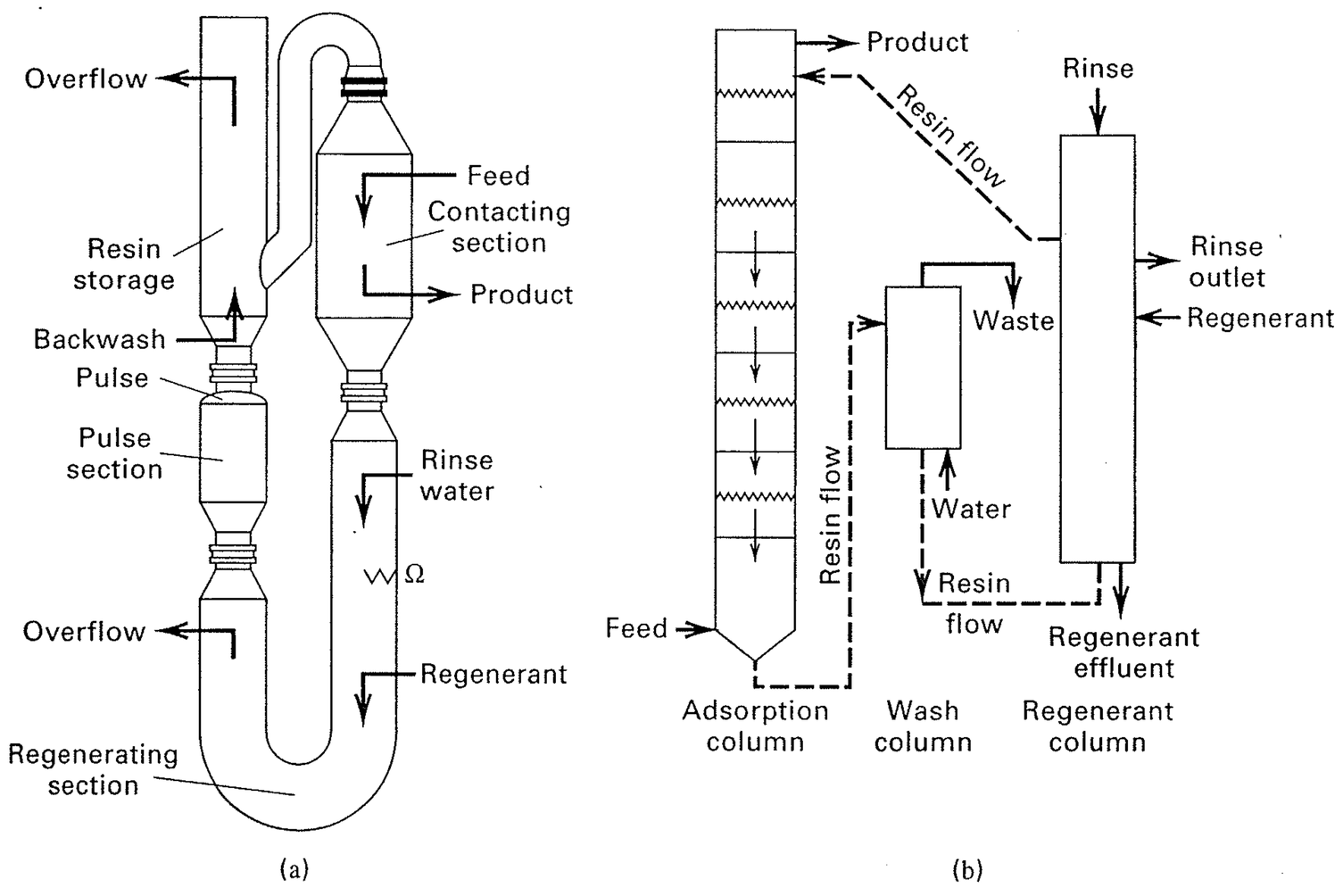

Figure 15.24 Continuous countercurrent ion-exchange contactors. (a) Higgins moving packed-bed process. (b) Himsley fluidized-bed process.

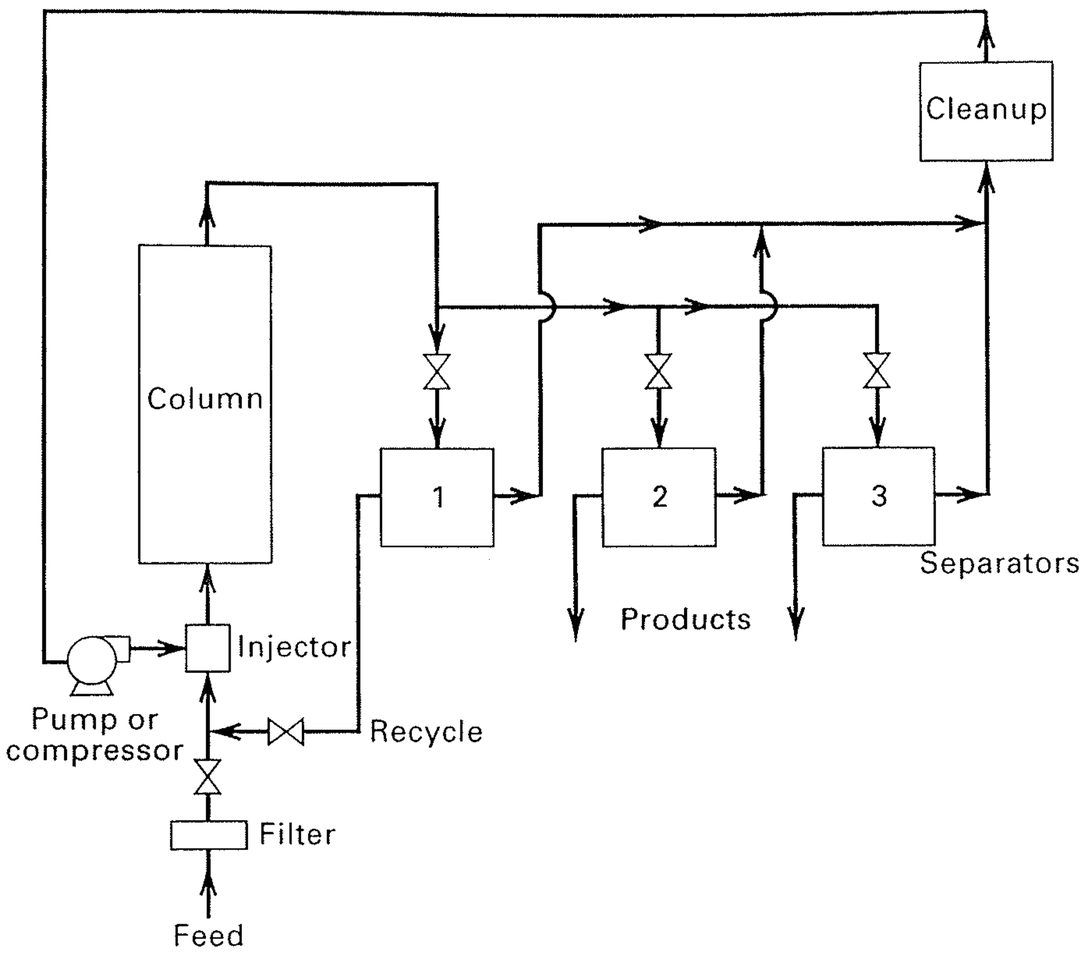

Figure 15.25 Large-scale, batch elution chromatography process.

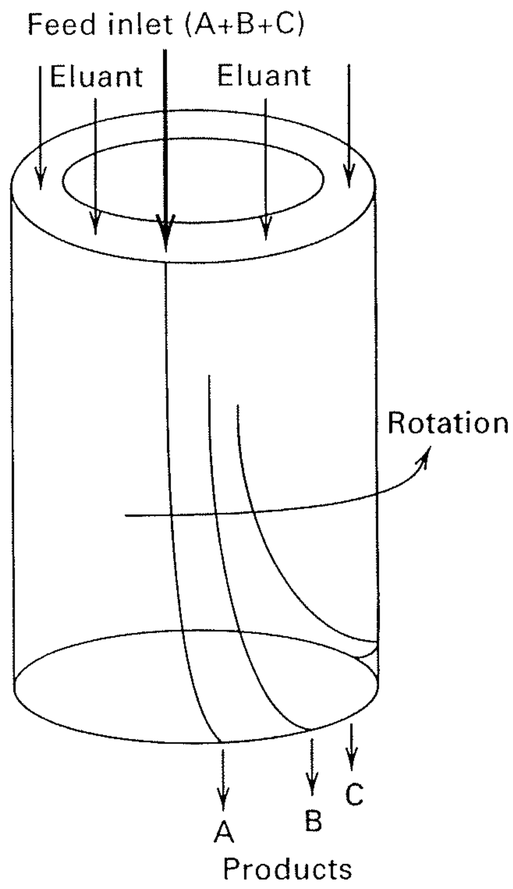

Figure 15.26 Rotating, cross-current, annular chromatograph.

Chromatography

Operation modes for large-scale, commercial application of chromatography are of two major types, as discussed in a book edited by Ganetsos and Barker [71]. The first, and the most common, is a transient mode that is a scaled-up version of an analytical chromatograph, referred to as large-scale, batch (or elution) chromatography. Packed columns of diameter up to 4.6 m and packed heights to 12 m have been reported. As shown in Figure 15.25 and discussed by Wankat in Chapter 14 of the *Handbook* edited by Rousseau [9], a recycled solvent or carrier gas is fed continuously into the sorbent-packed column. The feed mixture and recycle is pulsed into the column by an injector. A timer or detector (not shown) splits the effluent from the column, sending it to different separators (condensers, evaporators, distillation columns, etc.). Each separator is designed to remove a particular feed component from the carrier fluid. An additional cleanup step is required to purify the carrier fluid before it is recycled to the column. Separator one produces no product because it handles an effluent pulse that contains the carrier fluid and two or more of the feed components, which are recovered and recycled to the column. Thus, if properly designed and operated, the batch chromatograph operates somewhat like a batch-distillation column, producing a nearly pure cut for each component in the feed and slop cuts for recycle. The system shown in Figure 15.25 is designed to separate a binary system. If, say, three more separators are added, the system can separate a five-component feed into five nearly pure products.

The second major type of large-scale chromatograph is the countercurrent flow or simulated-moving-bed mode already discussed for adsorption. This mode is more efficient, but is more complicated and can only separate a mixture into two products. A third mode is the continuous, cross-current (or rotating) chromatograph, first conceived by Martin [72] and shown schematically in Figure 15.26. The packed annular bed rotates slowly about its axis, past the feed-inlet point. *Eluant* (solvent or carrier gas) enters the top of the bed uniformly over the entire cross-sectional area. Both feed and eluant are fed continuously and are carried downward and around by the rotation of the bed. Because of the different selectivities of the feed components for the sorbent, each component traces a different helical path since each spends a different amount of time in contact with the sorbent. Thus, each component is eluted from the bottom of the packed annulus at a different location. In principle, a multicomponent feed can be separated continuously into nearly pure components following separation of the carrier fluid from each eluted fraction. Units of up to 12 in. in diameter have successfully separated sugars, proteins, and metallic elements.

Slurry Adsorption (Contact Filtration)

Three modes of adsorption from a liquid in an agitated vessel are of interest. The first is the *batch mode* in which a batch of liquid is contacted with a batch of adsorbent for a period of time, followed by discharge of the slurry from the vessel, and filtration to separate the solids from the liquid. The second is the *continuous mode,* in which liquid and adsorbent are continuously added to and removed from the agitated vessel. In the third mode, called the *semibatch* or *semicontinuous mode,* the liquid is continuously fed to and removed from the agitated vessel, where it is contacted with the adsorbent, which is retained in a contacting zone of the vessel until it is nearly spent. Models for each of these three modes are developed next, followed by examples of their application. In all models, the slurry is assumed to be perfectly mixed by agitation in the turbulent regime to produce a fluidized bed of sorbent. Perfect mixing is approached by

using a liquid depth of from one to two vessel diameters, four vertical wall baffles, and one or two marine propellers or pitched-blade turbines on a vertical shaft. With a proper impeller rotation rate, the axial flow achieves complete suspension. For semicontinuous operation, a clear liquid region is maintained above the suspension region for liquid withdrawal.

Because small particles are used in slurry adsorption and because the relative velocity between the particles and the liquid in an agitated slurry is low (small particles tend to move with the liquid), the rate of adsorption is assumed to be controlled by external, rather than internal, mass transfer.

Batch Mode

The rate of adsorption of solute, as controlled by external mass transfer, is

$$-\frac{dc}{dt} = k_L a(c - c^*) \tag{15-77}$$

where c is the concentration of solute in the bulk liquid; c^* is the concentration in equilibrium with the loading on the adsorbent, q; k_L is the external liquid-phase mass-transfer coefficient; and a is the external surface area of the adsorbent per unit volume of liquid. Starting from feed concentration, c_F, the instantaneous bulk concentration, c, at time t, is related to the instantaneous adsorbent loading, q, by material balance:

$$c_F Q = cQ + qS \tag{15-78}$$

where the adsorbent is assumed to be initially free of adsorbate, Q is the liquid volume (assumed to remain constant for dilute feeds), and S is the mass of adsorbent. The equilibrium concentration, c^*, is given by an appropriate adsorption isotherm: a linear isotherm, the Langmuir isotherm (15-36), or the Freundlich isotherm (15-35). For example, a rearrangement of the latter gives

$$c^* = (q/k)^n \tag{15-79}$$

To solve the system of equations for c and q as a function of time, starting from c_F at $t = 0$, (15-78) is combined with the equilibrium isotherm, for example, (15-79), to eliminate q. The resulting equation is combined with (15-77) to eliminate c^* to give an ODE for c in t, which is integrated analytically or numerically. Corresponding values of q are then obtained from (15-78).

If the equilibrium is represented by a linear isotherm,

$$c^* = q/k \tag{15-80}$$

an analytical integration gives

$$c = \frac{c_F}{\beta}[\exp(-k_L a\beta t) + \alpha] \tag{15-81}$$

where

$$\beta = 1 + \frac{Q}{Sk} \tag{15-82}$$

$$\alpha = \frac{Q}{Sk} \tag{15-83}$$

As the contact time approaches infinity, adsorption equilibrium is approached and for the linear isotherm, from (15-81) or combining (15-78), with $c = c^*$, and (15-80):

$$c\{t = \infty\} = c_F \alpha/\beta \tag{15-84}$$

Continuous Mode

When both liquid and solids flow continuously through a perfectly mixed vessel, (15-77) is converted to an algebraic equation because, as in a perfectly mixed reaction vessel (CSTR), the concentration, c, throughout the vessel, is equal to the exit (outlet) concentration, c_{out}. Thus, in terms of the residence time in the vessel, t_{res}:

$$\frac{c_F - c_{\text{out}}}{t_{\text{res}}} = k_L a(c_{\text{out}} - c^*) \tag{15-85}$$

or, rearranging:

$$c_{\text{out}} = \frac{c_F + k_L a t_{\text{res}} c^*}{1 + k_L a t_{\text{res}}} \tag{15-86}$$

Equation (15-78) becomes

$$c_F Q = c_{\text{out}} Q + q_{\text{out}} S \tag{15-87}$$

where Q and S are now flow rates. An appropriate adsorption isotherm relates c^* to q_{out}.

For a linear isotherm, (15-80) becomes $c^* = q_{\text{out}}/k$, which when combined with (15-87) and (15-86) to eliminate c^* and q_{out}, gives

$$c_{\text{out}} = c_F\left(\frac{1 + \gamma\alpha}{1 + \gamma + \gamma\alpha}\right) \tag{15-88}$$

where α is given by (15-83) and

$$\gamma = k_L a t_{\text{res}} \tag{15-89}$$

The corresponding q_{out} is given by a rearrangement of (15-87):

$$q_{\text{out}} = \frac{Q(c_F - c_{\text{out}})}{S} \tag{15-90}$$

For a nonlinear adsorption isotherm, such as (15-35) or (15-36), (15-85) and (15-87) are combined with the isotherm equation, but it may not be possible to express the result explicitly in q_{out}. In that event, a numerical solution is required, as illustrated below in Example 15.10.

Semicontinuous Mode

The most difficult mode to model is the semicontinuous mode, where the adsorbent is retained in the vessel, but the feed liquid enters and exits the vessel at a fixed, continuous flow rate. Both concentration, c, and loading, q, vary with time. With perfect mixing, the outlet concentration is given by (15-86), where t_{res} is the residence time of the liquid in the suspension, and c^* is related to q in the suspension by an appropriate adsorption isotherm. The variation of q in the batch of solids is given by (15-77), rewritten in terms of the

change in q, rather than c:

$$S\frac{dq}{dt} = k_L a(c_{\text{out}} - c^*)t_{\text{res}}Q \qquad (15\text{-}91)$$

where, for this mode, S is the batch mass of adsorbent in the suspension and Q is the steady, volumetric-liquid flow rate.

Both (15-91) and (15-86) involve c^*, which can be replaced by a function of instantaneous q by selecting an appropriate isotherm. The resulting two equations are then combined to eliminate c_{out}. The resulting ODE is then integrated analytically or numerically to obtain q as a function of time, from which c_{out} as a function of time can be determined from (15-86) and the isotherm. The time-average value of c_{out} is then obtained by integration of c_{out} with respect to time. These steps are illustrated in the following example. For a linear isotherm, the derivation is left as an exercise.

EXAMPLE 15.10

An aqueous solution containing 0.010 mol phenol/L is to be treated at 20°C with activated carbon to reduce the concentration of phenol to 0.00057 mol/L. From Example 4.12, the adsorption equilibrium data are well fitted to the Freundlich equation:

$$q = 2.16c^{1/4.35} \qquad (1)$$

or

$$c^* = (q/2.16)^{4.35} \qquad (2)$$

where q and c are in mmol/g and mmol/L, respectively. In terms of kmol/kg and kmol/m^3, (2) becomes

$$c^* = (q/0.01057)^{4.35} \qquad (3)$$

All three modes of slurry adsorption are to be considered. From Example 4.12, the minimum amount of adsorbent is 5 g/L of solution. Laboratory experiments with adsorbent particles 1.5 mm in diameter in a well-agitated vessel have confirmed that the rate of adsorption is controlled by external mass transfer with $k_L = k_c = 5 \times 10^{-5}$ m/s. Particle surface area is 5 m^2/kg of particles.

(a) Using twice the minimum amount of adsorbent in an agitated vessel operated in the batch mode, determine the time in minutes to reduce the phenol content to the desired value.

(b) For operation in the continuous mode with twice the minimum amount of adsorbent, determine the required residence time in minutes in the agitated vessel. How does this compare to the batch time of part (a)?

(c) For operation in the semicontinuous mode with 1,000 kg of activated carbon, a liquid feed rate of 10 m^3/h, and a liquid residence time equal to 1.5 times the value computed in part (b), determine the run time to obtain a composite liquid product with the desired phenol concentration. Are the results reasonable, or should changes be made to the specifications?

SOLUTION

(a) Batch mode:

$$S/Q = 2(5) = 10\ \text{g/L} = 10\ \text{kg/m}^3$$
$$k_L a = 5 \times 10^{-5}(5)(10) = 2.5 \times 10^{-3}\text{s}^{-1}$$
$$c_F = 0.010\ \text{mol/L} = 0.010\ \text{kmol/m}^3$$

From (15-78),

$$q = \frac{c_F - c}{S/Q} = \frac{0.010 - c}{10} \qquad (4)$$

Substituting (4) into (3),

$$c^* = \left(\frac{0.10 - c}{0.1057}\right)^{4.35} \qquad (5)$$

Substituting (5) into (15-77),

$$-\frac{dc}{dt} = 2.5 \times 10^{-3}\left[c - \left(\frac{0.010 - c}{0.1057}\right)^{4.35}\right] \qquad (6)$$

where, $c = c_F = 0.010$ kmol/m^3 at $t = 0$ and we want t for $c = 0.00057$ kmol/m^3. By numerical integration of (6), $t = 1{,}140$ s $= 19$ min.

(b) Continuous mode:

Equation (15-85) applies, where all quantities are the same as those determined in part (a) and $c_{\text{out}} = 0.00057$ kmol/m^3. Thus,

$$t_{\text{res}} = \frac{c_F - c_{\text{out}}}{k_L a(c_{\text{out}} - c^*)}$$

where c^* is given by (3) with $q = q_{\text{out}}$, and q_{out} is obtained from (15-87). Thus,

$$t_{\text{res}} = \frac{0.010 - 0.00057}{2.5 \times 10^{-3}\left[0.00057 - \left(\frac{0.010 - 0.00057}{0.1057}\right)^{4.35}\right]}$$
$$= 6{,}950\ \text{s or } 1.93\ \text{h}$$

This residence time is appreciably longer than the batch time of 1,140 s. In the batch mode, the concentration driving force for external mass transfer is initially $(c - c^*) = c_F = 0.010$ kmol/m^3 and gradually declines to a much smaller final value, at 1,140 s, of

$$(c - c^*) = c_{\text{final}} - \left(\frac{0.010 - c_{\text{final}}}{0.1057}\right)^{4.35}$$
$$= 0.000543\ \text{kmol/m}^3$$

For the continuous mode with perfect mixing in the vessel, the concentration driving force for external mass transfer is always at the final batch value of 0.000543 kmol/m^3.

(c) Semicontinuous mode:

Equation (15-91) applies with

$S = 1{,}000$ kg, $\quad c_F = 0.010$ kmol/m^3
$Q = 10$ m^3/h, $\quad t_{\text{res}} = 10{,}425$ s, $\quad k_L a = 2.5 \times 10^{-3}$ s^{-1}
c^* is given in terms of q by (3) and c_{out} is given by (15-86).

Combining (15-91), (3), and (15-86) to eliminate c^* and c_{out} gives, after simplification,

$$\frac{dq}{dt} = \left(\frac{\gamma}{1+\gamma}\right)\frac{Q}{S}\left[c_F - \left(\frac{q}{0.01057}\right)^{4.35}\right] \qquad (7)$$

where γ is given by (15-89) and the time, t, is the time that the adsorbent remains in the vessel. For values of γ, Q/S, and c_F equal, respectively, to 26.06, 0.01 m^3/h-kg, and 0.010 kmol/m^3, (7) reduces to

$$\frac{dq}{dt} = 0.00963\left[0.010 - \left(\frac{q}{0.01057}\right)^{4.35}\right] \qquad (8)$$

where t is in hours and q is in kmol. By numerical integration of (8), starting from $q = 0$ at $t = 0$, we obtain q as a function of t as given in Table 15.8. Included are corresponding values of

Table 15.8 Results for Part (c), Semicontinuous Mode, of Example 15.10

		kmol/m^3	
Time t, h	q, kmol/kg	c_{out}	c_{cum}
0.0	0.0	0.000370	0.000370
5.0	0.000481	0.000371	0.000370
10.0	0.000962	0.000398	0.000375
15.0	0.001440	0.000535	0.000401
15.7	0.001506	0.000570	0.000407
20.0	0.001905	0.000928	0.000476
21.0	0.001995	0.001052	0.000501
22.0	0.002084	0.001195	0.000529
23.0	0.002172	0.001356	0.000561
23.2	0.002189	0.001390	0.000568
23.3	0.002197	0.001407	0.000572

c_{out} computed from (15-86) combined with (3) to eliminate c^*:

$$c_{out} = \frac{c_F + \gamma(q/0.01057)^{4.35}}{1+\gamma} = \frac{0.010 + 26.06(q/0.01057)^{4.35}}{27.06}$$

Also included in Table 15.8 are the cumulative values of c, for all of the liquid effluent that exits the vessel during the period from $t = 0$ to $t = t$, as obtained by integrating c_{out} with respect to time: $c_{cum} = \int_0^t c_{out}\, dt/t$.

From the results in Table 15.8, it is seen that the loading, q, increases almost linearly during the first 10 h, while the instantaneous phenol concentration c_{out} in the exiting liquid remains almost constant. At 15.7 h, c_{out} has increased to the specified value of 0.00057 kmol/m^3, but c_{cum} is only 0.000407 kmol/m^3. Therefore, the operation can continue. Finally, at between 23.2 and 23.3 h, c_{cum} reaches 0.00057 kmol/m^3 and the operation must be terminated. During operation, the vessel contains 1,000 kg or 2 m^3 of adsorbent particles. With a liquid residence time of almost 3 h, the vessel must contain 10(3) = 30 m^3. Thus, the vol% solids in the agitated vessel is 6.7. This is reasonable. If the mass of adsorbent in the vessel is increased to 2,000 kg, giving almost 12 vol% solids, the time of operation is doubled to 46.5 h.

Fixed-Bed Adsorption (Percolation)

In the continuous and semicontinuous modes of operation in slurry adsorption, the liquid exiting the vessel always contains unadsorbed solute. If a fixed bed is used, it is possible to obtain a nearly solute-free liquid or gas effluent until the adsorbent in the bed approaches saturation. A fixed bed is frequently used for gas purification and bulk separation.

Consider the flow, down through a fixed bed of adsorbent, of a fluid containing an adsorbable component (the solute). If (1) external and internal mass-transfer resistances are very small; (2) plug flow is achieved; (3) axial dispersion is negligible; (4) the adsorbent is initially free of adsorbate; and (5) the adsorption isotherm begins at the origin, then local equilibrium between the fluid and the adsorbent is achieved instantaneously, resulting, as shown in Figure 15.27, in a shock like wave, called a *stoichiometric front,* that moves as a sharp concentration front through the bed. This is *ideal (local equilibrium) fixed-bed adsorption.* Upstream of the front, the adsorbent is saturated with adsorbate and the concentration of solute in the fluid is that of the feed, c_F. The loading of adsorbate on the adsorbent is the q_F in equilibrium with c_F. The length (height) and weight of the bed section upstream of the front are LES and WES, respectively, where ES refers to the equilibrium section, called the *equilibrium zone.*

In the upstream region, the adsorbent is spent. Downstream of the stoichiometric front and in the exit fluid, the concentration of the solute in the fluid is zero, and the adsorbent is still adsorbate-free. In this section of the bed, the length and weight are LUB and WUB, respectively, where UB refers to unused bed.

After a period of time, called the *stoichiometric time,* the stoichiometric wave front reaches the end of the bed, the concentration of the solute in the fluid abruptly rises to the inlet value, c_F, no further adsorption is possible, and the adsorption step is terminated. This point is referred to as the *breakpoint* and the stoichiometric wave front becomes the ideal *breakthrough* curve.

For ideal fixed-bed adsorption, the location of the concentration wave front L, in Figure 15.27, as a function of time, is obtained solely by material balance and adsorption equilibrium considerations. Thus, at equilibrium, the loading in equilibrium with the feed is designated by $q_F = f\{c_F\}$, where $f\{c_F\}$ is given by an appropriate adsorption isotherm. By material balance on the adsorbate before breakthrough occurs: Solute in entering feed = adsorbate. Accordingly:

$$Q_F c_F t_{ideal} = q_F S L_{ideal}/L_B \qquad (15\text{-}92)$$

where Q_F is the volumetric flow rate of feed, c_F is the concentration of the solute in the feed, t_{ideal} is the time for an

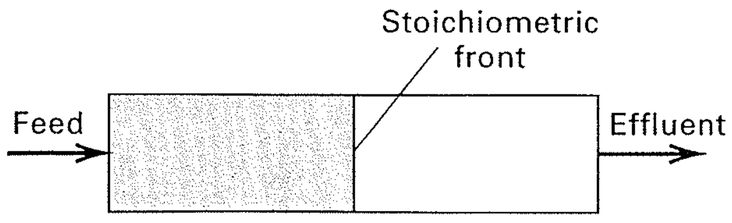

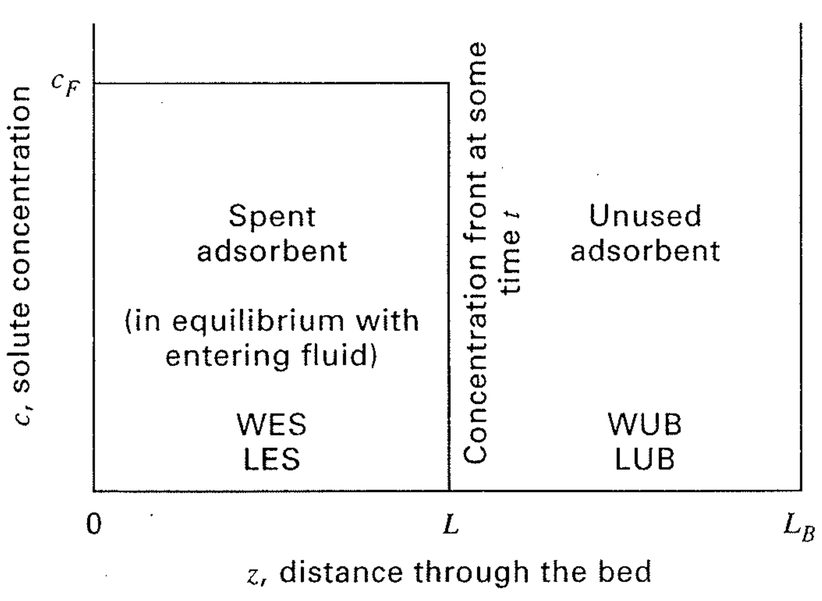

Figure 15.27 Stoichiometric (equilibrium) concentration front for ideal fixed-bed adsorption.

ideal front to reach $L_{\text{ideal}} < L_B$, q_F is the loading per unit mass of adsorbent that is in equilibrium with the feed concentration, S is the total mass of adsorbent in the bed, and L_B is the total bed length.

$$L_{\text{ideal}} = \text{LES} = \left(\frac{Q_F c_F t_{\text{ideal}}}{q_F S}\right) L_B \tag{15-93}$$

$$\text{LUB} = L_B - \text{LES} \tag{15-94}$$

$$\text{WES} = S\left(\frac{\text{LES}}{L_B}\right) \tag{15-95}$$

$$\text{WUB} = S - \text{WES} \tag{15-96}$$

In a real fixed-bed adsorber, the assumptions leading to (15-92) are not valid. Internal transport resistance and, in some cases, external transport resistance are finite. Axial dispersion can also be significant, particularly at low flow rates in shallow beds. These factors contribute to the development of broad concentration fronts like those in Figure 15.28. In Figure 15.28a, typical solute concentration profiles for the fluid are shown as a function of distance through the bed at increasing times t_1, t_2, and t_b from the start of flow through the bed. At t_1, no part of the bed is saturated. At t_2, the bed is almost saturated for a distance L_s. At L_f, the bed is almost clean. Beyond L_f, little mass transfer occurs at t_2 and the adsorbent is still unused. The region between L_s and L_f is called the mass-transfer zone, MTZ at t_2, where adsorption takes place. Because it is difficult to determine where the MTZ zone begins and ends, L_f can be taken where $c/c_F = 0.05$, with L_s at $c/c_F = 0.95$. From time t_2 to time t_b, the S-shaped front moves through the bed. At t_b, the leading point of the MTZ just reaches the end of the bed. This is the breakthrough point. Rather than using $c/c_F = 0.05$, the breakthrough concentration can be taken as the minimum detectable or maximum allowable solute concentration in the effluent fluid.

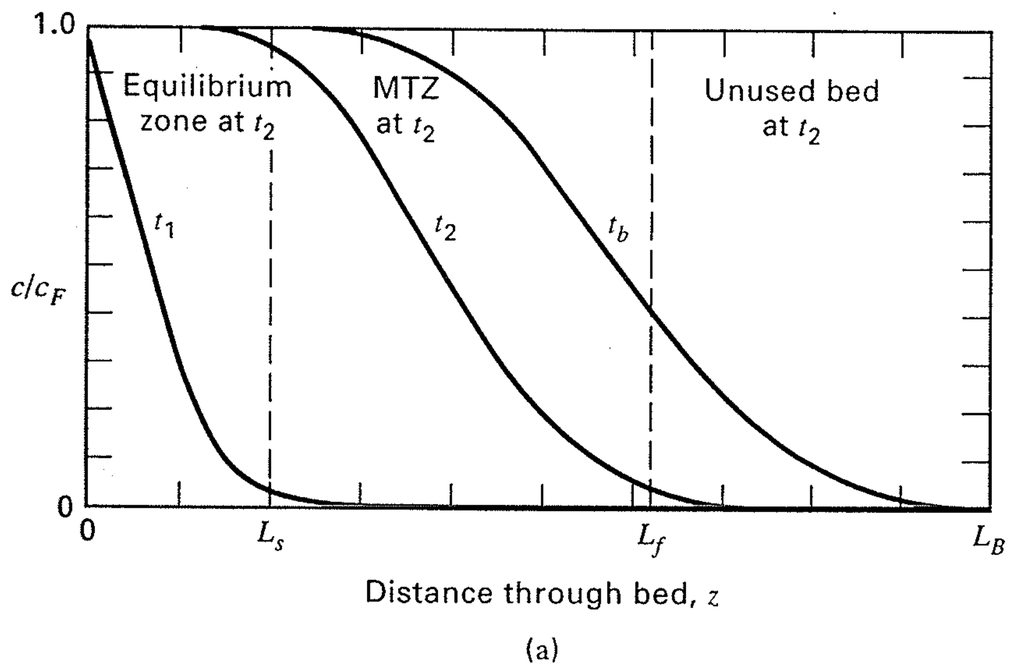

Figure 15.28 Solute wave fronts in a fixed-bed adsorber with mass-transfer effects. (a) Concentration–distance profiles. (b) Breakthrough curve.

Figure 15.28b is a typical plot of the ratio of the outlet-to-inlet solute concentration in the fluid as a function of time from the start of flow. The S-shaped curve is called the breakthrough curve. Prior to t_b, the outlet solute concentration is less than some maximum permissible value, say, $c_{\text{out}}/c_F = 0.05$. At t_b, this value is reached, the adsorption step is discontinued, and the regeneration part of the cycle is initiated or the spent adsorbent is discarded. If the adsorption step were to be continued for $t > t_b$, the outlet solute concentration would be observed to rise rapidly, eventually approaching the inlet concentration as the outlet end of the bed became saturated. The time to reach $c_{\text{out}}/c_F = 0.95$ is designated t_e.

The steepness of the breakthrough curve determines the extent to which the capacity of an adsorbent bed can be utilized. Thus, the shape of the curve is very important in determining the length of an adsorption bed. For the ideal case, with a stoichiometric wave front, (15-92) applies and all of the bed is utilized before breakthrough occurs. As the width of the breakthrough curve and the corresponding width of the MTZ for the concentration profiles increase, less and less of the bed capacity can be utilized. The situation is further complicated by the fact that the steepness of the concentration profiles shown in Figure 15.28a increases or decreases with time, depending on the shape of the adsorption isotherm, as shown by DeVault [73], in the following manner.

Assume: (1) plug flow of the fluid through the bed at a constant actual (interstitial) velocity, u; (2) instantaneous equilibrium of the solute in the bulk fluid with the adsorbate; (3) no axial dispersion; and (4) isothermal conditions. The bed is not initially free of adsorbate and/or the feed to the bed starting at time $t = 0$ is not at constant composition. The superficial fluid velocity is $\epsilon_b\, u$. A mass balance on the solute for the flow of fluid through a differential adsorption-bed length, dz, over a differential-time duration, dt, gives

$$\epsilon_b u A_b c|_z = \epsilon_b u A_b c|_{z+\Delta z} + \epsilon_b A_b \Delta z \frac{\partial c}{\partial t} + (1-\epsilon_b) A_b \Delta z \frac{\partial q}{\partial t} \tag{15-97}$$

Dividing by Δz and taking the limit as $\Delta z \to 0$ gives

$$\frac{\partial c}{\partial t} + u\frac{\partial c}{\partial z} + \frac{(1-\epsilon_b)}{\epsilon_b}\frac{\partial q}{\partial t} = 0 \tag{15-98}$$

where q is the adsorption loading/unit volume of adsorbent particles, given by an appropriate adsorption isotherm. By the chain rule:

$$\frac{\partial q}{\partial t} = \frac{\partial q}{\partial c}\frac{\partial c}{\partial t} \tag{15-99}$$

This hyperbolic PDE (15-98) gives $c = f\{z, t\}$. Therefore, by the rules of implicit partial differentiation:

$$u_c = \left(\frac{\partial z}{\partial t}\right)_c = -\frac{\left(\frac{\partial c}{\partial t}\right)}{\left(\frac{\partial c}{\partial z}\right)} \qquad (15\text{-}100)$$

where u_c is the velocity of the concentration wave front, $\partial z/\partial t$ at constant c. Combining (15-98) to (15-100):

$$u_c = \frac{u}{1 + \left(\frac{1-\epsilon_b}{\epsilon_b}\right)\frac{dq}{dc}} \qquad (15\text{-}101)$$

This equation gives the velocity of the concentration wave front for the solute in terms of the interstitial fluid velocity and the slope, dq/dc, of the adsorption isotherm. If dq/dc is constant, the wave front moves at a constant value.

In general, the concentration wave front moves through the bed at a velocity, u_c, that is much less than the interstitial fluid velocity. For example, suppose that $\epsilon_b = 0.5$ and the equilibrium adsorption isotherm is given by $q = 5{,}000c$. Then $dq/dc = 5{,}000$. Then, from (15-101), $u_c/u = 0.0002$. If the interstitial velocity is 3 ft/s, the velocity of the concentration wave front is only 0.0006 ft/s. If the bed were 6 ft in height, it would take 2.78 h for the concentration wave front to pass through the bed. If the adsorption isotherm is curved, regions of the wave front at a higher concentration move at a velocity different from regions at a lower concentration. Thus, for a linear isotherm (curve A in Figure 15.29a), the width of the MTZ and the wave pattern remain constant. For a favorable isotherm of the Freundlich or Langmuir type (curve B in Figure 15.29a), high-concentration regions move faster than low-concentration regions, and the wavefront steepens with time until a constant pattern front (CPF) is developed, as shown in Figure 15.29b. For the much less common unfavorable type of isotherm (Curve C in Figure 15.29a), low-concentration regions travel faster and the wavefront broadens with time.

For the general case where external and internal mass-transfer resistances are finite and/or axial dispersion is not negligible, methods for predicting concentration profiles and breakthrough curves have been the subject of much study. As will be shown, when mass-transfer resistances are a factor, the concentration fronts develop quite differently from the equilibrium fronts just described. Solutions for a number of simplified cases are discussed in detail by Ruthven [10]. The PDE for the governing dynamic behavior is a modification of (15-98):

$$-D_L\frac{\partial^2 c}{\partial z^2} + \frac{\partial(uc)}{\partial z} + \frac{\partial c}{\partial t} + \frac{(1-\epsilon_b)}{\epsilon_b}\frac{\partial \bar{q}}{\partial t} = 0 \qquad (15\text{-}102)$$

where the first term accounts for axial dispersion with eddy diffusivity D_L, the second term permits an axial variation in fluid velocity, and the fourth term is now based on $\bar{q}$, the volume-average adsorbate loading per unit mass. Thus, the latter term accounts for the variation of q throughout the adsorbent particle, due to internal mass-transfer resistance, by averaging the rate of adsorption over the adsorbent particle. The volume-average adsorbate loading for a spherical particle is given by

$$\bar{q} = \left(\frac{3}{R_p^3}\right)\int_0^{R_p} r^2 q\, dr \qquad (15\text{-}103)$$

where R_p is the radius of the adsorbent particle.

Equation (15-102) gives the concentration of solute in the bulk fluid as a function of time and location in the bed. Equation (15-68) gives the concentration of the solute in the fluid within the pores of an adsorbent particle. These two equations are coupled together by the continuity condition at the particle surface:

$$D_e\left(\frac{\partial c}{\partial r}\right)_{R_P} = k_c(c - c_{R_P}) \qquad (15\text{-}104)$$

where k_c is the external mass-transfer coefficient and D_e is the effective diffusivity in the particle, as discussed in Section 15.3. The simultaneous solution of (15-102), (15-103), (15-68), and (15-104) is a formidable task, which can be avoided by using the linear-driving-force (LDF) model formulated by Glueckauf [74, 75] and discussed in detail by Yang [25] and Ruthven [10]. This model, which is widely used to simulate and design fixed-bed adsorption, is based on the following relation, which replaces (15-68) and (15-104):

$$\frac{\partial \bar{q}}{\partial t} = k(q^* - \bar{q}) = kK(c - c^*) \qquad (15\text{-}105)$$

where q^* is the adsorbate loading in equilibrium with the solute concentration, c, in the bulk fluid; c^* is the concentration in equilibrium with average loading $\bar{q}$; k is the overall mass-transfer coefficient, which includes both external- and internal-transport resistances; and K is the adsorption-

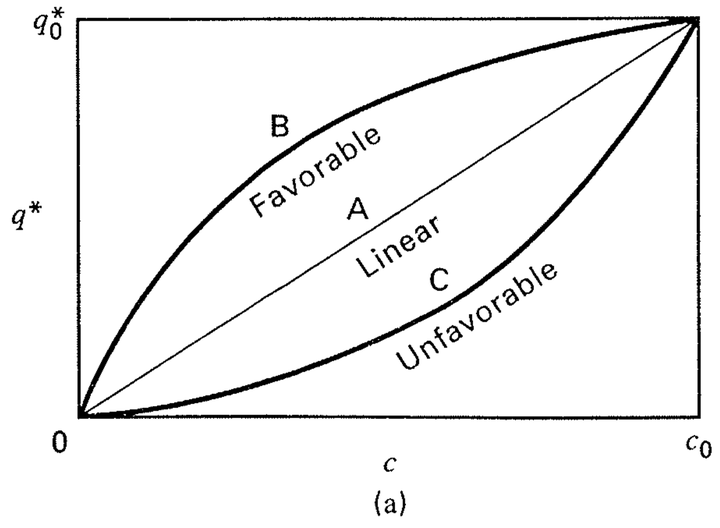

Figure 15.29 Effect of shape of isotherm on sharpness of concentration wavefront. (a) Isotherm shapes. (b) Self-sharpening wavefront caused by a favorable adsorption isotherm.

equilibrium constant for a linear adsorption isotherm of the form $q = Kc$.

A suitable relationship for the factor kK is

$$\frac{1}{kK} = \frac{R_p}{3k_c} + \frac{R_p^2}{15D_e} \tag{15-106}$$

where the first term on the RHS represents the external mass-transfer resistance, $k_c\, a_v$, since for a sphere, the surface area/unit volume, a_v, is given by

$$4\pi R_p^2 / \left[(4/3)\pi R_p^3\right] = 3/R_p$$

The second term in (15-106) represents the internal resistance, which was first developed by Glueckauf [75], but can also be derived by assuming a parabolic adsorbate loading profile, in the particle, as shown by Liaw et al. [76]. Thus, let

$$q = a_0 + a_1 r + a_2 r^2 \tag{15-107}$$

where the constants a_i depend on time and location in the bed, but are independent of r. Because $\partial q/\partial r = 0$ at $r = 0$ (symmetry condition), $a_1 = 0$. Equating Fick's first law for diffusion into the particle at the particle surface, to the rate of accumulation of adsorbate within the particle, assuming that effective diffusivity is independent of concentration, we obtain

$$\frac{\partial \bar{q}}{\partial t} = D_e a_v \left.\frac{\partial q}{\partial r}\right|_{r=R_p} = \frac{3D_e}{R_p} \left.\frac{\partial q}{\partial r}\right|_{r=R_p} \tag{15-108}$$

At the particle surface, from (15-107):

$$q_{R_p} = a_0 + a_2 R_p^2 \tag{15-109}$$

Substituting (15-107) with $a_1 = 0$ into (15-103) and integrating gives

$$\bar{q} = a_0 + \frac{3}{5} a_2 R_p^2 \tag{15-110}$$

Combining (15-109) and (15-110) to eliminate a_0 gives

$$a_2 = \frac{5}{2R_p^2}(q_{R_p} - \bar{q}) \tag{15-111}$$

From (15-107):

$$\left.\frac{\partial q}{\partial r}\right|_{r=R_p} = 2a_2 R_p \tag{15-112}$$

Combining (15-110), (15-111), and (15-108):

$$\frac{\partial \bar{q}}{\partial t} = \frac{15D_e}{R_p^2}(q_{R_p} - \bar{q}) \tag{15-113}$$

Comparing (15-105) with (15-113), we see that the internal resistance is given by the second term in (15-106).

The analytical solution of a simplified form of (15-102), which assumes negligible axial dispersion, constant fluid velocity, u, and the LDF mass-transfer model, is summarized by Ruthven [10] and discussed in detail by Klinkenberg [77]. The solution was first obtained in terms of Bessel functions by Anzelius [78] for the analogous problem of heating or cooling a packed bed of depth z with a fluid. A useful approximate solution is that of Klinkenberg [79]:

$$\frac{c}{c_F} \approx \frac{1}{2}\left[1 + \text{erf}\left(\sqrt{\tau} - \sqrt{\xi} + \frac{1}{8\sqrt{\tau}} + \frac{1}{8\sqrt{\xi}}\right)\right] \tag{15-114}$$

where

$$\xi = \frac{kKz}{u}\left(\frac{1-\epsilon_b}{\epsilon_b}\right) = \text{Dimensionless distance coordinate} \tag{15-115}$$

$$\tau = k\left(t - \frac{z}{u}\right) = \text{Dimensionless time coordinate corrected for displacement} \tag{15-116}$$

$$\text{erf}(-x) = -\text{erf}(x) \tag{15-117}$$

$$\text{erf}(x) = \frac{2}{\sqrt{\pi}} \int_0^x e^{-\eta^2} d\eta \tag{15-118}$$

where ξ and τ are coordinate transformations for z and t, which convert the equations to a much simpler form. The approximation (15-114) is accurate to <0.6% error for $\xi > 2.0$. The erf(x), which is included as a function in most spreadsheet programs, is 0.0 at $x = 0$ and asymptotically approaches a value of 1.0 for $x > 2.0$, where x is a dummy variable.

Klinkenberg [79] also includes the following approximate solution for profiles of solute concentration in equilibrium with the average sorbent loading:

$$\frac{c^*}{c_F} = \frac{\bar{q}}{q_F^*} \approx \frac{1}{2}\left[1 + \text{erf}\left(\sqrt{\tau} - \sqrt{\xi} - \frac{1}{8\sqrt{\tau}} - \frac{1}{8\sqrt{\xi}}\right)\right] \tag{15-119}$$

where $c^* = \bar{q}/K$ and $c^*/c_F = \bar{q}/q_F^*$, where q_F^* is the loading in equilibrium with c_F.

EXAMPLE 15.11

Air at 70°F and 1 atm, containing 0.9 mol% benzene, enters a fixed-bed adsorption tower at a flow rate of 23.6 lb/min. The tower is 2 ft in inside diameter and is packed to a height of 6 ft with 735 lb of 4 × 6 mesh silica gel (SG) particles having an effective diameter of 0.26 cm and an external void fraction of 0.5. The adsorption isotherm for benzene has been experimentally determined for the conditions of interest and found to be linear over the concentration range of interest, as given by

$$q = Kc^* = 5{,}120\, c^* \tag{1}$$

where

q = lb benzene adsorbed per ft^3 of silica gel particles

c^* = equilibrium concentration of benzene in the gas, in lb benzene per ft^3 of gas

Mass-transfer experiments, simulating the conditions of the 2-foot-diameter bed, have been carried out and fitted to a linear-driving-force (LDF) model:

$$\frac{\partial \bar{q}}{\partial t} = 0.206K(c - c^*) \tag{2}$$

where time is in minutes. The constant $k = 0.206$ min^{-1} includes resistances both in the gas film and in the adsorbent pores, with the latter resistance dominant.

Using the approximate concentration-profile equations of Klinkenberg [77], compute a set of breakthrough curves and determine the time when the concentration of benzene in the exiting air rises to 5% of the inlet concentration. Assume isothermal and isobaric operation. Compare the breakthrough time with the time predicted by the equilibrium model.

SOLUTION

For the equilibrium model, the bed becomes completely saturated with benzene at the inlet concentration.

MW of entering gas $= 0.009(78) + 0.991(29) = 29.44$
Density of entering gas $= (1)(29.44)/(0.730)(530) = 0.076$ lb/ft^3
Gas flow rate $= 23.6/0.0761 = 310$ ft^3/min

$$\text{Benzene flow rate in entering gas} = \frac{(23.6)}{29.44}(0.009)(78)$$
$$= 0.562 \text{ lb/min}$$

or

$$c_F = \frac{0.562}{310} = 0.00181 \text{ lb benzene/ft}^3 \text{ of gas}$$

From (1),

$$q = 5{,}120(0.00181) = 9.27 \frac{\text{lb benzene}}{\text{ft}^3 \text{ SG}}$$

The total adsorption of benzene at equilibrium

$$= \frac{9.27(3.14)(2)^2(6)(0.5)}{4} = 87.3 \text{ lb}$$

$$\text{Time of operation} = \frac{87.3}{0.562} = 155 \text{ min}$$

For the actual operation, taking into account external and internal mass-transfer resistances, from (15-115) and (15-116),

$$\xi = \frac{(0.206)(5{,}120)z}{u}\left(\frac{1-0.5}{0.5}\right) = 1{,}055\, z/u$$

$$u = \text{interstitial velocity} = \frac{310}{0.5\left(\frac{3.14 \times 2^2}{4}\right)} = 197 \text{ ft/min} \qquad (3)$$

$$\xi = \frac{1{,}055}{197} z = 5.36z$$

where z is in feet.

$$\text{When } z = \text{bed height} = 6 \text{ ft}, \xi = 32.2 \text{ and } \tau = 0.206\left(t - \frac{z}{197}\right) \qquad (4)$$

where t is in minutes. For $t = 155$ min (the ideal time), and $z = 6$ ft (the bed height), using (4), $\tau = 32$.

Thus, breakthrough curves should be computed from (15-114) for values of τ and ξ no greater than about 32. For example, when $\xi = 32.2$ (exit end of the bed), and $\tau = 30$, which corresponds to a time $t = 145.7$ minutes, the concentration of benzene in the exiting gas, from (15-114), is

$$\frac{c}{c_F} = \frac{1}{2}\left[1 + \text{erf}\left(30^{0.5} - 32.2^{0.5} + \frac{1}{8(30)^{0.5}} + \frac{1}{8(32.2)^{0.5}}\right)\right]$$
$$= \frac{1}{2}[1 + \text{erf}(-0.1524)] = \frac{1}{2}\text{erfc}(0.1524)$$
$$= 0.4147 \text{ or } 41.47\%$$

This far exceeds the specification of $c/c_F = 0.05$ or 5% at the exit. Thus, the time of operation of the bed is considerably less than the ideal time of 155 min. Figure 15.30 shows breakthrough curves computed from (15-114) over a range of the dimensionless time, τ, for values of the dimensionless distance, ξ, of 2, 5, 10, 15, 20, 25, 30, and 32.2, where the latter corresponds to the exit end of the bed. For $c/c_F = 0.05$ and $\xi = 32.2$, τ is seen to be about 20 (19.9 by calculation).

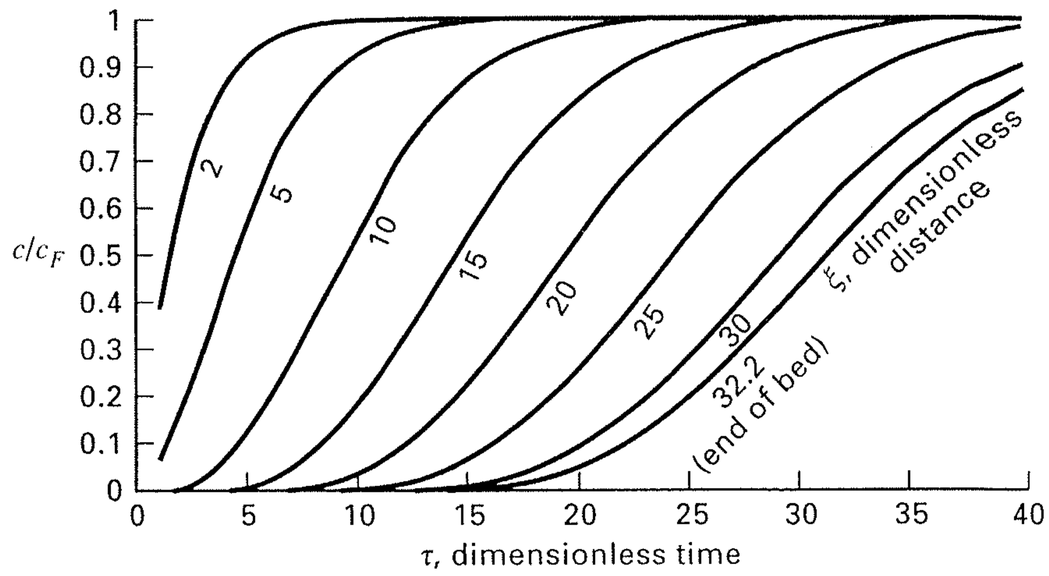

Figure 15.30 Gas concentration breakthrough curves for Example 15.11.

From (4), with $z = 6$ ft, the time to breakthrough is $t = \frac{20}{0.206} + \frac{6}{197} = 97.1$ min which is 62.3% of the ideal time.

Figure 15.30 or (15-114) can be used to compute the bulk concentration of benzene at various locations in the bed for $\tau = 20$. The results are as follows:

ξ	z, ft	c/c_F
2	0.373	1.00000
5	0.932	0.99948
10	1.863	0.97428
15	2.795	0.82446
20	3.727	0.53151
25	4.658	0.25091
30	5.590	0.08857
32.2	6.000	0.05158

We can also compute, at $\tau = 20$, the adsorbent loading, at various positions in the bed, from (15-119), using $q = 5{,}120c$. The maximum loading corresponds to c_F. Thus, $q_{\max} = 9.28$ lb benzene/ft^3 of SG. Breakthrough curves for the solid loading are plotted in Figure 15.31. As expected, those curves are displaced to the right

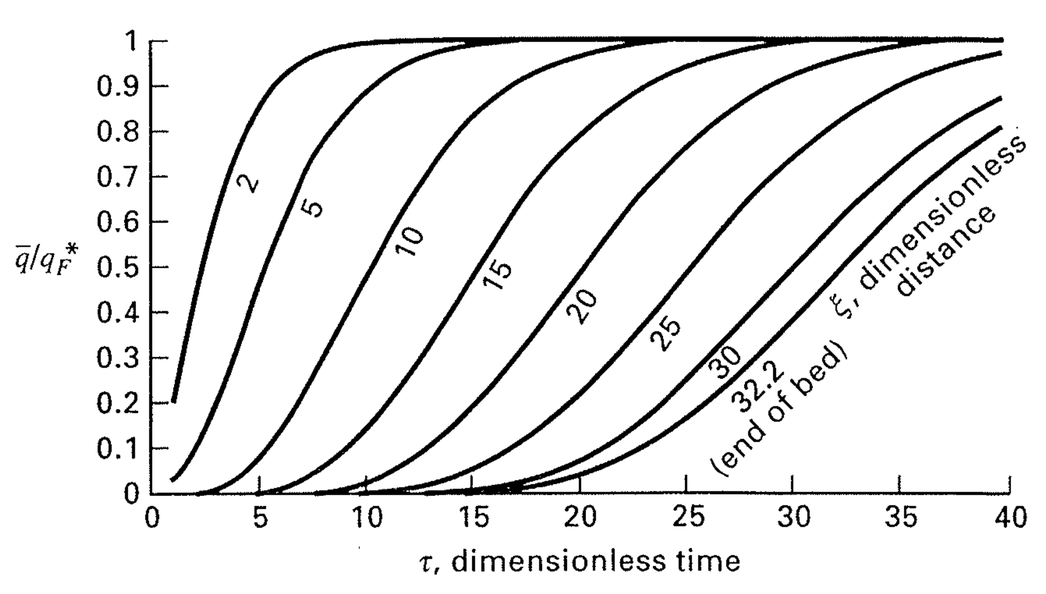

Figure 15.31 Adsorbent loading breakthrough curves for Example 15.11.

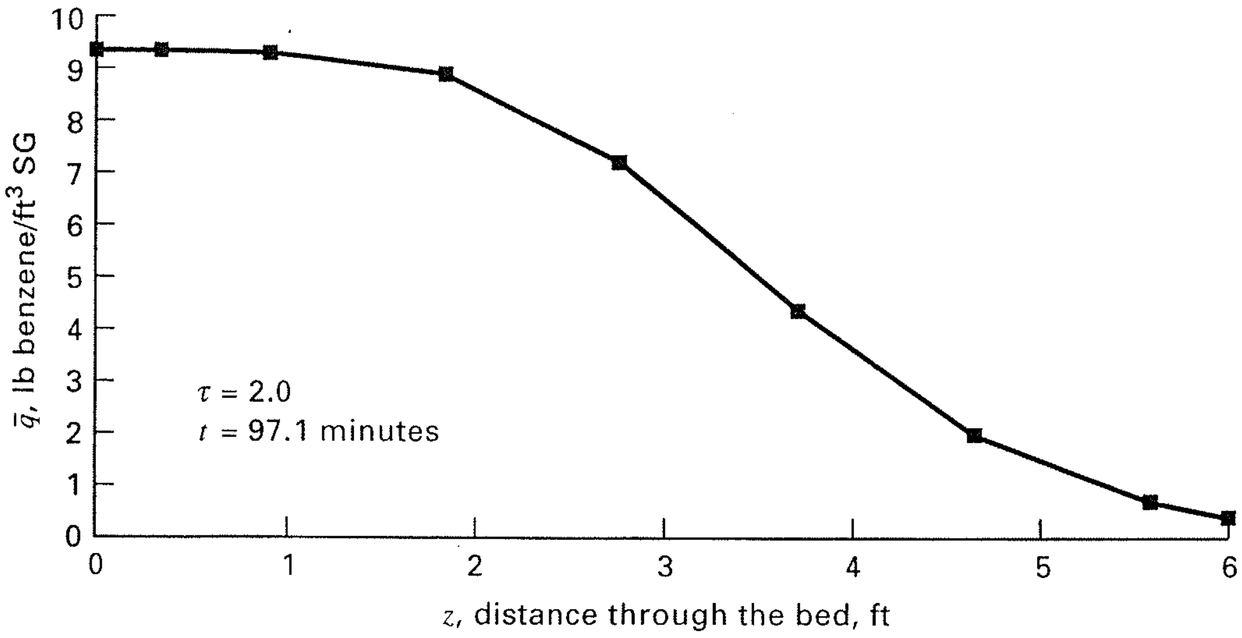

Figure 15.32 Adsorbent loading profile for Example 15.11.

from the curves of Figure 15.30. At $\tau = 20$:

ξ	z, ft	$\frac{c^*}{c_F} = \frac{\bar{q}}{q_F^*}$	$\bar{q}$, $\frac{\text{lb benzene}}{\text{ft}^3\text{SG}}$
2	0.373	0.99998	9.28
5	0.932	0.99883	9.27
10	1.863	0.96054	8.91
15	2.795	0.77702	7.21
20	3.727	0.46849	4.35
25	4.658	0.20571	1.909
30	5.590	0.06769	0.628
32.2	6.000	0.03827	0.355

The values of $\bar{q}$ in the preceding table are plotted in Figure 15.32 and integrated over the 6-foot bed length to obtain the average bed loading:

$$\bar{q}_{\text{avg}} = \int_0^6 \bar{q}dz/6$$

The result is 5.72 lb benzene/ft^3 of SG, which is 61.6% of the maximum loading based on the inlet benzene concentration.

If the bed were increased in height by a factor of 5, to 30 ft, $\xi = 161$. The ideal time of operation would be 780 min or 13 h. With mass-transfer effects taken into account, as before, the dimensionless operating time to breakthrough is computed to be $\tau = 132$, or breakthrough time from (4) is

$$t = \frac{132}{0.206} + \frac{30}{197} = 641 \text{ min}$$

which is 82.2% of the ideal time. This represents a substantial increase in bed utilization.

Scale-up for Constant-Pattern Front

In Example 15.11, the wavefront (of the type shown in Figure 15.28a), broadens as it moves through the bed. This is shown in Figure 15.33, where MTZ, the width of the mass-transfer zone, is plotted against the dimensionless time, τ, up to the value of 20 where the front breaks through the 6-foot-long bed. The MTZ in Figure 15.33 is based on a range of c/c_F from 0.95 to 0.05. As seen, MTZ increases from about 2 feet at $\tau = 6$ to about 4 feet at $\tau = 20$. As shown, with increasing τ, the rate of broadening slows. However, for a deeper bed, it is found that even at $\tau = 100$, the wavefront is still slowly broadening.

The continual broadening of the wavefront determined in Example 15.11 is typical of that obtained with a linear adsorption isotherm (curve A in Figure 15.29a). The wavefront also continues to broaden with an unfavorable isotherm (curve C in Figure 15.29a). But, when the isotherm is of the favorable Langmuir or Freundlich type (curve B in Figure 15.29a), wavefront broadening rapidly diminishes and an asymptotic or *constant-pattern front* (CPF) is developed. For such a front, MTZ becomes constant and curves of c/c_F and $\bar{q}/q^*$ become coincident.

The bed depth at which the CPF is approached depends upon the nonlinearity of the adsorption isotherm and the importance of adsorption kinetics. The mathematical proof of the existence of an asymptotic wavefront solution is given by Cooney and Lightfoot [80], including the case of axial dispersion. Initially, the wavefront broadens because of mass-transfer resistance and/or axial dispersion. Eventually, the opposite influence of a favorable isotherm, as shown in Figure 15.29b, comes into play and an asymptotic wavefront pattern is approached. For a constant-pattern front, Sircar and Kumar [81] present some analytical solutions and Cooney [82] presents a rapid approximate method, illustrated with the Freundlich and Langmuir isotherms, to estimate concentration profiles and breakthrough curves when mass-transfer and equilibrium parameters are available.

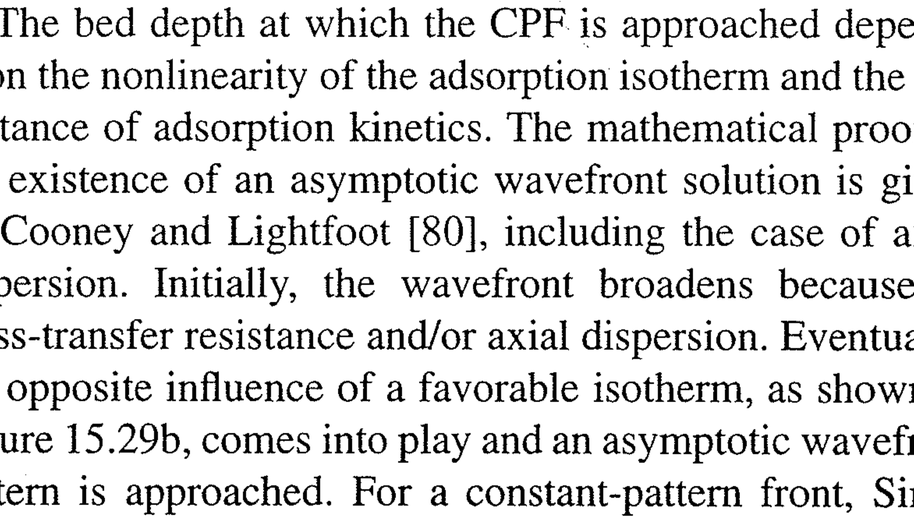

Figure 15.33 Broadening of wavefront in Example 15.11.

When the constant-pattern-front assumption is valid, it can be used to determine the length of a full-scale adsorbent bed from breakthrough curves obtained in small-scale laboratory experiments. This widely used technique is described by Collins [83] for purification applications. The adsorbent bed is considered to be the sum of two sections, analogous to those mentioned for ideal, fixed-bed adsorption. Thus, the total bed length is estimated to be the sum of the length, LES, of the ideal, fixed-bed adsorber plus an additional length, called the LUB, that depends on the observed width of the MTZ and the shape of the c/c_F profile within that zone. The total required bed length is

$$L_B = \text{LES} + \text{LUB} \tag{15-120}$$

For the ideal, fixed-bed adsorber, with MTZ = 0, LUB is not necessary, but if $L_B >$ LES, then LUB is the length of unused bed. However, when an MTZ is present, then an LUB is necessary and is referred to as the equivalent length of unused bed. To determine LUB from an experimental breakthrough curve, for the same feed composition and superficial velocity to be used in the commercial adsorber, and for a CPF, the front is located such that in Figure 15.34, area A is equal to area B. Then:

$$\text{LUB} = \text{Ideal wavefront velocity} \times (t_s - t_b) = \frac{L_e}{t_s}(t_s - t_b) \tag{15-121}$$

where L_e is the length of the experimental bed. For the ideal case, a solute mass balance for a cylindrical bed of diameter D gives

$$c_F Q_F t = q_F \rho_b \pi \frac{D^2}{4}(\text{LES}) \tag{15-122}$$

where t is the time to breakthrough, from which the LES can be determined.

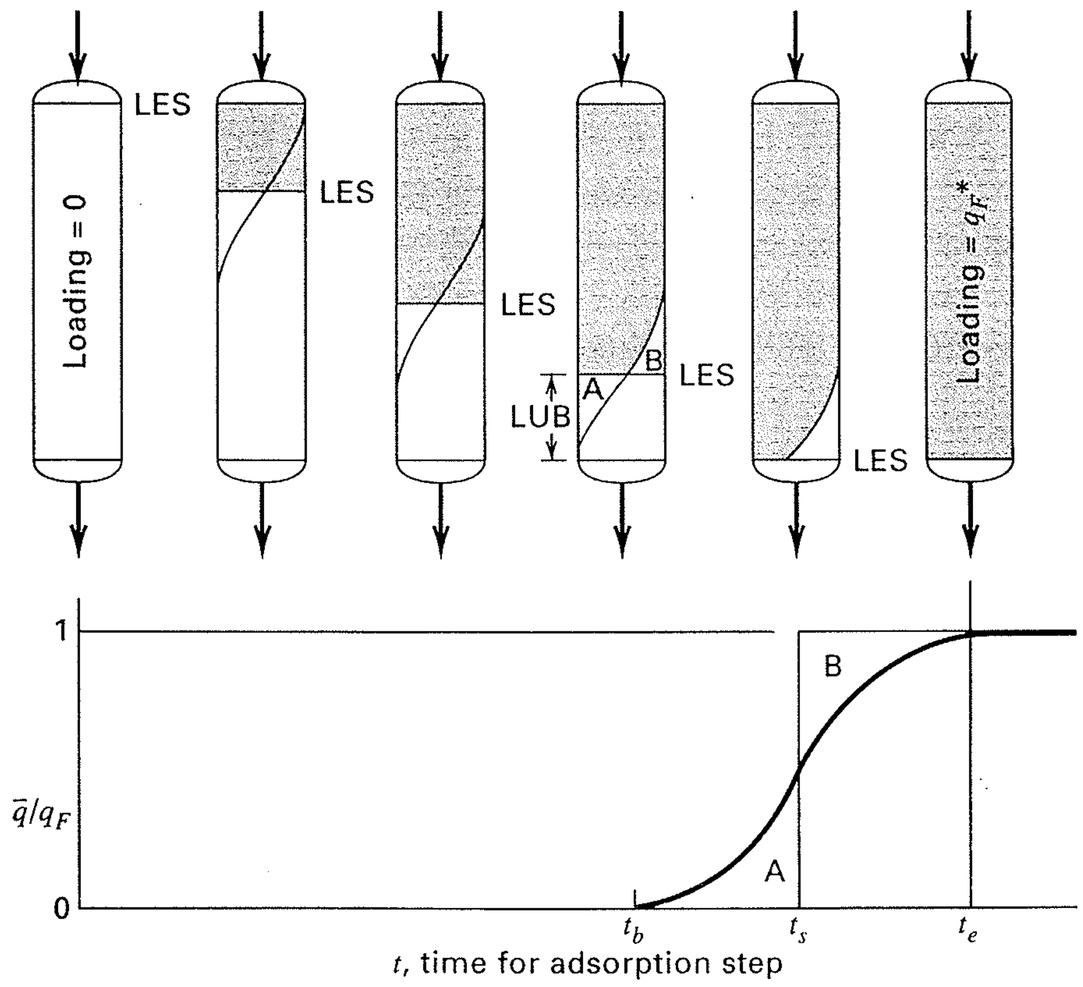

Figure 15.34 Determination of bed length from laboratory measurements.

Instead of positioning the stoichiometric front for equal areas in Figure 15.34, the LUB can be determined from the experimental breakthrough-curve data by computing t_s from

$$t_s = \int_0^{t_e} \left(1 - \frac{c}{c_F}\right) dt \tag{15-123}$$

If, in Figure 15.34, t_s is located midway between t_b and t_e, such that the shape of the experimental breakthrough curve below area B is equivalent to the curve above area A, then $LUB = \text{MTZ}/2$, i.e., one-half of the width of the mass-transfer zone. In the absence of experimental breakthrough data, a conservative estimate of MTZ is 4 ft.

EXAMPLE 15.12

Collins [83] presents the following experimental data for the adsorption of water vapor from nitrogen in a fixed bed of 4A molecular sieves:

Bed depth = 0.88 ft, temperature = 83°F (negligible temperature change), pressure = 86 psia (negligible pressure drop), G = entering gas molar velocity = 29.6 lbmol/h-ft^2, entering water content = 1,440 ppm (by volume), initial adsorbent loading = 1 lb/100 lb sieves, and bulk density of bed = 44.5 lb/ft^3. For the entering gas moisture content, c_F, the equilibrium loading, q_F, = 0.186 lb H_2O/lb solid.

c_{exit}, ppm (by volume)	Time, h	c_{exit}, ppm (by volume)	Time, h
<1	0–9.0	650	10.8
1	9.0	808	11.0
4	9.2	980	11.25
9	9.4	1,115	11.5
33	9.6	1,235	11.75
80	9.8	1,330	12.0
142	10.0	1,410	12.5
238	10.2	1,440	12.8
365	10.4	1,440	13.0
498	10.6		

Determine the bed height required for a commercial unit to be operated at the same temperature, pressure, and entering gas mass velocity and water content to obtain an exiting gas with no more than 9 ppm (by volume) of water vapor with a breakthrough time of 20 h.

SOLUTION

$$c_F = \frac{1{,}440(18)}{106} = 0.02592 \text{ lb } H_2O/\text{lbmol } N_2$$

$$G = \frac{Q_F}{\pi D^2/4} = 29.6 \text{ lbmol } N_2/\text{h-ft}^2 \text{ of bed cross-section}$$

Initial moisture content of bed = 0.01 lb H_2O/lb solid

From (15-122),

$$\text{LES} = \frac{(0.02592)(29.6)(20)}{(0.186 - 0.01)(44.5)} = 1.96 \text{ ft}$$

Use the integration method to obtain LUB. From the data:

Take $t_e = 12.8$ h (1,440 ppm) and $t_b = 9.4$ h (9 ppm)

By numerical integration of the breakthrough-curve data, using (15-123): $t_s = 10.93$ h

From (15-121),

$$\text{LUB} = \left(\frac{10.93 - 9.40}{10.93}\right)(0.88) = 0.12 \text{ ft}$$

From (15-120):
$L_B = 1.96 + 0.12 = 2.08$ ft or a bed utilization of $\frac{1.96}{2.08} \times 100\% = 94.2\%$.

Alternatively, the following approximate calculation can be made. Let t_b, the beginning of breakthrough, be 5% of the final ppm or 0.05(1440) = 72 ppm. Using the experimental data, this corresponds to $t_b = 9.76$ h. Let t_e, the end of breakthrough, be 95% of the final ppm or 0.95(1440) = 1370 ppm, corresponding to $t_e = 12.25$ h. Let t_s = the midpoint or $(9.76 + 12.25)/2 = 11$ h. The ideal wavefront velocity $= L_e/t_s = 0.88/11 = 0.08$ ft/h. From (15-121), $LUB = 0.08(11 - 9.76) = 0.1$ ft. That is, the $MTZ = 0.2$ ft and $L_B = 1.96 + 0.1 = 2.06$ ft.

Thermal-Swing Adsorption

Thermal (temperature)-swing adsorption (TSA), in its simplest configuration, is carried out with two fixed beds in parallel, operating cyclically, as in Figure 15.20b. While one bed is adsorbing solute at near-ambient temperature, $T_1 = T_{\text{ads}}$, the other bed is regenerated by desorbing adsorbate at a higher temperature, $T_2 = T_{\text{des}}$, at which the equilibrium adsorbate loading is much less for a given concentration of solute in the fluid, as illustrated in Figure 15.21. Although the desorption step might be accomplished in the absence of a purge fluid by simply vaporizing the adsorbate, readsorption of some solute vapor would occur upon cooling the bed. Thus, it is best to remove the desorbed adsorbate with a purge. The desorption temperature is high, but not so high as to cause deterioration of the adsorbent. TSA is best applied to the removal of contaminants present at low concentrations in the feed fluid. In that case, nearly isothermal adsorption and desorption is achieved. An ideal cycle involves four steps: (1) adsorption at T_1 to breakthrough, (2) heating of the bed to T_2, (3) desorption at T_2 to a low adsorbate loading, and (4) cooling of the bed to T_1. Practical cycles do not operate with isothermal steps. Instead, Steps 2 and 3 are combined for the regeneration part of the cycle, with the bed being simultaneously heated and desorbed with preheated purge gas until the temperature of the effluent approaches that of the inlet purge. Steps 1 and 4 may also be combined because, as discussed in detail by Ruthven [10], the thermal wave precedes the MTZ front. Thus, adsorption takes place at essentially the feed-fluid temperature.

The heating and cooling steps cannot be accomplished instantaneously because of the relatively low bed thermal conductivity. Although heat transfer can be done indirectly from jackets surrounding the beds or from coils located within the beds, bed temperature changes are more readily achieved by preheating or precooling a purge fluid, as shown in Figure 15.35. The purge fluid can be a portion of the feed or effluent, or some other fluid. The purge fluid can also be used in the desorption step. When the adsorbate is valuable and easily condensed, the purge fluid might be a noncondensable gas. When the adsorbate is valuable, but not easily condensed, and is essentially insoluble in water, steam may be used as the purge fluid, followed by condensation of the steam to separate it from the desorbed adsorbate. When the adsorbate is not valuable, fuel and/or air can be used as the purge fluid, followed by incineration. Often the amount of purge used in the regeneration step is much less than the amount of feed sent to the bed in the adsorption step. In Figure 15.35, the feed fluid is a gas. The spent bed is heated and regenerated with preheated feed gas, which is then cooled to condense the desorbed adsorbate.

Because of the time to heat and cool a fixed bed, cycle times for TSA are long, usually extending over periods of hours or days. The longer the cycle time, the longer the required bed length, and the greater the percent utilization of the bed during adsorption. However, for a given cycle time,

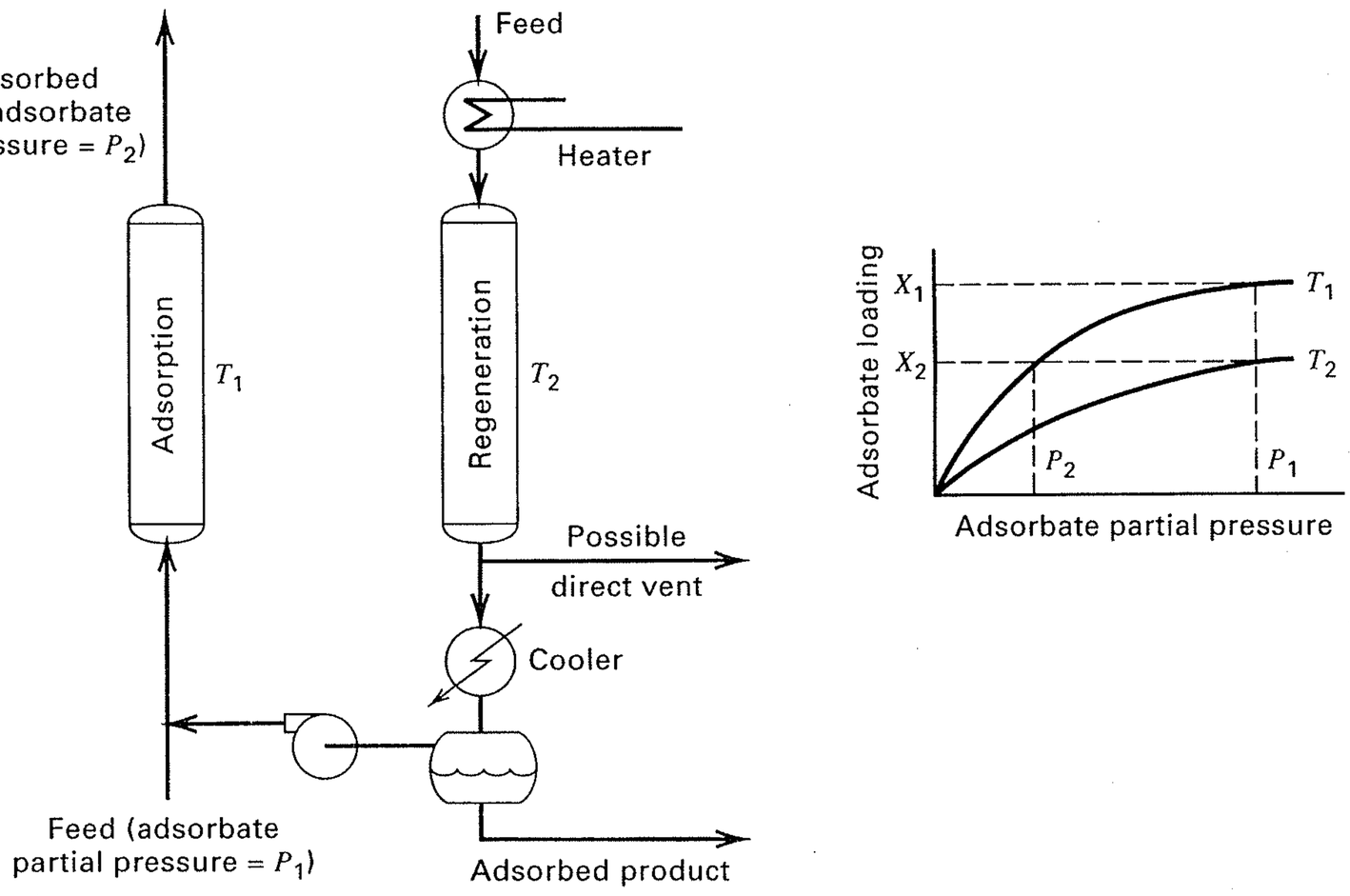

Figure 15.35 Temperature-swing adsorption cycle.

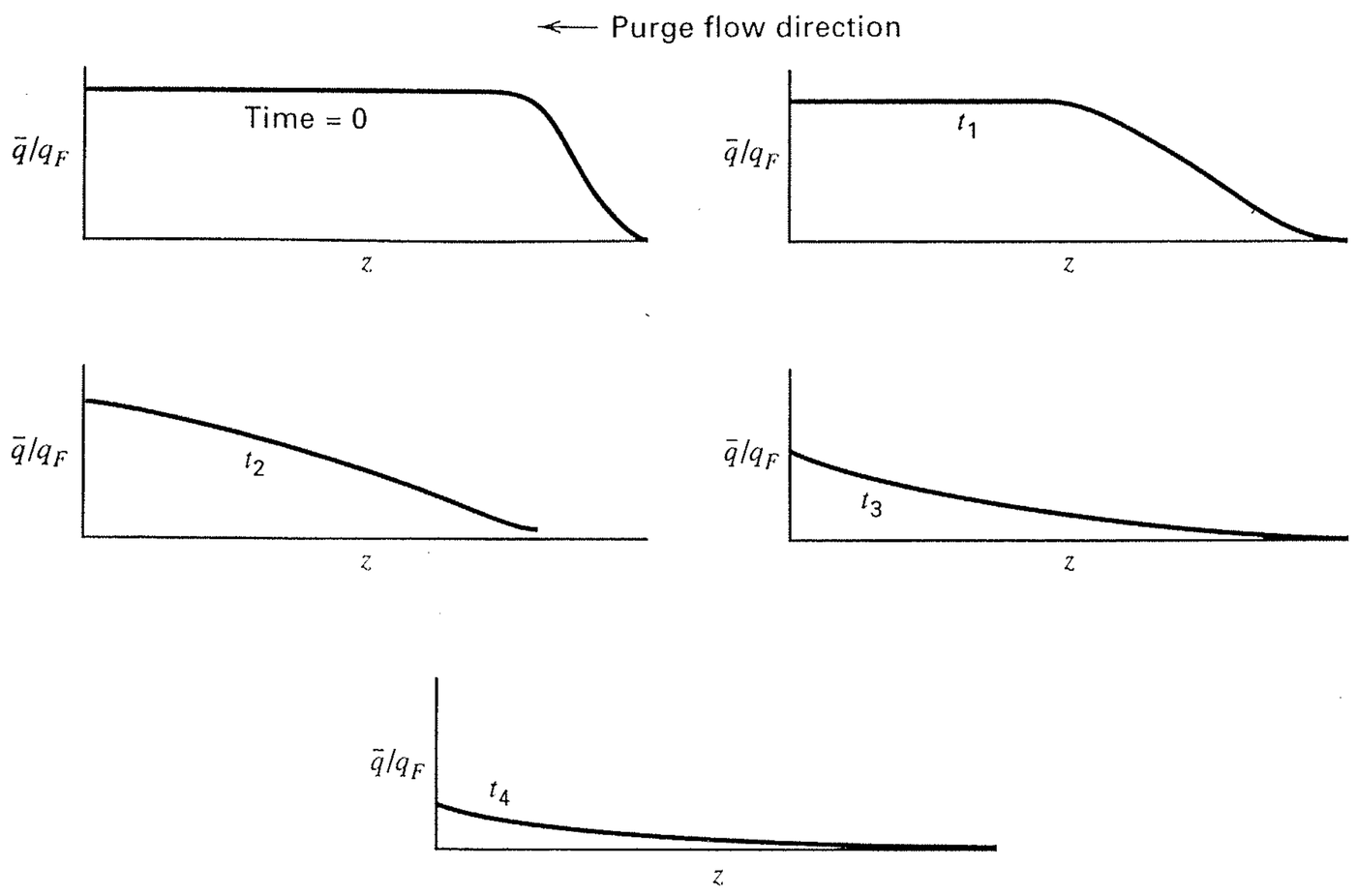

Figure 15.36 Sequence of loading profiles during countercurrent regeneration.

when the width of the MTZ is an appreciable fraction of the bed height, such that the capacity of the bed is poorly utilized, consideration should be given to a *lead-trim-bed* arrangement of two beds in series for the adsorption step. When the lead bed is spent, it is switched to regeneration. At this point in time, the trim bed has an MTZ occupying a considerable portion of the bed, and that bed becomes the lead bed, with a regenerated bed becoming the trim bed. In this manner only a fully spent bed is switched to regeneration. Thus, a total of three beds is used. If the flow rate of the feed stream is very high, beds in parallel may be required for both adsorption and desorption.

The adsorption step is usually conducted with the feed fluid flowing downward through the bed. The flow direction for desorption can be either downward or upward, but the upward, countercurrent direction is usually preferred because it is more efficient. Consider the sequence of loading fronts shown in Figure 15.36, for regeneration countercurrent to adsorption. Although the bed is shown in a horizontal position, it must be positioned vertically. The feed fluid flows downward, entering at the left and leaving at the right. At time $t = 0$, breakthrough has occurred, with a loading profile as shown at the top, where the MTZ is seen to be about 25% of the bed. If the purge fluid for regeneration also flows downward (entering at the left), all of the adsorbate will have to move through the unused portion of the bed. Thus, some of the desorbed adsorbate will be readsorbed in the unused section and then desorbed a second time. If countercurrent regeneration is used, the unused portion of the bed is never contacted with desorbed adsorbate. During a countercurrent regeneration step, the loading profile changes progressively, as shown for a series of times in Figure 15.36. The right-side end of the bed, where the purge enters, is desorbed first. At the end of regeneration, the residual loading may be uniformly zero or, more likely, finite and nonuniform as shown at the bottom of Figure 15.36. If the latter, then the useful cyclic capacity, called the *delta loading,* is as shown in Figure 15.37.

Calculations of the concentration and loading profiles during desorption are only approximated by (15-114) and (15-119) because the loading is not uniform at the beginning of desorption. A numerical solution for the desorption step can be obtained in the following fashion using a procedure discussed by Wong and Niedzwiecki [84]. Although their method was developed for the adsorption step, it is readily applied to desorption. In the absence of axial dispersion and for constant fluid velocity, (15-102) and (15-105) are rewritten as

$$u\frac{\partial \phi}{\partial z} + \frac{\partial \phi}{\partial t} + \left(\frac{1-\epsilon_b}{\epsilon_b}\right) kK(\phi - \psi) = 0 \qquad (15\text{-}123)$$

$$\frac{\partial \psi}{\partial t} = k(\phi - \psi) \qquad (15\text{-}124)$$

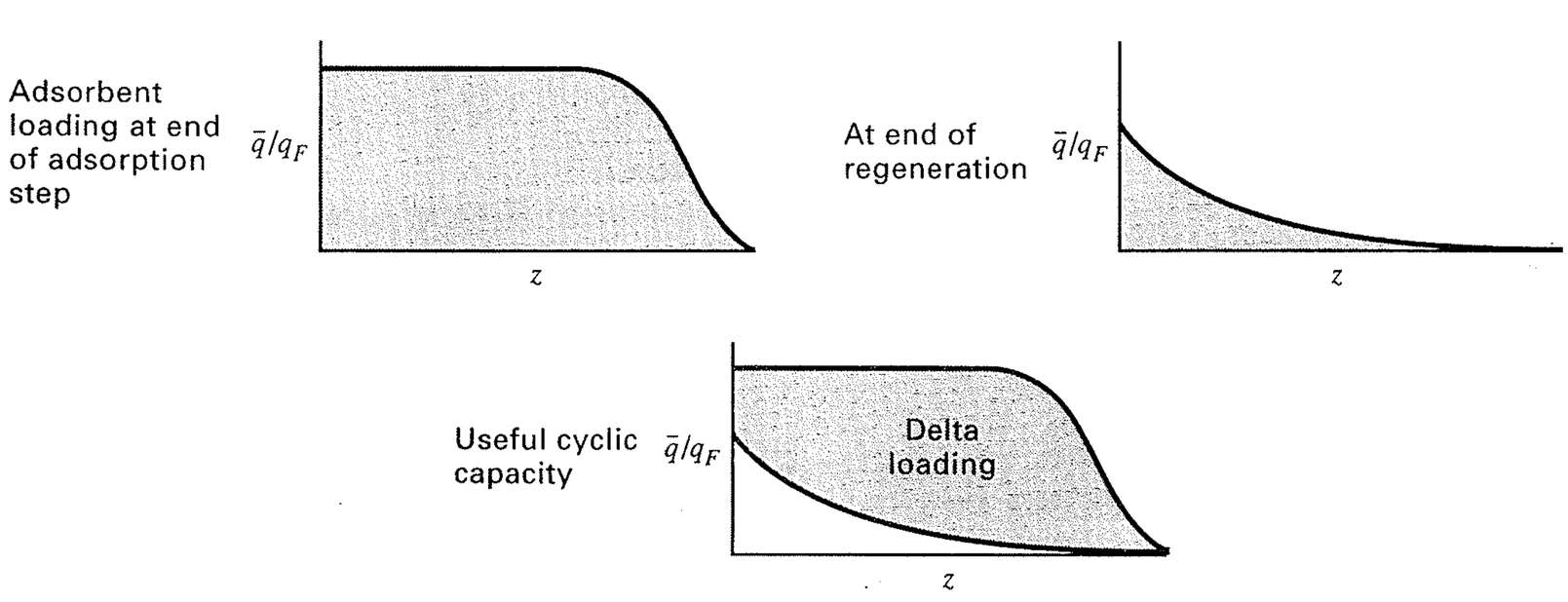

Figure 15.37 Delta loading for regeneration step.

where

$$\phi = c/c_F \tag{15-125}$$

$$\psi = \bar{q}/q_F^* \tag{15-126}$$

and c_F and q_F^* are the values at the beginning of the adsorption step. The boundary conditions are as follows:

At $t = 0$: $\phi = \phi\{z\}$ at the end of the adsorption step
$\psi = \psi\{z\}$ at the end of the adsorption step

where, for countercurrent desorption, it is best to let z start from the bottom of the bed (called z') and increase in the direction of purge-gas flow. Thus, u in (15-123) is positive.

At $z' = 0$: $\phi = 0$ (no solute in the entering purge gas)
$\psi = 0$

Partial differential equations (15-123) and (15-124) in independent variables z and t can be converted to a set of ordinary differential equations (ODEs) in independent variable t by the method of lines (MOL), which was first applied to parabolic PDEs by Rothe in 1930, as discussed by Liskovets [85], and subsequently to elliptic and hyperbolic PDEs. The MOL is developed in detail by Schiesser [86]. The lines refer to the z'-locations of the ODEs. To obtain the set of ODEs, the z'-coordinate is divided into N increments or $N + 1$ grid points that are usually evenly spaced. For many problems, 20 increments are sufficient. Letting i be the index for each grid point in z', starting from the end where the purge gas enters, and discretizing $\partial\phi/\partial z'$, (15-123) and (15-124) become

$$\frac{d\phi_i}{dt} = -u\left(\frac{\Delta\phi}{\Delta z'}\right)_i - \left(\frac{1-\epsilon_b}{\epsilon_b}\right)kK(\phi_i - \psi_i), \qquad i = 1, N+1 \tag{15-127}$$

$$\frac{d\psi_i}{dt} = k(\phi_i - \psi_i), \qquad i = 1, N+1 \tag{15-128}$$

where the initial conditions ($t = 0$) for ϕ_i and ψ_i are as given above. Before we can integrate (15-127) and (15-128), we must provide a suitable approximation for $(\Delta\phi/\Delta z')_i$. In general, for a moving-front problem of the hyperbolic type here for adsorption and desorption, the simple central difference

$$\left(\frac{\Delta\phi}{\Delta z'}\right)_i \approx \frac{\phi_{i+1} - \phi_{i-1}}{2\Delta z'}$$

is not adequate. Instead, Wong and Niedzwiecki [84] found that a five-point, biased, upwind, finite-difference approximation, discussed by Schiesser [87], is very effective. This approximation, which is derived from a Taylor's series analysis, places emphasis on conditions upwind of the moving front. At an interior grid point:

$$\left(\frac{\Delta\phi}{\Delta z'}\right)_i \approx \frac{1}{12\Delta z'}[-\phi_{i-3} + 6\phi_{i-2} - 18\phi_{i-1} + 10\phi_i + 3\phi_{i+1}] \tag{15-129}$$

Note that the coefficients of the ϕ-factors, inside the square brackets, sum to 0. At the last grid point, $N + 1$, where the purge gas exits, (15-129) is replaced by

$$\left(\frac{\Delta\phi}{\Delta z'}\right)_{N+1} \approx \frac{1}{12\Delta z'}[3\phi_{N-3} - 16\phi_{N-2} + 36\phi_{N-1} - 48\phi_N + 25\phi_{N+1}] \tag{15-130}$$

For the first three node points, the following approximations replace (15-129):

$$\left(\frac{\Delta\phi}{\Delta z'}\right)_1 \approx \frac{1}{12\Delta z'}[-25\phi_1 + 48\phi_2 - 36\phi_3 + 16\phi_4 - 3\phi_5] \tag{15-131}$$

$$\left(\frac{\Delta\phi}{\Delta z'}\right)_2 \approx \frac{1}{12\Delta z'}[-3\phi_1 - 10\phi_2 + 18\phi_3 - 6\phi_4 + \phi_5] \tag{15-132}$$

$$\left(\frac{\Delta\phi}{\Delta z'}\right)_3 \approx \frac{1}{12\Delta z'}[\phi_1 - 8\phi_2 + 0\phi_3 + 8\phi_4 - \phi_5] \tag{15-133}$$

However, because values of ϕ_1 (at $z' = 1$) are given as a boundary condition, (15-131) is not needed.

Equations (15-127) to (15-133) with boundary conditions for ϕ_1 and ψ_1 constitute a set of $2N$ ODEs as an initial-value problem, with time as the independent variable. However, the values of ϕ_i and ψ_i at the different axial locations can change with time at vastly different rates. For example, in Figure 15.36 for desorption fronts, if we divide the bed length, L, into 20 equal-width increments, starting from the right-hand side where the purge gas enters, we see that initially ψ_{21}, where the purge gas exits, is not changing at all, while ψ_5 is changing rapidly. Near the end of the desorption step, ψ_{21} is changing rapidly, while ψ_5 is not. The same observations hold for ϕ_i. This type of response is referred to as *stiffness,* as described by Schiesser [87] and in *Numerical Recipes* by Press et al. [88]. If we attempt to integrate the set of ODEs with simple Euler or Runge–Kutta methods, not only do we encounter truncation error, but, with time, the computed values of ϕ_i and ψ_i go through enormous instability, characterized by wild swings between large and impossible positive and negative values. Even if the length is divided into many more than 20 increments and very small time steps are used, instability is still often encountered.

The integration of a stiff set of ODEs is most efficiently carried out by variable-order/variable-step-size implicit methods of the type first developed by Gear [89]. These methods are included in a widely available software package called ODEPACK, described by Byrne and Hindmarsh [90]. The subject of stiffness is also discussed in Chapter 13.

EXAMPLE 15.13

In Example 15.11, benzene is adsorbed from air at 70°F and 1 atm onto silica gel in a fixed-bed adsorber, 6 ft in length. Breakthrough occurs at close to 97.1 min for $\phi = 0.05$. At that time, values of $\phi = c/c_F$ and $\psi = \bar{q}/q_F^*$ in the bed are distributed as follows, where z' is measured backwards from the exit of the bed for the adsorption step. These results were obtained by the numerical

method just described, as applied to the adsorption step, and are in close agreement with the approximate, analytical Klinkenberg solution given in Example 15.11.

z', ft	$\phi = c/c_F$	$\psi = \bar{q}/q_F^*$
0	0.05227	0.03891
0.3	0.07785	0.05913
0.6	0.11314	0.08776
0.9	0.16008	0.12690
1.2	0.22017	0.17850
1.5	0.29394	0.24387
1.8	0.38042	0.32310
2.1	0.47678	0.41459
2.4	0.57825	0.51469
2.7	0.67861	0.61786
3.0	0.77108	0.71728
3.3	0.84969	0.80603
3.6	0.91057	0.87858
3.9	0.95281	0.93207
4.2	0.97848	0.96690
4.5	0.99172	0.98636
4.8	0.99731	0.99531
5.1	0.99921	0.99857
5.4	0.99987	0.99960
5.7	1.00000	1.00000
6.0	1.00000	1.00000

If the bed is regenerated isothermally with pure air at 1 atm and 145°F, and the desorption of benzene during the heat-up period is neglected, determine the loading, $\bar{q}$, profile at times of 15, 30, and 60 min for pure stripping air interstitial velocities of: (a) 197 ft/min, and (b) 98.5 ft/min. At 145°F and 1 atm, the adsorption isotherm, in the same units as in Example 15.11, is

$$q = 1{,}000c^* \tag{1}$$

giving an equilibrium loading of about 20% of that at 70°F. Assume that k is unchanged from the value of 0.206 in Example 15.11.

SOLUTION

This problem is solved by the MOL with 20 increments in z', using the subroutine LSODE in ODEPACK to integrate the set of ODEs. The user supplies the FORTRAN MAIN program and the subroutine FEX, shown in Table 15.9, for the derivative functions given by (15-127) to (15-130) and (15-132) to (15-133). The program LSODE includes detailed instructions for writing these two routines. Note that the program in Table 15.9 actually includes both the adsorption and desorption steps for desorption conditions of 30 min at 197 ft/min.

The computed loading profiles for all conditions are plotted in Figures 15.38a and b, for desorption interstitial velocities of 197 and 98.5 ft/min, respectively, where z is the distance from the feed gas inlet end of the bed for the adsorption step. The curves are similar to those shown in Figure 15.30. For the 197 ft/min case, desorption is almost complete at 60 min with less than 1% of the bed still loaded with benzene. If this velocity were used, this would allow $97.1 - 60 = 37.1$ min for heating and cooling the bed before and after desorption. For the 98.5 ft/min case at 60 min, about 5% of the bed is still loaded with benzene. This may be acceptable, but the resulting adsorption step would take a little longer because initially the bed would not be clean. Several cycles are required to establish a cyclic steady state, whose development is considered in the next section on pressure-swing adsorption.

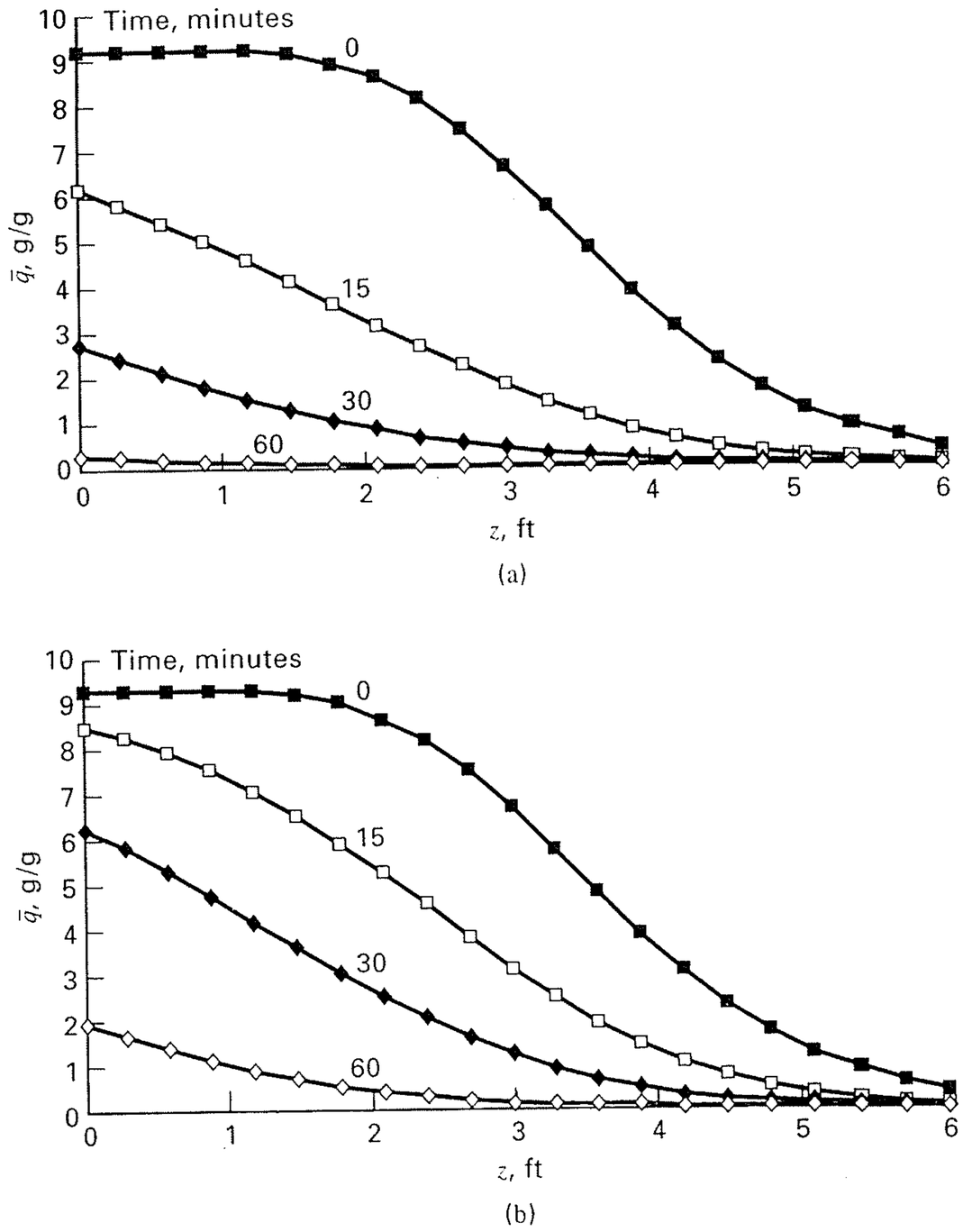

Figure 15.38 Regeneration loading profiles for Example 15.13.
(a) Regeneration air interstitial velocity = 197 ft/min.
(b) Regeneration air interstitial velocity = 98.5 ft/min.

Pressure-Swing Adsorption

Pressure-swing adsorption (PSA) and vacuum-swing adsorption (VSA), in their simplest configurations, are carried out with two fixed beds in parallel, operating in a cycle, as in Figure 15.39. Unlike TSA, where thermal means is used to effect the separation, PSA and VSA use mechanical work to increase the pressure or create a vacuum. While one bed is adsorbing at one pressure, the other bed is desorbing at a lower pressure, as was illustrated in Figure 15.21. Unlike TSA, which can be used to purify gases or liquids, PSA and VSA are used only with gases, because a change in pressure has little or no effect on the equilibrium loading for liquid adsorption. PSA was originally used only for purification, as in the removal of moisture from air by the "heatless drier," which was invented by C.W. Skarstrom in 1960 to compete with TSA. However, by the early 1970s, PSA was being applied to bulk separations such as the partial separation of air

Table 15.9 FORTRAN Computer Program for Example 15.13

```
      PROGRAM tsa
      IMPLICIT DOUBLE PRECISION(A-H, O-Z)
      EXTERNAL FEX
      DIMENSION C(40),ATOL(60),RWORK(4162),IWORK(90),CH(40),DL(40)
      COMMON CF,VEL,AK,A(20)
      open (unit=3,file='n1.out')
      write(3,*)'desorption velocity=197ft/min, desorption time=30min'
      NEQ=60
      CF0=0.00181
      CF1=0.0
      TCA=97.1
      NUMCYCLE=1
      MXSTEP=2000
      DO 55 I=1,20
55    C(I)=0.0

      DO 56 I=21,40
      C(I)=0.0
56    CONTINUE

      T=0.D0
      TOUT=0.0
      ITOL=2
      RTOL=1.D-6
      DO 57 I=1, 60
      ATOL(I)=1.0 D-12
57    CONTINUE

      ITASK=1
      ISTATE=1
      IOPT=1
      IWORK(6)=2000
      LRW=4162
      LIW=90
      MF=22

        CF=CF0
        C0=CF
        AK=5120.
        Q0=AK*C0

        CALL LSODE(FEX,NEQ,C,T,TOUT,ITOL,RTOL,ATOL,ITASK,ISTATE,
     1  IOPT,RWORK,LRW,IWORK,LIW,JEX,MF)
        WRITE(3,*)'CONDITIONS AT THE BEGINNING '
        WRITE(3,*)'TIME(SEC)=',TOUT
        WRITE(3,*)'CONC. GAS PHASE'
        WRITE(3,*)C0, (C(I),I=1,20)
        WRITE(3,*)'LODING gm/gm'
        WRITE(3,*)Q0,(C(I),I=21,40)
        write(3,128)
128      format(///)
       C0DL=1.0
       Q0DL=1.0
        DO 989 I=1,20
        DL(I)=C(I)/C0
        DL(I+20)=C(I+20)/Q0
989     CONTINUE
         WRITE(3,*)'DIMENSIONLESS CONDITIONS AT THE BEGINNING'
         WRITE(3,*)'TIME(SEC)=',TOUT
         WRITE(3,*)'DIMENSIONLESS GAS CONCENTRATION C/CF'
         WRITE(3,*)C0DL, (DL(I),I=1,20)
         WRITE(3,*)'DIMENSIONLESS LOADING Q/Q0'
         WRITE(3,*)Q0DL, (DL(I),I=21,40)
       write(3,129)
```

(*continued*)

Table 15.9 (*Continued*)

```
129       format(////////)
          DO 1000 KK=1,NUMCYCLE
C-------------------------------------------------------------------------
C------------ADSORPTION STEP--------------------------------------------
C-------------------------------------------------------------------------
          T=0.0

          CF=CF0
          C0=CF
          AK=5120.
          Q0=AK*C0

          VEL=197.0
          ISTATE=1
          TOUT= 97.1

          CALL LSODE(FEX,NEQ,C,T.TOUT,ITOL,RTOL,ATOL,ITASK,ISTATE,
     1    IOPT,RWORK,LRW,IWORK,LIW,JEX,MF)
          IF(KK.EQ.1)GOTO18
          IF((KK/25)*25.NE.KK)GOTO81
18         WRITE(3,*)'CONDITIONS AT THE END OF ADSORPTION STEP'
           WRITE(3,*)'STEP TIME(SEC)=',TOUT
           WRITE(3,*)'CONC. OF GAS PHASE'
           WRITE(3,*)C0,(C(I),I=1,20)
           WRITE(3,*)'LOADING gm/gm'
           WRITE(3,*)Q0,(C(I),I=21,40)
           WRITE(3,741)
741        FORMAT(///)
           C0DL=1.0
           Q0DL=1.0
           DO 990 I=1,20
           DL(I)=C(I)/C0
           DL(I+20)=C(I+20)/Q0
 990       CONTINUE
            WRITE(3,*)'DIMENSIONLESS CONDITIONS AT THE END OF ADSORPTION'
            WRITE(3,*)'STEP TIME(SEC)=',TOUT
            WRITE(3,*)'DIMENSIONLESS GAS CONCENTRATION C/CF'
            WRITE(3,*)C0DL,(DL(I),I=1,20)
            WRITE(3,*'DIMENSIONLESS LOADING Q/Q0'
            WRITE(3,*)Q0DL,(DL(I),I=21,40)
            WRITE(3,238)
238         FORMAT(////////)
C-------------------------------------------------------------------------
C-------DESORPTION BY TEMPERATURE SWING-----------------------------------
C-------------------------------------------------------------------------
81       T=0.0
         VEL=197.0
         TOUT=30.0
         ISTATE=1

         CF=CF1
         C0=CF
         AK=1000.0
         Q0=AK*C0

         DO 91 I=1,40
         CH(I)=C(I)
91       CONTINUE

         DO 92 I=1,19
         C(I)=CH(20-I)
92       CONTINUE
         C(20)=CF0

         DO 95 I=1,19
```

Table 15.9 (*Continued*)

```
95        C(20+I)=CH(40-I)
          C(40)=CF0*5120.
          CALL LSODE (FEX,NEQ,C,T,TOUT,ITOL,RTOL,ATOL,ITASK,
     1    ISTATE,IOPT,RWORK,LRW,IWORK,LIW,JEX,MF)

          DO 93 I=1,40
          CH(I)=C(I)
93        CONTINUE

          DO 94 I=1,19
          C(I)=CH(20-I)
          C(20+I)=CH(40-I)
94        CONTINUE
          C0=C(20)
          Q0=C(40)
          C(20)=CF1
          C(40)=1000.*CF1
          IF(KK.EQ.1)GOTO38
          IF((KK/25)*25.NE.KK)GOTO1000
38        WRITE(3,*)'CONDITIONS AT THE END OF DESORPTION '
          WRITE(3,*)'STEP TIME(SEC)=',TOUT
          WRITE(3,*)'CONC. OF GAS PHASE '
          WRITE(3,*)C0,(C(I),I=1,20)
          WRITE(3,*)'LOADING gm/gm'
          WRITE(3,*)Q0,(C(I),I=21,40)
          WRITE(3,264)
264       FORMAT (///)
           C0DL=C0/CF0
           Q0DL=Q0/(CF0*5210.)
           DO 991 I=1,20
           DL(I)=C(I)/CF0
           DL(I+20)=C(I+20)/(CF0*5120.)
991        CONTINUE
           WRITE(3,*)'DIMENSIONLESS CONDITIONS AT THE END OF DESORPTION'
           WRITE(3,*)'STEP TIME(SEC)=',TOUT
           WRITE(3,*)'DIMENSIONLESS GAS CONCENTRATION C/CF'
           WRITE(3,*)C0DL,(DL(I),I=1,20)
           WRITE(3,*)'DIMENSIONLESS LOADING Q/Q0'
           WRITE(3,*)Q0DL,(DL(I),I=21,40)
           WRITE(3,365)
365        FORMAT(////////)
1000      CONTINUE

 C-------------------------------------------------------------------------
 C-------------------------------------------------------------------------
 C-------------------------------------------------------------------------
          WRITE(3,60)IWORK(11),IWORK(12),IWORK(13)
  60      FORMAT(/12H NO. STEPS =,I4,11H NO. F-S =,I4,11H NO. J-S =,I4)
          STOP
  80      WRITE(3,90)ISTATE
  90      FORMAT(///22H ERROR HALT.. ISTATE =,I3)
          close(unit=3)
          STOP
          END
C-------------------------------------------------------------------------
          SUBROUTINE FEX (NEQ,T,C,CDOT)
          IMPLICIT DOUBLE PRECISION(A-H,O-Z)
          DIMENSION C(40), CDOT(40)
          COMMON CF,VEL,AK,A(20)
          E=0.5
          C0=CF
          Q0=AK*C0
          DZ=6.0/20.0       !FT
```

(*continued*)

Table 15.9 (*Continued*)

```
      AA=-VEL
      BB=-(1.0-E)/E

      R4FDX=1./(12.*DZ)
      A(1)=R4FDX*
     1  (-3.*C0-10.*C(1)+18.*C(2)-6.*C(3)+1.*C(4))

      A(2)=R4FDX*
     1  (1.*C0-8.*C(1)+0.*C(2)+8.*C(3)-1.*C(4))

      A(3)=R4FDX*
     1  (-1.*C0+6.*C(1)-18.*C(2)+10.*C(3)+3.0*C(4))

      DO 455 I=4,19
      A(I)=R4FDX*
     1  (-1.*C(I-3)+6.*C(I-2)-18.*C(I-1)+10.*C(I)+3.*C(I+1))
455   CONTINUE
      A(20)=R4FDX*
     1  (3.*C(16)-16.*C(17)+36.*C(18)-48.*C(19)+25.*C(20))

      DO 676 I=1,20
      CDOT(20+I)=0.206*(AK*C(I)-C(20+I))
      CDOT(I)=AA*A(I)+BB*CDOT(20+I)
676   CONTINUE

      RETURN
      END
```

to produce either nitrogen or oxygen and to the removal of impurities and pollutants from other gas streams. PSA can also be used for vapor recovery, as discussed and illustrated by Ritter and Yang [91].

A typical sequence of steps in the Skarstrom cycle, operating with two beds, is shown in Figure 15.40. Each bed operates alternately in two half-cycles of equal duration: (1) pressurization followed by adsorption, and (2) depressurization (blowdown) followed by a purge. The feed gas is used for pressurization, while a portion of the effluent product gas is used for purge. Thus, in Figure 15.40, while adsorption is taking place in bed 1, part of the gas leaving bed 1 is routed to bed 2 to purge that bed in a direction countercurrent to the direction of flow of the feed gas during the adsorption step. When moisture is to be removed from air, the dry-air product is produced during the adsorption step in each of the two beds. In Figure 15.40, the adsorption and purge steps represent less than 50% of the total cycle time. In many commercial applications of PSA, these two steps consume a much greater fraction of the cycle time because pressurization and blowdown can be completed rapidly. Therefore, cycle times for PSA and VSA are short, typically seconds to minutes. Thus, small beds have relatively large throughputs. With the valving shown in Figure 15.39, the

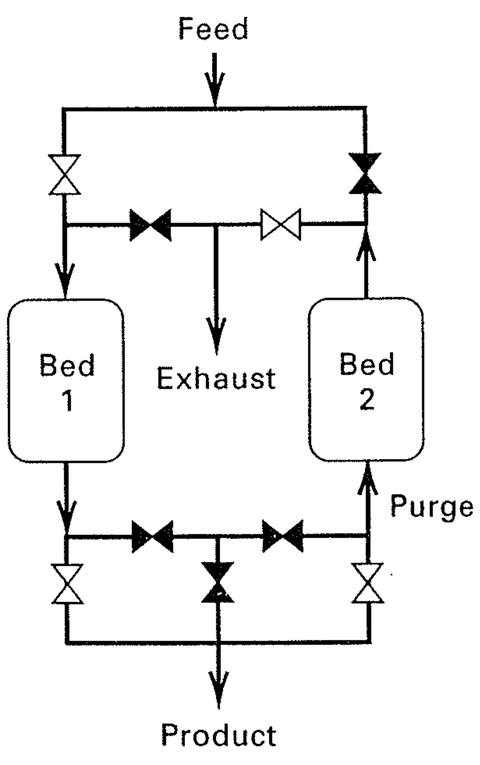

Figure 15.39 Pressure-swing-adsorption cycle.

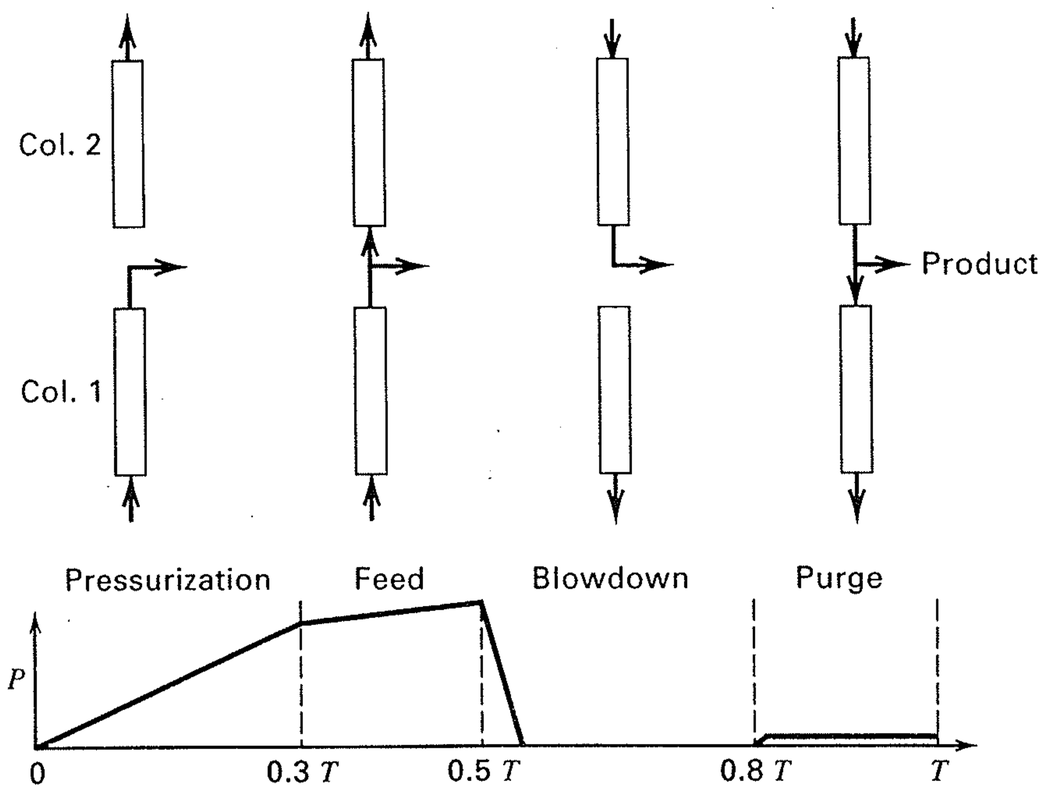

Figure 15.40 Sequence of cycle steps in PSA.

entire cyclic sequence can be programmed to operate automatically. With some valves open and others closed, as in Figure 15.39, adsorption takes place in Bed 1 and purge takes place in Bed 2. During the second half of the cycle, the valve openings and beds are switched.

Since the introduction of the Skarstrom cycle, numerous improvements have been made to increase product purity, product recovery, adsorbent productivity, and energy efficiency, as discussed by Yang [25] and by Ruthven, Farooq, and Knaebel [92]. Among these modifications are the use of (1) three, four, or more beds; (2) a pressure-equalization step in which both beds are equalized in pressure following purge of one bed and adsorption in the other; (3) pretreatment or guard beds to remove strongly adsorbed components that might interfere with the separation of other components; (4) purge with a strongly adsorbing gas; and (5) the use of an extremely short cycle time to approach isothermal operation, if a longer cycle causes an undesirable increase in temperature during adsorption and an undesirable decrease in temperature during desorption.

Separations by PSA and VSA are controlled by adsorption equilibrium or adsorption kinetics, where the latter refers to mass transfer external and/or internal to the adsorbent particle. Both types of control are important commercially. For the separation of air with zeolites, adsorption equilibrium is the controlling factor, with nitrogen more strongly adsorbed than oxygen and argon. For air with 21% oxygen and 1% argon, oxygen of about 96% purity can be produced. When carbon molecular sieves are used, oxygen and nitrogen have almost the same adsorption isotherms, but the effective diffusivity of oxygen is much larger than that of nitrogen. Consequently, a nitrogen product of very high purity (>99%) can be produced.

PSA and VSA cycles have been modeled successfully for both equilibrium and kinetic-controlled cases. The models and computational procedures are similar to those used for TSA. The models are particularly useful for optimizing cycles. Of particular importance in PSA and TSA is the determination of the cyclic steady state. In TSA, following the desorption step, the regenerated bed is usually clean. Thus, a cyclic steady state is closely approached in one cycle. In PSA and VSA, this is often not the case, and complete regeneration is seldom achieved or necessary. It is only required to attain a cyclic steady state whereby the product obtained during the adsorption step has the desired purity and at cyclic steady state, the difference between the loading profiles after adsorption and desorption is equal to the solute entering in the feed. Starting with a clean bed, the attainment of a cyclic steady state for a fixed cycle time may require tens or hundreds of cycles. Consider an example from a study by Mutasim and Bowen [93] on the removal of ethane and carbon dioxide from nitrogen with 5A zeolite, at ambient temperature with adsorption and desorption for 3 min each at 4 bar and 1 bar, respectively, in beds 0.25 m in length. Figures 15.41a and b show the computed development of the loading and gas concentration profiles at the end of each adsorption step for ethane, starting from a clean bed. At the end of the first cycle, the bed is still clean beyond about 0.11 m. By the end of the 10th cycle, a cyclic steady state has almost been attained, with a clean bed existing only near the very end of the bed. Experimental data points for ethane loading at the end of 10 cycles agree reasonably well with the computed profile from a mathematical model.

Modeling of PSA and VSA cycles is carried out with the same equations as for TSA. However, the assumptions of negligible axial diffusion and isothermal operation may be relaxed. For each cycle, the pressurization and blowdown steps are often ignored and the initial conditions for adsorption and desorption are the final conditions for the desorption and adsorption steps, respectively, of the previous cycle. This is illustrated in the following example. Calculations can also be made with Aspen Adsim of the Aspen Engineering Suite.

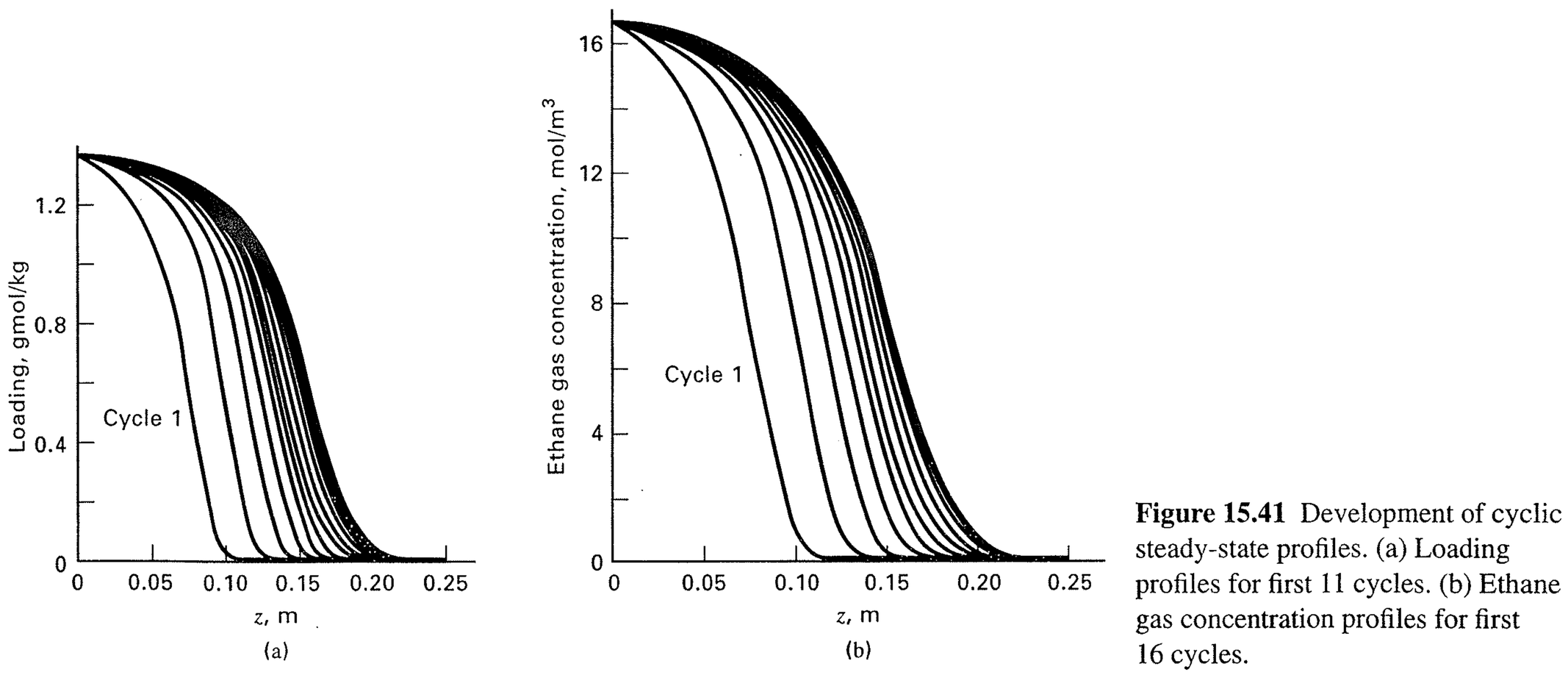

Figure 15.41 Development of cyclic steady-state profiles. (a) Loading profiles for first 11 cycles. (b) Ethane gas concentration profiles for first 16 cycles.

EXAMPLE 15.14

Ritter and Yang [91] conducted an experimental and theoretical study of the use of PSA to recover dimethyl methylphosphonate (DMMP) vapor from air. For the following data and operating conditions, starting with a clean bed, use the method of lines with a stiff integrator to estimate the concentration and loading profiles for the beds, the percent of the feed gas recovered as essentially pure air, and the average mole fraction of DMMP in the effluent gas leaving the desorption step during the third cycle.

Feed-Gas Conditions:

236 ppm by volume of DMMP in dry air at 294 K and 3.06 atm

Adsorbent:

BPL activated carbon, 5.25 g in each bed, 0.07 cm average particle diameter, and 0.43 bed porosity.

Bed dimensions: 1.1 cm i.d. by 12.8 cm each

Langmuir adsorption isotherm: $q = \dfrac{48{,}360 p_{\text{DMMP}}}{1 + 98{,}700 p_{\text{DMMP}}}$,

where q is in g/g and p is in atm.

Overall mass-transfer coefficient: $k = 5 \times 10^{-3}\ \text{s}^{-1}$

Cycle conditions (all at 294 K):

1. Pressurization with pure air from p_L to p_H in negligible time.
2. Adsorption at $p_H = 3.06$ atm with feed gas for 20 minutes. u = interstitital velocity = 10.465 cm/s.
3. Blowdown from p_H to p_L with no loss of DMMP from the adsorbent or gas in the voids of the bed in negligible time.
4. Desorption at $p_L = 1.07$ atm with product gas (pure air) for 20 minutes. Interstitial velocity, u, corresponding to use of 41.6% of the product gas leaving the adsorption step.

SOLUTION

This example can be solved using the same equations and numerical techniques employed in Example 15.13, but noting that the units of q are different and a Langmuir isotherm replaces Henry's law. If the bed is not clean following the first desorption step, the results for the second and third cycles will differ from the first. The results are not presented here, but the calculations are required in Exercise 15.30.

Continuous, Countercurrent Adsorption Systems

In previous subsections, slurry and fixed-bed modes of adsorption, shown in Figures 15.20a and b, were considered. While these are traditional modes of adsorber operation, the third mode of operation in Figure 15.20c, continuous, countercurrent operation, has an important advantage because, as in a heat exchanger, an adsorber, and other separation cascades, countercurrent flow maximizes the average driving force for transport. In adsorption, this increases the efficiency of adsorbent use.

In Figure 15.20c, both liquid or gas mixtures undergoing separation and the solid adsorbent particles move through the system. However, as discussed in detail by Ruthven and Ching (65) and Wankat (97), the advantage of countercurrent operation can also be achieved by a simulated-moving-bed (SMB) operation, with one widely used implementation shown in Figure 15.23, wherein adsorbent particles remain fixed in a bed. In this subsection, the continuous, countercurrent system shown in Figure 15.20c is considered, while the next subsection covers the SMB. Both types of operation can be applied to purification or bulk separation.

McCabe–Thiele and Kremser Methods for Purification

Consider a binary mixture, dilute in a solute that is to be removed by adsorption in a continuous, countercurrent system of the type shown in Figure 15.42a. Only the solute is adsorbed. Feed F, with solute concentration c_F, enters the adsorption section, ADS, at Plane P_1, from which adsorbent S leaves with a solute loading q_F. Purified feed called the raffinate, with solute concentration c_R, leaves the adsorption section at Plane P_2, countercurrent to adsorbent of loading q_R, which enters at the top of the bed. At Plane P_3, a purge called the desorbent, D, with solute concentration c_D, enters at the bottom of the desorption section, DES, from which the adsorbent leaves to enter the adsorption section. We assume that the desorbent does not adsorb and exits from the desorption

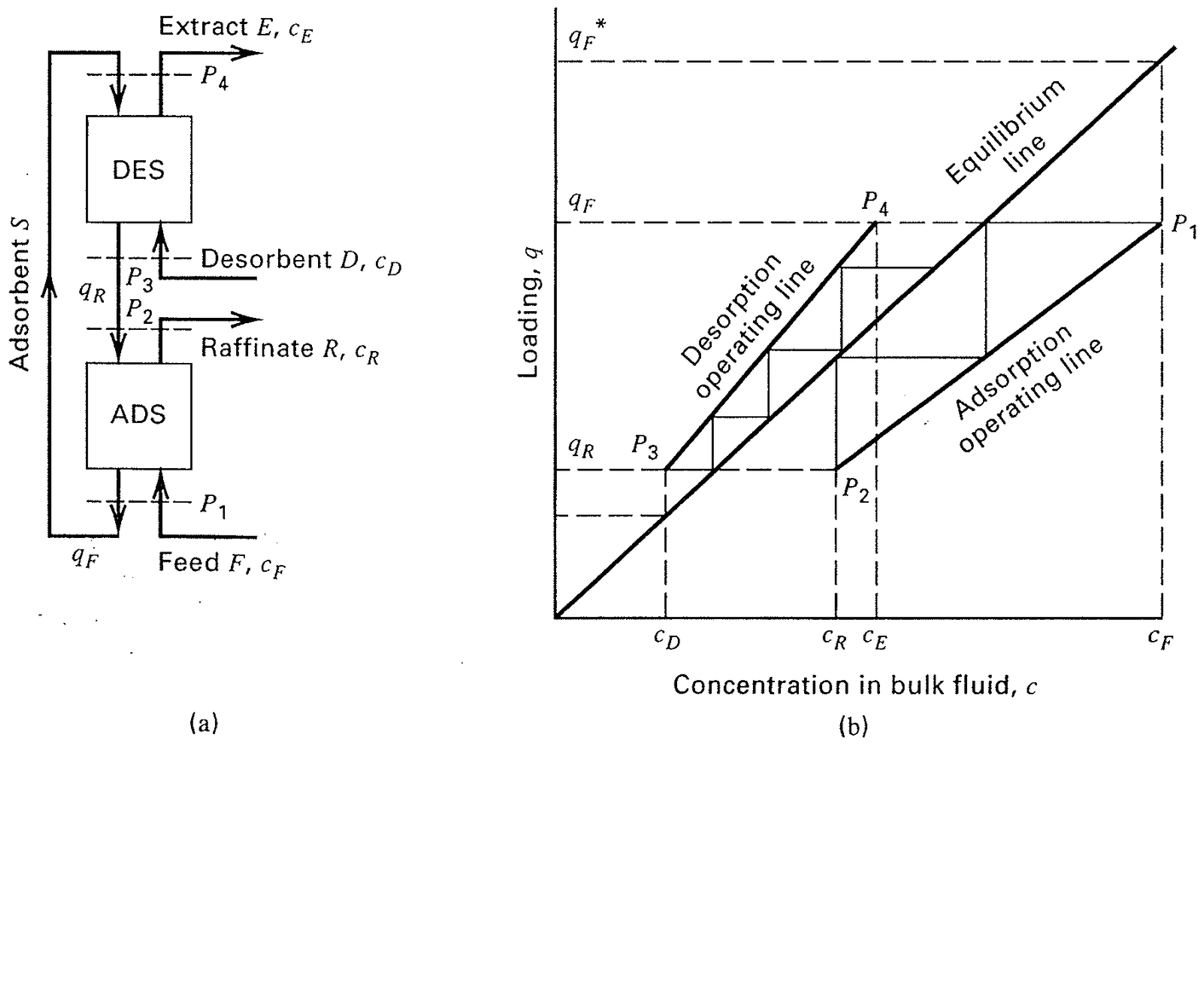

Figure 15.42 Continuous, countercurrent adsorption–desorption system. (a) System sections and flow conditions. (b) McCabe–Thiele diagram.

section as extract E, with solute concentration c_E, at Plane 4, where recycled adsorbent enters the desorption bed to complete the cycle.

If the system is dilute in the solute, if the solute adsorption isotherms for the feed solvent and the purge fluid are identical, and the system operates at constant temperature and pressure, the McCabe–Thiele diagram for the solute resembles that shown in Figure 15.42b, where the operating and equilibrium lines are straight because of the dilute condition. Note that the proper directions for mass transfer require that the adsorption and desorption operating lines lie below and above, respectively, the equilibrium line. These three lines are represented by the following equations:

Adsorption Operating Line:

$$q = \frac{F}{S}(c - c_F) + q_F \tag{15-134}$$

Desorption Operating Line:

$$q = \frac{D}{S}(c - c_D) + q_R \tag{15-135}$$

Equilibrium Line:

$$q = Kc \tag{15-136}$$

where F, S, and D are solute-free mass flow rates, and all solute concentrations are per solute-free carrier.

In Figure 15.42b, as the concentration of solute in the entering desorbent (purge), c_D, approaches zero, and solute concentration in the exiting raffinate, c_R, approaches zero, in order to avoid a large number of stages, it is necessary to select the adsorbent and desorbent flow rates so that

$$\frac{F}{S} < K < \frac{D}{S}$$

Thus, because more purge, D, than feed, F, is required, this system is only economical when the purge fluid is inexpensive. From the equilibrium and operating lines in Figure 15.42b, 2 and 3.3 equilibrium stages are determined for the adsorption and desorption sections, respectively, by stepping off stages in the McCabe–Thiele diagram. When the equilibrium and operating lines are straight, as in Figure 15.42b, the algebraic Kremser method, rather than the graphical McCabe–Thiele method, can be employed. The Kremser equation, discussed in Section 6.4, is written in the following end-point form for the adsorption or desorption section:

$$N_t = \frac{\ln\left[\dfrac{c_1 - q_1/K}{c_2 - q_2/K}\right]}{\ln\left[\dfrac{c_1 - c_2}{q_1/K - q_2/K}\right]} \tag{15-137}$$

where 1 and 2 refer to opposite ends of the section, such as Planes 1 and 2 in Figure 15.42a, which are chosen so that $q_1 > q_2$.

If the operating conditions, e.g., temperature, for the two sections can be altered so as to place the equilibrium line for desorption below that for adsorption, it becomes possible to use a portion of the raffinate for desorption. This situation, shown in Figure 15.43, is achieved by desorbing at elevated temperature or, in the case of gas adsorption, at reduced pressure. Now, as shown in Figure 15.43, F/S can be greater than D/S. With a portion of raffinate used in Bed 2 (DES), the net raffinate product is $F - D$. Note that in this case, the two operating lines must intersect at the point (q_R, c_R). By adjusting D/F, this point can be moved closer and closer to the origin so as to achieve any raffinate purity, c_R, desired, but at the expense of more theoretical stages and, therefore, deeper beds.

For a number of theoretical stages, N_t, in either the adsorption or desorption sections, bed height L can be determined from

$$L = N_t(\text{HETP}) \tag{15-138}$$

Values of HETP, which depend on mass-transfer resistances and axial dispersion, must be determined from experimental measurements. For large-diameter beds, typical values of HETP are in the range of 0.5–1.5 ft [97, 98].

McCabe–Thiele Method for Bulk Separation

Figure 15.44 shows a continuous, countercurrent adsorption–desorption process for bulk separation of a binary mixture.

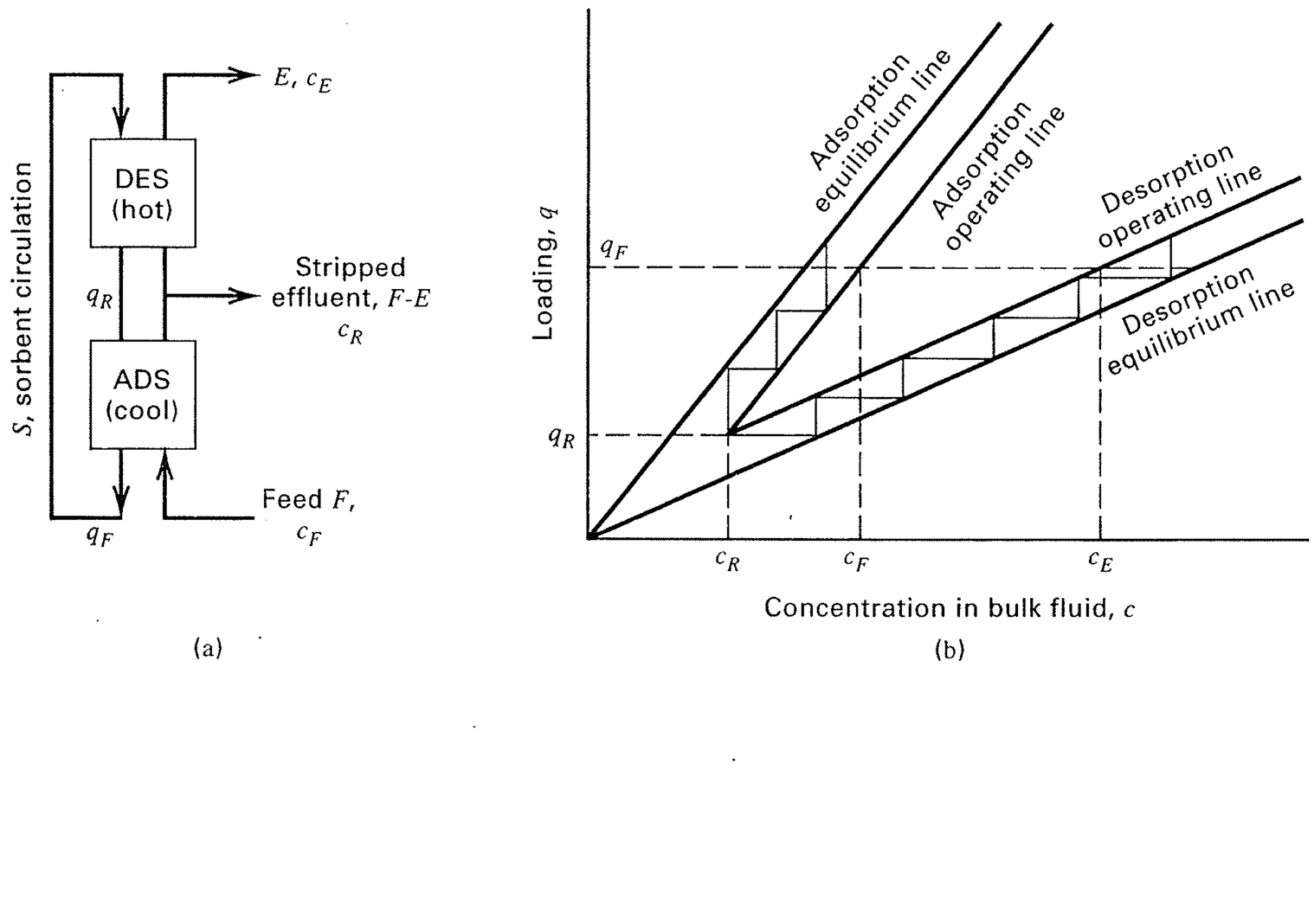

Figure 15.43 Continuous, countercurrent system with a temperature swing. (a) System sections and flow conditions. (b) McCabe–Thiele diagram.

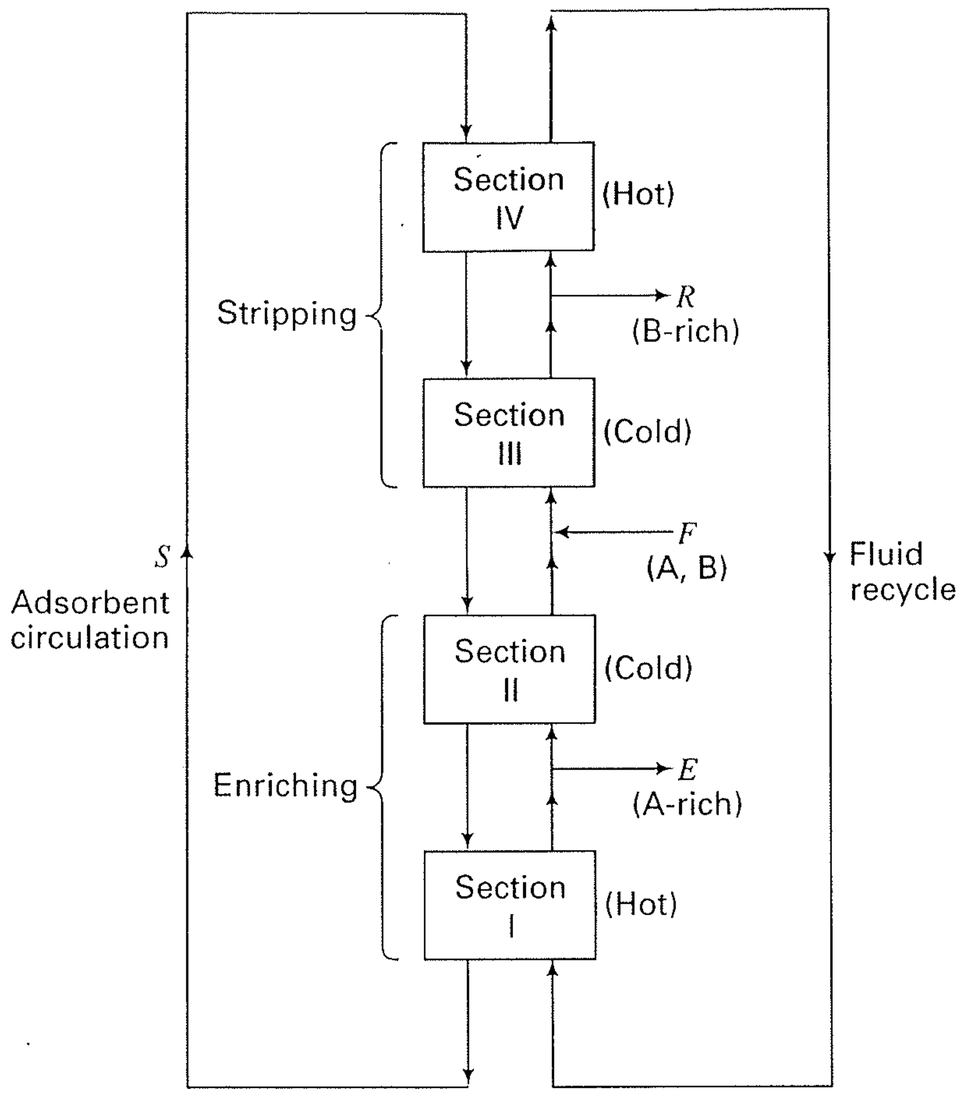

Figure 15.44 Continuous, countercurrent system for bulk separation.

The feed consists of component A, which is more strongly adsorbed, and B, which is less strongly adsorbed. The process consists of four sections (also called zones), numbered from the bottom up. Adsorbent S is circulated through the system, passing downward through the four sections, preferentially adsorbing A, leaving B to preferentially pass upward. To provide flexibility, a thermal swing is used, with Sections II and III operating at low or ambient temperature, while Sections I and IV operate at elevated temperature. The feed, F, enters between Sections II and III, passing up through Section III, where A is preferentially adsorbed at a relatively cold temperature. Product R, rich in B, is removed between Sections III and IV. At the higher temperature in Section IV, residual A and B is desorbed, with the fluid leaving from Section IV recycled to Section I. Adsorbent with mainly adsorbed A passes downward from Section III to Section II and then to Section I, where component A is desorbed to produce product E, rich in A, which is removed between Sections I and II. The system resembles an inverted distillation column, with the top two sections (III and IV) providing a stripping action to produce a product rich in the less strongly adsorbed component, while the bottom two sections provide an enriching action to produce a product rich in the more strongly adsorbed component. An equipment arrangement similar to that in Figure 15.44 was used in the Hypersorption moving bed process [66] for separating hydrogen and methane from ethane and heavier hydrocarbons, except that Section IV was a cooler, Section I was a steam stripper, and gas leaving Section IV was used to lift the adsorbent from Section I to Section IV. Additional flexibility can be achieved for the system in Figure 15.44 by providing separate adsorbent-circulation loops for the top two and bottom two sections.

EXAMPLE 15.15

One hundred pounds per minute (dry basis) of air at 80°F and 1 atm with 65% relative humidity is dehumidified isothermally and isobarically to 10% relative humidity in a continuous, countercurrent moving-bed adsorption unit. The adsorbent is dry silica gel (SG) having a particle-diameter range of 1.42 to 2.0 mm. Over the water-partial-pressure range of interest, the adsorption isotherm is given by measurements of Eagleton and Bliss [94] as

$$q_{H_2O} = 29c_{H_2O} \tag{1}$$

with concentration in lb H_2O/lb dry air and loading in lb H_2O/lb dry SG. If 1.5 times the minimum flow rate of silica gel is used, determine the number of equilibrium stages required.

SOLUTION

For relative humidities of 65% and 10%, the corresponding moisture contents are, from a humidity chart, 0.0143 and 0.0022 lb H_2O/lb dry air, respectively.

In this case, Figure 15.42b applies for the adsorption section. Using the nomenclature in that figure:

$$F = 100 \text{ lb/min}, \quad c_F = 0.0143 \text{ lb } H_2O\text{/lb dry air},$$
$$c_R = 0.0022 \text{ lb } H_2O\text{/lb dry air}, \quad \text{and } q_R = 0.$$

The value of q_F depends on adsorbent flow rate, S, which is 1.5 times the minimum value. At minimum-adsorbent rate, exiting adsorbent is in equilibrium with the entering gas. Therefore, from (1): $q_F^* = 29(0.0143) = 0.415$ lb H_2O/lb dry SG. The amount of water vapor adsorbed is $F(c_F - c_R) = 100(0.0143 - 0.0022) = 1.21$ lb/min. Therefore: $S_{min} = \frac{1.21}{0.415} = 2.92$ lb dry SG/min. If 1.5 times the minimum amount of silica gel is used: $S = 1.5\,S_{min} = 1.5(2.92) = 4.38$ lb dry SG/min. By material balance: $q_F = \frac{1.21}{4.38} = 0.276$ lb H_2O/lb dry SG. From (15-137), with $K = 29$ from (1) and letting F be at plane 1 and R at plane 2:

$$N_t = \frac{\ln\left[\dfrac{0.0143 - 0.276/29}{0.0022 - 0}\right]}{\ln\left[\dfrac{0.0143 - 0.0022}{0.276/29 - 0}\right]} = 3.2 \text{ stages}$$

Simulated-Moving-Bed Systems

Continuous, countercurrent, moving-bed systems, often referred to as "true-moving-bed" (TMB) systems, encounter operating difficulties, including abrasion of adsorbent particles, failure to approach a plug flow of the particles as they move downward, and channeling of fluid through the moving bed. Alternatively, as shown in one implementation in Figure 15.23, a continuous countercurrent operation can be simulated by using a column containing a series of fixed beds and periodically moving the locations at which streams enter and leave the column. "Simulated-moving-bed" (SMB) systems have found widespread commercial application for liquid separations in the petrochemical, food, biochemical, pharmaceutical, and fine chemical industries, say of components A and B, when employing a circulating desorbent D (also called a diluent or eluent) to aid in the separation. In some cases the properties of D are such that,

like A and B, it can be adsorbed. Then, D can displace A and/or B from the sorbent pores, while A and/or B can displace D. In that case, a hybrid process of SMB adsorption and distillation, as shown in Figure 15.23, is often utilized, where following the SMB, a D-free extract of A and a D-free raffinate of B are obtained by distillation, with recovered D recycled to the SMB. In other cases, D is a component of the feed and is not adsorbed, but simply acts as a carrier and stripping agent for separation of A from B. For example, an aqueous solution of glucose and fructose is often separated by an SMB into an extract of aqueous glucose and a raffinate of aqueous fructose, which may be the final products. In the literature, simulated-moving-bed operations are often referred to as chromatographic, rather than adsorptive, separations.

An SMB can be treated as a countercurrent cascade of sections (or zones), rather than stages, where stream entry or withdrawal points bound the sections. As discussed by Zang and Wankat [99], two-, three-, and four-section systems for producing two products, and a nine-section system for three products are described in the literature, with the four-section system, shown in Figure 15.45a, being the most common commercial design. More recently, Kim and Wankat [100] proposed SMB designs with from 12 to 32 sections for separation of quaternary mixtures.

Operation of a simulated moving bed is best understood by studying the two representations of a four-section system and the accompanying fluid composition profile in Figure 15.45. The schematic representation in Figure 15.45a shows a TMB, with circulation of solid adsorbent S down through four dense-bed sections in a closed cycle, while Figure 15.45b represents an actual SMB system, comprised of four sections divided into 12 fixed-bed subsections, shown as rectangles, with periodic movement of fluid inlet and outlet ports, shown as circles. The sections in Figure 15.45a are sometimes

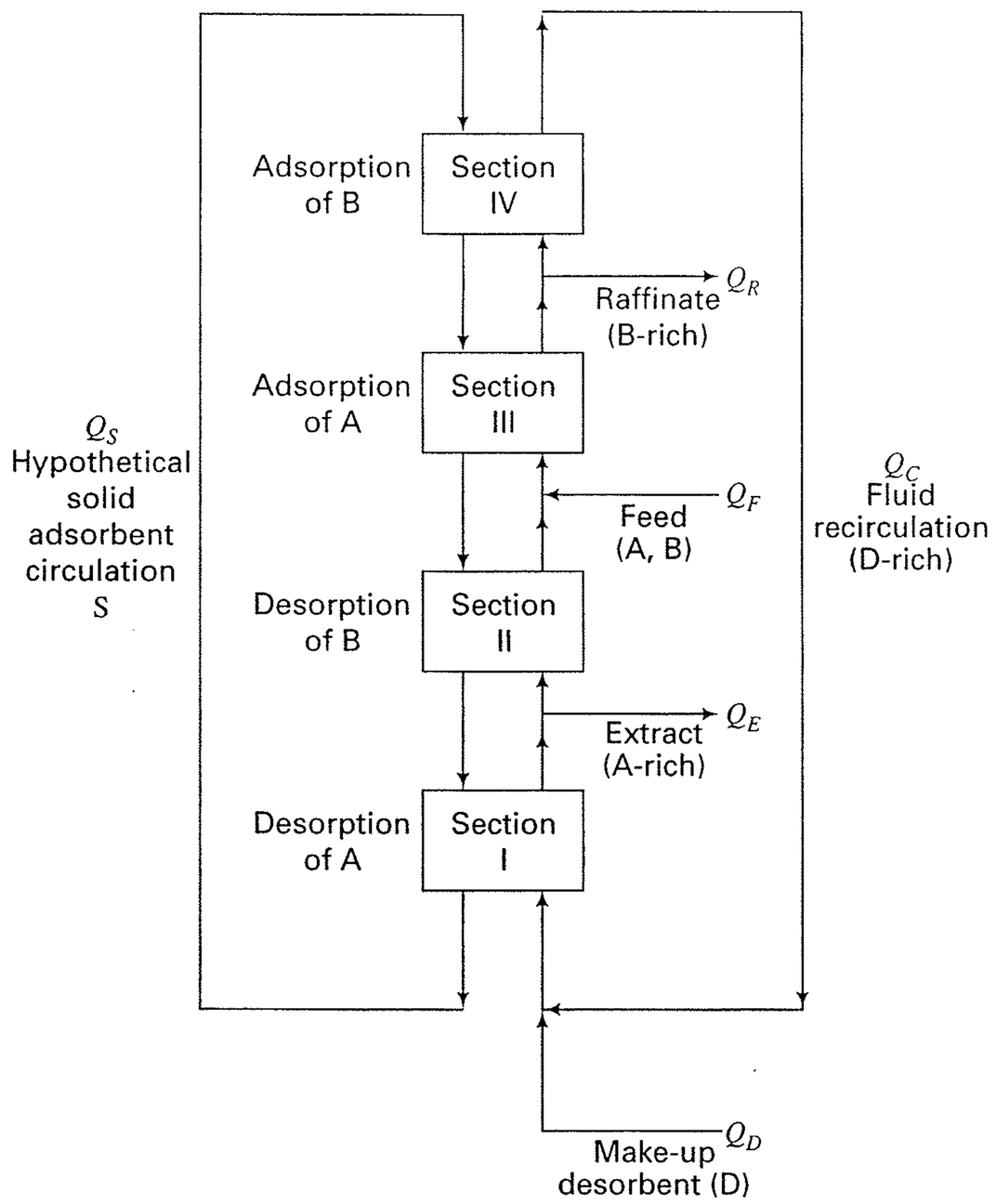

(a) Schematic representation of a true moving bed.

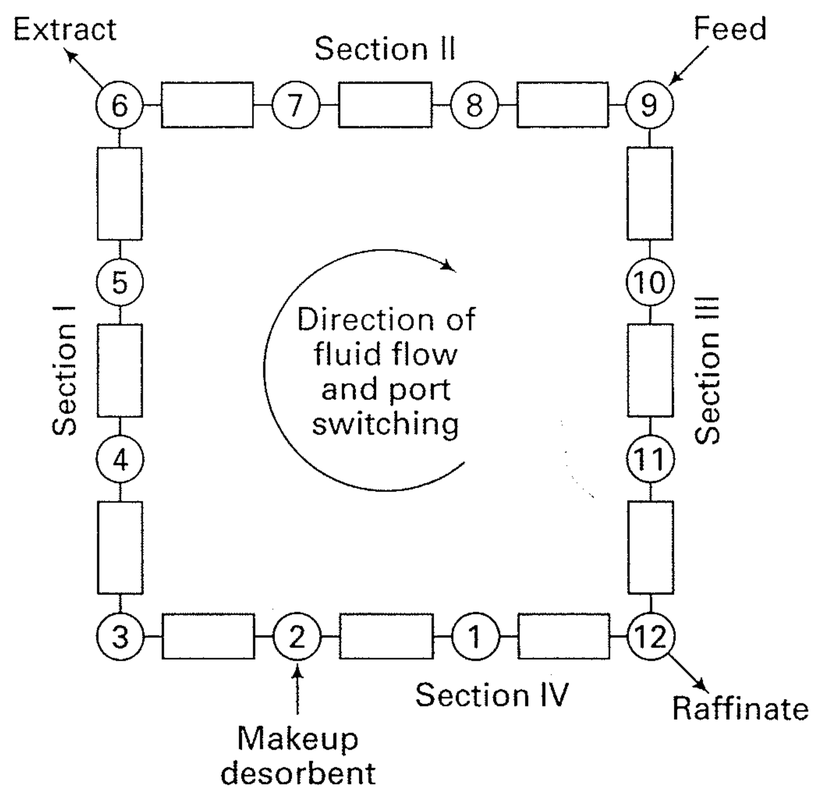

(b) Simulated-moving-bed system with port switching

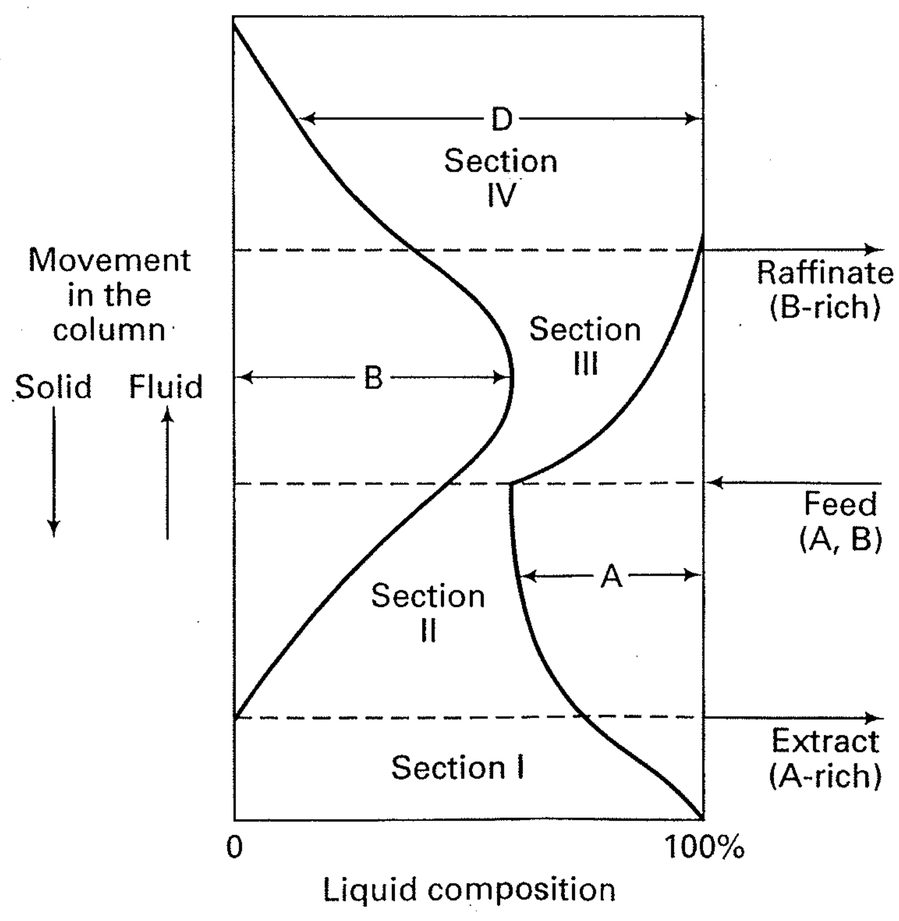

(c) Component composition profile

Figure 15.45 Four-section system.

referred to as zones, and the fixed-bed subsections in Figure 15.45b are often referred to as beds and sometimes columns. In the equivalent TMB case of Figure 15.45a, fluid of changing composition with respect to feed components A and B, and desorbent D, flows upward through the downward-flowing adsorbent beds. From the top of Section IV, fluid rich in D is recirculated to Section I. Fluid feed is shown as a binary mixture of A and B, which enters between Sections II and III. Component A is more strongly adsorbed than D, which is more strongly adsorbed than B. The desired result is that A is almost completely separated from B. However, appreciable amounts of D may appear in both the B-rich raffinate and A-rich extract. Thus, makeup D is added to the recirculated fluid.

Each of the four sections in Figure 15.45a performs a different primary function, listed in Figure 15.45a. More detail follows for the case where D, as well as A and B, are adsorbed. A typical component composition profile is shown in Figure 15.45c.

Section I: Desorb A. Entering S contains adsorbed A and D. Ideally, entering fluid is nearly pure D. Exiting S contains adsorbed D. Exiting fluid is A and D, part of which is withdrawn as A-rich extract.

Section II: Desorb B. Entering S contains adsorbed A, B, and D. Entering fluid is A and D. Exiting S contains adsorbed A and D. Exiting fluid is A, B, and D.

Section III: Adsorb A. Entering S contains adsorbed B and D. Entering fluid is A, B, and D from section II and fresh feed of A and B. Exiting S contains adsorbed A, B, and D. Exiting fluid is B and D, part of which is withdrawn as B-rich raffinate.

Section IV: Adsorb B. Entering S contains adsorbed D. Entering fluid is B and D. Exiting S contains adsorbed B and D. Ideally, exiting fluid is nearly pure D.

The steady-state separation achieved by the TMB in Figure 15.45a can be a close approximation to that achieved by the SMB, shown for a commercial Sorbex system in Figure 15.23 and by a simpler representation in Figure 15.45b. In both figures, it is seen that four sections are provided with a total of 12 ports for fluid feeds to enter, or fluid products to exit. In Figure 15.45b, it is clear that ports divide each section into subsections, four for Section I, three for Section II, three for Section III, and two for Section IV. As each section is divided into more subsections (thereby adding more ports), the SMB system more closely approaches the separation achieved in the corresponding TMB. In Figure 15.45b, only ports 2, 6, 9, and 12 are open. After an increment of time (called the switching time or port switching interval, t^*), those ports are closed and 3, 7, 10, and 1 are opened. In this manner, the ports are closed and opened in sequence in the direction shown. By periodically shifting feed and product positions by one port position in the direction of fluid flow, movement of solid adsorbent in the opposite direction within the sections is simulated. Because of stream additions and withdrawals between sections, flow rates in each of the four sections are different. Figure 15.23 shows a pump for controlling the fluid flow rate at the bottom of the SMB. Although sections are switched, the pump is not. Therefore, the pump must be programmed for four different flow rates depending on the section to which the pump is currently connected.

A number of models have been developed for designing and analyzing SMBs. These include: (1) TMB equilibrium-stage model using a McCabe–Thiele-type analysis, (2) TMB local adsorption-equilibrium model, (3) TMB rate-based model, and (4) SMB rate-based model. The first three assume steady-state conditions with continuous, countercurrent flows of fluid and solid adsorbent, approximating SMB operation with a TMB. The SMB rate-based model applies to transient operation for start-up, approach to a cyclic steady state, and shut-down. The simplest of the four approaches is the TMB equilibrium-stage model, but it is difficult to apply to multicomponent systems with nonlinear adsorption-equilibrium isotherms. The TMB local adsorption-equilibrium model, although ignoring the effects of axial dispersion and fluid-particle mass transfer, has proved useful for establishing reasonable operating flow rates in multiple sections of an SMB because, for many applications, behavior of an SMB is determined largely by adsorption equilibria. For a linear adsorption isotherm, Wankat [102] has successfully applied this method to SMBs with up to 32 sections for feeds dilute in the solutes. Methods for solving the TMB local adsorption equilibrium model for multicomponent systems, including concentrated mixtures, with nonlinear adsorption isotherms, have been presented by a number of investigators, including Storti et al. [103], who extended the pioneering work of Rhee, Aris, and Amundson [104] for a single section to the commonly used four-section unit, and Mazzotti et al. [105] for multicomponent systems. For a final design, rate-based models are preferred. These models, which account for axial dispersion in the bed, particle-fluid mass-transfer resistances, and nonlinear adsorption isotherms, are available in the program Aspen Chromatography, of the Aspen Engineering Suite, for both TMB steady-state operation and SMB dynamic operation. The local adsorption equilibrium and rate-based models are described next, followed by illustrative examples, two of which are solved using Aspen Chromatography. Equations are presented for four-section units, but are readily extended to more sections.

Steady-state Local Adsorption Equilibrium TMB Model

The TMB model describes continuous, steady-state, multicomponent adsorption with countercurrent flow of the fluid and solid adsorbent, as shown in Figure 15.46 for a single section of height Z of a multisection system, subject to these

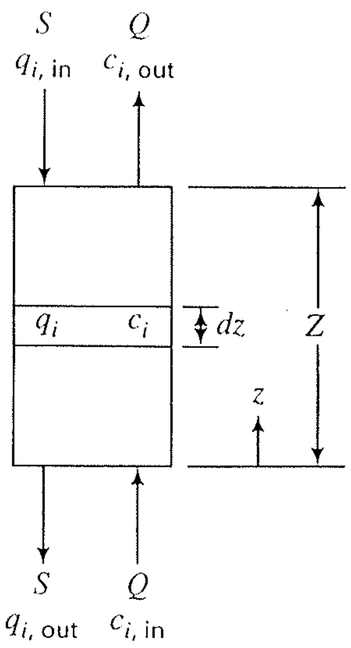

Figure 15.46 TMB local-adsorption-equilibrium model for a single section.

assumptions:

- One-dimensional plug flow of both phases with no channeling.
- Constant volumetric flow rates, of Q for the liquid and Q_S for the solid.
- Constant external void fraction, ϵ_b, of the solids bed.
- Negligible axial dispersion and particle-fluid mass-transfer resistances.
- Local adsorption equilibrium between solute concentrations, c_i, in the bulk liquid and adsorption loading, q_i, on the solid.
- Isothermal and isochoric conditions.

For a differential-bed thickness, dz, where component i undergoes mass transfer between the two phases, this mass balance applies:

$$Q\frac{dc_i}{dz} - S\frac{dq_i}{dz} = 0 \qquad \text{(15-138)}$$

Boundary conditions are

$$z = 0,\ c_i = c_{i,\text{in}} \quad \text{and} \quad z = Z,\ q_i = q_{i,\text{in}}$$

The solution to (15-138) depends on the equilibrium adsorption isotherm. Typically, when the fluid is a liquid dilute in solutes, a linear (Henry's law) isotherm, $q_i = K_i c_i$, is used, where q_i is on a particle volume basis so that K_i is dimensionless. For the bulk separation of liquid mixtures, where concentrations of the feed components and desorbent are not small, a nonlinear, extended-Langmuir-equilibrium-adsorption isotherm of the constant-selectivity form, from Example (15.6) applies

$$q_i = \frac{(q_i)_m K_i c_i}{1 + \sum_j K_j c_j} \qquad \text{(15-139)}$$

In either case, the solution of Rhee, Aris, and Amundson [104], when extended to multiple (e.g., four) sections, as by Storti et al. [103], predicts constant component concentrations in each section, but with discontinuities at either one or both section boundaries. Typical concentration profiles are shown in Figure 15.47 for a four-solute system (1, 2, 3, and 4), where a set of stationary rectangular (shock-like) waves of constant concentration exists in the fluid phase in each section. The concentration profile for the desorbent (component 5) is not shown. Note that the concentrations of the four solutes for this local equilibrium assumption are negligible in Sections I and IV, where only desorbent is present.

The usefulness of local equilibrium theory is in approximate determinations of required solid adsorbent and fluid flow rates in each section of a TMB in order to achieve a perfect separation of two solutes. The description of the method, first developed by Ruthven and Ching [106] and extended by Zhong and Guiochon [107], is facilitated by applying local adsorption-equilibrium theory to the simple case of a feed dilute in binary solutes, A and B, that are to be completely separated. Assume diluent, D, does not adsorb and Henry's law governs adsorption equilibrium, with $K_A > K_B$ (i.e., A is more strongly adsorbed). First, we define a set of flow rate ratios, m_j, one for each section, j, as

$$m_j = \frac{Q_j}{Q_s} = \frac{\text{volumetric fluid phase flow rate}}{\text{volumetric solid particle phase flow rate}} \qquad \text{(15-140)}$$

For conditions of local adsorption equilibrium, the following necessary and sufficient conditions apply to each section for

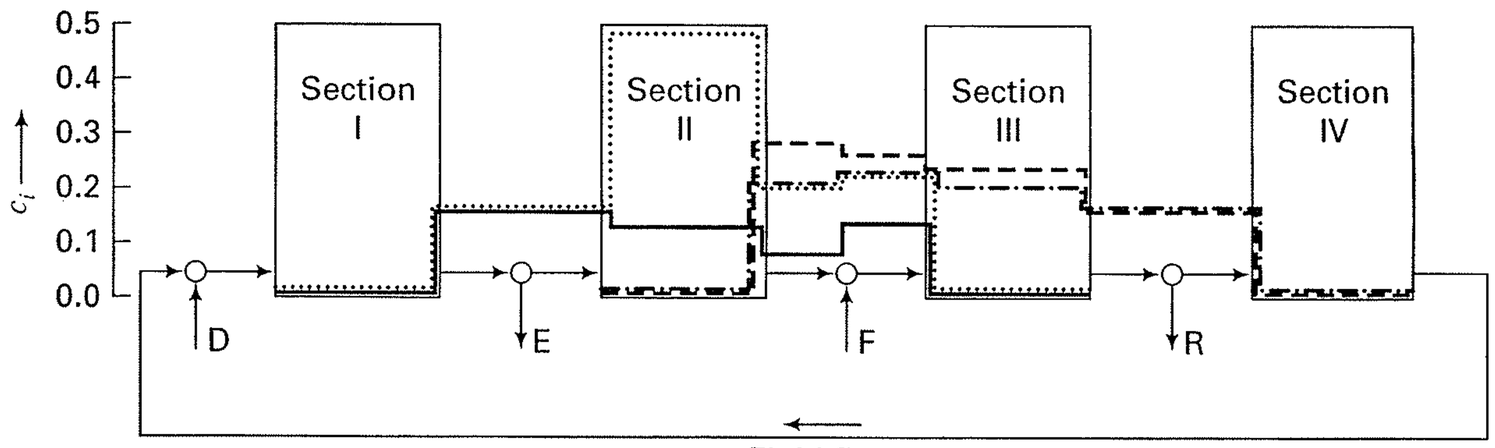

Component		Relative adsorption selectivity
1	—·—·—·	1.00
2	– – – – –	1.12
3	.....	2.86
4	———	5.71
5	(not shown)	1.90

Figure 15.47 Typical solute-concentration profiles for local adsorption equilibrium in a four-section unit.

complete separation:

$$K_A < m_I < \infty \tag{15-141}$$

$$K_B < m_{II} < K_A \tag{15-142}$$

$$K_B < m_{III} < K_A \tag{15-143}$$

$$0 < m_{IV} < K_B \tag{15-144}$$

Constraint (15-142) ensures that net flow rates of components A and B will be positive (upward) in section I. Constraint (15-144) ensures that the net flow rates of components A and B will be negative (downward) in Section IV. Constraints (15-142) and (15-143) are most important because they ensure sharpness of the separation. They cause net flow rates of A and B to be negative (downward) and positive (upward), respectively, in the two central sections II and III. Inequality constraints (15-141) to (15-144) may be converted to equality constraints, where β, the safety margin, is discussed shortly.

$$Q_I/Q_S = K_A\beta \tag{15-145}$$

$$(Q_I - Q_E)/Q_S = K_B\beta \tag{15-146}$$

$$(Q_I - Q_E + Q_F)/Q_S = K_A/\beta \tag{15-147}$$

$$(Q_I - Q_E + Q_F - Q_R)/Q_S = K_B/\beta \tag{15-148}$$

Solving (15-145) to (15-148) by eliminating Q_I gives

$$Q_S = \frac{Q_F}{K_A/\beta - K_B\beta} \tag{15-149}$$

$$Q_E = Q_S(K_A - K_B)\beta \tag{15-150}$$

$$Q_R = Q_S(K_A - K_B)/\beta \tag{15-151}$$

Then, using (15-145),

$$Q_I = Q_C + Q_D = Q_S K_A\beta \tag{15-152}$$

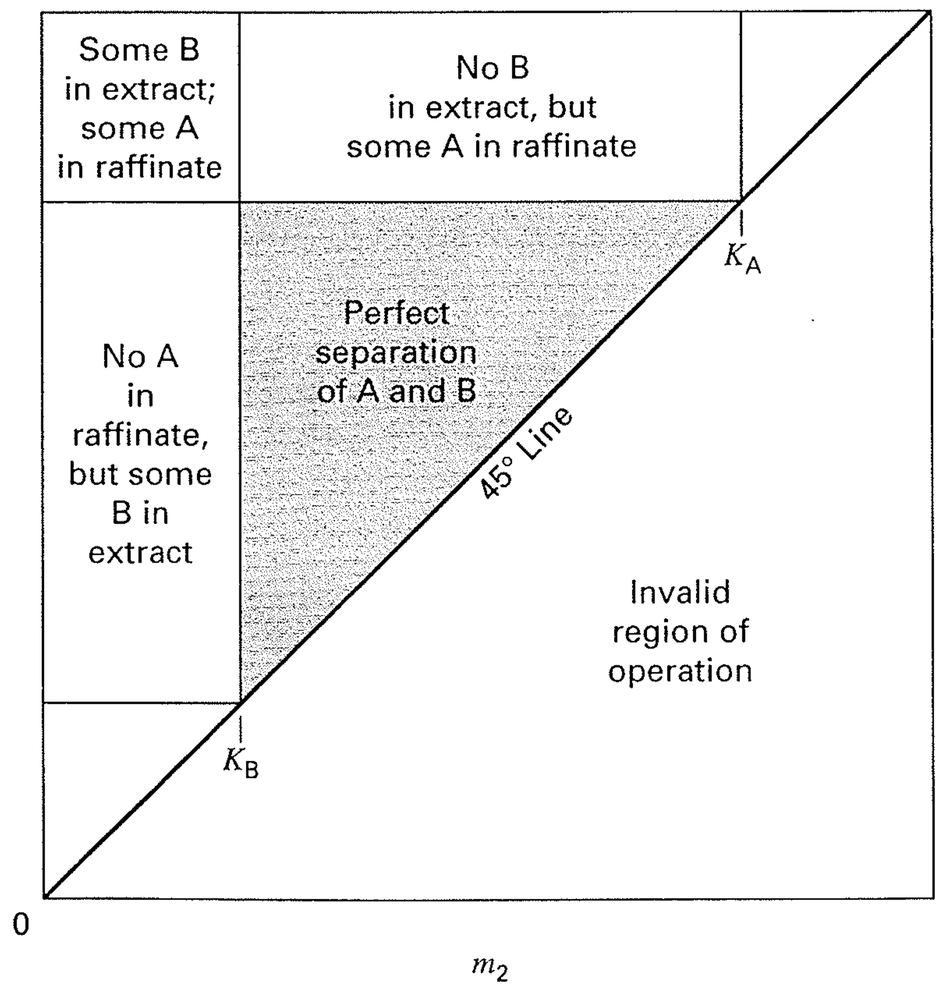

Figure 15.48 Triangle method for determining necessary values of flow rate ratios.

Therefore,

$$Q_C = Q_S K_A\beta - Q_D \tag{15-153}$$

where Q_C = fluid recirculation rate before adding makeup desorbent. By an overall material balance,

$$Q_D = Q_E + Q_R - Q_F \tag{15-154}$$

Restrictions on flow rate ratios, m_{II} and m_{III} in inequality constraints (15-142) and (15-143), are conveniently represented by the *triangle method* of Storti et al. [107], as shown in Figure 15.48. If values of m_{II} and m_{III} within the triangular region are selected, a perfect separation is possible. However, if $m_{II} < K_B$, some B will appear in the extract; if $m_{III} > K_A$, some A will appear in the raffinate. If $m_{II} < K_B$ and $m_{III} > K_A$, extract will contain some B and raffinate will contain some A.

The permissible range for safety margin, β, in (15-145) to (15-151) is determined from inequality constraints (15-142) and (15-143). Let

$$\gamma_{i,j} = \frac{m_j}{K_i} = \frac{Q_j}{Q_S K_i} \tag{15-155}$$

In Section II, we require that $\gamma_{A,II} > 1$ and $\gamma_{B,II} < 1$. In terms of safety margin, β, we can apply (15-155) to give corresponding equalities, $Q_{II}/Q_S = K_A/\beta$ and $Q_{II}/Q_S = K_B\beta$, assuming equal β in all four sections. Equating these two equalities for the same safety margin gives $\beta = \sqrt{K_A/K_B}$, which is the maximum value of β for a perfect separation, the minimum value being 1.0. Above the maximum value of β, some sections will encounter negative fluid flow rates. Below a β value of 1.0, a perfect separation will not be achieved. As the value of β increases from minimum to maximum, fluid flow rates in the sections increase, often exponentially. Thus, estimation of operating flow rates is generally carried out using a value of β close to, but above, 1.0, e.g., 1.05 (unless it exceeds the maximum value of β). Note that as the separation factor, K_A/K_B, approaches 1.0, not only does the separation become more difficult, but also, the permissible range of β becomes smaller. In the triangle method, illustrated in Figure 15.48, the upper left corner of the triangle corresponds to $\beta = 1$, while the maximum value of β occurs when $m_{II} = m_{III}$, which falls on the 45° line between the values K_A and K_B. Extensions of the above binary procedures for estimating operating flow rates to cases of both constant selectivity Langmuir adsorption isotherms and to more complex nonlinear isotherms are given by Mazzotti et al. [109] and for multicomponent systems by Mazzotti et al. [105]. With nonlinear adsorption isotherms, the right triangle of Figure 15.48 is distorted to a shape with one or more curved sides.

EXAMPLE 15.16

Fructose (A) is separated from glucose (B) in a four-section SMB unit. The aqueous feed of 1.667 mL/min contains 0.467 g/min of A, 0.583 g/min of B, and 0.994 g/min of water. For the adsorbent and

expected concentrations and temperature of the operation, Henry's law holds, with constants of $K_A = 0.610$ and $K_B = 0.351$ for fluid concentrations in g/mL and loadings in g/mL of adsorbent particles. Water is assumed not to adsorb. Estimate operating flow rates in mL/min to achieve a perfect separation of fructose from glucose for a TMB. Note that the extract will contain fructose, while raffinate will contain glucose. Conversion of the results to SMB operation will be made in Example 15.17.

SOLUTION

Equations (15-149) to (15-154) apply. The minimum value of β is 1.0, while the maximum value is $\sqrt{K_A/K_B} = \sqrt{0.610/0.351} = 1.32$. Calculations are most conveniently carried out with a spreadsheet. With reference to Figure 15.45 for the case of a TMB, the results for values of β = 1.0, 1.05, 1.20 are:

	Volumetric Flow Rates, mL/min		
	β = 1.0	β = 1.05	β = 1.20
Feed, Q_F	1.667	1.667	1.667
Solid particles, Q_S	6.436	7.848	19.132
Extract, Q_E	1.667	2.134	5.946
Raffinate, Q_R	1.667	1.936	4.129
Recirculation, Q_C	2.259	2.624	5.596
Make-up desorbent, Q_D	1.667	2.403	8.408
Q_{I}	3.926	5.027	14.004
Q_{II}	2.259	2.893	8.058
Q_{III}	3.926	4.560	9.725
Q_{IV}	2.259	2.624	5.596

Note that the lowest section fluid flow rates, Q_{I}–Q_{IV}, correspond to β = 1.0. At β = 1.2, section fluid flow rates, as well as the adsorbent particles flow rate, become significantly higher. The most concentrated products (extract and raffinate) and the smallest flow rate of make-up desorbent are also achieved with the lowest β value.

Steady-state TMB Model

This model, which assumes plug flow at isothermal, isobaric, and constant-fluid-velocity conditions in each section, j, ($j = 1$ to 4) requires for each component, i ($i = 1$ to C) the following equations, where each section begins at $z = 0$, where the fluid enters, and ends at $z = L_j$. Unlike the previous local adsorption-equilibrium model, axial dispersion and fluid-particle mass transfer are taken into account.

(1) Mass-balance equation for the bulk fluid phase, f, [similar to (15-102)]:

$$-D_{L_j}\frac{d^2c_{i,j}}{dz^2} + u_{f_j}\frac{dc_{i,j}}{dz} + \frac{(1-\epsilon_b)}{\epsilon_b}J_{i,j} = 0 \quad (15\text{-}156)$$

where the first term accounts for axial dispersion, J_i is the mass-transfer flux between the bulk fluid phase and the sorbate in the pores of the solid, and u_f is the interstitial fluid velocity, where for an adsorbent bed of cross-sectional area, A_b,

$$u_{f_j} = \frac{Q_j}{\epsilon_b A_b} \quad (15\text{-}157)$$

(2) Mass-balance equation for the sorbate, s, on the solid phase:

$$u_s\frac{d\bar{q}_{i,j}}{dz} - J_{i,j} = 0 \quad (15\text{-}158)$$

where u_s is the true moving-solid velocity, where

$$u_s = \frac{Q_S}{(1-\epsilon_b)A_b} \quad (15\text{-}159)$$

(3) Fluid-to-solid mass transfer [similar to (15-105)]:

$$J_{i,j} = k_{i,j}(q^*_{i,j} - \bar{q}_{i,j}) \quad (15\text{-}160)$$

(4) Adsorption isotherm [e.g., the multicomponent, extended-Langmuir equation of (15-139)]:

$$q^*_{i,j} = f\{\text{all } c_{i,j}\} \quad (15\text{-}161)$$

This system of $4C$ second-order ODEs and $4C$ first-order ODEs, together with the algebraic equations for mass-transfer rates and adsorption equilibria, requires $12C$ boundary conditions, i.e., $3C$ for each section.

At the entrance, $z = 0$, to each section, we require a boundary condition that accounts for axial dispersion. This has been discussed extensively in the literature, e.g., Danckwerts [110]. Most often used is

$$u_{f_j}(c_{i,j,0} - c_{i,j}) = -\epsilon_b D_{L_j}\frac{dc_{i,j}}{dz} \quad (15\text{-}162)$$

where $c_{i,j,0}$ is the concentration of component i entering ($z = 0$) section j.

For continuity of bulk fluid concentrations and sorbate loadings in moving from one section to another, the following boundary conditions apply at boundaries of adjacent sections:

At Sections I and II where extract is withdrawn:

$$c_{i,\mathrm{I},z=L_j} = c_{i,\mathrm{II},z=0} \quad (15\text{-}163)$$

$$q_{i,\mathrm{I},z=L_j} = q_{i,\mathrm{II},z=0} \quad (15\text{-}164)$$

At Sections III and IV where raffinate is withdrawn:

$$c_{i,\mathrm{III},z=L_j} = c_{i,\mathrm{IV},z=0} \quad (15\text{-}165)$$

$$q_{i,\mathrm{III},z=L_j} = q_{i,\mathrm{IV},z=0} \quad (15\text{-}166)$$

At Sections II and III where the feed enters:

$$c_{i,\mathrm{III},z=0} = \frac{Q_{\mathrm{II}}}{Q_{\mathrm{III}}}c_{i,\mathrm{II},z=L_{\mathrm{II}}} + \frac{Q_F}{Q_{\mathrm{III}}}c_{i,F} \quad (15\text{-}167)$$

$$q_{i,\mathrm{II},z=L_j} = q_{i,\mathrm{III},z=0} \quad (15\text{-}168)$$

At Sections IV and I where make-up desorbent enters:

$$c_{i,\mathrm{I},z=0} = \frac{Q_{\mathrm{IV}}}{Q_{\mathrm{I}}}c_{i,\mathrm{IV},z=L_{\mathrm{II}}} + \frac{Q_D}{Q_{\mathrm{I}}}c_{i,D} \quad (15\text{-}169)$$

$$q_{i,\mathrm{IV},z=L_j} = q_{i,\mathrm{I},z=0} \quad (15\text{-}170)$$

where the volumetric fluid flow rates, which change from section to section, are subject to

$$Q_{\mathrm{I}} = Q_{\mathrm{IV}} + Q_D \tag{15-171}$$

$$Q_{\mathrm{II}} = Q_{\mathrm{I}} - Q_E \tag{15-172}$$

$$Q_{\mathrm{III}} = Q_{\mathrm{II}} + Q_F \tag{15-173}$$

$$Q_{\mathrm{IV}} = Q_{\mathrm{III}} - Q_E \tag{15-174}$$

It is important to note that for an SMB, solid particles do not flow down through the unit, but are retained in stationary beds in each section. To obtain the same true velocity difference between the fluid and solid particle phase, the upward fluid velocity in the SMB must be the sum of the absolute true velocities in the upward-moving fluid and downward-moving solid particle phases in the TMB. Thus, using (15-157) and (15-159),

$$(Q_j)_{\mathrm{SMB}} = (Q_j)_{\mathrm{TMB}} + \left(\frac{\epsilon_b}{1-\epsilon_b}\right)(Q_S)_{\mathrm{TMB}} \tag{15-175}$$

The TMB model can be solved by any of a number of techniques, as discussed by Constantinides and Mostoufi [111], with the Newton shooting method being preferred. An example of the application of the steady-state TMB model is given after the next subsection that treats dynamic SMB models.

Dynamic SMB Model

The equations are subject to the same assumptions as the steady-state TMB model. Changes in the equations permit the model to take into account time of operation, t, and to use a fluid velocity relative to the stationary solid particles. In addition, equations now must be written for each bed subsection (also referred to as a column), k, between adjacent ports, as shown in Figure 15.45b. The revised equations are

(1) Mass-balance equation for the bulk fluid phase, f [similar to (15-102)]:

$$\frac{\partial c_{i,k}}{\partial t} - D_{L_j}\frac{\partial^2 c_{i,k}}{\partial z^2} + u_{f_k}\frac{\partial c_{i,k}}{\partial z} + \frac{(1-\epsilon_b)}{\epsilon_b}J_{i,k} = 0 \tag{15-176}$$

(2) Mass-balance equation for sorbate on the solid phase:

$$\frac{\partial \bar{q}_{i,k}}{\partial t} - J_{i,k} = 0 \tag{15-177}$$

where the interstitial fluid velocity for SMB operation is related to that for TMB operation at a particular location by

$$(u_f)_{\mathrm{SMB}} = (u_f)_{\mathrm{TMB}} + |(u_s)|_{\mathrm{TMB}} \tag{15-178}$$

SMB and TMB models are further connected by an equation that relates solid velocity in the TMB model to a port-switching time, t^*, and bed height between adjacent ports, L_k, for use in this SMB model:

$$u_s = \frac{L_k}{t^*} \tag{15-179}$$

The boundary conditions for the TMB model apply to SMB models. In addition, initial conditions are needed for fluid concentrations, $c_{i,j}$, and sorbate loadings, $\bar{q}_{i,j}$, throughout the adsorbent beds; e.g., at $t = 0$, $c_{i,k} = 0$ and $\bar{q}_{i,k} = 0$.

The SMB model, which involves PDEs, rather than ODEs, is much more difficult to solve than the steady-state TMB, because it involves moving concentration fronts. In Aspen Chromatography, the dynamic SMB equations are solved by discretizing the first- and second-order spatial terms of the PDEs to obtain a large set of ODEs and algebraic equations, which constitute a DAE (differential algebraic equations) system. A number of discretization or differencing methods are provided. Each complete cycle of the SMB model provides a different result, which ultimately leads to a cyclic steady state. Studies have shown that if the number of bed subsections per section is at least four and the number of cycles is 10 or more, the steady-state TMB result closely approximates the SMB result. Therefore, if only steady-state results are of interest, the simpler steady-state TMB model is best employed.

All four models can be applied to a gas or liquid mixture, with the latter being the most widely applied to industrial separations. Regardless of the model used for design of an SMB (dynamic SMB or steady-state TMB), the basic information required is:

1. Flow rate and composition of the feed (binary of A and B, or multicomponent).
2. Selection of a suitable adsorbent, S, and desorbent, D.
3. Nominal bed operating temperature, T, and pressure, P.
4. A suitable adsorption isotherm for all components, with known constants at the bed operating conditions.
5. Desired separation, which may be purity (on a desorbent-free basis) and desired recovery of the most strongly adsorbed component in the extract.

Not initially known, but required before calculations can be made, are:

6. Total bed height and inside diameter of the adsorption column.
7. Amount of adsorbent in the column.
8. Desorbent recirculation rate.
9. Flow rates of extract and raffinate.
10. Overall mass-transfer coefficients for transport of solutes between bulk fluid and sorbate layer on the adsorbent.
11. Eddy diffusivity for axial dispersion.
12. Spacing of inlet and outlet ports.

Some guidance on initial values for items 6, 10, and 11 is sometimes provided in patents for similar separations. For example, for the separation of xylene mixtures using para diethylbenzene as desorbent, Minceva and Rodrigues [112] suggest:

- Molecular-sieve zeolite adsorbent with a spherical particle diameter, d_p, between 0.25 and 1.00 mm and a particle density, ρ_p, of 1.39 g/cm^3.

- Operating temperature between 140°C and 185°C with an operating pressure sufficient to maintain a liquid phase.
- Liquid interstitial velocity, u_f, between 0.4 and 1.2 cm/s.
- Four sections with eight to 24 subsections (beds).

For a commercial-size unit, the following are suggested:

- Bed height, L_k, in each subsection from 40 to 120 cm.
- Equation (15-106) for estimating overall mass-transfer coefficient, $k_{i,j}$, for solute transport between bulk fluid and sorbate layer on the adsorbent.
- An axial diffusivity, D_{L_j}, defined in terms of a Peclet number, where

$$N_{\text{Pe}} = \frac{u_f(\text{characteristic length})}{D_L} \qquad (15\text{-}180)$$

Characteristic lengths equal to bed depth or particle diameter have been used. Most common for TMB and SMB is bed depth, with Peclet numbers in the 1000–2000 range.

EXAMPLE 15.17

Use the results of the fructose-glucose separation of Example 15.16, for $\beta = 1.05$, with the steady-state TMB model of Aspen Chromatography to estimate product compositions obtained with the following laboratory-size SMB unit:

Number of sections = 4

Number of subsections (beds) in each section (column) = 2

All bed diameters = 2.54 cm

All bed heights = 10 cm

Bed void fraction = 0.40

Particle diameter = 500 microns (0.5 mm)

Overall mass-transfer coefficient for A and B = 10 min^{-1}

Peclet number high enough that axial dispersion is negligible

SOLUTION

To use Aspen Chromatography, the recirculating liquid flow rate for a TMB must be converted to a SMB using (15-175), and solid-particle flow rate must be converted to a port switching time given by (15-179). From (15-175), using the results for $\beta = 1.05$ in Example 15.16,

$$(Q_C)_{\text{SMB}} = 2.624 + \left(\frac{0.40}{1 - 0.40}\right) 7.848 = 7.856 \text{ mL/min}$$

The total liquid rate in Section I of the SMB is

$$(Q_{\text{I}})_{\text{SMB}} = (Q_C)_{\text{SMB}} + Q_D = 7.856 + 2.403 = 10.259 \text{ mL/min}$$

This is the maximum volumetric flow rate in the SMB and it is of interest to calculate the corresponding interstitial fluid velocity. From (15-157),

$$(u_{f\text{I}})_{\text{SMB}} = \frac{(Q_{\text{I}})_{\text{SMB}}}{\epsilon_b A_b} = \frac{10.259}{0.40\left[\dfrac{3.14(2.54)^2}{4}\right]}$$

$$= 5.06 \text{ cm/min} = 0.0844 \text{ cm/s}$$

This fluid velocity is low, but it corresponds to a desirable bed diameter-to-particle diameter ratio of 2.54/0.05 = 49. To increase fluid velocity to, say, 0.4 cm/s, the bed diameter would be decreased to 1.17 cm, giving a bed diameter-to-particle diameter of 23, which would still be acceptable.

From (15-159), the true velocity of the solid particles in each bed is

$$u_s = \frac{Q_S}{(1 - \epsilon_b)A_b} = \frac{7.848}{(1 - 0.40)\left[\dfrac{3.14(2.54)^2}{4}\right]} = 2.58 \text{ cm/min}$$

From (15-179), port-switching time for subsection bed height, L, of 10 cm is,

$$t^* = \frac{L}{u_s} = \frac{10}{2.58} = 3.88 \text{ min}$$

The following results were obtained from Aspen Chromatography for a steady-state TMB:

	Feed	Desorbent	Extract	Raffinate
Flow rate, mL/min	1.667	2.403	2.134	1.936
Concentrations, g/L:				
Fructose	280.0	0.0	211.6	12.7
Glucose	350.0	0.0	8.4	295.3
Water	596.0	996.0	861.7	795.8
Mass fraction on water-free basis:				
Fructose	0.444		0.962	0.040
Glucose	0.556		0.038	0.960

As seen in the table, a reasonably sharp separation between fructose and glucose is achieved. In Exercise 15.39, modifications to the input data are studied in an attempt to improve separation sharpness.

EXAMPLE 15.18

Minceva and Rodrigues [112] consider the industrial-scale separation of paraxylene from a liquid mixture of C_8 aromatics in a four-section SMB. Feed to the unit is 1,450 L/min with the composition shown in a table below, which also contains results for this example. The adsorbent is a molecular-sieve zeolite with a particle density of 1.39 g/cm^3 and a particle diameter of 0.092 cm that packs a bed with an external void fraction of 0.39. The desorbent is paradiethylbenzene (PDEB). With reference to Figure 15.45, the number of subsections is 6, 9, 6, and 3, respectively, in Sections I to IV. The height of each bed subsection is 1.135 m, with a bed diameter of 4.117 m. The operation takes place at 180°C and a pressure above 12 bar, sufficient to prevent vaporization. At these conditions, the extended Langmuir adsorption isotherm (15-139) correlates adsorption equilibrium, yielding the following constants. Note that this is a constant-selectivity isotherm; therefore, the selectivity relative to paradiethylbenzene is tabulated.

Component	q_m, mg/g	K, cm^3/mg	Selectivity
Paraxylene	130.3	1.0658	0.9969
Paradiethylbenzene	107.7	1.2935	1.0000
Ethylbenzene	130.3	0.3067	0.2689
Metaxylene	130.3	0.2299	0.2150
Orthoxylene	130.3	0.1884	0.1762

Note that the desorbent does not have the most desirable equilibrium adsorption property because its selectivity does not lie between that of paraxylene and the C_8 components of the feed. Take the overall mass-transfer coefficient between sorbate and bulk fluid, in (15-160), as 2 min^{-1} for each component. For axial dispersion, assume a Peclet number of 700 in (15-180) with a characteristic length of bed height.

Using Aspen Chromatography with the TMB model as an approximation of the SMB, determine steady-state flow rates and compositions of extract and raffinate, together with the composition profiles in the four sections for the following operating conditions:

Extract flow rate = 1,650 L/min

Raffinate flow rate = 2,690 L/min

Circulation flow rate, $(Q_C)_{SMB}$, before adding makeup DPEB = 5,395 L/min

Port-switching interval, $t^* = 1.15$ min

SOLUTION

By an overall material balance, the DPEB makeup flow rate is

$$Q_D = Q_E + Q_R - Q_F = 1{,}650 + 2{,}690 - 1{,}450 = 2{,}890 \text{ L/min}$$

From the switching time, using (15-179), with a 1.135-m bed height,

$$u_s = 1.135/1.15 = 0.987 \text{ m/min} = 98.7 \text{ cm/min}$$

The adsorbent bed cross-sectional area, $A_b = 3.14(4.117)^2/4 = 13.31$ m^2.

From (15-159), the volumetric flow rate of the solid particles in a TMB is

$$Q_S = u_s(1-\epsilon)A_b = 0.987(1-0.39)(13.31)$$
$$= 8.014 \text{ m}^3/\text{min} = 8{,}014 \text{ L/min}$$

Liquid flow rates in the four sections are as follows, where both $(Q_j)_{SMB}$ and $(Q_j)_{TMB}$ flow rates are included, where the former are computed by material balance and the latter from (15-175). For example,

$$(Q_I)_{SMB} = (Q_C)_{SMB} + Q_D = 5{,}395 + 2{,}890 = 8{,}285 \text{ L/min}$$
$$(Q_I)_{TMB} = (Q_I)_{SMB} - [0.39/(1-0.39)]Q_S$$
$$= 8{,}285 - 0.639(8{,}014) = 3{,}164 \text{ L/min}$$

Section in Figure 15.45	$(Q_j)_{SMB}$, L/min	$(Q_j)_{TMB}$, L/min
I	8,285	3,164
II	6,635	1,514
III	8,085	2,964
IV	5,395	274

Results of the Aspen Chromatography calculations for the steady-state TMB model, but on an SMB basis are:

Wt% of component	Feed	Desorbent	Extract	Raffinate
Ethylbenzene	14.0	0.0	0.00	7.63
Metaxylene	49.7	0.0	0.00	27.09
Orthoxylene	12.7	0.0	0.00	6.92
PDEB	0.0	100.0	80.79	57.85
Paraxylene	23.6	0.0	19.21	0.51

Note that an excellent separation between paraxylene and the other feed components of the feed is achieved. However, both the extract and raffinate contain a substantial fraction of desorbent, PDEB. The desorbent in both products is recovered by the hybrid SMB-distillation process shown in Figure 15.23. Component concentration profiles in the four sections, as computed by Aspen Chromatography, are shown in Figure 15.49. In Sections I and III particularly, they differ considerably from the flat profile predictions of the simple, local-equilibrium TMB model. The circulating desorbent is predicted to be essentially pure PDEB.

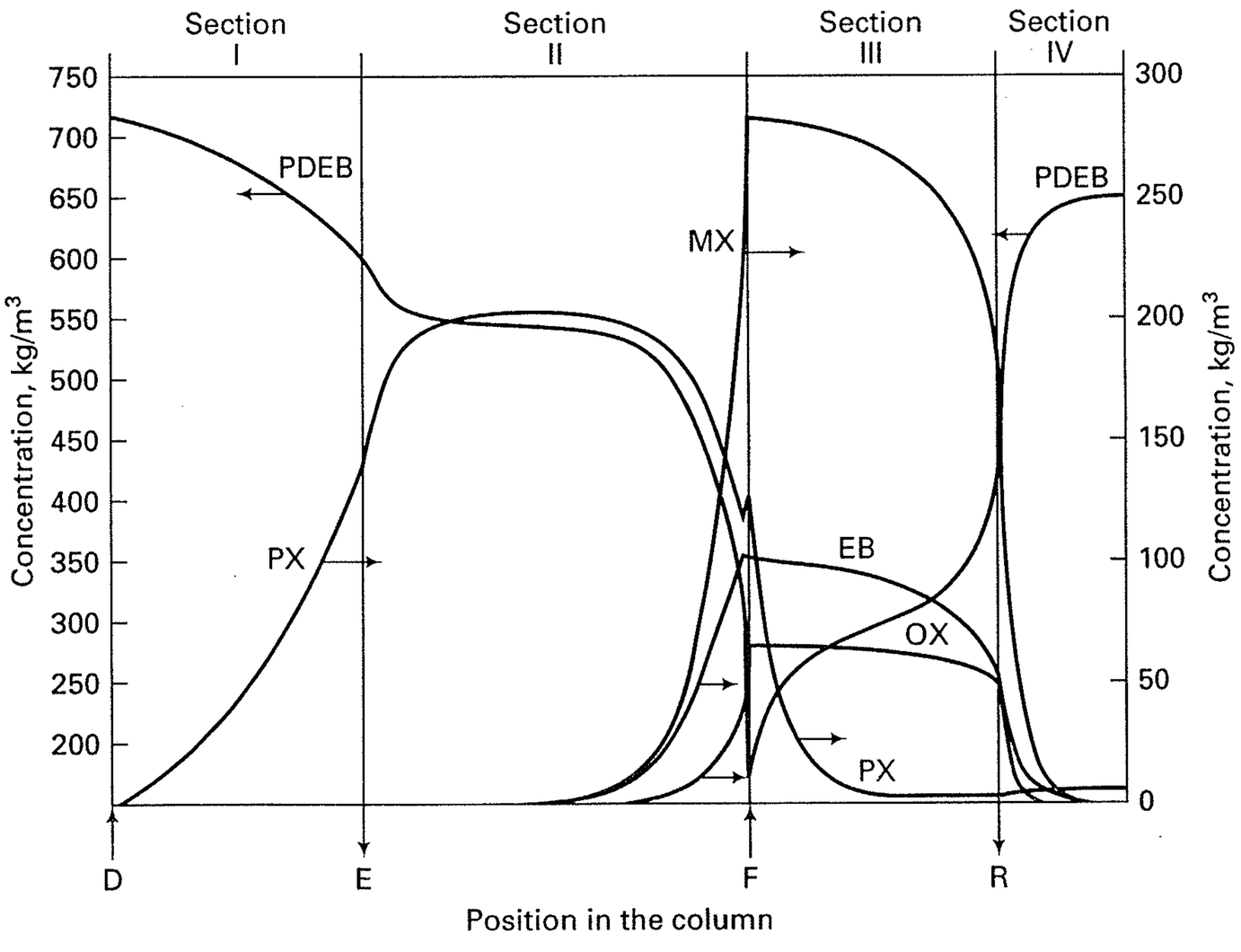

Figure 15.49 Concentration profiles in the liquid for SMB of Example 15.18.

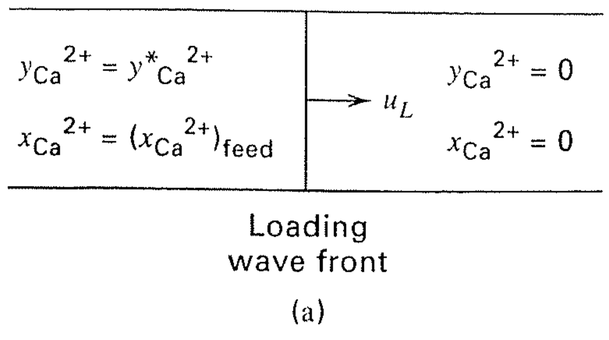

Figure 15.50 Ion exchange in a cyclic operation with a fixed bed. (a) Loading step. (b) Displacement and regeneration steps.

Ion-Exchange Cycle

Although ion exchange has a wide range of applications, water softening with gel resins continues to be the major one. Usually a fixed bed is used, which is operated in a cycle of four steps: (1) loading, (2) displacement, (3) regeneration, and (4) washing. The solute ions removed from water in the loading step are mainly Ca^{2+} and Mg^{2+}, which are absorbed by resin while an equivalent amount of Na^+ is transferred from resin to water as feed solution flows down through the bed. If mass transfer is rapid, the solution and resin are at equilibrium at all points in the bed. With a divalent ion (e.g., Ca^{2+}) replacing a monovalent ion (e.g., Na^+), the equilibrium expression is given by (15-44), where A is the divalent ion. If $(Q/C)^{n-1}K_{A,B} \gg 1$, equilibrium for the divalent ion is very favorable (see Figure 15.29a) and a self-sharpening front of the type shown in Figure 15.29b develops. In that case, which is common, ion exchange is well approximated using simple stoichiometric or shock-wave front theory for adsorption, assuming plug flow. As the front moves down through the bed, the resin behind or upstream of the front is in equilibrium with the feed composition. Ahead or downstream of the front, water is essentially free of the divalent ion(s). Breakthrough occurs when the front reaches the end of the bed.

Suppose the only cations in the feed are Na^+ and Ca^{2+}. Then, from (15-44):

$$K_{Ca^{2+},Na^+}\left(\frac{Q}{C}\right) = \frac{y_{Ca^{2+}}(1 - x_{Ca^{2+}})}{x_{Ca^{2+}}(1 - y_{Ca^{2+}})} \qquad (15\text{-}181)$$

where Q is total concentration of the two cations in the resin, in eq/L of bed of wet resin, and C is total concentration of the two ions in the solution, in eq/L of solution. One mole of Na^+ is 1 equivalent, while 1 mole of Ca^{2+} is 2 equivalents. The quantities y_i and x_i are equivalent (rather than mole) fractions. From Table 15.5, using (15-45), the molar selectivity factor is

$$K_{Ca^{2+},Na^+} = 5.2/2.0 = 2.6$$

For a given loading step during water softening, values of Q and C remain constant. Thus, for a given equivalent fraction, $x_{Ca^{2+}}$ in the feed, (15-181) is solved for the equilibrium $y_{Ca^{2+}}$. By material balance, for a given bed volume, the time t_L for the loading step is computed. The loading wavefront velocity is $u_L = L/t_L$ where L is the height of the bed. Equivalent fractions ahead of and behind the loading front are shown in Figure 15.50a. Typically, feed-solution superficial mass velocities are about 15 gal/h-ft^2, but can be much higher at the expense of larger pressure drops.

At the end of the loading step, the bed voids are filled with feed solution, which must be displaced from the bed. This is best done with a regeneration solution, which is usually a concentrated salt solution that flows upwards through the bed. Thus, the displacement and regeneration steps are combined. Following displacement, mass transfer of Ca^{2+} from the resin beads to the regenerating solution takes place while an equivalent amount of Na^+ is transferred from the solution to the resin. In order for equilibrium to be favorable for regeneration with Na^+, it is necessary for $(Q/C)K_{Ca^{2+},Na^+} \ll 1$. In that case, which is just the opposite for loading, the wavefront during regeneration sharpens quickly into a shock-like wave. This criterion can be satisfied by using a saturated salt solution to give a large value for C.

During displacement and regeneration, two concentration waves move through the bed. The first is the displacement front; the second, the regeneration front. For plug flow and negligible mass-transfer resistance, the resin and solution are in equilibrium at all locations in the bed. Again (15-181) is used to solve for the equilibrium equivalent fractions, which are shown for the displacement and regeneration steps in Figure 15.50b. The displacement time, t_D, is determined from the interstitial velocity, u_D, of the fluid during displacement:

$$t_D = L/u_D \qquad (15\text{-}182)$$

The regeneration time, t_R, is determined by material balance, from which the regeneration wavefront velocity is $u_R = L/t_R$. In general, the mass velocity of the regeneration solution is less than that of the feed solution. The cycle is completed by displacing, with water, the salt solution in the bed voids. The cycle calculations are illustrated by the following example.

EXAMPLE 15.19

Hard water, containing 500 ppm (by weight) of magnesium carbonate and 50 ppm of NaCl, is to be softened at 25°C in an existing fixed bed of gel resin of a cation capacity of 2.3 eq/L of bed volume. The bed is 8.5 ft in diameter and packed to a height of 10 ft, with a wetted-resin void fraction of 0.38. During the loading step, the recommended throughput is 15 gal/min-ft^2. During displacement, regeneration, and washing, the flow rate is reduced to 1.5 gal/min-ft^2. The displacement and regeneration solutions are water saturated with NaCl (26 wt%). Determine: (a) flow rate of feed solution, L/min, (b) loading time to breakthrough, h, (c) loading wavefront velocity, cm/min, (d) flow rate of regeneration solution, L/min, (e) displacement time, h, (f) additional time for regeneration, h, (g) regeneration wavefront velocity, cm/min, (h) amount of regeneration solution for one cycle, L, and (i) Washing time, h.

SOLUTION

Molecular weight, M, of $MgCO_3 = 83.43$

$$\text{Concentration of } MgCO_3 \text{ in feed} = \frac{500(1{,}000)}{83.43(1{,}000{,}000)}$$
$$= 0.006 \text{ mol/L or } 0.012 \text{ eq/L}$$

M of NaCl = 58.45

$$\text{Concentration of NaCl in feed} = \frac{50(1{,}000)}{58.45(1{,}000{,}000)}$$
$$= 0.000855 \text{ mol/L or eq/L}$$

(a) Bed cross-section area $= 3.14(8.5)^2/4 = 56.7$ ft^2.

Feed-solution flow rate $= 15(56.7)$
$= 851$ gpm or 3,219 L/min

(b) Behind the loading wavefront:

$$x_{Ca^{2+}} = \frac{0.012}{0.012 + 0.000855} = 0.9335$$

Since no NaCl in the feed is exchanged: $C = 0.012$ eq/L and $Q = 2.3$ eq/L

From Table 15.5,

$$K_{Mg^{2+},Na^+} = 3.3/2 = 1.65$$

From (15-181), for Mg^{2+} instead of Ca^{2+} as the exchanging ion, with $x_{Mg^{2+}}$ = that of the feed from Figure 15.50a:

$$1.65\left(\frac{2.3}{0.012}\right) = \frac{(y^*_{Mg^{2+}})(1 - 0.9335)}{(0.9335)(1 - y^*_{Mg^{2+}})}$$

Solving: $y^*_{Mg^{2+}} = 0.9998$. Thus, sodium ion is displaced from the resin almost completely.

Bed volume $= (56.7)(10) = 567$ ft^3 or 16,060 L

Total bed capacity $= 2.3\,(16{,}060) = 36{,}940$ eq

Mg^{2+} absorbed by resin $= 0.9998(36{,}940) = 36{,}930$ eq

Mg^{2+} entering bed in feed solution $= 0.012(3{,}219) = 38.63$ eq/min

$$t_L = \frac{36{,}930}{38.63} = 956 \text{ min or } 15.9 \text{ h}$$

(c) $u_L = L/t_L = 10/956 = 0.01046$ ft/min or 0.319 cm/min.

(d) Flow rate of regeneration solution $= (1.5/15)(3{,}219) =$ 321.9 L/min.

(e) Displacement time = time for 321.9 L/min to displace liquid in the voids.

$$\text{Void volume} = 0.38\,(16{,}060) = 6{,}103 \text{ L and } t_D = \frac{6103}{321.9} = 19 \text{ min}$$

(f) For a 26 wt% NaCl solution at 25°C, density from *Perry's Chemical Engineers' Handbook* = 1.19443 g/cm^3.

Flow rate of Na^+ in regeneration solution

$$= \frac{321.9(1{,}000)(1.19443)(0.26)}{58.45} = 1{,}710 \text{ eq/min}$$

$$\text{NaCl concentration in regenerating solution} = \frac{1{,}710}{321.9}$$
$$= 5.31 \text{ eq/L} = c_R$$

From (15-181), noting conditions in Figure 15.49:

$$\frac{Q}{c_R} K_{Mg^{2+},Na^+} = 1.65\left(\frac{2.3}{5.31}\right) = 0.715$$

This is less than 1, but not much less than 1. Therefore, the regeneration wavefront may not sharpen rapidly. Assume a shock-wave-like front anyway.

From (15-181),

$$0.715 = \frac{(0.09998)(1 - x^*_{Mg^{2+}})}{x^*_{Mg^{2+}}(1 - 0.9998)}$$

Solving: $x^*_{Mg^{2+}} = 0.9998$

So downstream of the regeneration wavefront, but upstream of the displacement wavefront, the liquid contains very few sodium ions.

Chromatographic Separations

The separation of multicomponent mixtures into more than two products usually requires more than one separation device. For example, if a four-component mixture (A, B, C, D) is to be separated by distillation into pure products, a sequence of three trayed columns is almost always used. If the order of decreasing volatility is A, B, C, and D, the first column might produce a distillate of nearly pure A; the second column a distillate of nearly pure B; and the third column a distillate of nearly pure C and a bottoms of nearly pure D. Four other sequences are possible, depending upon the selection of the split for each column.

Chromatography is one of the few separation techniques that can separate a multicomponent mixture into nearly pure components in a single device, generally a column packed with a suitable sorbent. The degree of separation depends upon column length and differences in component affinities for the sorbent.

As an example, consider a mixture of three components, A, B, and C, in order of decreasing affinity for the sorbent, S. If the separation is achieved by adsorption, then A is the most strongly adsorbed. A feed mixture, insufficient to load the sorbent, is introduced as a pulse into one end (feed end) of the packed chromatographic column. The resulting initial concentrations for the three components are shown in Figure 15.51a, where most of the bed remains clean of adsorbates. An *elutant,* such as a carrier gas or solvent that has little or no affinity for the sorbent, is now introduced continuously into the feed end of the bed, causing the three components to desorb, with C desorbing most readily. However, as the desorbed components are carried down the bed by the elutant into cleaner regions of the bed, the components are successively readsorbed and then redesorbed to produce three waves, as shown in Figure 15.51b. Because of differences in affinities for the sorbent, the three waves, which initially overlap considerably, gradually overlap less (Figure 15.51c), and finally, if the column is long enough, become completely separated, as in Figure 15.51d and e. In that case, the components are eluted from the column, one at a time. In Figure 15.51e, all components but A have been eluted. As the separated waves elute, the area under each component wave is proportional to the mass of the component moving through the packed column.

Chromatography, as discussed here, is limited to batch processes in which feed is introduced as pulses into an elutant carrier gas or solvent, which then contacts the sorbent. All feed components have affinities for the sorbent, but the elutant does not. This type of chromatography is sometimes

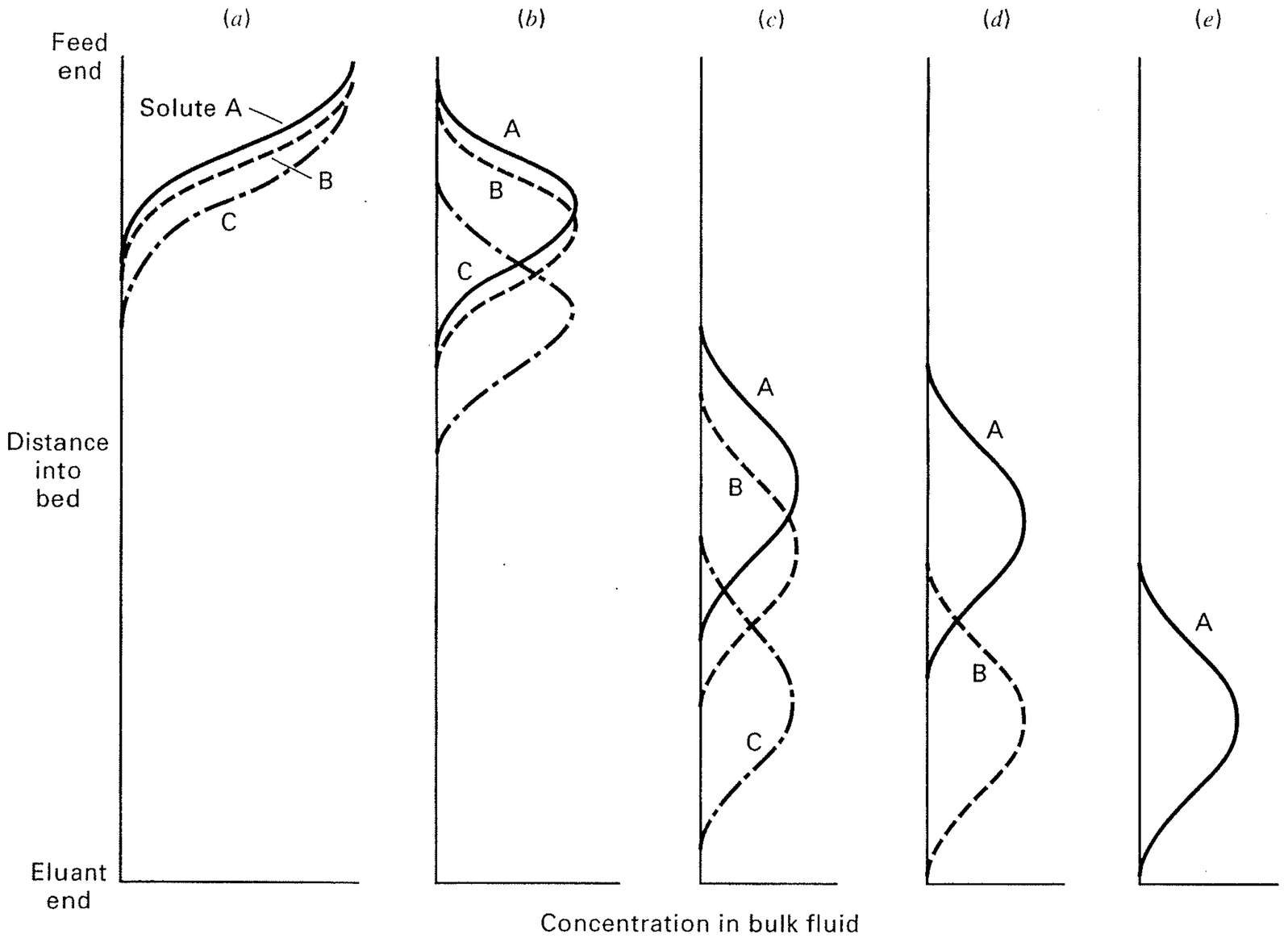

Figure 15.51 Movement of concentration waves during separation in a chromatographic column.

referred to as batch or elution chromatography. Chromatography in the broader sense, as mentioned by Ruthven [10], refers to any separation process involving partitioning of components between a flowing fluid and a solid adsorbent (or a solid-supported liquid absorbent). The previously presented simulated-moving-bed (SMB) system, which uses a circulating desorbent that may also partition, may be viewed as a chromatographic process.

Equilibrium Wave Pulse Theory for Linear Isotherm

A simple and useful wave theory for chromatography is based on isothermal, plug flow, negligible axial dispersion, and local equilibrium everywhere. This theory, when developed for adsorption, results in the stoichiometric wavefront that was shown in Figure 15.27. For chromatography, where solutes are pulsed into the column, a wave pulse rather than a wavefront results, as shown in Figure 15.52a. For a stoichiometric (equilibrium) wave, the pulse is a square wave rather than a Gaussian-distribution-like wave of the type shown in Figure 15.51c. The latter type of wave results when axial dispersion occurs, mass-transfer resistances are important, radial variations of the fluid velocity occur, and/or the pulse of solutes is not a square wave.

If the sorbent is nonporous, such as a gel, and the adsorption isotherm is linear for each solute i ($q = Kc$), then (15-101) applies and each solute wave velocity, u_i, in terms of the interstitial fluid velocity is given by

$$u_i = \frac{u}{1 + \dfrac{1 - \epsilon_b}{\epsilon_b} K_i} \tag{15-183}$$

This equation applies to both the leading and trailing edges of the feed pulse to produce solute movement diagrams, used extensively by Wankat [95]. When the elutant is dilute in the solutes, such that the sorption equilibrium constants do not depend on composition, but only on temperature, (15-183) applies independently to each solute in a multicomponent mixture. For a strongly sorbed solute, such as B in Figure 15.52b, K is large, and the second term in the

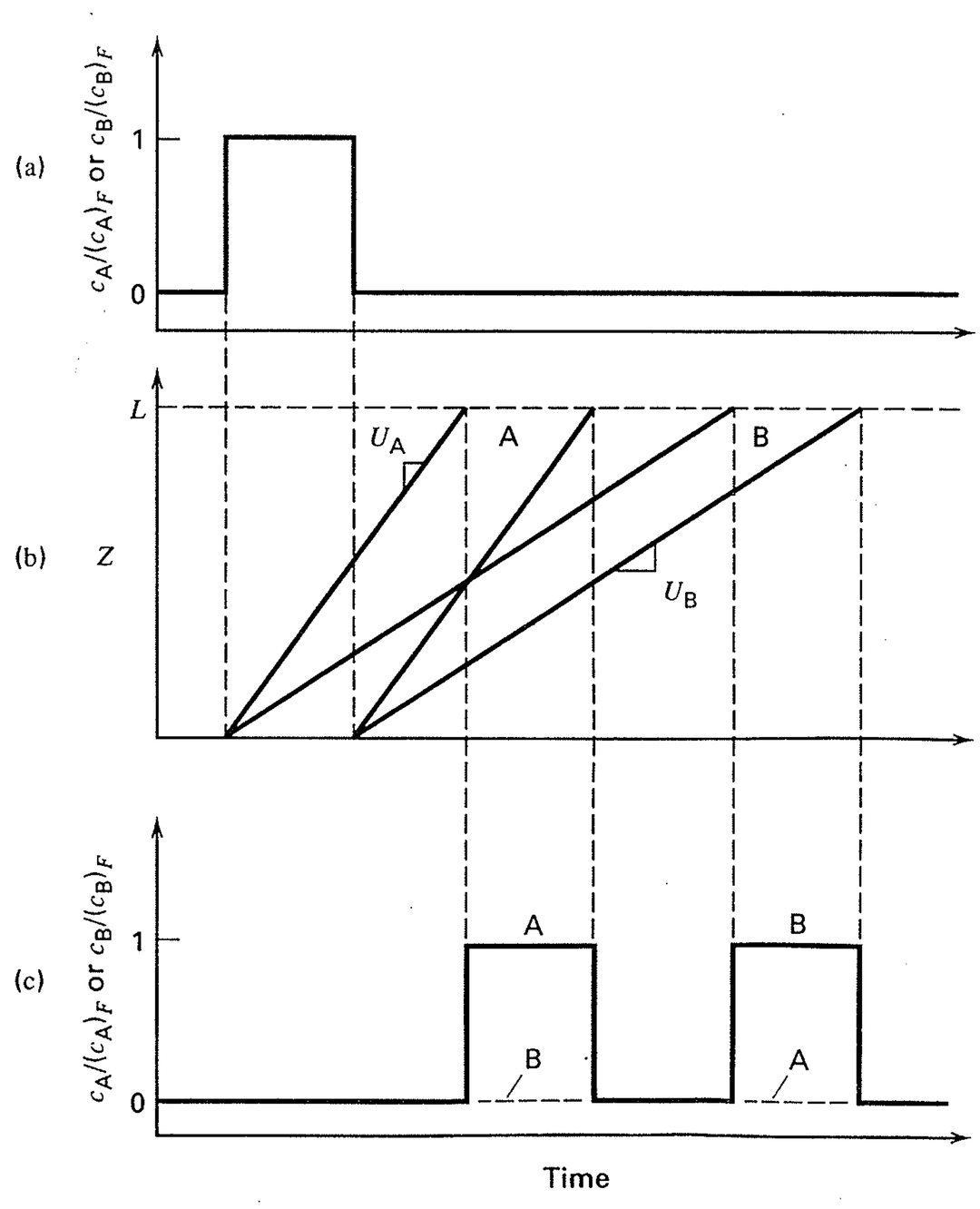

Figure 15.52 Ideal solute wave pulses in a chromatographic column.

denominator dominates, so that solute moves much slower through the bed than does the elutant. For a weakly sorbed solute, such as A in Figure 15.52b, K is small and the denominator is not much greater than 1. For such a solute, its velocity may not be significantly smaller than the elutant velocity.

In Figure 15.52b, the wave velocities of both the leading and trailing edges of the wave pulses are constant, with $u_A > u_B$. For each solute, the pulse time to move through a column of length L is $t_i = L/u_i$. The wave pulse of A reaches the end of the column in less time than the B wave pulse. In Figure 15.52c, the product-concentration ratios, c_A/c_{A_F} and c_B/c_{B_F}, are shown at the end of the bed as a function of time. The widths of these product waves are identical to the widths of the feed pulses, as illustrated in the following example. This simple, equilibrium-wave pulse theory for linear isotherms can be used to obtain an approximate estimate of the separation achievable in a chromatographic column. Unfortunately, the estimate is not conservative when computing the necessary column length, because the pulses broaden, as shown after the following example.

EXAMPLE 15.20

An aqueous solution of 3 g/cm^3 each of glucose (G), sucrose (S), and fructose (F) is to be separated in a chromatographic column, packed with an ion-exchange resin of the calcium form. In the range of expected solute concentrations, the sorption isotherms are linear and independent, with $q_i = K_i c_i$, where q_i is in grams sorbent per 100 cm^3 resin and c_i is in grams solute per 100 cm^3 solution. From experiment:

Solute	K
Glucose	0.26
Sucrose	0.40
Fructose	0.66

The superficial solution velocity is 0.031 cm/s and bed void fraction is 0.39. If a 500-second pulse, t_P, of feed is followed by elution with pure water, what length of column packing is needed to separate the three solutes if sorption equilibrium is assumed? How soon after the first pulse begins can a second 500-second pulse begin?

SOLUTION

Interstitial solution velocity $= 0.031/0.39 = 0.0795$ cm/s.

Wave velocity for glucose from (15-183):

$$u_G = \frac{0.0795}{1 + \left(\frac{1 - 0.39}{0.39}\right)(0.26)} = 0.0565 \text{ cm/s}$$

Similarly,

$$u_S = 0.0489 \text{ cm/s} \quad \text{and} \quad u_F = 0.0391 \text{ cm/s}$$

The smallest difference in wave velocities is between glucose and sucrose. Therefore, the separation between these two waves determines the column length. The minimum column length, assuming equilibrium, corresponds to the time at which the trailing edge of the glucose wave pulse, together with the leading edge of the sucrose wave pulse, leaves the column. Thus, if t_P is the duration of the first pulse and L is the length of the packing:

$$t_P + \frac{L}{u_G} = \frac{L}{u_S} \tag{1}$$

Thus,

$$500 + \frac{L}{0.0565} = \frac{L}{0.0489}$$

Solving, length of packing, $L = 182$ cm. The glucose just leaves the column at

$$500 + \frac{182}{0.0565} = 3{,}718 \text{ s}$$

The locations of the three wave fronts in the column at 3,718 s are shown in Figure 15.53.

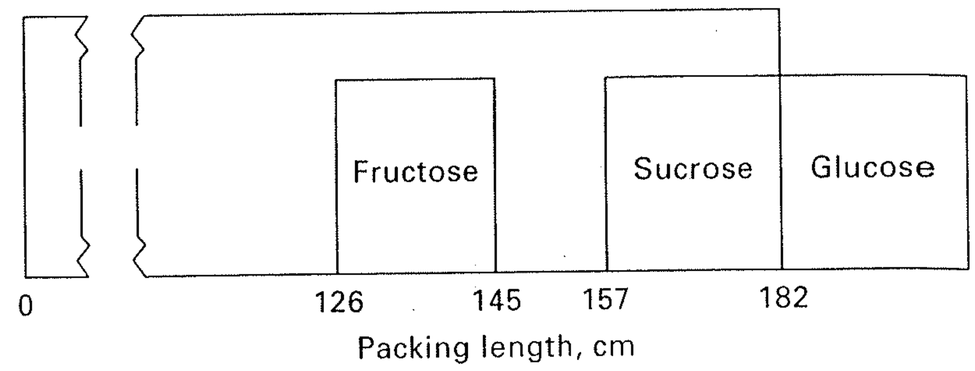

Figure 15.53 Locations of solute waves of first pulse for Example 15.20 at 3,718 s.

The time at which the second pulse begins is determined so that the trailing edge of the first fructose wave pulse just leaves the column as the second pulse of glucose begins to leave the column. This time, based on the fructose, is $500 + 182/0.0391 = 5{,}155$ s. It takes the leading edge of a glucose wave $182/0.0565 = 3{,}220$ s to pass though the column. Therefore, the second pulse can begin at $5{,}155 - 3{,}220 = 1{,}935$ s. This establishes the following ideal cycle: pulse: 500 s, elute: 1,435 s, pulse: 500 s, elute: 1,435 s, etc. In the real case, where we account for mass-transfer resistance, as shown in the next example, the column will have to be longer.

Analytical Solution for Rate-based Chromatography with Linear Isotherm

A plot of solute concentrations in the elutant as a function of time is a chromatogram. When mass-transfer resistances, axial dispersion, and other non-ideal phenomena are not negligible, the solute concentrations in a chromatogram will not appear as square waves, but will exhibit the wave shapes in Figure 15.51. Carta [96] developed analytical solutions for chromatographic response to periodic injections of rectangular feed pulses, taking into account mass-transfer resistances for solute mixtures having linear, independent adsorption isotherms. Carta's solution for the LDF approximation is readily applied to the determination of the necessary length of packing and frequency of feed pulses for the chromatographic separation of a feed mixture.

For each solute in the feed, (15-102) is simplified by neglecting axial dispersion and assuming a constant interstitial fluid velocity, u, through the packing:

$$\frac{\partial c_i}{\partial t} + u\frac{\partial c_i}{\partial z} + \frac{(1 - \epsilon_b)}{\epsilon_b}\frac{\partial \bar{q}_i}{\partial t} = 0 \tag{15-184}$$

The linear driving force approximation (15-105), the linear isotherm, and (15-106) for the overall mass-transfer resistance are assumed to apply for each solute. For periodic, rectangular feed pulses, the boundary conditions for feed pulses of duration, t_F, each followed by an elution period of duration, t_E, are for each solute concentration, $c_i\{z, t\}$:

Initial condition:

$$\text{At } t = 0,\ c_i\{z, 0\} = 0 \tag{15-185}$$

Feed pulse:

$$\begin{aligned}&\text{At } z = 0,\ c_i\{0, t\} = (c_i)_F \\ &\quad \text{for } (j-1)(t_F + t_E) < t < j(t_F + t_E) - t_E\end{aligned} \tag{15-186}$$

Elution period:

$$\begin{aligned}&\text{At } z = 0,\ c_i\{0, t\} = 0 \\ &\quad \text{for } j(t_F + t_E) - t_E < t < j(t_F + t_E)\end{aligned} \tag{15-187}$$

where $j = 1, 2, 3, \ldots$ is an index that accounts for the periodic nature of the feed and elution pulses. Thus, with $j = 1$, the feed pulse takes place from $t = 0$ to $t = t_F$ and the elution pulse is from t_F to $t_F + t_E$.

Carta solved the linear system of (15-184), (15-105), and (15-106) for conditions (15-185) to (15-187) by the Laplace transform method to obtain the following series solution, in terms of dimensionless parameters, which is applied to each solute in the feed pulse:

$$X = \frac{r_F}{2r} + \frac{2}{\pi}\sum_{m=1}^{\infty}\left[\frac{1}{m}\exp\left(-\frac{m^2 n_f}{m^2 + r^2}\right)\sin\left(\frac{m\pi r_F}{2r}\right)\right.$$
$$\left.\times\cos\left(\frac{m\theta_f}{r} - \frac{m\pi r_F}{2r} - \frac{m\beta n_f}{r} - \frac{mrn_f}{m^2 + r^2}\right)\right] \tag{15-188}$$

where

$$X = c/c_F \tag{15-189}$$

$$r = \frac{k}{2\pi K}(t_F + t_E) \tag{15-190}$$

$$r_F = \frac{k}{\pi K}t_F \tag{15-191}$$

$$n_f = \frac{(1-\epsilon_b)kz}{\epsilon_b u} \tag{15-192}$$

$$\theta_f = \frac{kt}{K} \tag{15-193}$$

$$\beta = \frac{\epsilon_b}{(1-\epsilon_b)K} \tag{15-194}$$

$$K = q/c \tag{15-195}$$

and where

$$k = \frac{1}{\dfrac{R_p}{3k_c} + \dfrac{R_p^2}{15D_e}} \tag{15-196}$$

When nonlinear adsorption isotherms such as the Freundlich equation (15-35), the Langmuir equation (15-36), or extensions thereof to multicomponent mixtures [e.g., concentration forms of (15-32) or (15-33)] are necessary, the analytical solution of Carta is not applicable. However, the method of lines, using five-point, biased, upwind, finite-difference approximations, as described earlier in the section on thermal-swing adsorption, can be applied to obtain a numerical solution.

EXAMPLE 15.21

Use Carta's equation with the following properties to compute the chromatogram for the conditions of Example 15.20 with a packing length of 182 cm. Does a significant overlap of peaks result?

Property	Glucose	Sucrose	Fructose
K	0.26	0.40	0.66
D_e, cm^2/s	1.1×10^{-8}	1.8×10^{-8}	2.8×10^{-8}
k_c, cm/s	5.0×10^{-3}	5.0×10^{-3}	5.0×10^{-3}

$\epsilon_b = 0.39$, $R_p = 0.0025$ cm, $u = 0.0795$ cm/s,
$z = 182$ cm, $t_E = 2{,}000$ s, and $t_F = 500$ s

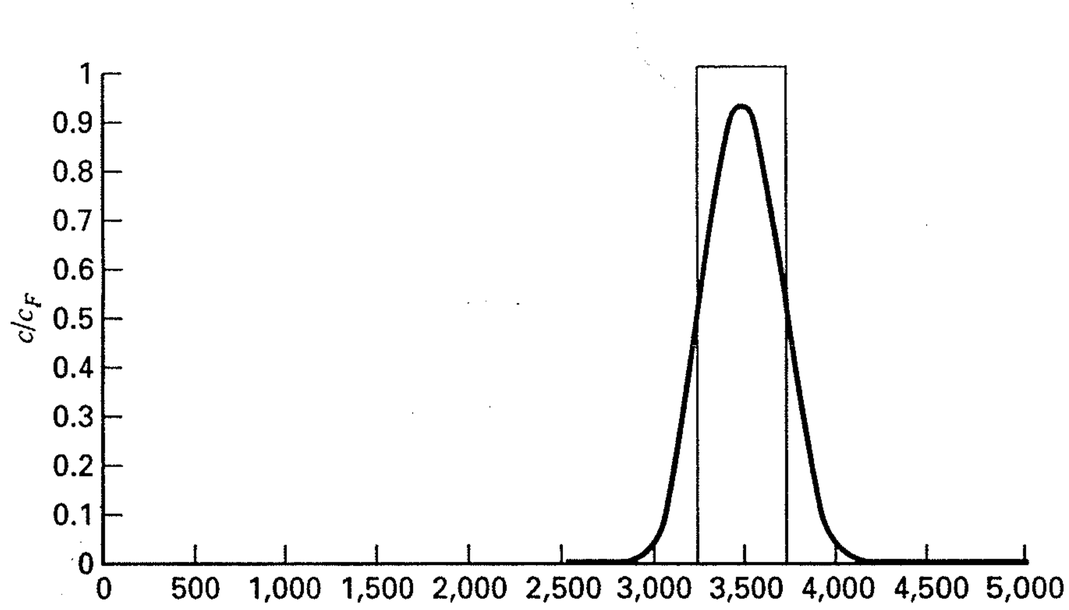

Figure 15.54 Computed chromatograms for Example 15.21.
(a) Comparison of ideal to nonideal wave for fructose.
(b) Computed chromatogram for nonideal eluant.

SOLUTION

Values of k and the computed dimensionless parameters from (15-148) to (15-152) are as follows:

	Glucose	Sucrose	Fructose
r	40.22	42.66	40.06
r_F	16.09	17.07	16.03
n_f	94.13	153.6	238.0
θ_f	$0.1011\,t$	$0.1072\,t$	$0.1007\,t$
β	2.459	1.598	0.9687
k, s^{-1}	0.0263	0.0429	0.0665

where t is in seconds.

Values of $X = c/c_F$ are computed with these parameters using (15-188) for values of time, t, in the neighborhood of times for the equilibrium-based waves. The resulting chromatogram for glucose is shown in Figure 15.54a, compared to the equilibrium rectangular wave (shown as a dashed line) determined in Example 15.20 using (15-183). The areas under the two curves should be identical. The equilibrium-based wave appears to be centered in time within the mass-transfer-based wave.

In Figure 15.54b, the complete computed chromatogram is plotted for the three carbohydrates. It is seen that the effect of mass transfer is to cause the peaks to overlap significantly. To obtain a sharp separation, it is necessary to lengthen the column or reduce the feed pulse time, t_F.

SUMMARY

1. Sorption is a generic term for the selective transfer of a solute from the bulk of a liquid or gas to the surface and/or into the bulk of a solid or liquid. Thus, sorption includes adsorption and absorption. The sorbed solute is commonly called the sorbate.

2. For commercial applications, a sorbent should have high selectivity, high capacity, rapid solute transport rates, stability, strength, and ability to be regenerated. An adsorbent should have small pores so as to give a large surface area per unit volume.

3. Physical adsorption of pure gases and gas mixtures is easily measured. Adsorption of pure liquids and liquid mixtures is not easily measured.

4. The most widely used commercial adsorbents are carbon (activated and molecular-sieve), molecular-sieve zeolites, silica gel, and activated alumina.

5. The most widely used ion exchangers are water-swellable, solid gel resins based on the copolymerization of styrene and a cross-linking agent, such as divinylbenzene. They can be cation or anion exchangers. Ions are exchanged stoichiometrically on an equivalent basis. Thus, Ca^{2+} is exchanged for 2 Na^{+}.

6. Sorbents for chromatographic separations are typically solid adsorbents, liquid absorbents supported on or bonded to an inert solid, or a gel.

7. The most commonly used adsorption isotherms for gases and liquids are Henry's law (linear isotherm), the Freundlich isotherm, and the Langmuir isotherm. The latter asymptotically approaches the linear isotherm at low concentrations and an asymptotic value, representing maximum surface coverage, at high concentrations. For mixtures, extended versions of the Freundlich and Langmuir isotherms are often used.

8. Ion-exchange equilibrium is most commonly represented by an equilibrium constant based on the law of mass action. Because of the dilute conditions common in chromatography, a linear equilibrium isotherm is commonly employed.

9. For physical adsorption, the rate of adsorption is almost instantaneous after the solute reaches the sorbing surface. Thus, only external and internal mass-transfer resistances need be considered. External mass-transfer coefficients are generally obtained from empirical correlations of the Chilton–Colburn j-factor type. Internal mass transfer is generally based on a modified Fick's first law using an effective diffusivity that depends on particle porosity, pore tortuosity, bulk molecular diffusivity, and surface diffusivity. Diffusivities in ion-exchange resin gels depend strongly on the degree of cross-linking.

10. A wide variety of sorption systems are used, including slurry adsorption in various modes of operation, fixed-bed adsorption, and simulated, continuous, countercurrent adsorption. When sorbent regeneration is necessary, the system must be operated on a cycle. For fixed beds, the most common cycles are temperature-swing adsorption (TSA) and pressure-swing adsorption (PSA). Ion exchange almost always includes a regeneration step, using a displacement fluid. In a chromatographic separation, adsorption and regeneration take place in the same column.

11. For the design and operation of all sorption systems, the adsorption isotherm is of great importance because it relates, at equilibrium, the concentration of the solute in the fluid to its loading as a sorbate in and/or on the sorbent. Most commonly, the overall rate of adsorption is expressed in the form of a linear driving force (LDF) model, where the driving force is the difference between bulk concentration and concentration in equilibrium with the loading. The coefficient in the LDF equation is a combined overall mass-transfer coefficient and area for sorption.

12. In ideal, fixed-bed operation, solute–sorbate equilibrium between the flowing fluid and the static bed is assumed everywhere. For plug flow and negligible axial dispersion, the result is a sharp concentration front that moves like a shock wave (stoichiometric front) through the bed. Upstream of the front, the sorbent is spent and in equilibrium with the feed mixture. Downstream of the front, the sorbent is clean of sorbate. Typically, the stoichiometric front travels through the bed at a much slower velocity than the interstitial velocity of the fluid feed. The time for the concentration front to reach the end of the bed is the breakthrough time.

13. When mass-transfer effects are taken into account, the concentration front broadens into an S-shaped curve such that at breakthrough only a portion of the sorbent is fully loaded. When mass-transfer coefficients and sorption isotherms are known, these curves can be readily computed with the Klinkenberg equations. Alternatively, when the shapes of experimental concentration fronts appear to exhibit a constant pattern, because of favorable adsorption equilibrium, commercial-size adsorption beds can be scaled-up directly from experimental breakthrough data by the method of Collins.

14. Thermal-swing adsorption (TSA) can be used to remove small concentrations of solutes from gas and liquid mixtures. Typically, adsorption is carried out at ambient temperature and desorption at an elevated temperature. Because bed heating and cooling between the adsorption and desorption steps is not instantaneous, TSA cycles are long, typically hours or days. The desorption step, starting with a partially loaded bed, can be computed numerically by the method of lines, using a stiff integrator.

15. Pressure-swing adsorption (PSA) is used to separate air and enrich hydrogen-containing streams. Adsorption is carried out at an elevated or ambient pressure, whereas desorption occurs at ambient pressure or in a vacuum; the latter is often referred to as vacuum-swing adsorption (VSA). Because pressure swings can be made rapidly, PSA cycles are short, typically seconds or minutes. Usually, it is not necessary to regenerate the bed completely. When that circumstance exists and the cycle is fixed, a number of cycles may be needed to approach a cyclic steady-state operation.

16. Although continuous, countercurrent adsorption with a moving bed is difficult to achieve successfully in practice, an SMB system is becoming popular, particularly for separation of solutes in dilute aqueous solutions and for bulk-liquid separations. Design procedures for SMB systems, which require solution of systems of differential-algebraic equations, are highly developed.

17. Design calculations for ion-exchange operations are based on the equilibrium assumption for both the loading and regeneration steps.

18. In chromatography, the feed is periodically pulsed into a column packed with sorbent. Between feed pulses, an elutant is passed through the column, causing the less strongly sorbed solutes to move through the column more rapidly than other solutes. If the column is long enough, a multicomponent feed can be completely separated, with solutes eluted one by one from the column. In the absence of mass-transfer resistances, a rectangular feed pulse is separated into individual solute rectangular pulses, whose position–time curves are readily established. When mass-transfer effects are important, the rectangular pulses take on a Gaussian distribution that can be predicted by the analytical solution of Carta, provided that a linear adsorption isotherm applies and axial dispersion is negligible.

REFERENCES

1. KELLER, G.E. II, in *Industrial Gas Separations,* T.E. Whyte, Jr., C.M. Yon, and E.H. Wagner, eds., ACS Symposium Series No. 223, American Chemical Society, Washington, D.C., p. 145 (1983).
2. MILTON, R.M., U.S. Patents 2,882,243 and 2,882,244 (1959).
3. SKARSTROM, C.W., U.S. Patent 2,944,627 (1960).
4. BROUGHTON, D.B., and C.G. GERHOLD, U.S. Patent 2,985,589 (May 23, 1961).
5. ETTRE, L.S., and A. ZLATKIS, Eds., *75 Years of Chromatography—A Historical Dialog,* Elsevier, Amsterdam (1979).
6. BONMATI, R.G., G. CHAPELET-LETOURNEUX, and J.R. MARGULIS, *Chem. Engr.,* **87** (6), 70–72 (1980).
7. BERNARD, J.R., J.P. GOURLIA, and M.J. GUTTIERREZ, *Chem. Engr.,* **88** (10), 92–95 (1981).
8. WHITE, D.H., JR., and P.G. BARKLEY, *Chem. Eng. Progress,* **85** (1) 25–33 (1989).
9. ROUSSEAU, R.W., Ed., *Handbook of Separation Process Technology,* Wiley-Interscience, New York (1987).
10. RUTHVEN, D.M., *Principles of Adsorption and Adsorption Processes,* John Wiley and Sons, New York (1984).
11. BRUNAUER, S., P.H. EMMETT, and E. TELLER, *J. Am. Chem. Soc.,* **60,** 309 (1938).
12. SATTERFIELD, C.N., *Heterogeneous Catalysis in Practice,* McGraw-Hill, New York (1980).
13. RUTHVEN, D.M., in *Kirk-Othmer Encyclopedia of Chemical Technology,* Vol. 1, 4th ed., Wiley-Interscience, New York (1991).
14. BARRER, R.M., *Zeolites and Clay Minerals as Sorbents and Molecular Sieves,* Academic Press, New York (1978).
15. BRECK, D.W., *Zeolite Molecular Sieves,* John Wiley and Sons, New York (1974).
16. ADAMS, B.A., and E.L. HOLMES, *J. Soc. Chem. Ind.,* **54,** 1–6T (1935).
17. MCWILLIAMS, J.D., *Chem. Engr.,* **85** (12), 80–84 (1978).
18. DORFNER, K., *Ion Exchangers, Properties and Applications,* 3rd ed., Ann Arbor Science, Ann Arbor, MI (1971).
19. SEWELL, P.A., and B. CLARKE, *Chromatographic Separations,* John Wiley and Sons, New York (1987).
20. BRUNAUER, S., L.S. DEMING, W.E. DEMING, and E. TELLER, *J. Am. Chem. Soc.,* **62,** 1723–1732 (1940).
21. BRUNAUER, S., *The Adsorption of Gases and Vapors,* Vol. I, *Physical Adsorption,* Princeton University Press (1943).
22. TITOFF, A., *Z. Phys. Chem.,* **74,** 641 (1910).
23. VALENZUELA, D.P., and A.L. MYERS, *Adsorption Equilibrium Data Handbook,* Prentice-Hall, Englewood Cliffs, NJ (1989).
24. RAY, G.C., and E.O. BOX, JR., *Ind. Eng. Chem.,* **42,** 1315–1318 (1950).
25. YANG, R.T., *Gas Separation by Adsorption Processes,* Butterworths, Boston (1987).
26. FREUNDLICH, H., *Z. Phys. Chem.,* **73,** 385–423 (1910).
27. MANTELL, C.L., *Adsorption,* 2nd ed., McGraw-Hill, New York, p. 25 (1951).
28. LANGMUIR, J., *J. Am. Chem. Soc.,* **37,** 1139–1167 (1915).
29. MARKHAM, E.C., and A.F. BENTON, *J. Am. Chem. Soc.,* **53,** 497–507 (1931).
30. YON, C.M., and P.H. TURNOCK, *AIChE Symp. Series,* **67** (117), 75–83 (1971).
31. BROUGHTON, D.B., *Ind. Eng. Chem.,* **40,** 1506–1508 (1948).
32. MYERS, A.L., and J.M. PRAUSNITZ, *AIChE J.,* **11,** 121–127 (1965).
33. MILLER, G.W., K.S. KNAEBEL, and K.G. IKELS, *AIChE J.,* **33,** 194–201 (1987).
34. RITTER, J.A., and R.T. YANG, *Ind. Eng. Chem. Res.,* **26,** 1679–1686 (1987).
35. RUTHVEN, D.M., and F. WONG, *Ind. Eng. Chem. Fundam.,* **24,** 27–32 (1985).
36. KIPLING, J.J., *Adsorption from Solutions of Nonelectrolytes,* Academic Press, London (1965).
37. RADKE, C.J., and J.M. PRAUSNITZ, *AIChE J.,* **18,** 761–768 (1972).
38. ANDERSON, R.E., "Ion-Exchange Separations," in *Handbook of Separation Techniques for Chemical Engineers,* 2nd ed., P.A. Schweitzer, Ed., McGraw-Hill, New York (1988).
39. BONNER, O.D., and L.L. SMITH, *J. Phys. Chem.* **61,** 326–329 (1957).
40. BAUMAN, W.C., and J. EICHHORN, *J. Am. Chem. Soc.,* **69,** 2830–2836 (1947).

41. BAUMAN, W.C., J.R. SKIDMORE, and R.H. OSMUN, *Ind. Eng. Chem.,* **40,** 1350–1355 (1948).

42. SUBBA RAO, H.C., and M.M. DAVID, *AIChE Journal,* **3,** 187–190 (1957).

43. SELKE, W.A., and H. BLISS, *Chem. Eng. Prog.,* **46,** 509–516 (1950).

44. SELKE, W.A., and H. BLISS, *Chem. Eng. Prog.,* **47,** 529–533 (1951).

45. MYERS, A.L., and S. BYINGTON, in *Ion Exchange: Science and Technology,* A.E. Rodrigues, Ed., Martinus Nijhoff, Boston, pp. 119–145.

46. RANZ, W.E., and W.R. MARSHALL, JR., *Chem. Eng. Prog.,* **48,** 141–146 (1952).

47. RANZ, W.E., and W.R. MARSHALL, JR., *Chem. Eng. Prog.,* **48,** 173–180 (1952).

48. RANZ, W.E., *Chem. Eng. Prog.,* **48,** 247–253 (1952).

49. GAMSON, B.W., G. THODOS, and O.A. HOUGEN, *Trans. AIChE,* **39,** 1–35 (1943).

50. CHILTON, T.H., and A.P. COLBURN, *Ind. Eng. Chem.,* **26,** 1183–1187 (1934).

51. SEN GUPTA, A., and G. THODOS, *AIChE J.,* **9,** 751–754 (1963).

52. PETROVIC, L.J., and G. THODOS, *Ind. Eng. Chem. Fundamentals,* **7,** 274–280 (1968).

53. DWIVEDI, P.N., and S.N. UPADHAY, *Ind. Eng. Chem. Process Des. Dev.,* **16,** 157–165 (1977).

54. WAKAO, N., and T. FUNAZKRI, *Chem. Eng. Sci.,* **33,** 1375–1384 (1978).

55. KUNII, D., and O. LEVENSPIEL, *Fluidization Engineering,* 2nd ed., Butterworth-Heinemann, Boston, Chap. 3 (1991).

56. THIELE, E.W., *Ind. Eng. Chem.,* **31,** 916–920 (1939).

57. WHEELER, A., *Advances in Catalysis,* Vol. 3, Academic Press, New York, pp. 249–327 (1951).

58. SCHNEIDER, P., and J.M. SMITH, *AIChE J.,* **14,** 886–895 (1968).

59. RIEKERT, L., *AIChE J.,* **31,** 863–864 (1985).

60. SLADEK, K.J., E.R. GILLILAND, and R.F. BADDOUR, *Ind. Eng. Chem. Fundam.,* **13,** 100–105 (1974).

61. KAPOOR, A., R.T. YANG, and C. WONG, "Surface Diffusion," *Catalyst Reviews,* **31,** 129–214 (1989).

62. HELFFERICH, F., *Ion Exchange,* McGraw-Hill, New York (1962).

63. SOLDANO, B.A., *Ann. NY Acad. Sci.,* **57,** 116–124 (1953).

64. KELLER, G.E., "Separations: New Directions for an Old Field," *AIChE Monograph Series,* **83** (17) (1987).

65. RUTHVEN, D.M., and C.B. CHING, *Chem. Eng. Sci.,* **44,** 1011–1038 (1989).

66. BERG, C., *Trans. AIChE,* **42,** 665–680 (1946).

67. BROUGHTON, D.B., *Chem. Eng. Progress,* **64** (8), 60–65 (1968).

68. GEMBICKI, S.A., A.R. OROSKAR, and J.A. JOHNSON, in *Encyclopedia of Chemical Technology,* 4th edition, Vol. 1, John Wiley, New York, pp. 573–600 (1991).

69. HIGGINS, I.R., and J.T. ROBERTS, *Chem. Engr. Prog. Symp. Ser.,* **50** (14), 87–92 (1954).

70. HIMSLEY, A., Canadian Patent 980,467 (Dec. 23, 1975).

71. GANETSOS, G., and P.E. BARKER, Ed., *Preparative and Production Scale Chromatography,* Marcel Dekker, New York (1993).

72. MARTIN, A.J.P., *Disc. Faraday Soc.,* **7,** 332 (1949).

73. DEVAULT, D., *J. Am. Chem Soc.,* **65,** 532–540 (1943).

74. GLUECKAUF, E., *Trans. Faraday Soc.,* **51,** 1540–1551 (1955).

75. GLUECKAUF, E., and J.E. COATES, *J. Chem. Soc.,* 1315–1321 (1947).

76. LIAW, C.H., J.S.P. WANG, R.A. GREENKORN, and K.C. CHAO, *AIChE J.,* **25,** 376–381 (1979).

77. KLINKENBERG, A., *Ind. Eng. Chem.,* **46,** 2285–2289 (1954).

78. ANZELIUS, A., Z., *Angew. Math u. Mech.,* **6,** 291–294 (1926).

79. KLINKENBERG, A., *Ind. Eng. Chem.,* **40,** 1992–1994 (1948).

80. COONEY, D.O., and E.N. LIGHTFOOT, *IEC Fundamentals,* **4,** 233–236 (1965).

81. SIRCAR, S., and K. KUMAR, *Ind. Eng. Chem. Process Des. Dev.,* **22,** 271–280 (1983).

82. COONEY, D.O., *Chem. Eng. Comm.,* **91,** 1–9 (1990).

83. COLLINS, J.J., *Chem. Eng. Prog. Symp. Ser.* **63** (74), 31–35 (1967).

84. WONG, Y.W., and J.L. NIEDZWIECKI, *AIChE Symposium Series,* **78** (219), 120–127 (1982).

85. LISKOVETS, O.A., *Differential Equations* (a translation of *Differentsial'nye Uravneniya*) **1,** 1308–1323 (1965).

86. SCHIESSER, W.E., *The Numerical Method of Lines Integration of Partial Differential Equations,* Academic Press, San Diego (1991).

87. SCHIESSER, W.E., *Computational Mathematics in Engineering and Applied Science,* CRC Press, Boca Raton, FL (1994).

88. PRESS, W.H., S.A. TEUKOLSKY, W.T. VETTERLING, and B.P. FLANNERY, *Numerical Recipes in FORTRAN,* 2nd ed., Cambridge University Press, Cambridge (1992).

89. GEAR, C.W., *Numerical Initial Value Problems in Ordinary Differential Equations,* Prentice-Hall, Englewood Cliffs, NJ (1971).

90. BYRNE, G.D., and A.C. HINDMARSH, *J. Comput. Phys.,* **70,** 1–62 (1987).

91. RITTER, J.A., and R.T. YANG, *Ind. Eng. Chem. Res.,* **30,** 1023–1032 (1991).

92. RUTHVEN, D.M., S. FAROOQ, and K.S. Knaebel, *Pressure-Swing Adsorption,* VCH, New York (1994).

93. MUTASIM, Z.Z., and J.H. BOWEN, *Trans. I. Chem. E.,* **69,** Part A, 108–118 (March 1991).

94. EAGLETON, L.C., and H. BLISS, *Chem. Eng. Progress,* **49,** 543–548 (1953).

95. WANKAT, P.C., *Rate-Controlled Separations,* Elsevier Applied Science, New York (1990).

96. CARTA, G., *Chem. Eng. Sci.,* **43,** 2877–2883 (1988).

97. WANKAT, P.C., *Large-Scale Adsorption and Chromatography,* Vols. I and II, CRC Press, Inc., Boca Raton (1986).

98. BROUGHTON, D.B., R.W. NEUZIL, J.M. PHARIS, and C.S. BREARBY, *Chem. Eng. Prog.,* **66** (9), 70–75 (1970).

99. ZANG, Y., and P.C. WANKAT, *Ind. Eng. Chem. Res.,* **41,** 5283–5289 (2002).

100. KIM, J.K., and P.C. WANKAT, *Ind. Eng. Chem. Res.,* **43,** 1071–1080 (2004).

101. HUMPHREY, J.L., and G.E. Keller II, *Separation Process Technology,* McGraw-Hill, New York (1997).

102. WANKAT, P.C., *Ind. Eng. Chem. Res.,* **40,** 6185–6193 (2001).

103. STORTI, G., M. MASI, S. CARRA, and M. MORBIDELLI, *Chem. Eng. Sci.,* **44,** 1329 (1989).

104. RHEE, H.-K., R. ARIS, and N.R. AMUNDSON, *Phil. Trans. Royal Soc. London, Series A,* **269** (No. 1194), 187–215 (Feb. 5, 1971).

105. MAZZOTTI, M., G. STORTI, and M. MORBIDELLI, *AIChE Journal,* **40,** 1825–1842 (1994).

106. RUTHVEN, D.M., and C.B. CHING, *Chem. Eng. Sci.,* **44,** 1011–1038 (1989).

107. ZHONG, G., and G. GUIOCHON, *Chem. Eng. Sci.,* **51,** 4307–4319 (1996).

108. STORTI, G., M. MAZZOTTI, M. MORBIDELLI, and S. CARRA, *AIChE Journal,* **39,** 471–492 (1993).

109. MAZZOTTI, M., G. STORTI, and M. MORBIDELLI, *J. Chromatography* A, **769,** 3–24 (1997).

110. DANCKWERTS, P.V., *Chem. Eng. Sci.,* **2,** 1 (1953).

111. CONSTANTINIDES, A., and N. MOSTOUFI, *Numerical Methods for Chemical Engineers with MATLAB Applications,* Prentice Hall PTR, Upper Saddle River, NJ (1999).

112. MINCEVA, M. and A. E. RODRIGUES, *Ind. Eng. Chem. Res.,* **41,** 3454–3461 (2002).

EXERCISES

Section 15.1

15.1 Porous particles of activated alumina have a BET surface area of 310 m^2/g, a particle porosity of 0.48, and a particle density of 1.30 g/cm^3. Determine: (a) specific pore volume in cm^3/g, (b) true solid density, g/cm^3, and (c) approximate pore diameter in angstroms from (15-2).

15.2 Carbon molecular sieves are available in two forms from a Japanese manufacturer:

	Form A	Form B
Pore volume, cm^3/g	0.18	0.38
Average pore diameter	5 Å	2.0 μm

Estimate the surface area of each form.

15.3 Representative properties of small-pore silica gel are as follows: pore diameter = 24 Å; particle porosity = 0.47; particle density = 1.09 g/cm^3; and specific surface area = 800 m^2/g

(a) Are these values reasonably consistent? (b) If the adsorption capacity for water vapor at 25°C and 6 mmHg partial pressure is 18% by weight, what fraction of a monolayer is adsorbed?

15.4 The following data were obtained in a BET apparatus for adsorption equilibrium of nitrogen on silica gel (SG) at –195.8°C. Estimate the specific surface area in m^2/g of silica gel. How does your value compare with that in Table 15.2?

N_2 Partial Pressure, torr	Volume of N_2 Adsorbed in cm^3 (0°C, 1 atm) per gram SG
6.0	6.1
24.8	12.7
140.3	17.0
230.3	19.7
285.1	21.5
320.3	23.0
430	27.7
505	33.5

15.5 Estimate the maximum ion-exchange capacity in meq/g resin for an ion-exchange resin made from 8 wt% divinylbenzene and 92 wt% styrene.

Section 15.2

15.6 Shen and Smith [*Ind. Eng. Chem. Fundam.,* **7,** 100–105 (1968)] measured equilibrium-adsorption isotherms at four different temperatures for pure benzene vapor on silica gel, having the following properties: surface area = 832 m^2/g, pore volume = 0.43 cm^3/g, particle density = 1.13 g/cm^3, and average pore diameter = 22 Å.

The adsorption data are as follows:

Partial Pressure of Benzene, atm	Moles Adsorbed/g Gel × 10^5			
	70°C	90°C	110°C	130°C
5.0×10^{-4}	14.0	6.7	2.6	1.13
1.0×10^{-3}	22.0	11.2	4.5	2.0
2.0×10^{-3}	34.0	18.0	7.8	3.9
5.0×10^{-3}	68.0	33.0	17.0	8.6
1.0×10^{-2}	88.0	51.0	27.0	16.0
2.0×10^{-2}	—	78.0	42.0	26.0

(a) For each temperature, obtain a best fit of the data to (1) linear, (2) Freundlich, and (3) Langmuir isotherms. Which isotherm(s), if any, fit the data reasonably well?

(b) Do the data represent less than a monolayer of adsorption?

(c) From the data, estimate the heat of adsorption. How does this value compare to the heat of vaporization (condensation) of benzene?

15.7 The separation of propane and propylene is accomplished by distillation, but at the expense of more than 100 trays and a reflux ratio of greater than 10. Consequently, the use of adsorption has been investigated in a number of studies. Jarvelin and Fair [*Ind. Eng. Chem. Research,* **32,** 2201–2207 (1993)] measured adsorption-equilibrium data at 25°C for three different zeolite molecular sieves (ZMSs) and activated carbon. The data were fitted to the Langmuir isotherm with the following results:

Adsorbent	Sorbate	q_m	K
ZMS 4A	C_3	0.226	9.770
	$C_3^=$	2.092	95.096
ZMS 5A	C_3	1.919	100.223
	$C_3^=$	2.436	147.260
ZMS 13X	C_3	2.130	55.412
	$C_3^=$	2.680	100.000
Activated carbon	C_3	4.239	58.458
	$C_3^=$	4.889	34.915

where q and q_m are in mmol/g and p is in bar.

(a) Which component is most strongly adsorbed by each of the adsorbents? (b) Which adsorbent has the greatest adsorption capacity? (c) Which adsorbent has the greatest selectivity? (d) Based on equilibrium considerations, which adsorbent is best for the separation?

15.8 Ruthven and Kaul [*Ind. Eng. Chem. Res.,* **32,** 2047–2052 (1993)] measured adsorption isotherms for a series of gaseous aromatic hydrocarbons on well-defined crystals of NaX zeolite over ranges of temperature and pressure. For 1,2,3,5-tetramethylbenzene

at 547 K, the following equilibrium data were obtained with a vacuum microbalance:

q, wt%	7.0	9.1	10.3	10.8	11.1	11.5
p, torr	0.012	0.027	0.043	0.070	0.094	0.147

Obtain a best fit of the data to the linear, Freundlich, and Langmuir isotherms, with q in mol/g and pressure in atm. Which isotherm gives the best fit?

15.9 Lewis, Gilliland, Chertow, and Hoffman [*J. Am. Chem. Soc.*, **72,** 1153–1157 (1950)] measured adsorption equilibria for pure propane, pure propylene, and binary mixtures thereof, on activated carbon and silica gel. Adsorbate capacity was high on carbon, but selectivity was poor. Selectivity was high on silica gel, but capacity was low. For silica gel (751 m^2/g), the following pure component data were obtained at 25°C:

Propane		Propylene	
P, torr	q, mmol/g	P, torr	q, mmol/g
11.1	0.0564	34.2	0.3738
25.0	0.1252	71.4	0.7227
43.5	0.1980	91.6	0.7472
71.4	0.2986	194.3	1.129
100.0	0.3850	198.3	1.168
158.9	0.5441	271.5	1.401
227.5	0.7020	353.2	1.562
304.2	0.843	550.7	1.918
387.0	1.010	555.2	1.928
468.0	1.138	760.6	2.184
569.0	1.288		
677.8	1.434		
775.0	1.562		

The following mixture data were measured at 25°C, over a pressure range of 752–773 torr:

Total Pressure, torr	Millimoles of Mixture Adsorbed/g	y_{C_3}, Mole Fraction in Gas Phase	x_{C_3}, Mole Fraction in Adsorbate
769.2	2.197	0.2445	0.1078
760.9	2.013	0.299	0.2576
767.8	2.052	0.4040	0.2956
761.0	2.041	0.530	0.2816
753.6	1.963	0.5333	0.3655
766.3	1.967	0.5356	0.3120
754.0	1.974	0.6140	0.3591
753.6	1.851	0.6220	0.5550
754.0	1.701	0.6252	0.7007
760.0	1.686	0.7480	0.723
—	2.180	0.671	0.096
760.0	1.993	0.8964	0.253
760.0	1.426	0.921	0.401

(a) Fit the pure component data to Freundlich and Langmuir isotherms. Which gives the best fit? Which component is most strongly adsorbed?

(b) Use the results of the Langmuir fits in part (a) to predict binary-mixture adsorption using the extended Langmuir equation, (15-32). Are the predictions adequate?

(c) Ignoring the pure-component data, fit the binary-mixture data to the extended Langmuir equation, (15-32). Is the fit better than that obtained in part (b)?

(d) Ignoring the pure-component data, fit the binary mixture data to the extended Langmuir–Freundlich equation, (15-33). Is the fit adequate? Is the fit better than that in part (c)?

(e) For the binary-mixture data, compute the relative selectivity,

$$\alpha_{C_3,C_3^=} = y_{C_3}(1 - x_{C_3})/[x_{C_3}(1 - y_{C_3})]$$

for each condition. Does α vary widely or is the assumption of constant α reasonable?

15.10 In Example 15.6, pure-component, liquid-phase adsorption data are used with the extended-Langmuir isotherm to predict a binary-solute data point. Use the following mixture data to obtain the best fit to an extended Langmuir–Freundlich isotherm of the form

$$q_i = \frac{(q_0)_i k_i c_i^{1/n_i}}{1 + \sum_j k_j c_j^{1/n_j}} \tag{1}$$

Data for binary-mixture adsorption on activated carbon (1000 m^2/g) at 25°C for acetone (1) and propionitrile (2) are as follows:

Solution Concentration, mol/L		Loading, mmol/g	
c_1	c_2	q_1	q_2
5.52E − 5	7.46E − 5	0.0192	0.0199
6.14E − 5	7.71E − 5	0.0191	0.0198
1.06E − 4	1.35E − 4	0.0308	0.0320
1.12E − 4	1.46E − 4	0.0307	0.0319
3.03E − 4	2.32E − 3	0.0378	0.263
3.17E − 4	2.34E − 3	0.0378	0.264
3.25E − 4	3.89E − 4	0.0644	0.0672
1.42E − 3	1.58E − 3	0.161	0.169
1.42E − 3	1.61E − 3	0.161	0.169
1.43E − 3	1.60E − 3	0.161	0.169
2.09E − 3	3.84E − 4	0.250	0.0390
2.17E − 3	3.85E − 4	0.251	0.0392
4.99E − 3	5.24E − 3	0.291	0.307
5.06E − 3	5.31E − 3	0.288	0.305
7.41E − 3	2.42E − 2	0.237	0.900
7.52E − 3	2.47E − 2	0.236	0.896
2.79E − 2	7.59E − 3	0.802	0.251
4.00E − 2	3.44E − 2	0.715	0.822
4.02E − 2	3.42E − 2	0.717	0.834

15.11 Sircar and Myers [*J. Phys. Chem.*, **74,** 2828–2835 (1970)] measured liquid-phase adsorption at 30°C for a binary mixture of cyclohexane (1) and ethyl alcohol (2) on activated carbon. Assuming no adsorption of ethyl alcohol, they used (15-34) to obtain the

following results:

x_1	q_1^e, mmol/g	x_1	q_1^e, mmol/g
0.042	0.295	0.440	0.065
0.051	0.485	0.470	0.000
0.072	0.517	0.521	−0.129
0.148	0.586	0.537	−0.362
0.160	0.669	0.610	−0.643
0.213	0.661	0.756	−1.230
0.216	0.583	0.848	−1.310
0.249	0.595	0.893	−1.180
0.286	0.532	0.920	−1.230
0.341	0.383	0.953	−0.996
0.391	0.192	0.974	−0.470

(a) Plot the data as q_1^e against x_1. Explain the shape of the curve.

(b) In what regions of concentration could the Freundlich isotherm be fitted to the data? Make the fits.

15.12 Both the adsorptive removal of small amounts of toluene from water and small amounts of water from toluene are important in the process industries. Activated carbon is particularly effective for removing soluble organic compounds (SOCs) from water. Activated alumina is effective for removing soluble water from toluene. Fit each of the following two sets of equilibrium data for 25°C to both the Langmuir and Freundlich isotherms. For each case, which isotherm provides the better fit? Could a linear isotherm be used?

Toluene (in Water)		Water (in Toluene)	
Activated Carbon		Activated Alumina	
c, mg/L	q, mg/g	c, ppm (by Weight)	q, g/100g
0.01	12.5	25	1.9
0.02	17.1	50	3.1
0.05	23.5	75	4.2
0.1	30.3	100	5.1
0.2	39.2	150	6.5
0.5	54.5	200	8.2
1	90.1	250	9.5
2	70.2	300	10.9
5	125.5	350	12.1
10	165	400	13.3

15.13 Derive (15-44). Use this equation to solve the following problem. Sulfate ion is to be removed from 60 L of water by exchanging it with chloride ion on 1 L of a strong-base resin with relative molar selectivities as listed in Table 15.6 and an ion-exchange capacity of 1.2 eq/L of resin. The water to be treated has a sulfate-ion concentration of 0.018 eq/L and a chloride-ion concentration of 0.002 eq/L. Following the attainment of equilibrium ion exchange, the treated water will be removed and the resin will be regenerated with 30 L of 10 wt% aqueous NaCl.

(a) Write the ion-exchange reaction.

(b) Determine the value of $K_{SO_4^{2-},Cl^-}$.

(c) Calculate equilibrium concentrations $c_{SO_4^{2-}}$, c_{Cl^-}, $q_{SO_4^{2-}}$, and q_{Cl^-} in eq/L for the initial ion-exchange step.

(d) Calculate the concentration of Cl^- in eq/L for the regenerating solution.

(e) Calculate $c_{SO_4^{2-}}$, c_{Cl^-}, $q_{SO_4^{2-}}$, and q_{Cl^-} upon reaching equilibrium in the regeneration step.

(f) Are the separations sufficiently selective?

15.14 Silver ion in methanol was exchanged with sodium ion using Dowex 50 cross-linked with 8% divinylbenzene by Gable and Stroebel [*J. Phys. Chem.*, **60,** 513–517 (1956)]. The molar selectivity coefficient was found to vary somewhat with the equivalent fraction of Na^+ in the resin as follows:

x_{Na^+}	0.1	0.3	0.5	0.7	0.9
K_{Ag^+,Na^+}	11.2	11.9	12.3	14.1	17.0

If the wet capacity of the resin is 2.5 eq/L and the resin is initially saturated with Na^+, calculate the equilibrium equivalent fractions if 50 L of 0.05-M Ag^+ in methanol is treated with 1 L of wet resin.

15.15 Ion exclusion is a process that uses ion-exchange resins to separate nonionic organic compounds from ionic species contained in a polar solvent, usually water. The resin is presaturated with the same ions as in the solution, thus eliminating ion exchange. However, in the presence of the polar solvent, resins undergo considerable swelling by absorbing the solvent. Experiments have shown that a nonionic solute will distribute between the solution outside the resin and the solution within the resin, while the ions can only exchange.

A feed solution of 1,000 kg contains 6 wt% NaCl, 35 wt% glycerol, and 47 wt% water. This solution is to be treated with Dowex-50 ion-exchange resin in the sodium form, after prewetting with water, to recover 75% of the glycerol. The following data for the glycerol distribution coefficient,

$$K_d = \frac{\text{mass fraction in solution inside resin}}{\text{mass fraction in solution outside resin}}$$

were reported by Asher and Simpson [*J. Phys. Chem.*, **60,** 518–521 (1956)]:

Mass Fraction Glycerol in Solution Outside Resin	K_d	
	6 wt% NaCl	12 wt% NaCl
0.10	0.75	0.91
0.20	0.80	0.93
0.30	0.83	0.95
0.40	0.85	0.97

If the prewetted resin contains 40 wt% water, determine the kilograms of resin (dry basis) required.

Section 15.3

15.16 Benzene vapor in an air stream is adsorbed in a fixed bed of 4 × 6 mesh silica gel packed to an external void fraction of 0.5. The bed is 2 feet in inside diameter and the air flow rate is 25 lb/min (benzene-free basis). At a location in the bed where the pressure is 1 atm, the temperature is 70°F, and the bulk mole fraction of benzene is 0.005, estimate the external, gas-to-particle mass-transfer and heat-transfer coefficients.

15.17 Water vapor in an air stream is to be adsorbed in a 12.06-cm-inside-diameter column packed with 3.3-mm-diameter Alcoa F-200 activated alumina beads with an external porosity of 0.442. At a location in the bed where the pressure is 653.3 kPa, the temperature is 21°C, the gas flow rate is 1.327 kg/min, and the

dew-point temperature is 11.2°C, estimate the external, gas-to-particle mass-transfer and heat-transfer coefficients.

15.18 For the conditions of Example 15.8 estimate the effective diffusivity of acetone vapor in the pores of activated carbon with the following properties: particle density = 0.85 g/cm^3, particle porosity = 0.48, average pore diameter = 25 Å, and tortuosity = 2.75.

Consider both bulk and Knudsen diffusion, but ignore surface diffusion.

15.19 For the conditions of Exercise 15.16, estimate the effective diffusivity of benzene vapor in the pores of silica gel with the following properties: particle density = 1.15 g/cm^3, particle porosity = 0.48, average pore diameter = 30 Å, and tortuosity = 3.2.

Consider all mechanisms of diffusion. The adsorption equilibrium constant is given in Example 15.11, and the differential heat of adsorption is −11,000 cal/mol.

15.20 For the conditions of Exercise 15.17, estimate the effective diffusivity of water vapor in the pores of activated alumina with the following properties: particle density = 1.38 g/cm^3, particle porosity = 0.52, average pore diameter = 60 Å, and tortuosity = 2.3.

Consider all mechanisms of diffusion except surface diffusion.

Section 15.4

15.21 Adsorption with activated carbon, made from bituminous coal, of soluble organic compounds (SOCs) to purify surface and ground water is a proven technology, as discussed by Stenzel [*Chem. Eng. Prog.*, **89** (4), 36–43 (1993)]. The less-soluble organic compounds, such as chlorinated organic solvents and aromatic solvents, are the more strongly adsorbed. Water containing 3.3 mg/L of trichloroethylene (TCE) is to be treated with activated carbon to obtain an effluent with only 0.01 mg TCE/L. At 25°C, adsorption equilibrium data for TCE on activated carbon are correlated with the following Freundlich equation:

$$q = 67\, c^{0.564} \tag{1}$$

where

q = mg TCE/g carbon and c = mg TCE/L solution

The TCE is to be removed by slurry adsorption using a powdered form of the activated carbon, with an average particle diameter of 1.5 mm. In the absence of any laboratory data on mass-transfer rates, assume that the rate of adsorption for the small particles is controlled by external mass transfer with a Sherwood number of 30. Particle surface area is 5 m^2/kg. The molecular diffusivity of TCE in low concentrations in water at 25°C may be determined from the Wilke–Chang equation.

(a) Determine the minimum amount of adsorbent needed.

(b) For operation in the batch mode with twice the minimum amount of adsorbent, determine the time to reduce the TCE content to the desired value.

(c) For operation in the continuous mode using twice the minimum amount of adsorbent, determine the required residence time.

(d) For operation in the semicontinuous mode at a feed rate of 50 gpm and for a liquid residence time equal to 1.5 times that computed in part (c), determine the amount of activated carbon to give a reasonable vol% solids in the tank and a run time of not less than 10 times the liquid residence time.

15.22 Repeat Exercise 15.21 for water containing 0.324 mg/L of benzene (B) and 0.630 mg/L of m-xylene (X).

Adsorption isotherms at 25°C for these low concentrations are essentially independent and are given by

$$q_B = 32\, c_B^{0.428} \tag{1}$$

$$q_X = 125\, c_X^{0.333} \tag{2}$$

The feed concentrations of the SOCs in the feed are to be reduced to 0.002 mg/L each.

15.23 Repeat Exercise 15.21 for water containing 0.223 mg/L chloroform, whose concentration is to be reduced to 0.010 mg/L. The adsorption isotherm at 25°C is given by

$$q = 10\, c^{0.564} \tag{1}$$

15.24 Three fixed-bed adsorbers containing 10,000 lb of granules of activated carbon (ρ_b = 30 lb/ft^3) each are to be used to treat 250 gpm of water containing 4.6 mg/L of 1,2-dichloroethane (D) to reduce the concentration to less than 0.001 mg/L. Each carbon bed has a height equal to twice the diameter. Two beds are to be placed in series so that when Bed 1 (the lead bed) becomes saturated with D at the feed concentration, that bed is removed. Bed 2 (the trailing bed), which is partially saturated at this point, depending upon the width of the MTZ, becomes the lead bed, and previously idle Bed 3 takes the place of Bed 2. While Bed 1 is off-line, its spent carbon is removed and replaced with fresh carbon. The spent carbon is incinerated. The equilibrium adsorption isotherm for D is given by $q = 8\, c^{0.57}$, where q is in mg/g and c is in mg/L. Once the cycle is established, how often must the carbon in a bed be replaced? What is the maximum width of the MTZ that will allow saturated loading of the lead bed?

15.25 The fixed-bed adsorber series arrangement of Exercise 15.24 is to be used to treat 250 gpm of water containing 0.185 mg/L of benzene (B) and 0.583 mg/L of m-xylene (X). However, because the two solutes may have considerably different breakthrough times, more than two operating beds in series may be needed. The adsorption isotherms are given in Exercise 15.22, where q is in mg/g and c is in mg/L. From laboratory measurements, the widths of the mass-transfer zones are estimated to be MTZ_B = 2.5 ft and MTZ_X = 4.8 ft. Once the cycle is established, how often must the carbon in the bed be replaced?

15.26 Air at 80°F, 1 atm, 80% relative humidity, and a superficial velocity of 100 ft/min passes through a 5-ft-high bed of 2.8-mm-diameter spherical particles of silica gel (ρ_b = 39 lb/ft^3). The adsorption equilibrium isotherm at 80°F is given by

$$q_{H_2O} = 15.9\, p_{H_2O} \tag{1}$$

where q is in lb H_2O/lb gel and p is in atm. The overall mass-transfer coefficient can be estimated from (15-106), using an effective diffusivity of 0.05 cm^2/s and with k_c estimated from (15-65). Using the approximate concentration-profile equations of Klinkenberg, compute a set of breakthrough curves and determine the time when the humidity of the exiting air reaches 0.0009 lb H_2O/lb dry air. Assume isothermal and isobaric operation. Compare the time to breakthrough with the time for the equilibrium model. At breakthrough, what is the approximate width of the mass-transfer zone. What is the average loading of the bed at breakthrough?

15.27 A train of four 55-gallon cannisters of activated carbon is to be used to reduce the nitroglycerine (NG) content of 400 gph of

wastewater from 2,000 ppm by weight to less than 1 ppm. Each cannister has a diameter of 2 ft and holds 200 lb activated carbon ($\rho_b = 32$ lb/ft^3). Each cannister is equipped with a liquid-flow distributor to promote plug flow through the bed of carbon. The effluent from the first cannister is monitored so that when a 1 ppm threshold of NG is reached, that cannister is removed from the train and a fresh cannister is added to the end of the train. The spent carbon is mixed with coal for use as a fuel in a coal-fired power plant at the process site. Using the following pilot-plant data, estimate how many cannisters are needed each month and the monthly cannister cost at $700 per cannister.

Pilot-plant data:

Tests with the same 55-gallon cannister to be used in the commercial process; water flow rate = 10 gpm; NG content in feed = 1,020 ppm by weight.

Breakthrough correlation:

$t_B = 3.90\,L - 2.05$, where t_B = time, h, at breakthrough of the 1 ppm threshold and L = bed depth of carbon in feet.

15.28 Air at a flow rate of 12,000 scfm (60°F, 1 atm) and containing 0.5 mol% ethyl acetate (EA) and no water vapor is to be treated with activated carbon (C) ($\rho_b = 30$ lb/ft^3) with an equivalent particle diameter of 0.011 ft in a fixed-bed adsorber to remove the ethyl acetate, which will be subsequently stripped from the carbon by steam at 230°F. Based on the following data, determine the diameter and height of the carbon bed, assuming adsorption at 100°F and 1 atm and a time-to-breakthrough of 8 h with a superficial gas velocity of 60 ft/min. If the bed height-to-diameter is unreasonable, what change in design basis would you suggest?

***Adsorption isotherm data (100°F) for* EA:**

p^{EA}, atm	q, lb EA/lb C	p^{EA}, atm	q, lb EA/lb C
0.0002	0.125	0.0020	0.227
0.0005	0.164	0.0050	0.270
0.0010	0.195	0.0100	0.304

Breakthrough data at 100°F and 1 atm for EA in air at a gas superficial velocity of 60 ft/min in a 2-ft dry bed:

Mole Fraction EA in Effluent	Time, Min	Mole Fraction EA in Effluent	Time, Min
0.00005	60	0.00100	95
0.00010	66	0.00250	120
0.00025	75	0.00475	160
0.00050	84		

15.29 In Examples 15.11 and 15.13, benzene is adsorbed from air at 70°F in a 6-ft-high bed of silica gel and then stripped with air at 145°F. If the bed height is changed to 30 ft, the following data are obtained for breakthrough at 641 minutes for the adsorption step:

z, ft	$\phi = c/c_F$	$\psi = \bar{q}/q_F^*$	z, ft	$\phi = c/c_F$	$\psi = \bar{q}/q_F^*$
0–12	1.000	1.000	14	1.000	1.000
13	1.000	1.000	15	1.000	1.000
16	0.999	0.999	24	0.599	0.575
17	0.997	0.997	25	0.468	0.444
18	0.992	0.990	26	0.343	0.321
19	0.978	0.975	27	0.235	0.217
20	0.951	0.944	28	0.150	0.137
21	0.901	0.890	29	0.090	0.081
22	0.825	0.808	30	0.050	0.044
23	0.722	0.701			

If the bed is regenerated isothermally with pure air at 1 atm and 145°F, and the desorption of benzene during the heatup period is neglected, determine the loading, $\bar{q}$, profile at a time sufficient to remove 90% of the benzene from the bed if an interstitial pure air velocity of 98.5 ft/min is used. Values of k and K at 145°F are given in Example 15.13.

15.30 Use the method of lines with a five-point, biased, upwind finite-difference approximation and a stiff integrator to perform PSA cycle calculations that approach the cyclic steady state for the data and design basis in Example 15.14, starting from: (a) a clean bed, and (b) a bed saturated with the feed. Are the two cyclic steady states essentially the same?

15.31 Solve Example 15.14 for $P_L = 0.12$ atm and an interstitial velocity during desorption that corresponds to the use of 44.5% of the product gas from the adsorption step.

15.32 For the separation of air by PSA, adsorption of both O_2 and N_2 must be considered. Develop a model for this case taking into account two species mass balances, overall mass balance, two species mass-transfer rates, and two extended-Langmuir isotherms. Each of the two main steps can be isothermal and isobaric. Can your PDE equations still be solved by the method of lines with a stiff integrator? If so, outline a procedure for doing it.

15.33 Two adsorption-based separation processes not considered in this chapter because of lack of significant commercial application are (1) parametric pumping, first conceived by R.H. Wilhelm in the early 1960s, and (2) cycling-zone adsorption, invented by R.L. Pigford and co-workers in the late 1960s. The status of and future for these two processes was assessed by Sweed in 1984 [*AIChE Symp. Series,* **80** (233), 44–53 (1984)]. Describe in detail each of these processes. Can either be used for both gas-phase and liquid-phase adsorption?

15.34 A gas mixture containing 55 mol% propane and 45 mol% propylene is to be separated into products containing 10 and 90 mol% propane by adsorption in a continuous, countercurrent adsorption system operating at 25°C and 1 atm. The adsorbent is silica gel, for which equilibrium data are given in Exercise 15.9. Determine by the McCabe–Thiele method: (a) the adsorbent flow rate per 1,000 m^3 of feed gas at 25°C and 1 atm if 1.2 times the minimum rate is used, and (b) the number of theoretical stages required.

15.35 Repeat Example 15.19, except for a feed containing 400 ppm (by weight) of $CaCl_2$ and 50 ppm of NaCl.

15.36 An aqueous solution, buffered to a pH of 3.4 by sodium citrate and containing 20 mol/m^3 each of glutamic acid, glycine, and valine, is separated in a chromatographic column, packed with Dowex 50W-X8 in the sodium form to a depth of 470 mm. The resin is 0.07 mm in diameter and packs to a bed void fraction

of 0.374. Equilibrium data follow Henry's law, as in Example 15.20, with the following dimensionless constants, determined by Takahashi and Goto [*J. Chem. Eng. Japan,* **24,** 121–123 (1991)]:

Solute	K
Glutamic acid	1.18
Glycine	1.74
Valine	2.64

The superficial solution velocity is 0.025 cm/s. Using equilibrium theory, what pulse duration can be used to achieve complete separation? How long must the elution step be before the second pulse can begin?

15.37 Repeat Exercise 15.36, but using Carta's equation to account for mass transfer with the following effective diffusivities:

Solute	D_e, cm^2/s
Glutamic acid	1.94×10^{-7}
Glycine	4.07×10^{-7}
Valine	3.58×10^{-7}

Assume $k_c = 1.5 \times 10^{-3}$ cm/s. Establish a cycle of feed pulses and elution periods that will give the desired separation.

15.38 A dilute feed of 3-phenyl-1-propanol (A) and 2-phenyl ethanol (B) in a 60/40 wt% ratio, methanol–water mixture is to be fed to a four-section laboratory SMB to separate A from B. The feed rate is 0.16 mL/min with 0.091 g/L of A and 0.115 g/L of B. The desorbent is a 60/40 wt% methanol–water mixture. For this dilute mixture of A and B and the adsorbent to be used, Henry's law applies with $K_A = 2.36$ and $K_B = 1.40$. Assume that neither the methanol nor the water adsorb. The external void fraction of the adsorbent beds, ϵ_b, is 0.572. A switching time of 10 minutes is to be used. Using the steady-state, local-composition TMB model for a perfect separation of A from B with $\beta = 1.15$, estimate initial values for the volumetric flow rates of the extract, raffinate, desorbent, and the solid particles. Convert the value of the recirculation rate for the TMB to that for the SMB and compute the resulting volumetric-liquid flow rates in each of the four sections.

15.39 In the steady-state TMB run of Example 15.17, results for Example 15.16, from the application of the steady-state, local-equilibrium TMB model, were used with a β of 1.05 to establish the flow rates of the raffinate, extract, makeup desorbent, recirculation, and solid particles so as to approach a perfect separation between fructose and glucose. While the separation was not perfect, it was reasonably good. What results are achieved in Example 15.17 if the overall mass-transfer coefficients approach infinity?